ACOUSTIC EMISSION CHARACTERISTICS OF METALS

by

LAITH SALIM SULAIMAN

A thesis submitted for the degree of

Doctor of Philosophy

in the

Department of Mechanical Engineering

at the

University of Aston in Birmingham

NOVEMBER 1979

To my parents to whom I will be

indebted all my life

ACOUSTIC EMISSION CHARACTERSTICS OF

METALS

Laith Salim Sulaiman

Ph.D.

1979

Summary

This work was concerned with the study of the characteristics of the acoustic emission from various metals and with obtaining more information about this phenomena. Low and medium carbon steels, Aluminium, Copper and Brass were used in this work.

Notched and unnotched flat and round tensile specimens of different dimensions were used. Three-point bending tests were carried out on steel specimens with different notch root radii.

The frequency bandwidth of the acoustic emission monitoring system used was 100-300KHz. The output signals were recorded on a magnetic tape recorder and an on-line mini-computer was used to analyse the recorded signals. The results showed that the number of acoustic emissions was affected by many factors such as type of metal, micro-structure, the notch size, and specimen size.

However, the frequency content of the acoustic emission signals was less affected by the above factors, but the frequency ranges of the analysed signals was found to be affected by the type of test carried out i.e. tensile or three-point bending test.

The results showed that acoustic emission is a very useful technique in material research and a valuable method for non-destructive testing.

Key Words

Acoustic Emission counts
Acoustic Emission rate
Non-destructive testing
Fast Fourier transformation (F.F.T.).

ACKNOWLEDGEMENTS

I would like to express my most sincere thanks to my supervisor, Professor E. Downham, for suggesting the project, his helpful suggestions and encouragement throughout the course of this work.

Also I would like to express my thanks to Professor J.T. Barnby of the Department of Metallurgy for his helpful advice.

My thanks also to Dr. Noori S. Noori, Hana and Muna Al-Khashab for their help during the preparation of this thesis.

CONTENTS

LIST OF FIGURES

Page

Page

CHAPTER 1

1.1. Introduction

Acoustic emission (stress wave) is the phenomena produced by the energy released as a solid material undergoes plastic deformation and fracture. Part of this energy is converted into elastic waves which propagate through the material and can be detected by high sensitivity sensors at the surface of the material.

The emissions provide a method of detecting crack formation and growth in a solid material and also can be used as an indicator of impending failure of the material, with the advantages that it can be accomplished remotely and at the time cracks are forming. This is important because it allows loads to be reduced, perhaps preventing catastrophic failure, and enables monitoring to be done in dangerous regions, such as places of high radioactivity, low pressure, or high and low temperatures.

The counting techniques have been the primary means of acoustic emission investigation and have yielded much information about the phenomena. However, these techniques do not always have sufficient capabilities to resolve differences in the features of the stress waves that are generated by dissimilar processes. Also, a number of empirical relationships have been established which relate, for example, fracture toughness or fatigue crack growth to some power of the cumulative count, but such relationships are found to be strongly affected by microstructural variables and by factors such as the type of transducer and threshold level employed.

The frequency analysis technique is found to be a very useful method of obtaining information concerning mechanical deformation mechanisms that cannot be obtained by conventional amplitude counting techniques.

A limited number of studies have been made on the characteristics of acoustic emission signals. Kaiser analysed a photographic record of acoustic emission signals in a variety of materials, including aluminium and steel. He observed that the acoustic emission characteristics frequencies increased as a function of strain. He reported that the predominant frequency of acoustic emission resulting from tensile loading increased from 3-7KHz at the outset to a maximum of 15-30KHz at yield and decreased thereafter.

Schofield (1) used a magnetic tape recorder and a variable bandpass filter to repeatedly scan an acoustic emission signal at different band widths. He reported that the frequency increased with stress increase. he did not observe the maximum frequency at yield as did Kaiser.

Hutton (2) used visual analysis of oscilliscope traces of acoustic emission signal and reported that acoustic emission, during plastic deformation of a steel, has an average frequency of 5KHz for the continuous emission and 20KHz for the burst emission.

Beattie, A.G. (3) studied the acoustic emission signals generated by the Fcc to Fct phase transformation in the alloy. The frequency response of the entire monitoring systems including transducers, was reasonably flat, ±1dB, between 100KHz and 3MHz. The average result of analysis showed a fairly wide-band signal between 50KHz and 200KHz with a maximum near the 100KHz.

Graham and Alers (4) used a simple technique for obtaining the frequency spectra of individual acoustic emission from propagation of cracks in metals and in ceramics. They modified a Sony video tape recorder in such a way that individual acoustic emission bursts could be recorded and subsequently played back into a Hewlett-Packard Spectrum Analyser. This system makes possible the rapid determination of the frequency content of the burst from 0-3MHz. It also permits the measurement of the amplitude distribution of any series of burst emitted during a particular time interval of a mechanical deformation test. Tests were carried out on aluminium alloys, titanium alloys, some steel and single crystal MgO. No appreciable variation in frequency with deformation was observed. Tests carried out on A533-B steel showed a high frequency signal (Peak $\sim$ 1MHz) associated with plastic flow and lower frequency (Peak $\sim$ 200KHz) signals associated with the crack propagation were reported.

Bassim, Hay and Lanteigne (5) investigated the acoustic emission signals from flawed and unflawed specimens. Tensile specimens were used (AISI 1015 steel). They used a transducer with a flat response over a wide range of 0.1 to 0.5 MHz. Emissions continuously recorded on a modified Sony video tape recorder.

They concluded that the amplitude of the signal from the flawed specimen is larger than that from the unflawed specimen. The frequency of the signal emitted from the unflawed specimen is higher than that from the flawed specimen by 0.06MHz within each region. The unflawed specimen, with its microscale plastic deformation, has a boarder band spectra content.

Kline, R.A. (6) studied the acoustic emission signals frequency contents from the tensile tests of 70-30 brass specimens and HF-1 steel specimens. The specimens used were round tensile. HF-1 steel specimens were quenched and tempered. He used a tensile machine which was designed to be quiet in operation. The monitoring system used by Kline consisted of a wide-band transducer, pre-amplifier bandpass filter counter and video tape recorder (V.T.R.). The combination of the above instruments has the capability of 100dB gain over a frequency range from 100KHz to 3MHz ±3dB.

Kline concluded that the acoustic emission from the tensile loading of yellow brass tends to exhibit higher frequencies at higher strains. For HF-1 steel three distinct acoustic emission spectra corresponding to microplasticity, plasticity were observed.

Hartman and Kline (7) studied the acoustic emission signals from HF-1 steel. They used the setting and instrumentation as Kline used. They concluded that acoustic emission from the tensile loading of HF-1 exhibited three different frequency spectra, corresponding to microplasticity, plasticity and deformation after recovery.

The aim of this work is to obtain more information about the characteristics of the acoustic emission from metals. Because the frequency spectra of the acoustic emission signals contain valuable information about the source of these signals and the stage of deformation, particular emphasis was placed upon documenting the changes induced in the acoustic emission spectra with variation in the mechanism of deformation. Specimens were chosen from different types of steel, and non-ferrous metals (Aluminium, Copper, and Brass). Tensile tests and three-point bending tests were carried out on these specimens.

1.2. Historical Review

Acoustic Emission is a phenomena generated internally during dynamic processes in various materials. The dynamic processes may be the result of an externally applied stress or the result of some other unstable situation, e.g. phase transition or on a large scale, a shifting mine slope. The actual source of the stress waves depends on the material. It may be dislocation or crack motion in a metal, interparticle movement in a soil, or fibre breaking in a composite or wood.

Historically, the earliest use of acoustic emission phenomena occurred in the study of seismology. Analysis of elastic waves produced by an earthquake was used to characterize fault movements in terms of the energy released, location and depth. The possibility of detecting rockbursts in coal mines was appreciated at an early date.

Hodgson (8) (1943, 1958) in Canada and Obert (1941) and Obert and Duvall (1942, 1945, 1957, 1961) in the United States were all interested in predicting rockbursts in mines using the sub-audible "microseisms" generated in rocks. Their work started in the late 1930s. The transducer, called a geophone, was a bimorphic piezoelectric crystal 63.5mm long by 19mm wide by 6.35mm thick mounted as a cantilever in a steel tube 31.75mm in diameter and about 203mm long. It was designed to be the size of a stick of power so it would be inserted in a rock-drill hole. When the geophone is subjected to a subandible mechanical impulse, the crystal suffers a slight flexure which results in the generation of a transient voltage between the two terminals of the crystals. The output of the geophone has to travel as much as 300 metres of cable to the amplifier. The amplifier used has a flat frequency response between 150 to 10,000 Hz. The output has been recorded on a special paper, of which the result can be seen in time. The equipment was built by the workers themselves.

It was found during this work that microseisms (sub-audible rock noises) do not occur in shallow mines evidently because the pressure is not high enough there. Usually observation had to be made at a depth of at least 600 metres to observe microseisms. The ability to use microseisms as a means of predicting rock-bursts depends very strongly on the type of mine investigated. Due to dispersion in the attenuation of elastic waves in rock, the high frequency components of a microseism were dampened more rapidly than the low frequency of the microseism, the distance to the source.

The predictability of rock-burst via microseism count has been found to be reasonably good in certain mines. The criteria for rock-burst prediction was the following: "when the number of recorded noises increased in any interval (not exceeding 24 hours) by a factor of two or more, a dangerous condition is indicated. Furthermore, if after such an increase, the number of noises continue to increase, the state of danger is presumed to persist".

Obert and Duvall (1945) tried to ascertain whether the microseisms originate from intermovement along fissures, seams, or fractures of geological origin or from the homogeneous rock itself. They observe that microseisms can originate from initially homogeneous material and also observed a general behaviour in emission rate versus stress.

The Russians have been very active in using rock noise (Seismoacoustics) to predict rock-bursts. Their work started in 1952, considerably later than the American and Canadian workers. The Russian workers favoured electrodynamic geophones, with some work in piesoelectric types.

1.2.A. <u>Single Crystal and Polycrystalline Specimens</u>

Mason et al. (1948, Mason 1950) observed what appeared to be acoustic emissions in the ultrasonic frequency region during the mechanical twinning of a very small tin specimen. A plane quartz crystal was used as the detector. This work gave some of the first indirect evidence for the existence of dislocations in a mechanical process (twinning).

Dr. Joseph Kaiser (9) in 1950 indicated that all metals examined, including Zinc, Steel, Aluminium and Lead, exhibited acoustic emission phenomena. He attributed emission activity to grain boundary sliding during plastic deformation.

Kaiser reported that the predominant frequency of acoustic emission resulting from tensile loading increased from 3 to 7KHz at the outset to a maximum of 15 to 30KHz at yield and decreased thereafter. Lead was an exception, it exhibited no predictable change in its frequency contents.

Also Kaiser reported that the pulses were not repeated when the samples were reloaded to the previous stress level. This property of irreversibility was later exploited in the fabrication of passive stress sensors, although it was shown to be a reduction in magnitude and not truly an irreversible effect.

Schofield (10) (1955) investigated an extensive investigation on acoustic emission phenomena. He used aluminium and zinc single crystals, commercial copper, 24S-T4 aluminiums, lead, and 70-30 brass. The primary purpose of this early work was to determine the source of emission, and the single crystal work showed conclusively that grain boundary effects were not the only source of emission.

Schofield was the first to make a real distinction between burst-type (discrete) and continuous-type emissions. The "Kaiser effect" was also verified. He was able to show that twin production and grain boundary re-orientation (in a bicrystal) produced extremely large noises.

Schofield (11) found that a thin oxide surface layer on aluminium enhanced the emission activity, as did lightly cold-working the surface. He also found that the removal of surface material by etching tended to inhibit the initial response.

After more than five years of investigation, Schofield concluded that the oxide coating on metals does not contribute significantly to acoustic emission response; rather the surface and its condition play only a secondary role in influencing emission response in as much as they do affect the deformation characteristics.

His studies indicated that both the continuous-type and burst-type emissions result from emission source mechanisms of a transient, spike nature, as opposed to long duration oscillatory vibrations.

Schofield examined the effect on condition by removing the oxide layer and by lightly cold-working the specimen surfaces.

Also observed were appreciable differences between acoustic emission characteristics of various metals. These differences were: (a) the strain at which the emission initiated; (b) the strain at which the emission rate reached a maximum; and (c) the relative proportions of high amplitude, low-frequency bursts, and low-amplitude, high-frequency, quasi-continuous emission.

Schofield found that the acoustic emission response from polycrystalline copper and lead specimens was very similar to that from single crystals of aluminium. However, a 24S-T4 aluminium alloy exhibited a considerable increase in the number of burst-type signals during deformation over that from pure, single crystal aluminium specimens (11). A crack, which was found during testing of the 24S-T4 specimen, increased the amount of high frequency emissions and the overall emission pattern. Carbon steel specimens exhibited both continuous and burst-type emission response, with the quantity of burst-type signals being about the same as from aluminium alloys.

Liptai employed oriented, single crystal specimens of 99.99+% aluminium in an attempt to establish the mechanisms governing acoustic emission sources (12). He mounted ADP Piezoelectric crystals on the end of test specimens which were loaded to produce up to 2% strain. Liptai concluded that the micro-mechanisms associated with the emission source are the same as those which control slip band formation. He thought that the emission pulses were the result of a dislocation avalanche intersecting the surface of the specimen, and that the strain energy was dissipated by producing a new surface, heat, and elastic stress waves.

Liptai also investigated the Kaiser effect and found that the emission during retesting was equivalent to about 15% of the original acoustic emission activity, based on an average of nine retests.

He found that variations in thickness of an anodic oxide coating affected the acoustic response pattern. Thicker films shifted the most active period of emission activity to higher strains, indicating that a larger strain energy was necessary for dislocation arrays to break through the oxide barrier coating, generally producing emission pulses with greater amplitudes.

Tatro and Liptai (13) concluded that acoustic emission was a surface-associated phenomenon. They used 2011-T3 aluminium tensile specimens with a reduced centre section. They examined the effects of various surface treatments such as sand-blasting, oxide coating of various thicknesses, electro-polishing, anodizing, electron bombardment, annealing, hand sanding, and various combinations of these. One particularly interesting experiment consisted of loading an as-machined specimen to about 1% strain, removing the load, and reloading to 1% strain. The normal acoustic emission response was observed during the first loading. Upon reloading, as would be predicted on the basis of the Kaiser effect, there was a marked reduction in emission response. However, when the test section of this specimen was electropolished after the second loading, the acoustic emission activity in the pre-yield regine was dramatically restored. Tatro and Laptai noted that only about 0.127mm of material had been removed from the surfaces of these specimens.

Fisher and Lally (14) investigated the acoustic emission behaviour of single crystals of copper and magnesium and these were tension tested as strain rates ranging from $1X10^{-4}$/sec. to $3X10^{-2}$/sec. They found that the acoustic emission rate was proportional to the strain-rate and was of the order of 10^{3} pulse/sec. for strain-rate of about 10^{-3}/sec. The magnitude of observed acoustic emission pulses increased with increasing strain-rate. From these observations they concluded that the strain increment per emission pulse was about 10^{-6} to 10^{-7}.

Fisher and Lally found that no emission pulses were produced until the first appearance of slip markings.

The pulse rate was also proportional to the crystal length when the applied strain rates were equal. However, there was no comparable effect on emission rates when the cross-sectional area was varied from about 10 to 80mm^2.

Also they reported that the acoustic emission response from polycrystalline specimens of copper, brass, iron, and steel was essentially the same as that from single crystals. The pulse rate usually reached a maximum after the onset of plastic flow and then decreased gradually with increasing strain. Their equipment was capable of recording signals in the 3KHz to 20KHz bandwidth and their tests were performed by hydraulic loading in tension.

Liptai, Dunegan and Tatro (15) investigated the acoustic emission generated during phase transformation in metals and alloys. They used a 90KHz to 120KHz bandwidth to measure the acoustic emission pulses while heating and cooling cylindrical specimens in a liquid medium. They found that martenstic transformations generated elastic energy,whereas nucleation and growth transformations did not. From the Au-47.5 a/. Cd alloy cubic $\rightleftarrows$ orthorhombic transformation, it was found that the emission energy was nearly two orders of magnitude larger on heating than on cooling.

As the temperature is increased, the emission rate increases to a maximum value, and decays very rapidly, whereas on cooling, the rate builds up very rapidly and decreases more gradually. It was conjectured that emission activity (both summation and rate) was proportional to the fraction of material transformed.

Agarwal (16) has investigated the load and unload emission characteristics of several polycrystalline metals. Specimens of 99.99% aluminium, 1020 steel, 2024, 6061, and Alcoa-195 aluminium were loaded in uniaxial tension. A PZT-5 senser was mounted on one end of the specimen, and its output was amplified and processed through a 2 to 20KHz band-pass filter. Agarwal concluded that most of the emission burst contain a dominant frequency component of 10KHz.

Agarwal also found that the cumulative unload emission counts depended upon the maximum stress reached, the volume of stressed material and the hardness. Also the surface area and surface finish showed no effect on the unload emission response. The unload emission response from the tension test and compression test appear identical. Also, he observed an increase in unload emission with increased hardness.

Frederick (17) investigated the relation between the cumulative emission (emission count) and the average grain diameter from 99.99% pure aluminium specimens. Frederick found that the cumulative acoustic emission that is obtained for a given applied stress depends on the grain size of the aluminium. For small or large grain size the emission is low, but at an intermediate size there is a maximum total acoustic emission. The acoustic emission shape of relation between the acumulative acoustic emission and the grain size obtained in a frequency bandwidth of 6-20KHz.

Frederick explains the above phenomena using the dislocation source model, which showed that as the grain size increased the dislocation glide distance increased and a larger strain pulse was produced. This means that there are fewer grain boundary sources of dislocations. Hence a reduction in the emission is to be expected. The maximum emission occurs at a grain size of about 340μm. Acoustic emission activity declines at a rate inversely proportional to the grain size increased beyond a certain value. Hence, since the grain boundary surface area in a specimen is inversely proportional to the grain size, the acoustic emission activity is proportional to the grain boundary surface area. From this it is concluded that the grain boundaries act as an unstable source of dislocations when slip progress from one grain to an adjacent grain takes place (18).

Graham and Alers (4) used a videotape recorder with a 3MHz bandwidth to study the spectral content of acoustic emission from 88.9mm thick plate of A533-B steel.

The electronic amplifiers, filters, and videotape recording system provided a bandwidth which extended from 20KHz to 3MHz. Tensile tests were carried out by using a 10,000Kg capacity Instron machine at constant cross-head speeds of

0.127mm/minute to 12.7mm/minute.

From the spectral analysis they obtained a correlation between the frequency spectra of the observed emissions and the mode of failure.

Graham and Alers interpreted their data as suggesting that the "low frequency" emissions (where most of the energy was below 200KHz) were associated with brittle (cleavage) fracture, and the "high frequency" emissions (with significant energy content at about 800KHz) were associated with plastic ductile (shear) deformation.

Graham and Alers found that the higher frequency spectra shifted to low frequencies during the later stages of the tensile test, which was attributed to the work hardening effects. Also they concluded that acoustic emission characteristic spectra were dependent on the specimen geometry to a very limited extent.

Schayler and Feiertag (19) published their data after two years' work. The work involved a tensile test of several metals. Material investigated included aluminium, copper, berylco-25, iron, several carbon and stainless steels, vascomax-250, nickel, inconel, and titanium. These tensile samples were given various heat-treatments in air, argon, and vacuum. An instron machine of 5,000Kg capacity was used to perform the tensile tests. Several cross-head speeds were used. The transducer had a sharp resonance peak at 156KHz and the signal processing system had about 90dB gain.

Their report included discussions of general response trends and several unique characteristics were observed during testing.

1.2.B. Notched or Pre-cracked Specimens

Acoustic emission has greater potential for detecting cracks and other flaws. These flaws act as stress concentrators and produce localized plastic deformation at macroscopic stress levels well below general yielding. The localized plastic deformation in general produced acoustic emissions and the emissions can thus be used to detect the onset of such flaws. Hence acoustic emission is probably better than any other non-destructive test, allowing the monitoring of engineering structures for integrity against such flaws.

Early work in this particular area used rather low sensitivity acoustic emission measurements to determine the "Pop-in" stress for cracked (notched) specimens (20). The fracture toughness can be computed from the pop-in stress and the appropriate equations for the stress intensity factor (unstable factor of growing crack, K, is equal to the fracture toughness of the material).

Dunegan, Harris and Tatro (21) were interested in developing a non-destructive method of determining the fracture characteristics of flawed structures, so a programme was initiated to determine the acoustic characteristics of parts containing realistic cracks. This was accomplished by using single-edge-notched (SEN) fracture toughness specimens in a testing machine designed specially for acoustic emission tests. Experiments were also performed in this machine on unflawed specimens to determine the differences in the characteristic emission between the flawed and unflawed specimens.

Results of these studies of the acoustic emission characteristic of A50A beryllium and 7075 aluminium indicated that there is a marked different in the acoustic emission from an unflawed tensile and one containing a sharp crack. A theoretical model shows that the acoustic emission from a cracked specimen should vary as the fourth power of the stress intensity factor, whereas experimental results show a variation between the sixth and eighth power.

Dunegan obtained an expression for Penny-Sharp cracks but here it is not possible to directly determine (K) from the acoustic emission without also knowing the flaw size. Thus from theory it would appear that acoustic emission measurements would allow the determination of the flaw condition.

Measurements on single-edge-notch (SEN) fracture toughness specimens have shown the exponent (n) in the expression

$$N \propto K^n$$

to be more like 4-6 for 7075-T6 aluminium and about 8 for beryllium. Work on multiple crack specimens has also shown that the emission is again controlled by (K).

Also Dunegan and Harris have devised a scheme whereby they can say whether cracks are growing at a fixed load or have grown during repeated proof loads. If, while holding a cracked specimen at a proof load, emission occurs, then the crack is propagating. If emissions occur at a load less than the proof load then crack growth must have taken place during the proof loading scheme.

Gerberich and Hartbower (22) have found some very interesting and potentially useful empirical relations between crack parameters and acoustic emission. It was found that the number and size of the acoustic emissions seemed to bear a unique relationship to the amount of slow crack growth. A semi-empirical relationship was developed from elasticity theory. The result was:

$$\Delta A \simeq (\Sigma g)^2 \, {}^{E}/_{K^2}$$

where ΔA is the incremental area swept out by the crack. Σg is the sum of the stress wave amplitudes associated with the increments of growth. (E) is the elastic modules, and (K) is the applied stress intensity factor.

Also they found that a reasonably linear relationship exists between (Σg)/cycle and crack growth increment/cycle.

Hartbower et al. (23) tested specimens of 7075-T6 aluminium alloy and HY-80 steel using single-edge-notched (SEN) tensile specimens of varying width and thickness. Measurements were made of the number and amplitudes of stress wave emission (SWE) and in addition the time intervals between signals. It had been noted in tough strength materials like 18% nickel maraging steel that plane strain instability was marked by a large increase in amplitude of stress wave emission (SWE) and the approach of fracture was accompanied by an increase in both count rate and amplitude of stress wave emission (SWE). For the 7075-T6 aluminium alloy (which was more brittle) the approach of the plane stress instability was notable for an increase in the number of large stress waves.

The result of the HY-80 steel showed few stress wave emissions (SWE) were recorded and it was assumed that the system sensitivity was too low. Unstable crack growth, accompanied by large stress wave emission (SWE) (which saturated the recording system) characterized this material after maximum load. In contrast, all crack growth in the 7075-T6 was accompanied by detectable stress wave emission (SWE).

Jones and Brown (24) conducted a study to assess the usefulness of acoustic emission for determining plane-strain fracture toughness(K_{IC}) values. They used only a ceramic phonograph cartridge and a magnetic tape recorder as an acoustic detection system. Load and emission responses were simultaneously recorded. The test results showed definite acoustic indications of pop-in which were often too small to be detected with a compliance gauge. It was found that the transient nature of the wave forms from crack growth could usually be distinguished from the background noise. The (K_{IC}) values based on initial acoustic emission were usually slightly lower than those based on compliance gauge readings due to the higher sensitivity of the acoustic emission technique. Also they concluded that the disadvantage of the acoustic technique was susceptability to extraneous noise which could be confused with actual pop-in indication.

Baker (25) tested 18% nickel maraging steel in bending, the surface strain at one stage during the test reaching a value of 50%. This suggested that the material was ductile rather than brittle. The specimens contained a number of inclusions from which cracks were found to nucleate. No stress wave emission (SWE) attributable to those cracks was detected until, after repeated bendings, large cracks of areas of 6.25×10^{-3}mm were finally formed. After Pre-cracking in fatigue and testing there were a few stress wave emissions (SWE). Cracked specimens were also tested for failure, the stress wave emission (SWE) being less than that from D6ac steel, but readily measurable.

Baker also investigated the effects of test temperatures from $-100^{o}F$ to $+250^{o}F$, and strain rates from 0.01 to 0.001 per minute. Emission response decreased below room temperatures for the D6ac specimens, but was relatively unaffected by temperature for the maraging steel specimens.

Total emission counts appeared to be primarily dependent on total strain. Emission rate variations were proportional to strain rate. Surface finish effects were significant compared with the variations in emission amplitude and emission rate.

Pollock and Randon (26) studied the acoustic emission generated during fracture toughness of mild steel specimens. These investigations were carried out over a wide range of temperatures.

They concluded that acoustic emissions at low amplitude levels were detected between the brittle jumps in all tests. At $-135^{\circ}C$ the emission rate showed no dependence on stress intensity. At $-60^{\circ}C$ the emission rate showed some dependence on the stress intensity and the emissions are ascribed to ductile tearing which took place between the brittle jumps. More emissions were observed at $-60^{\circ}C$ than at $-135^{\circ}C$.

Randon and Pollock (27) investigated the acoustic emission in mild steels and Al-alloys during fracture toughness. They employed sensitive instrumentation capable of counting and analysing emissions covering frequencies from 25 up to 250KHz. Tests were carried out on mild steel specimens at low temperature ($-135^{\circ}C$) and on Al-alloy at $21^{\circ}C$. They correlated the emission amplitudes with the energy released.

They concluded that emissions observed in Al-alloy bear a one-to-one relationship with macroscopic crack movements, and the amplitudes of the emissions correlated with the energy released during crack movements. In large crack movements a higher fraction of the energy released appears as acoustic emission.

The elastic energy released in a crack movement (in steel) is proportional to the distance travelled by the crack.

Dunegan (28) studied the possibilities of using the acoustic emission techniques to estimate the stress intensity factor of a growing crack.

He concluded that the combination of acoustic emission and linear fracture mechanics can provide quantitative information regarding structural failure. For certain situations, acoustic emission techniques can be used to accurately estimate the stress intensity factor (K) at a growing crack and therefore provide predictive information regarding structural failure.

Ying and Grigor (29) investigated the acoustic emission phenomena from heavy section steel plates. Acoustic emission experiments have been conducted during tensile tests of heavy section flawed specimens. Emissions from both longitudinal and transverse base metal test specimens were studied in 152.4mm-thick plate (A533 Grade B steel). The flaw of each specimen was created by a local fatigue of a mechanical notch. The characteristics of acoustic emission from the specimens were confirmed in $\frac{1}{6}$ scale models (25.4mm-thick flawed specimens). These tests were carried out at various temperatures in the transition runs.

They concluded that the rate of change of emission with respect to strain prior to elastic limit depends on the test temperature. The rate of emission in logarithmatic scale from the base metal increased with the test temperature. The acoustic emission recorded from the 152.4mm-thick specimens was greater than that from a $\frac{1}{6}$ scale model.

Mirabile (30) studied the relation between the energy released and the frequency spectra of the signals and how it could be related to the number of acoustic emission counts. That is; Mirabile tried to identify the nature of the event taking place.

He concluded that from his theoretical research the energy produced by the acoustic emission may be regarded as the energy released by one or several moving disclocations in the vicinity of the point of observation. Also the length of propagation of a crack equal to several grain diameter is accompanied by an emission having an energy level of the order of 105 erg cm^{-2}.

The experimental results showed that the total number of pulses is not an effective means of distinguishing between two emission mechanisms: between plastic deformation and propagation of a crack and between brittle fracture and a ductile fracture.

Mirabile found that the total energy and the power spectra are far more sensitive and better able to distinguish between these mechanisms. Also he concluded that the possibility of distinguishing between brittle fracture and ductile fracture by combining energy measurements with measurements of the power density spectra was feasible.

Bassim, Hay and Lanteigne (31) studied the acoustic emission characteristics from the deformation of flawed and unflawed specimens. Mild steel AISI 1015 used for this study, which undergoes considerable deformation before fracture and which is a good acoustic emitter. They used a wide band transducer which was attached near the middle of the specimen. The transducer had a flat response over the range of 0.1 to 0.5MHz. The signal was then directed to a pre-amplifier and post-amplifier equipped with band pass filter of 0.1 to 2MHz for a total gain of 92dB. Emissions were continuously recorded on a modified Sony video tape recorder.

They concluded that the total acoustic emissions from flawed specimen are less than those from the unflawed specimen. Also the average maximum of the signal at a given strain is somewhat larger from the flawed specimen than from the unflawed specimen.

The frequency distribution from the flawed and unflawed specimens lies within two distinctive regions. The acoustic signals from the unflawed specimen generally have higher frequency than those from the flawed specimen. The shift in frequency from the flawed to the unflawed specimen is about 0.06MHz.

1.3. The Origin of Acoustic Emission

Acoustic Emission Analysis (35) helps in understanding, measuring and analyzing of a high frequency elastic wave phenomenon, which sometimes occurs in a solid (or liquid) medium with local, sometimes extremely small, instabilities.

1.3.a. Local instabilities

A system strives forever toward a state of lower energy, but because within a system there is seldom total homogeneity, an overall change will be proceded by local (micro-) instabilities.

The instabilities manifest themselves in many cases as (micro-) deformations and, in this way, are the direct cause for the occurence of acoustic emission.

The formation of micro-cavities, slip lines, martensitic phase transformations, moving Luder lines, grain re-orientation, local bubble formation before a liquid boils, minimal rock-crystal movements preceding an earth-quake, etc., indicate many local instabilities. Whatever deformation process is present, whatever material is being tested, or whatever construction is being controlled, acoustic emission is the most sensitive indicater of local instability known to this day.

Because local instabilities can grow into catastrophies, their early detection is worth a great effort.

1.3.b. Deformation phases

Deformation of solid material can be represented in four phases: elastic, micro-elastic, plastic and finally the crack. With this simple representation one must remember that during 'the deformation' other deformation phases are actually simultaneously occurring.

Deformation in the elastic area means that the deformation macroscopically is entirely reversible; as soon as the stress is taken away, the material returns to the state in which it was prior to receiving stress.

Under micro-plastic deformation is understood the non-reversible deformation with which the working of micro-mechanisms can be explained, for example, the dislocation-kinetic in crystals. Instead of micro-plastic deformation, the form macro-elastic transformation is also used. The behaviour of polycrystalline material during plastic deformation is still difficult to render using the concept for micro-plastic deformation which are valid for crystals.

During fracture the material parts are broadly separated; the applied stress disappears as well as the elastic deformation.

With acoustic emission analysis the problems point to the question, what deforms and how does it deform? From this we can see that further explanation of the deformation phases given above within the framework of acoustic emission will be necessary.

(1) Elasticity

During elastic deformation no acoustic emission occurs, at least if it is an elastic deformation only which is being considered, such as that possible with "Whiskers" (dislocation-free crystals). If one places stress on construction materials, then under the yield point, next to the elastic (reversible) transformation, micro-plastic (irreversible) transformation also occurs.

(2) Micro-plasticity

The connection between micro-plasticity and acoustic emission is being studied by a number of researchers. The dislocation-kinetic was only recently explained by James. On the basis of abroad study of literature and critical observations, he came up with a proportion between the 'change per unit time of the mobile dislocation density' and the 'acoustic emission intensity' P(number of acoustic emission pulses per unit time).

The proportion given likewise stands for a deviation given by Sedgwick of a connection between acoustic emission intensity and the change per unit time of the total dislocation density.

The acceleration and slowing of the dislocations also signify changes in energy state which are manifested in the form of elastic 'radiation' phenomenon (acoustic emission).

James' observations on the stimulated breaking loose of dislocations and the acoustic emission connected with it also can give an explanation for the acoustic emission perceived before the yield point is reached. He distinguishes between primary and secondary disclocations barriers . In very pure well-tempered crystals, he deals only with secondary dislocations barriers, meaning that the energy which is needed to detach a dislocation from this barrier is equal for all barriers. A uniform increase in the acoustic emission intensity to a maximim in the neighbourhood of the yield point is a manifestation of the uniform progression of the detaching of the dislocations.

Detachment of primary barriers costs significantly more in energy, which in addition can also significantly cost more in energy, which in addition can also significantly differ between different types of primary barriers. In polluted crystals, for example radiated crystals, primary barriers are also present. Limited erratic acoustic emission-count rate below the yield point means that now and then dislocations break loose from secondary anchorages. Upon reaching the yield point a small excitation, for example, originating from a dislocation movement of a secondary barrier, is enough to bring about a snowball effect. A sudden high of acoustic emission-count rate is a measurable manifestation of this occurrence.

The observations coming from Battelle-Frankfurt as well as those of James deal in essence with the velocity changes of dislocations. It is therefore not unreasonable to think that these two trends of thought could eventually lead to similar results and with this a significant step will be made in the science of fundamental deformation mechanisms.

Fast velocity transformations can also be taken as micro-plastic deformations. Martensitic (folding over) processes, for example, cause a lot of acoustic emission, especially when the filling in of the original lattice is bed, and because of this, during transformation considerable stresses are built up which lead to micro-plastic deformation.

As the degree of phase-transformation requires more time it will be more difficult to show the transformation with acoustic emission analysis. There is reason to suppose that, for example, during the cooling of steel, the martensitic formation, as well as the plastic deformation, which is the result of high internal tensions that have occurred during the transformation, cause different acoustic emission-signal images and hence can be distinguished as such.

As far as is known, little research has been done with respect to the twin-formation and acoustic emission. That twin-formation is one of the clearest and earliest known causes of acoustic emission has been known for a long time.

Dunegan,among others, has performed measurements with Beryllium.

Other micro-plastic phenomenon such as shrinkage are left undiscussed here. The results of shrinkage, for example local weakening of the material, can certainly be indicated with acoustic emission.

(3) Plasticity

As mentioned above, deformation after the crossing of the yield point is called plastic deformation, although, of course, even then elastic and micro-plastic deformation occurs.

With many experiments with materials whereby the stress is shown graphically against the deformation, the determination of the yield point is an arbitrary matter. Many curves display a flowing transition from the elastic to the plastic part. The acoustic emission analysis appears by far to be a suitable means for defining a sharp yield point; a point where detachment of dislocation-avalanches are the cause of significant acoustic emission-count rate. This high emission peak is observed with the deformation of a large number of materials. As the (plastic) deformation proceeds, the acoustic emission-count rate decreases sharply, which corresponds to the theories concerning the change of the mobile dislocation density. This same phenomenon can also readily be perceived with steel.

The occurrence of Luder line indicates a relatively high acoustic emission-count rate, the following of the line causes an acoustic emission which is a few degrees in size smaller.

1.3.c. Cracking

Cracking is the most extreme form of deformation. That 'the cracking' often causes a noise (acoustic emission) is already known. An important aim of acoustic emission research is the prevention of cracking. The prevention requires study of the material under extreme stress. Cracking occurs and there is always a discontinuity in the material. The fracture mechanics is in particular concerned with the research of these extreme states in the material. Fracture mechanics experiments lend themselves particularly to the use of acoustic emission analysis.

About the occurrence of acoustic emission with cracking, little more can be said than that a portion of the built-up elastic energy is released upon cracking in the form of elastic vibrations (= acoustic emission).

1.4. Factors Affecting Acoustic Emission Response

There are many factors that can influence the acoustic emission response from material such as thickness, the basic crystalline structure of the material, the history of the material and also the sensitivity of the instrumentation used to detect the acoustic emission response.

The micro-structure of the material plays a major role in its acoustic emission response, with signal amplitude level. Also the condition of the material, whether it is in the case or wrough condition, and many other factors, such as heat treatment etc.

Ono, Huang and Hatano (36) investigated the acoustic emission signals recorded during tensile tests and fracture toughness testing of three structural steels. These include (1) C-Mn steels with three levels of (S) (0.006%, 0.03% and 0.027%); (2) an AISI 4130 steel with five different heat treatments; (3) SA533B steel plates.

They found that the acoustic activity was little affected by the variation in the (S) content. The amplitude of acoustic emission signal was found to be dependent on the (S) content. They found from the amplitude distribution of the acoustic emission signal that the acoustic emission activities continued through 5% (for a low S content specimen) to 10% (for a high S specimen) plastic strain. The level of the signal amplitude was found to be strongly dependent on the (S) content. The level was found to be five times the background in the high (S) specimen. Also it was found that in low (S) specimen numerous burst-type signals were found in addition to the continuous acoustic emission signals. These burst signals decay to the level of continuous signals within 100 to 200µ sec. When (S) content is increased to 0.027% the number of burst-type signals was about twice that observed in the low (S) specimen and the decay time was increased to 200 to 400 µ sec.

They carried out a tensile test on specimens of 4130 steel. These specimens were furnace cooled or quenched and tempered at 650°C (resulting in spheroidized pearlite plus ferrite or in spheroidized carbides plus ferrite micro-structure).

Specimens given spheroidization anneal showed that low levels of acoustic emission activities persisted in the early part of work hardening. Normalized (bainitic) specimens exhibited strong acoustic emission activities, which started at one half of the macroscopic yield stress and reached the maximum at the yielding. Specimens quenched and tempered at 430°C also showed strong acoustic emission activities at the yielding.

The microstructure of SA533B steel specimens consisted of tempered bainite and tempered martensite. Numerous large inclusions were visible with a low power microscope. They concluded that continuous or quasi-continuous emissions originate from the tempered bainitic or matensitic matrix, whereas burst-type emissions arise from inclusions.

Pollock and Randon (26) studied the acoustic emission phenomena generated during the fracture toughness test of mild steel specimens over a range of temperatures. At higher temperatures (-70°C and above) and the increasing amounts of plastic deformation, the emission rate was dependent on the stress intensity factor K. However, at low temperature (below -130°C) this dependence was not found. They found that the total number of emissions decreased considerably with lower test temperatures.

Thickness effects also influence the amplitude of the burst-type emissions, where higher amplitude acoustic emission signals are obtained from thicker specimens. Ying and Grigory (29) investigated the acoustic emission activity from flawed heavy section steel plates. They tested a 152.4mm, and a 25.4mm thick flawed tensile specimen. These tests were carried out at various temperatures in the transition temperature range.

They concluded that the rate of change of emission with respect to strain prior to elastic limit depends on the test temperature. The rate of emission in logarithmic scale from the base metal increased with test temperature. Also the emission counts obtained from a 152.4mm thick specimen were greater than that from a 25.4mm thick model.

The possible causes, extent and nature of the influence of thickness on amplitude were believed to be (37):

(a) The crack front in the thicker specimens is exposed to more material and hence is exposed to much higher non-metallic inclusions.

(b) The triaxial stress in the vicinity of a crack is higher for thicker specimens, hence cleavage type fracture is possible. This reason is believed to be a more logical explanation for higher amplitude in thicker specimens.

Amongst the major factors that markedly affect acoustic emission are:-

(1) Homogeneity; where the presence of discontinuities, inclusions, second phase etc. result in an entirely different response compared with that of matrix alone.

(2) Material history; the mechanical working, stress relief, heat treatment and other processes play an important role in the variation of the acoustic response. the large grain sizes, the low dislocation density, and the random orientation of the crystalline structure (in the as-cast material), promote large amplitude acoustic emission signals when the material conditions are changed, i.e. heat treatments, cold-worked, cross-rolled, where the crystalline structure is refined, the acoustic emission characteristics differ very much.

(3) Field strength; material with higher strength showing a marked increase in signal amplitude. This is shown

by Green (38) when he tested specimens from 6AI-4V-Ti of standard and extra low interstitial (ELI) grade and from different heat treatment conditions of D6aC steel (both materials were of 2.54mm thickness). These specimens were tested at a constant stress rate and instrumentation gain. Parry (39) reported that significant increase in the acoustic emission amplitude occurred when a pressure vessel material was irradiated. Ireland et al. (40) investigated this effect from an A533 pressure vessel steel tested at cryogenic and ambient temperatures in the irradiated and unirradiated conditions and also confirmed that the amplitude of the acoustic emission signals increased at the lower temperatures over that at room temperature, while the irradiated material was noiser at all temperatures than the unirradiated material. Both irradiation and cryogenic temperatures will increase the yield strength of mild steel. Nevertheless, it is plausible that it is not the increase in yield strength, but some other effect such as a change from ductile to cleavage fracture that is causing the increase in the amplitude of the signals at cryogenic temperatures.

(4) The sensitivity of the instrumentation that is required to detect acoustic emission response is also an important factor.

1.5. Fields of Applications of Acoustic Emission

In recent years Acoustic Emission has found many fields of applications in industry and is no longer a laboratory research tool. Many researchers forecast that this recent development is an area which is going to receive much attention in future (32). Amongst the fields of industrial applications are:

(1) The area of non-destructive testing: NDT applications include:

(a) Historically, the acoustic emission was first used for monitoring pressure vessels and is still one of the most attractive practical applications. This type of application requires that the source of emission be located and that the ratic of emission signal to the backgroundnoise be as high as possible.

(b) Acoustic emission has been widely used in the past in studies of rock mechanics. This is an area of application that has great potential for practical application. Work in this area includes the utilization of acoustic emission to study the degree of the stability of the underground gas reservoirs, the pressure at which the reservoir exhibits initial instability, the location of the point at which initial reservoir instability occurs and the direction and rate of propagation of any resulting fractures in the rock.

(c) Weld monitoring during the in-process, where the weld was found to crack before its final completion - due to the contamination with Tantalum or Titanium. Also there was slag cracking in the submerged arc welds.

(d) Weld monitoring to detect cold post-weld cracking. A correlation between crack appearance in weld and acoustic emission activity was found (33).

(e) The utilization of acoustic emission for non-destructive evaluation of wire rope is another area that has recently been investigated (32). Faulty cables were found to be easily distinguished by acoustic emission, where faulty cables showed more acoustic emission at a given load compared with virgin cables.

(f) A final example of the application of acoustic emission to industrial problems is its use to provide process-control information for metal forming operations (34). This is another area of great potential that will probably grow rapidly in the near future.

This application, in particular, is the interest of this present study. In this application, acoustic emission - defined as elastic waves produced in metal as it undergoes plastic deformation and fracture - was found to give a much greater degree of resolution in surveillance of metal deformation and cracking than any other available technique. Also compared with the old members of the family of the non-destructive testing techniques, acoustic emission was unique in several respects (32). The elastic waves propagate through the material and can be detected at its surface by high sensitivity sensors. Therein lies the basis for utilizing acoustic emission as a technique to remotely detect the formation or growth of cracks in the material.

(2) Acoustic emission lends itself to continuous, remote surveillance of the structure, and does not require scanning with a detecter as does conventional ultrasonic or eddy current techniques.

(3) Acoustic emission technique is not applicable to detection of static flows or discontinuities, there must be some plastic deformation or crack growth occurring to generate the elastic waves.

(4) Potential resolution attainable with acoustic emission far exceeds that of the conventional techniques (ultrasonic, eddy current and radiography).
The capability is inherent to detect fracture of a single grain. It is questionable that a single dislocation movement involves sufficient energy to produce a detectable signal, but some level of dislocations, pile-up and breakaways, does fall within the detection threshold. This level of resolution qualifies acoustic emission as a tool which is very useful to basic fracture mechanics and material study.

(5) The emission source or crack can be located, using remote sensors, by determining the difference in time of signal arrival at three or more sensors.

However, attempts to relate acoustic emission counts to fracture mechanics terms have met limited success, partly because the mechanical process which causes acoustic emission is complicated and partly because of limitations in instrumentation and experimental procedure. Also great difficulties are still encountered in separating the acoustic emission of interest from extraneous background noise .

It can be concluded from the above that the utilization of acoustic emission in the assessment of structural integrity has begun but is still in its infancy. It is foreseen that the future in this area is limited. Therefore, much additional work remains to be done in characterising acoustic emission events and relating them to the structural changes of the material.

Studies of the sourses of acoustic emission can lead to extend the applications of the acoustic emission techniques in the areas of disclocations dynamics and the deformation of materials. The rapid advance in the field of electronics allows for the modification of the instrumentation and more advanced equipment is readily available, and can help to separate acoustic emission signal from background noise to facilitate the application of acoustic emission techniques to study the deformation properties of the material, such as stress, strain, and to relate them to the acoustic emission properties such as the number of counts. Furthermore, it helps to relate the number of counts to other acoustic emissions parameters such as frequency amplitude etc. It is intended in this study to draw out the above relationships. This requires acoustic emission responses from widely differing materials with varied mechanical history, heat treatment, and states of stress and strain.

CHAPTER 2

Some Fundamental Aspects of the Theory of Acoustic Emission

2.1 Introduction

Acoustic emission is defined as the elastic stress waves generated in the material due to the energy released by mechanisms that govern its deformation and fracture behaviour.

The fundamental mechanism or mechanisms giving rise to acoustic emission pulses have not yet been positively identified, but various investigators (41) have suggested that the generation of these emissions is related to the dynamic behaviour of dislocations during some fundamental deformation processes i.e. pile-ups, breakaway of dislocation, sudden initial and discontinuous movements of dislocation. Also attempts were made in early work to relate acoustic emission with strain, strain rate, and other parameters related to the strain with the microstructure.

It is the intention here to review these correlations, outline the formulated relationships, then present a detailed illustration of the relationships best suited to the purpose of this study.

Dislocations react to acoustic emission in different ways. A brief account of examples of these reactions can be given as follows:

(1) <u>Acoustic Emission from a Moving Dislocation</u>

A moving dislocation radiates energy due to:

(a) Changes in the dislocation core.

(b) And more importantly due to the sinusoidal Peierls force.

The stress to offset this loss of energy by radiation is of the order of (41,42):

$\sigma = (\pi^3/4) \times (v/c)^2 \mu$

where, μ = shear modules

v = dislocation velocity

c = shear wave velocity

(2) <u>Acoustic Emission from Dislocation Breakaway</u>

A pinned dislocation breaks away at some critical stress and the concurrent relaxation of strain energy is accompanied by the emission of sound waves. The force applied to cause the breakaway is:

$F = 2T\cos \phi_c/2$

$F = \mu b^2 \cos \phi_c/2$

where, $T \approx \mu b^2/2$ = line tension

ϕ_c = included angle between the adjacent arms of dislocation

ϕ_c depends on the strength of the obstacle where:

$\phi_c = 170^\circ$ for weak pinning and

$\phi_c \lesssim 90^\circ$ for strong pinning

If the pinning point is strong the dislocation cannot breakaway, instead dislocations multiply by Frank-Read source. The force associated with the Frank-Read source is:

$F = \mu b^2/2R$

where, $2R$ = distance between major pinning points.

For (n) dislocations are activated simultaneously the force associated with the burst of dislocations is

$F = n\mu b^2/2R$

(3) Acoustic Emission from the Grain Boundary

The stress associated by the operation of dislocations from the grain boundary is:

$\sigma = \alpha\mu bm(8/\pi)^{\frac{1}{2}}$

where, m = ledge density in the grain boundary

α = constant

(4) Acoustic Emission from Breakaway of Dislocation Pile-Ups

The breakaway of a pile-up of dislocations also produces acoustic emission. There is a stress concentration at the tip of the pile-up, hence the force associated with this pile-up is:

$F = nb\sigma$

where, n = No. of dislocations in the pile-up.

This force is large in the region of the general yield, which gives the largest acoustic emission amplitudes compared with the amplitudes of acoustic emission from the dislocation motions and breakaways.

The above processes were firmly established when the importance of the dislocation processes in the generation of acoustic emission in the crystalline metals were readily confirmed in the following works, and many investigators were tempted to describe this generation process physically and attempted to derive mathematical relationships. A general theory was derived from the simple uniaxial tension during the uniform deformation, where dislocation motions on the average are relatively homogeneous throughout the specimen and tend to produce uniform plastic strain.

Most of the power generated by these motions is ultimately dissipated as heat in the crystal lattice; the details of this heat dissipation processes as they relate to acoustic emission, investigated earlier, are presented below:

(1) When a material is strained slowly under uniaxial stress during elastic region $\sigma = E\varepsilon$ and work done

$= (1/2)\sigma\varepsilon = \frac{1}{2}\sigma \times \frac{\sigma}{E} = \frac{\sigma^2}{2E}$

This work is increased at $d\varepsilon$ beyond the yield to $\sigma\, d\varepsilon$, where the increment of flow stress is $Hd\varepsilon$ where, H = local tangent modulus $H \ll E$. Therefore the elastically recoverable strain energy increased from $\sigma^2/2E$ to $(\sigma + Hd\varepsilon)^2/2E$ i.e. by the amount $(H\sigma\, d\,\varepsilon/E)$, which is much less than the external work and the excess of work over the increase of strain energy is $(1-H/E)\sigma\, d\varepsilon$, which is transferred to the surrounding according to the first law of thermodynamics. Most of this energy is changed into heat and a small portion is stored in microstructural alterations.

(2) The analysis above was taken further to quantify the amount of energy dissipated as heat, and formulated how the

operative processes can be linked with acoustic emission.

(3) A process that directly links acoustic emission to the plastic deformation is shown as:

(a) The simultaneous motion of the dislocation extends a deformation band into a loss strained region of the crystal. Such an event, although intensely localised, tends towards a uniform specimen strain.

(b) So, for a propagation increment of the deformation band ΔL a strain increment ε was assumed as in fig. (1a).

The consequent plastic extension $\varepsilon\Delta L$ was found to be large compared with the crosshead displacement that occurs during the propagation of this increment (43). The region suddenly receiving this fairly large local strain increment relaxes the stress throughout the specimen by an amount plastic strain* elastic modulus* fractional volume of the region. This stress relaxation (shown as micro-yield drops in the stress-strain curve in fig. (1b) is propagated as a pair of longitudinal elastic stress waves from the region towards the specimen ends. These elastic waves are the signals detected as acoustic emission.

(4) These acoustic emission waves cause the vibration of dislocation line segments between points where they are strongly impeded by obstacle, and the oscillating fields of these dislocation segments will radiate energy by this interaction with the waves.

(5) Not all the energy in the microyield drops is transformed to vibrating dislocations, some is used in plastic deformation that is not associated with acoustic emission.

A mathematical theory was developed, i.e. formulated in terms of a partition function that specifies the fractional plastic strain which is homogeneous and which produces detectable emissions. This is described below:

With a tension specimen of length L, x-sectional area A and elastic modules E, deformed in a testing M/Ce of stiffness K at constant crosshead speed S, then;

$St = (\sigma A/K) + (\sigma/E + \varepsilon p)L$

where t = time

σ = axial stress

σ/E = axial elastic strain

εp = specimen elongation caused by plastic deformation.

From this equation:

$St/L = \sigma/E(1+AE/KL) + \varepsilon p$

where S/L = nominal applied strain rate or cross specific head rate

$E/(1+AE/KL)$ = effective modulus of specimen.

In this there are two plastic deformations; the homogeneous contributes to the cumulative plastic strain in the ordinary way.

The instantaneous strain due to the propagation increment of the deformation band $(\epsilon \Delta L)$. This implies for a very short time δt.and the two plastic strains are the homogeneous = (S/L) st which is negligible compared with the instantaneous = ($\varepsilon\Delta L/L$).

Therefore, no change of the length of specimen occurs due to the crosshead movement, instead the local jump in plastic deformation relaxes the elastic strain and produces a microyield drop. The magnitude of this drop is:

$\delta\sigma = E\ (\Delta L/L)\ \varepsilon/(1 + AE/KL)$

where $(1 + AE/KL)$ = factor describing the relative relaxation of elastic deformation

when $K\to\infty$, all the relaxation occurs in the specimen, however, K has a finite value and there will be a specimen elongation δL associated with the machine relaxation rather than the crosshead motion. The magnitude of this deformation is:

$\delta L/L = \varepsilon\Delta L/(1 + \frac{KL}{AE})$

Therefore, the plastic strain jumps contribute little to the macroscopic specimen strain, they merely convert elastic specimen and machine strain to plastic specimen internally. A partition function F equal to the total plastic strain that results from conversion from elastic strain and a second partition function F which is the fraction of the plastic strain rate than can be attributed to jumps are introduced.

For Δt corresponding to the period for one strain jump, the total strain increment $\Delta\varepsilon$

$\Delta\varepsilon = \Delta\sigma/E + \Delta\varepsilon^p$

$\quad = (H/E)\Delta\varepsilon + (1-H/E)\Delta\varepsilon$

and

$(S/L)\Delta t = ((HE/)\ (1+AE/KL)+(1-H/E))\Delta\varepsilon$

$\varepsilon p = ((H/E)\ (AE/KL)+1)\Delta\varepsilon$

and the strain rate

$= (1-H/E)\ (S/L)/(1+AH/KL)$

During Δt only one elastic to plastic strain conversion occurs where the strain increment was found as:

$\varepsilon(\Delta L/L) = (1+AE/KL)\ (\delta\sigma/E)$.

and the average strain rate is:

$\varepsilon = \varepsilon(\Delta L/\Delta tL) = (1+AE/KL)\ (\delta\sigma/E\Delta t)$

and

$f = \varepsilon/\varepsilon p = (1+AE/KL)\ (\delta\sigma/E\Delta t)\ /\ (1-H/E)\ (S/L)\ /\ (1+AH/KL)$

in this equation Δt was related to the acoustic emission count rate N as $N = m/\Delta t$ where m = No. of counts caused by $\delta\sigma$.

The above equations derived from the mathematical theory of acoustic emission reviewed in this Chapter provide complete formulation and relationships between the acoustic emission parameters and deformation properties of the material that can satisfy the objective of this study. It remains to investigate through experimental results.

The validity of these equations and their accuracy with respect to the practical measurable values of the acoustic emission parameter i.e. counts, frequency, amplitude. The response of these formulations to the experimental values of strain, stress, microstructures of the material are to the analysed in the hope to contribute to the information established to facilitate the application of acoustic emission techniques to study the deformation properties of the material. This is the subject of the next two chapters where experimental work carried out in this respect is outlined, then the results obtained from these experiments are presented in an orderly way for further analysis.

2.2. Type of Acoustic Emission

When a metal is stressed, a stress concentration occurs at the tip of defects contained in the metal. As stress increases, relaxation occurs in these regions and may take the form of plastic flow, micro-cracking or large scale cracking. These processes produce continuous emissions of small amplitude and discrete bursts of higher amplitude. These acoustic emission signals show the following characteristics:

(a) Continuous type of emissions are usually observed in plastic deformation, associated with micro-defects such as dislocation pile-up or breakaway, twining and granular re-orientations. This signal is of extremely low energy and consequently difficult to detect without high amplification, but the amplitude and emission rate of the signal in as low a frequency range as 100KHz can be seen to increase rather dramatically as gross yield occurs. There are no well-defined beginnings or endings of individual events as with the case of burst emission as shown in Fig. (2.a). These signals, therefore, cannot easily be used to locate the source of the yielding.

Continuous type of acoustic emission displays an irreversible nature named the 'Kaiser effect', that is a metal once stressed gives little or no emission during a subsequent deformation up to the previous level.

(b) Burst-type emission is thought to represent higher level, say macroscopic, defect growth and is most often associated with crack extension. The signals are significantly higher in energy than continuous emission, and appear as burst of sharp impulses with large amplitude, low emission rates and frequency contents as high as 1MHz. The rapid rise time and exponential decay characteristic of these signals is shown in Fig. (2.b).

The 'Kaiser effect' in burst-type acoustic emission is not so evident since micro- or macro-crack extension in a metal creates a new fracture surface which may cause the stress redistribution in the metal.

2.3. Amplitude Distribution of Acoustic Emission Signals

It is essential to analyse the emission characteristics which might be useful both in determining the criticality of the crack which emits the signals and to gaining an understanding of the emission mechanisms.

In early work where emission signals were observed and analysed, particular emphasis was placed on obtained amplitude distribution of emission signals, because it is important to monitor the growth of the cracks. The growth is a stochastic process in which the amount of each growth increment is determined by the balance between the amount of energy required to produce additional crack surface area and the amount of energy available. Both amounts have their statistical distribution along a crack tip in a heterogeneous medium and since this balance of energy is influenced by the stress level at the crack tip, some variation of emission amplitude distribution with stress level is expected.

The amplitude distribution is also related to the way a crack propagates and for this reason it can be expected to supply important data for understanding fracture mechanisms.

The amplitude distribution of acoustic emission signals were studied from fractures of mild steel (which is the interest of this study) and aluminium alloys, in different ranges of dimensions, as:-

(a) By investigating subcritical crack growth at microscopic level, prior to critical growth.

(b) Extending the investigation for critical crack growth which occurs when the critical stress intensity is reached.

The amplitude can be considered to be a measure of the released energy where the amplitude was found to be proportional to the square root of the energy incident on the sensor within the frequency band of the instrument response, thus the square of the observed amplitude is a rough measure of the energy released at the emission source.

The amplitude distribution was found to have a great significance in terms of the fracture properties of the material. The manner of the distribution indicates the nature of the fracture. The lack of small amplitudes in early investigations proved that energy cannot be released in a small amount, that is the material can store a relatively large amount of strain energy without causing a local instability.

The amplitude distribution peak was observed to shift towards larger emission amplitudes with increasing stress intensity factor and this can be interpreted qualitatively as a result of the progressively larger amount of energy available locally as the stress intensity factor increases.

From these observations it was concluded that the acoustic emission amplitude distribution is related to the distributions of the local strain energy level and the threshold level which, in turn, are determined by the material properties, thus it would be feasible to use the amplitude distribution of acoustic emission signals for determining the criticality of defects in materials.

The usefulness of the amplitude of acoustic emission as a source of information were further discussed (44) and was found undoubtedly a meaningful method of characterizing acoustic emissions, where it can be an alternative technique used when counting does not tell the required.

2.4. Frequency in the Acoustic Emission Signals

Determining the frequency content of individual acoustic emission bursts has two uses (45). The first is the possible identification of the source mechanisms (which include dislocation motion, crack propagation, phase transformations, twinning, etc.) and the insight into the physical parameters associated with their operation. The second is identifying the differences between the acoustic emission generated by any of the sources above. This is useful essentially to separate the signals from the background noise because if the frequency content of the signals and noises are both known, filtering or other electronic means can help very much in reducing the amount of unwanted noise.

As far as the first use, three distinct frequency spectra were observed (7). These correspond to the microplasticity i.e., plasticity and deformation.

Studies were carried out in this respect to relate observed emission pulses to the formation of slip lines and dislocation dynamics. It was confirmed that the burst type pulses are generated by small but rapid increments of plastic strain. The amount of plastic strain which accompanies each pulse and the time interval over which it occurs were determined as:

$\bar{E}_a = E/N$ (a)

where $\bar{E}_a$ = average strain/acoustic pulse

N = total number of pulses

That is the instantaneous strain is much greater than the applied strain rate. Thus the tiny bursts of plastic strain are essentially microscopic yield points.

This helped to discuss the slip events in terms of dislocation dynamics, where extensive studies by Transmission Electron Microscopy showed that the strain produced by each slip event is given by:

$\varepsilon = nba/LA$

where n = No. of dislocations (b)

b = Burger's vector

a = Area of slipped plane

L = length of crystal

A = Area of crystal

The value of strain given by equation (b) is much smaller than the strain indicated in equation (a); this indicated that the area must be the full cross-section of the crystal which in turn indicates that numerous slip events occur essentially simultaneously so that in effect slip does occur across the whole crystal. It was believed that the plastic strain associated with each pulse increases slowly at first because of the movement of individual dislocations, until it reaches a critical value and a large avalanche occurs. The stress needed for dislocation of opposite signs to pass each other is greatly reduced where the density of dislocations increases beyond a critical point; this is due to acoustic microyield points.

The studies also concluded that a small stress concentration is required to cause dislocations to move at high velocity of about $2X10^{3}$ cm/sec.

The second use of frequency is of more technological interest. In this respect early studies of frequency content of acoustic emission were limited to a low range because of limitations of techniques available and the result of identification of acoustic emission signals from noise depended much upon the geometry of the specimen. This tendency for the lower frequency modes of structures has advantages amongst it that acoustic emission tends to vary broad banded in frequency content, while many mechanical components content such as gears, cams, bearings etc. excite only the low-frequency components. This can allow the discrimination of one against the other by simple electronic means. There are also other types of mechanically and hydraulically produced noises which cover the same general frequency range as flaw-generated bursts. This can be troublesome, and to be able to frequency analyse these acoustic bursts in detail, it is essential to have a broad frequency range in order to find characteristic features and their spectra which can be used to distinguish them from acoustic emission.

Recently instrumentation has been developed for the broad band frequency analysis, the three most promising methods are:

(1) Digital conversion with computer analysis.

(2) Auto-correlation techniques.

(3) Recording then playing back with a tape recorder.

This recording method has the advantage of being able to record every acoustic emission event for later analysis, and therefore was used in this study.

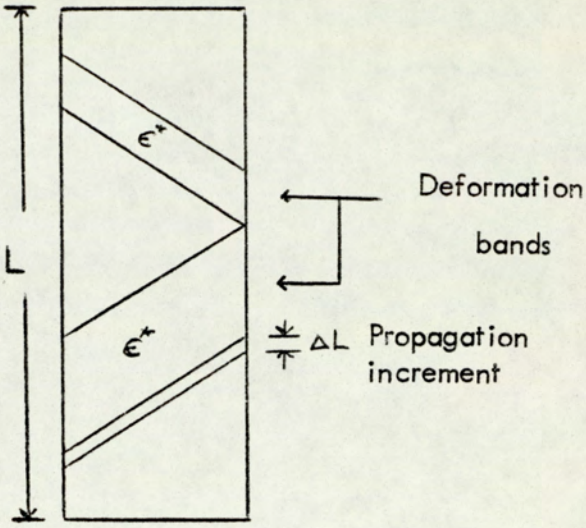

Fig. 1.a. Propagation of deformation bands in amonocrystalline specimen.

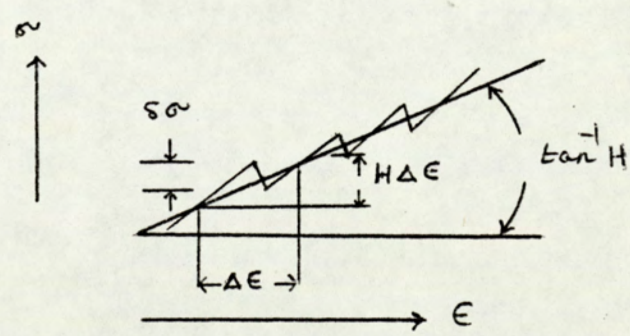

Fig. 1.b. Magnified portion of stress versus strain curve showing microyield drops.

Fig. 1. Deformation of monocrystalline.

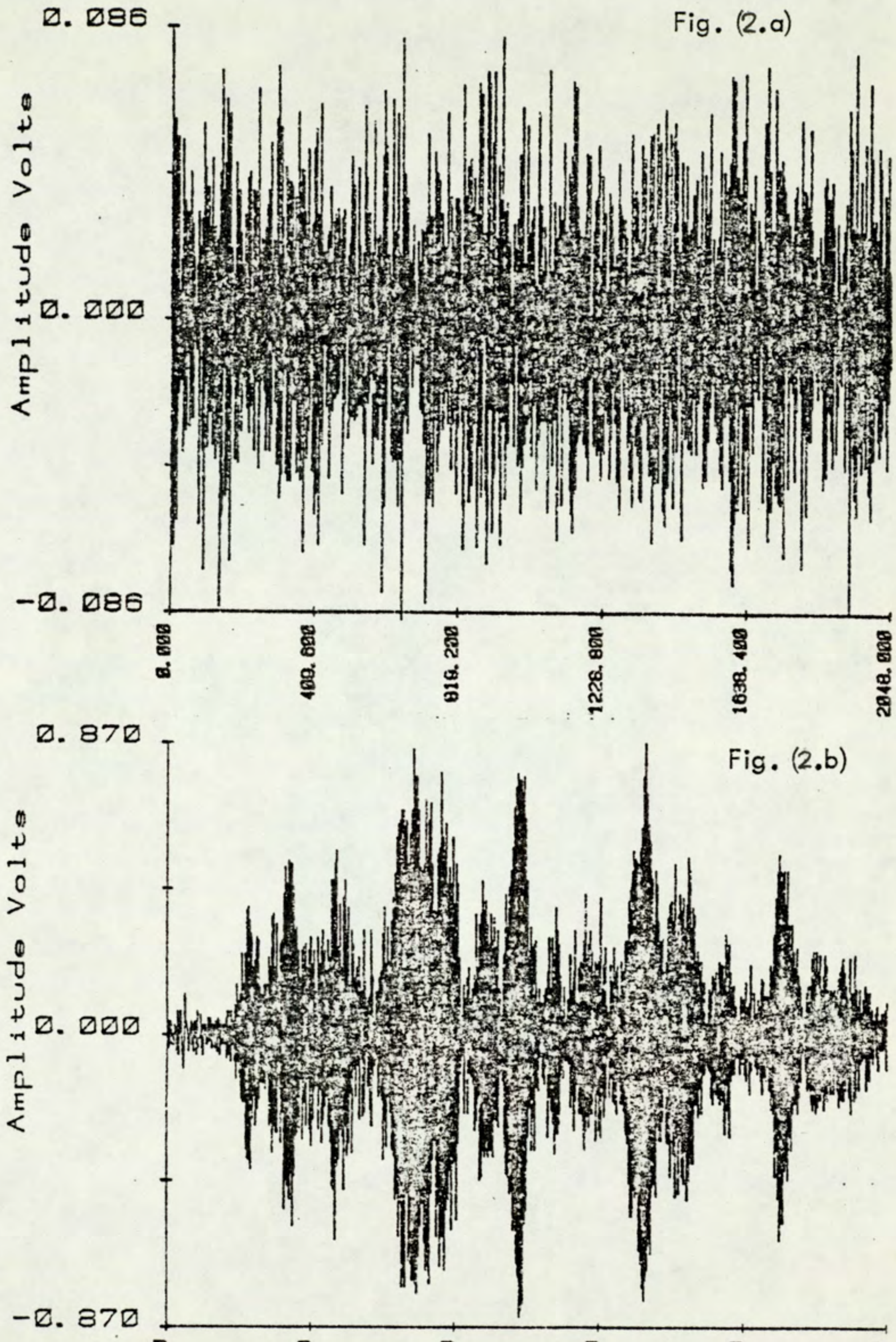

Fig. (2) Acoustic emission signals (a) continous type-emission.
(b) burst type-emission.

CHAPTER 3

Instrumentation

3.1. Introduction

Acoustic emission technique is a new method for non-destructive testing being introduced to a wide field of applications and the results show the validity of this method to give rapid and accurate results.

The necessary equipment is required to measure low level signals in the presence of noise. As methods of improving the signal-to-noise ratio are developed, the equipment can be expected to become more sophisticated.

The frequency characteristics of the stress wave emission at the present time appear to be determined largely by the instrumentation employed and the size and shape of the specimen.

Many commercial instruments (46) have been introduced to the market by many manufacturers (mostly American). Acoustic Emission Technology Corporation introduced to the market a multichannel, real-time, Acoustic Emission Analysis System. This system can accommodate 64 channels. It also has the facilities for permanent recording, a low noise pre-amplifier with a fixed gain (40 and 60dB), and various bandwidth that are selectable by use of plug-in filters.

Another instrument called "The Locator" was produced by the same company which designed for in-process weld monitoring.

Dunegan/Endevco Corporation markets a Flaw Locator Module for use with two sensors, a complete source location system for use with multisensors.

Dunegan/Endevco 3000 series equipment employs a module in conjunction with a "Data Bus" concept by which signals from various modules can be interconnected. Some of the available modules include: (a) a totalizer which provides selectable filtering and amplification, a digital counter and display unit, and a digital-to-analog. converter; (b) a log converter that provides for logarithmic scaling of emission counts and count rate. A reset clock to provide various timing functions. (c) A digital innerface which provides a binary coded digital (BCD) output for multiple channel sampling. A voltage controlled gate, a digital envelope processor.

These modules have been designed to be expanded by connection with another module as it becomes available.

Trodyne Corporation introduced many modules for acoustic emission testing. One of these instruments is designed to monitor and control resistance spot welding.

Another instrument called "Structure Integrity Monitoring System" (SIMS) includes power/audio, amplifier, signal processing and quantizing and display.

The Exxon Nuclear Company Inc. provide a commercial acoustic emission monitoring device using mobile acoustic emission equipment which they refer to as "Acoust" system. The "Acoust" systems are installed in specially built, self-contained mobile test units, some of which are transportable by air. The "Acoust" system includes provisions for acoustic energy release analysis and computerized emission sources location.

Panametrics, Inc. make a system called "Acoustic Emission Simulation Test Set". This device is provided with a pulser and needle-tipped probe for introducing the acoustic pulse to the structure to verify that the acoustic emission monitoring system is functioning. Also the company introduced a low-noise pre-amplifier with a switchable gain (40 and 60dB). This pre-amplifier has a bandwidth of (80-100KHz) which can be adjusted to suit the particular requirements.

3.2. Acoustic Emission Monitoring System

A basic single channel system for detection of acoustic emission consisted of: transducer, pre-amplifier, counter, tape recorder, filter, X-Y plotters and on-line mini-computer to analyse the signal.

(a) Sensor (Transducer)

The most vital part of the monitoring system is the sensor, Most investigators applying acoustic emission techniques to metals have been and are still using a piezoelectric crystal placed in direct contact with the specimen or structure. Early investigators used piezoelectric materials such as Ammonium Dihydrogen Phosphate (ADP), Rochelle Salts and Quartz as their acoustic emission transducer material. Development of ferroelectric ceramics in recent years has led to superior detection ability. PZT-5 is one such material that has proved very useful for acoustic emission transducers.

Piezoelectric transducers (PZT-5) have been used. The transducers are longitudinally poled and disc-shaped PZT (Lead-Zirconate-Titanate) model S140B (Dunegan/Endevco).

The fundamental resonance falls in the range 100 to 300KHz. The frequency response of the transducer used is shown in Fig. (3). The transducer can be bonded to the test specimen by mechanical stresses, and a thin layer of silicon grease is interposed between the transducer and the

UNIVERSITY LIBRARY

specimen for acoustic coupling and electrical insulation.

(b) Pre-amplifier

The pre-amplifier is probably the second most important component in the monitor system because this is where the system noise level is established.

A fixed gain (60dB) pre-amplifier has been used of model 802PA (Dunegan/Endevco). The pre-amplifier was provided with a filtering circuit to eliminate the unwanted signals before they get into the signal conditioning.

The pre-amplifier operated either single-ended or differential configuration by differing selector.

Power can be conveniently supplied to the pre-amplifier over the cable that routes the output signals to the totalizer.

The noise level is 3μvolts (RMS), the output voltage 10Vp-p and the bandpass filter is 100KHz-300KHz.

(c) The Totalizer

The model 310 totalizer (Dunegan/Endevco), was used which accepts acoustic emission signals from the pre-amplifier (model 802PA). This signal may then be additionally amplified by as much as 40dB, and continuously adjustable. Total system gain of 100db can be attained. Signals exceeding 1 volt peak are then counted by digital IC counters, having an adjustable full scale from 1000 to 1000,000 counts. The totalizer frequency response is from 20KHz to 1.25MHz. The summation of acoustic emission counts is obtained from the 310 totalizer. The totalizer has two outputs:

(1) For oscilliscope or tape recorder monitoring of AC acoustic emission signal 10Vp-p, 20KHz-1.25MHz bandwidth at -3dB points.

(2) DC output from digital-to-analog. converter, to the plotter, proportional to the counter counts. Full scale 10.0±0.1Vd.c.

(d) Magnetic Tape Recorder

A multichannel recorder type Ampex Model FR-1300 recorder/ reproducer was used. The recorder has six tape speeds: 1.524, .762, .381, .19, .095, and .0476 met. per second (MPS). Tape speed is controlled by a drive survo system associated with the selector. The standard bandwidths for a given speed are as follows:

Speed (MPS)	Bandwidth
1.524	300cps to 300 Kc ± 3dB
.762	150cps to 150 Kc ± 3dB
.381	100cps to 75 Kc ± 3dB
.19	50cps to 38 Kc ± 3dB
.095	50cps to 19 Kc ± 3dB
.0476	50cps to 10 Kc ± 3dB

Input level 1.0Vrms nominal (0dB) to produce normal recording level, operated from 0.2 to 10 Volts rms by adjustment of input potentiometer.

The frequency response of the recorder is shown in Fig. (4) and the calibration curve for the relation between the tape recorder counter and time is shown in Fig. (5).

A second tape recorder model RACAL-STORE 4 recorder/reproducer was used. Seven recording speeds were provided from 0.023 to 1.524 metre per second (MPS), selectable by means of a rotary switch.

The standard bandwidths for a given speed are tabulated below:

Speed (MPS)	Bandwidth
1.524	20,000Hz
.762	10,000Hz
.381	5,000Hz
.19	2,500Hz
.095	1,250Hz
.0476	625Hz
.0238	313Hz

(e) Filter

This was a model 3103(R) wide-range bandpass filter manufactured by the Krohn-Hito Corporation of Massachusetts, U.S.A. It has a low cut-off frequency range adjustable continuously from 10Hz to 1MHz and a high cut-off range from 30Hz to 3MHz. Maximum input amplitude is 3 volts rms, decreasing to 2.5 volts at 3MHz.

Maximum output voltage is 3 volts rms, decreasing to 2.5 volts at 3MHz. The output noise is less than 150μV.

(f) <u>On-Line Minicomputer</u>

The on-line minicomputer analysis equipment consists of the following units:

1. The Hewlett-Packard 9825A calculator has a memory of 21778 bytes.

2. The Hewlett-Packard 9885M flexible disc unit has a total storage capacity of about 500,000 bytes of data or programme.

3. The Hewlett-Packard 3437A system voltmeter is a burst reading DVM interfaced with the HP9825A calculator. Maximum sampling rate is 5700Hz and the maximum number of data points is 9999.

4. The Hewlett-Packard 9872A graph plotter, the Hewlett-Packard 9878A I/O expander and the Hewlett-Packard 9866B thermal printer.

The Fast Fourier transform analysis programmes were stored on the flexible disc and the signal to be processed is input to the voltmeter.

(g) Also other equipments were used during the tests and the analysis-like oscilliscope, Y-Y-T plotter, signal generator and frequency meter.

3.3 Data Recording

The following technique was employed to obtain the analysis of the acoustic emission signal:-

a) A transducer was attached to the surface of the specimen to be tested. This transducer was fixed rigidly to the surface of the specimen by insulation tape to prevent generating noise which might be picked up by the transducer. Also a silicon vacuum grease was applied between the surface of the specimen and the transducer to eliminate (or at least reduce) the background noise.

   It is worthy to mention that the transducer was attached at the middle of the gauge length of the flat specimens. But in the case of round tensile specimens the transducer was fixed to one of the grips because the diameter of the specimen was small i.e. 10mm diameter which did not allow the transducer to rest comfortably on the curved surface of the specimens. Fig. (6) shows how the transducer was attached to the specimen.

b) The output of the transducer was connected to a pre-amplifier. The pre-amplifier,which has a fixed gain of 60dB, was connected to the counter (totalizer). This is shown in Fig. (7).

(c) The amplified acoustic emission signal comes into the counter which has a built-in amplifier of a variable gain of 40dB maximum.

d) The counter gives two outputs, i.e. it was connected to the X-Y plotter which receives the D.C. output, and also the counter was connected to an "ampex" type recorder. This recorder receives the A.C. output (the acoustic emission pulses). It is useful to mention at this stage that the D.C. output was registered as acoustic emission counts against time on the X-Y plotter, while the A.C. output was recorded on the recorder at a speed of 1500mm/sec. as acoustic emission pulses. This is shown in Fig. (8).

At the same time an oscilliscope was connected to the input and the output of the recorder in order to monitor the signals while they were recorded.

The above data recording procedure was carried out during the mechanical tests, i.e. tensile test and three-point bending test. The tensile tests were carried out on the Mand Precision Tensile Machine, with maximum load capacity of 10 Tons. The three-point bending tests were carried out on the Instron.

3.4 Data Analysis

This second stage was carried out after the mechanical test. In this stage the recorder (Ampex FR-1300) was replayed at a speed of 47mm/sec. into a second recorder (Recal) which recorded the output of the first recorder at a speed of 1500mm/sec. By this method it was possible to reduce the frequency of acoustic emission signals by about 32 times.

This is shown in Fig. (9.a).

In the third stage, the second recorder (type Recal) was replayed at a speed of 47mm/sec. - at this stage the frequency of the signals was reduced by about 1,000 times and the output was fed into the computer through a filter (this filter was set at a bandwidth between 60-500Hz to remove the unwanted signals, especially those coming from the instrumentation). The programme used in the computer was the Fast Fourier transformation shown in Appendix The results of the computer were plotted on an X-Y plotter, first as a pulse and second as a fast fourier transformation spectrum. Fig. (9.b) shows the third stage setting.

It is worth mentioning that the reason for reducing the frequency by a factor of 1000 times was that the computer was limited to about 4000Hz, while the frequency of the real acoustic emission signal is between 100-300KHz. Therefore, after obtaining the analysis from the computer the values of the frequency were multiplied by a thousand to get back to the real frequency which is between 100-300KHz. Fig. (10) shows the complete on-line mini-computer analysis equipment with the two magnetic tape recorders.

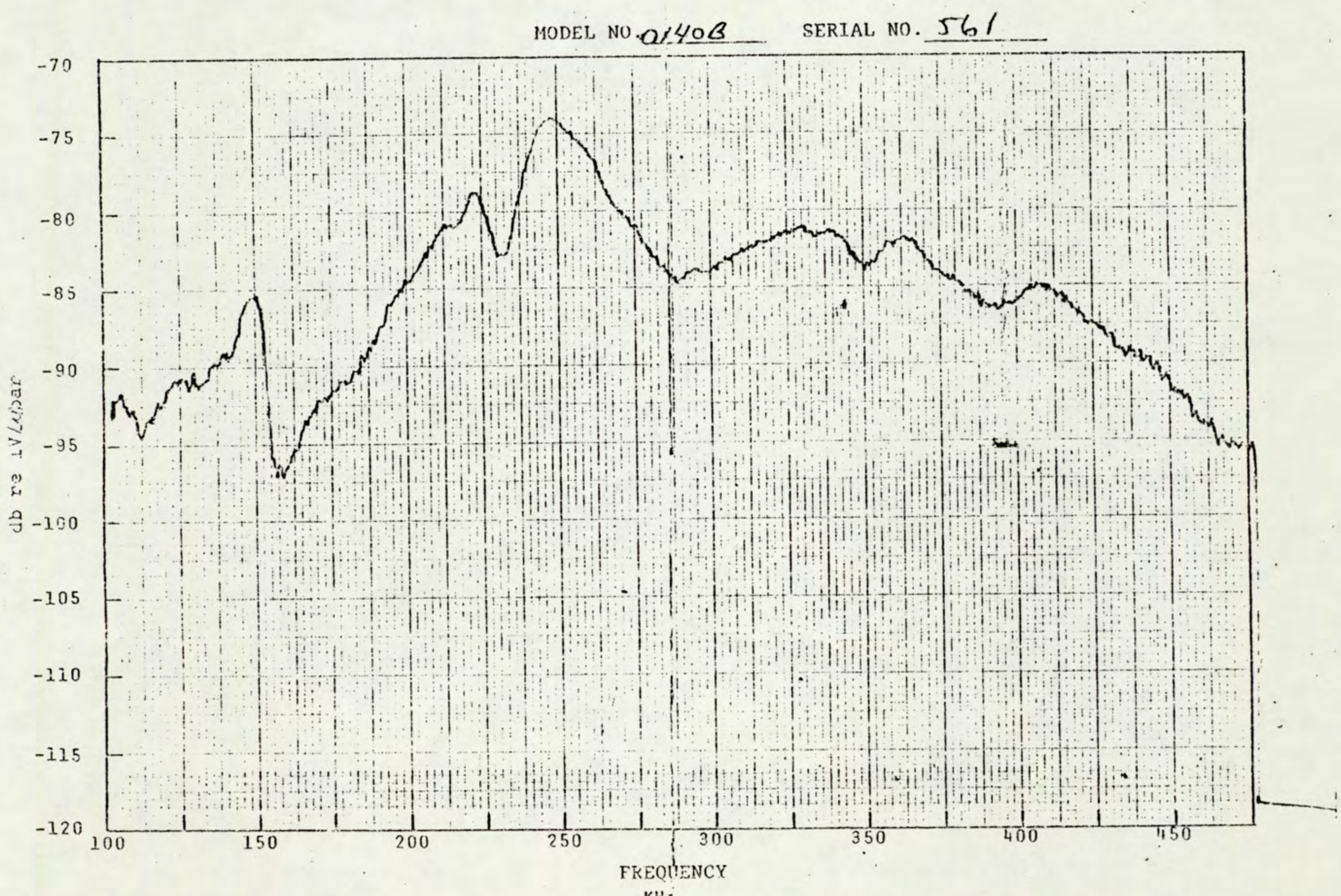

Fig. 3. Calibration curve for the transducer.

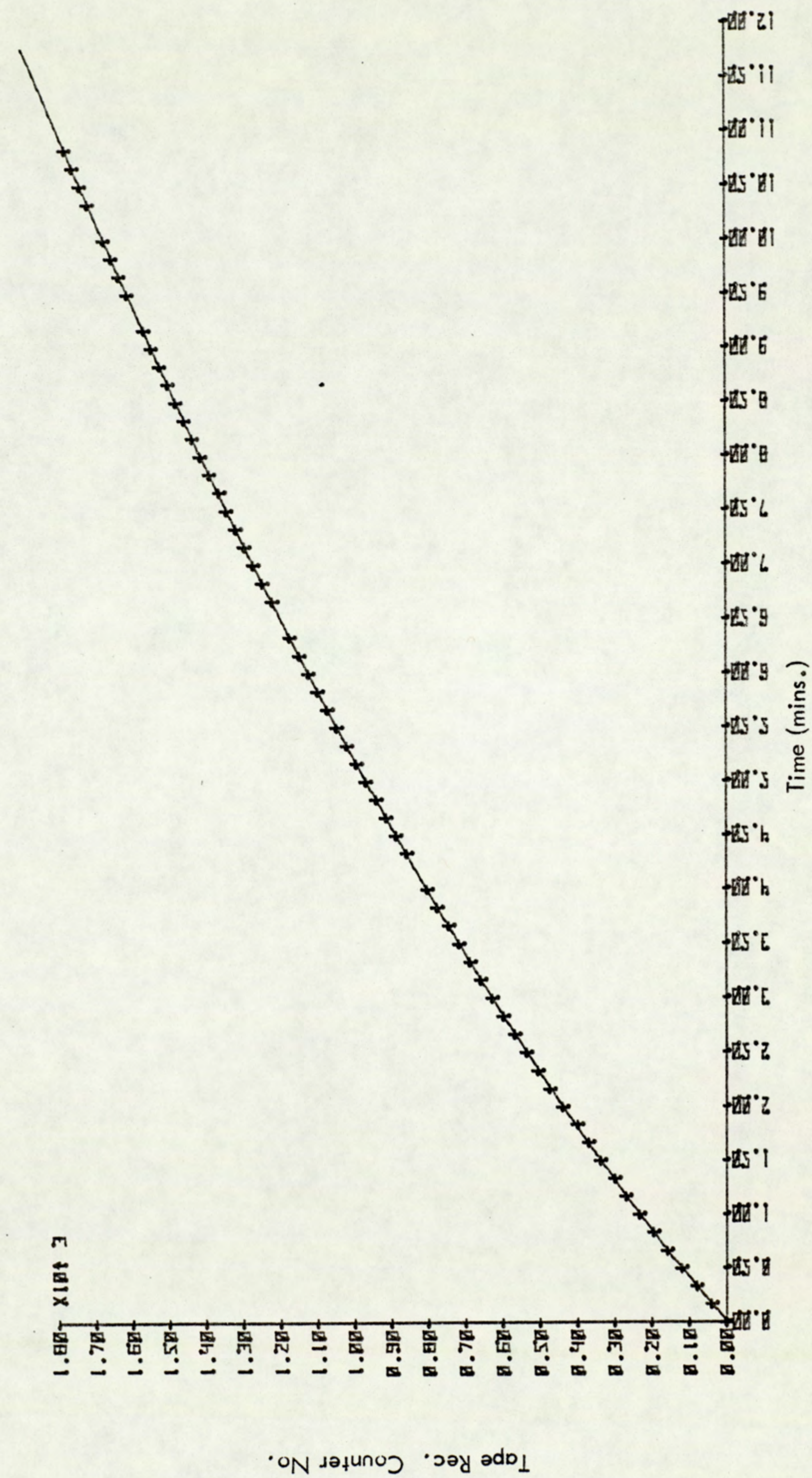

Fig. 5. Relation between tape recorder counter with time.

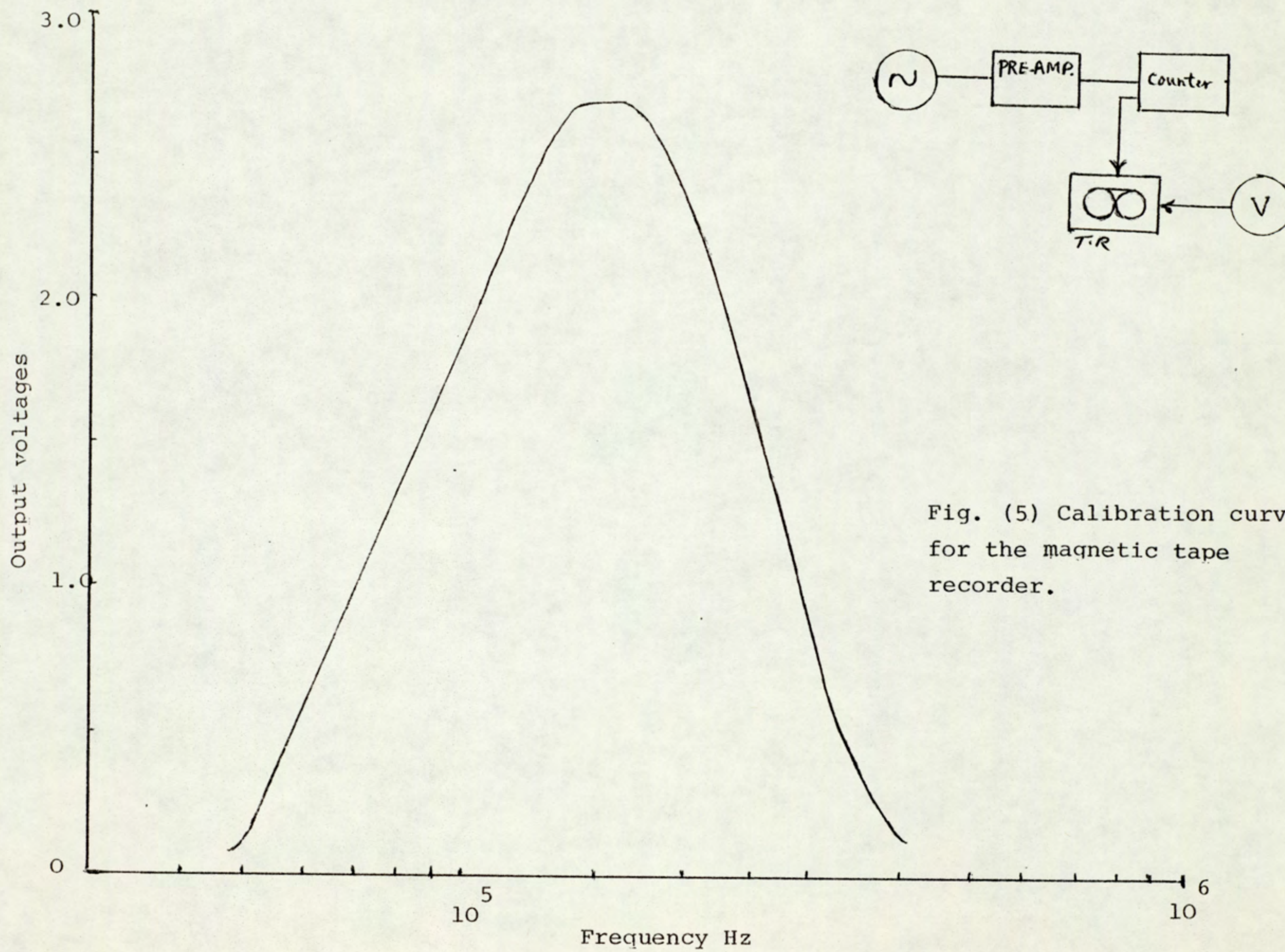

Fig. (5) Calibration curve for the magnetic tape recorder.

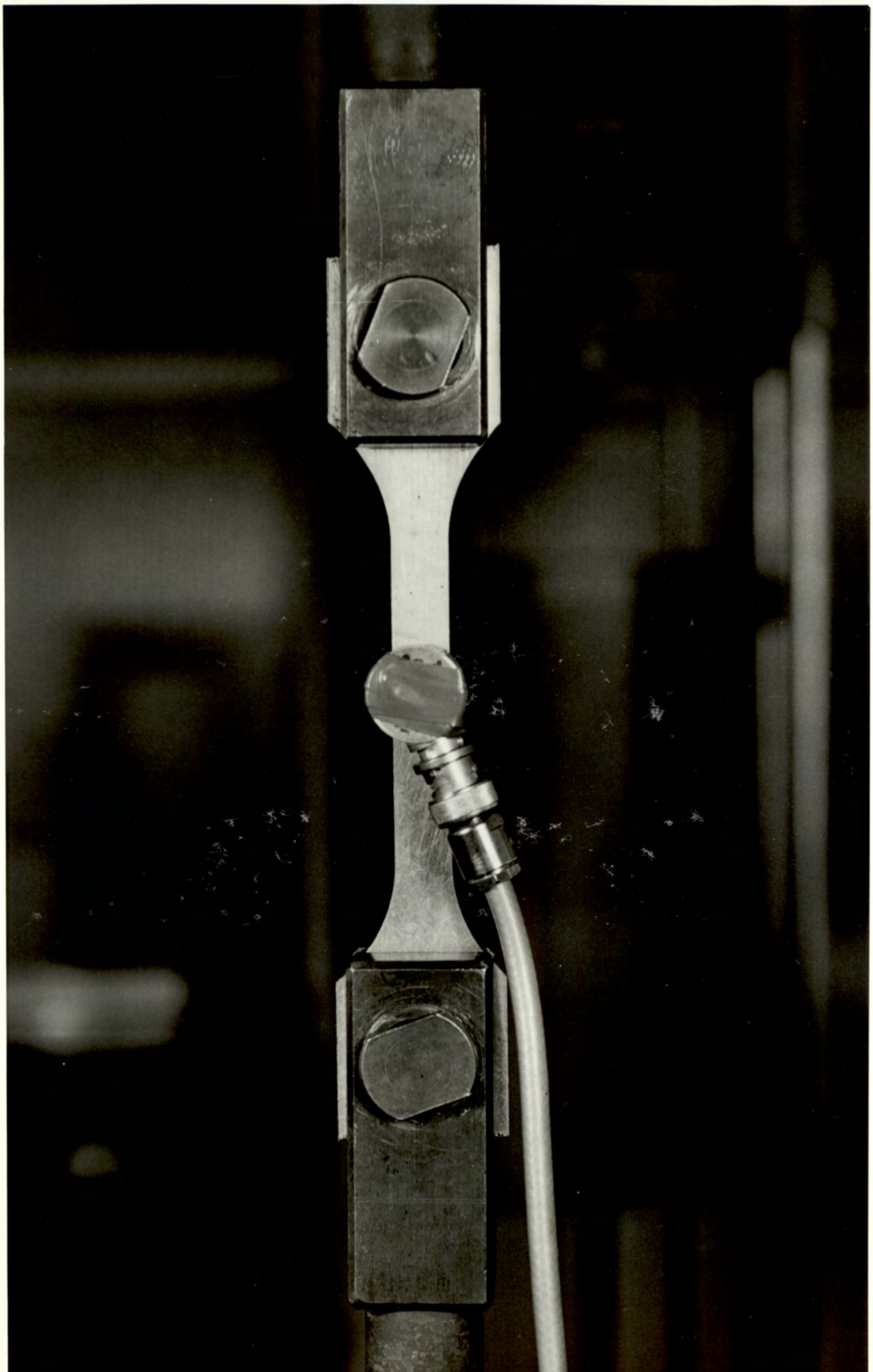

Fig. 6. Specimen ready for test.

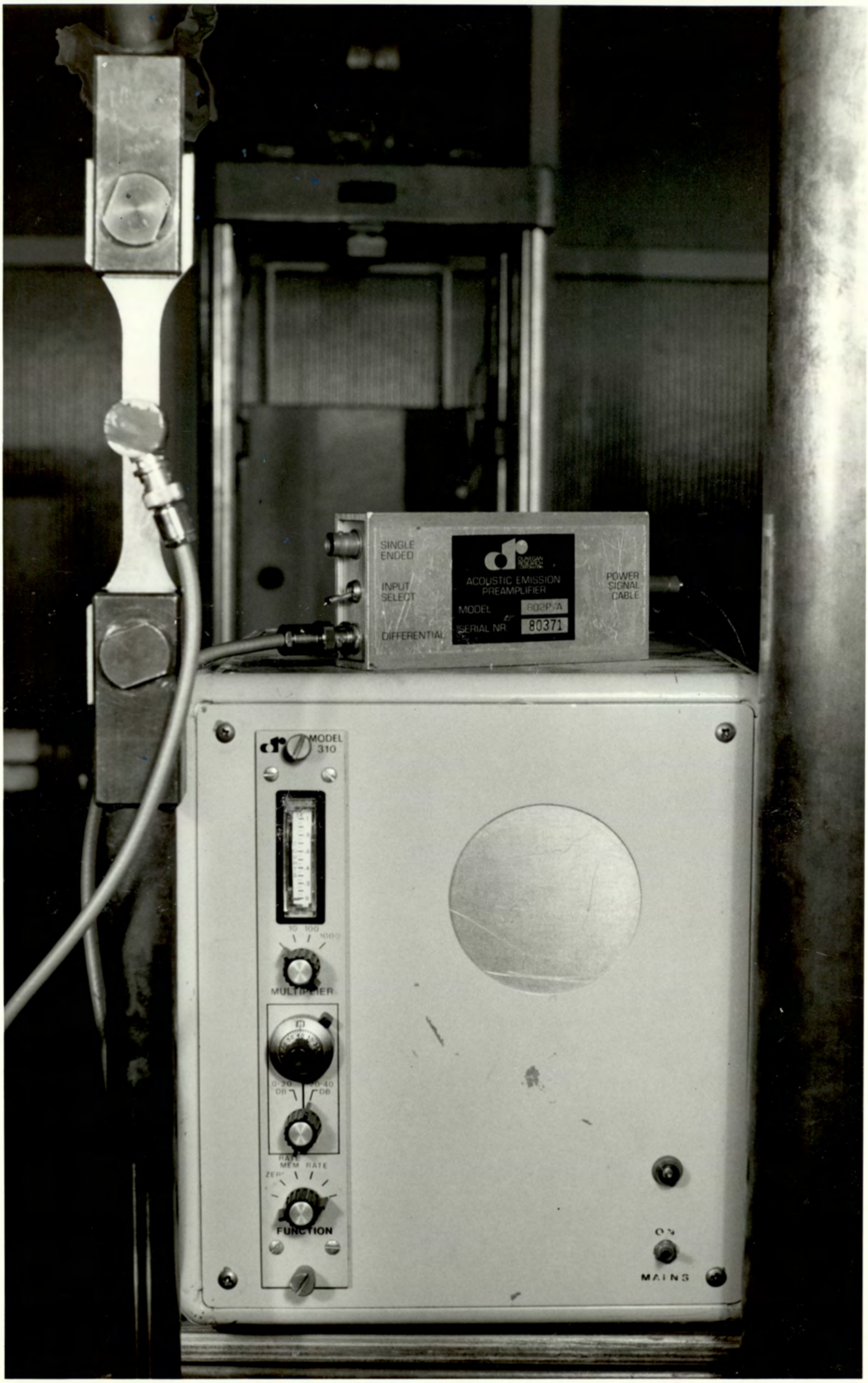

Fig. 7. A.E. monitoring system.

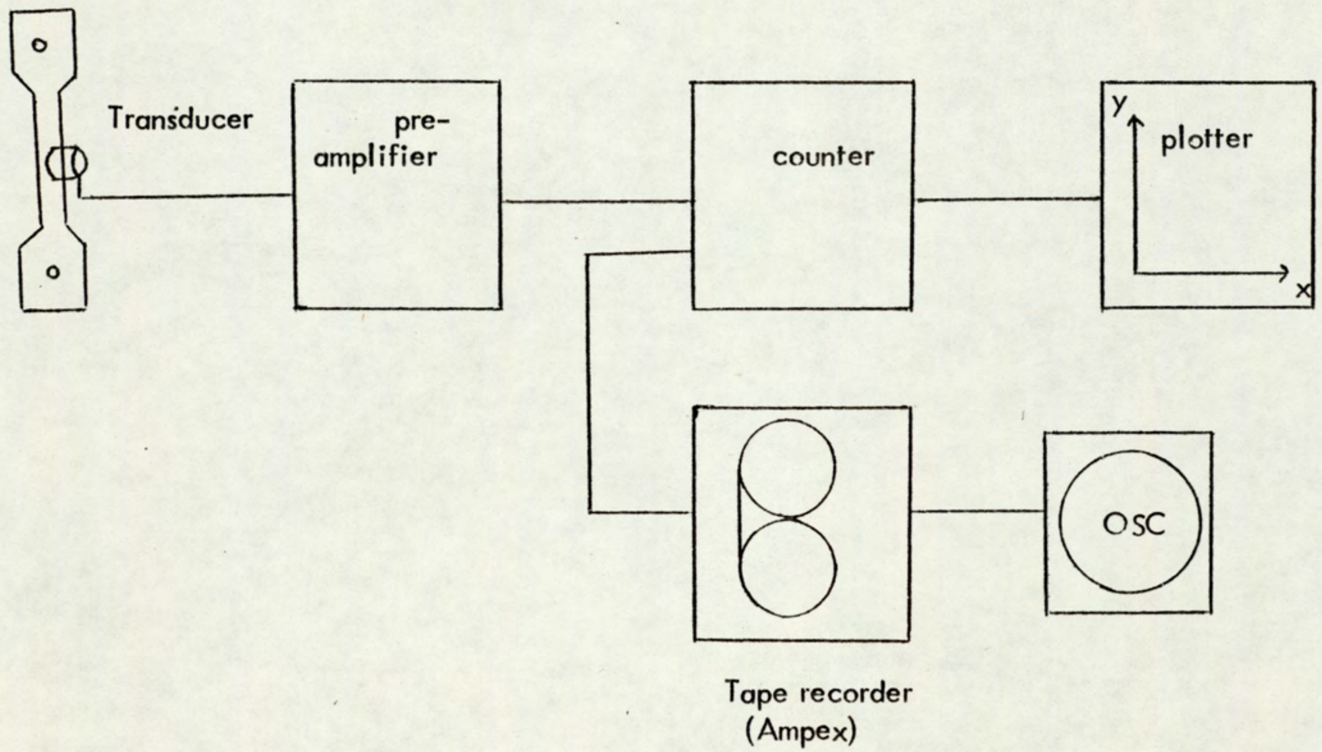

Fig. 8. Stage (1) data recording diagram.

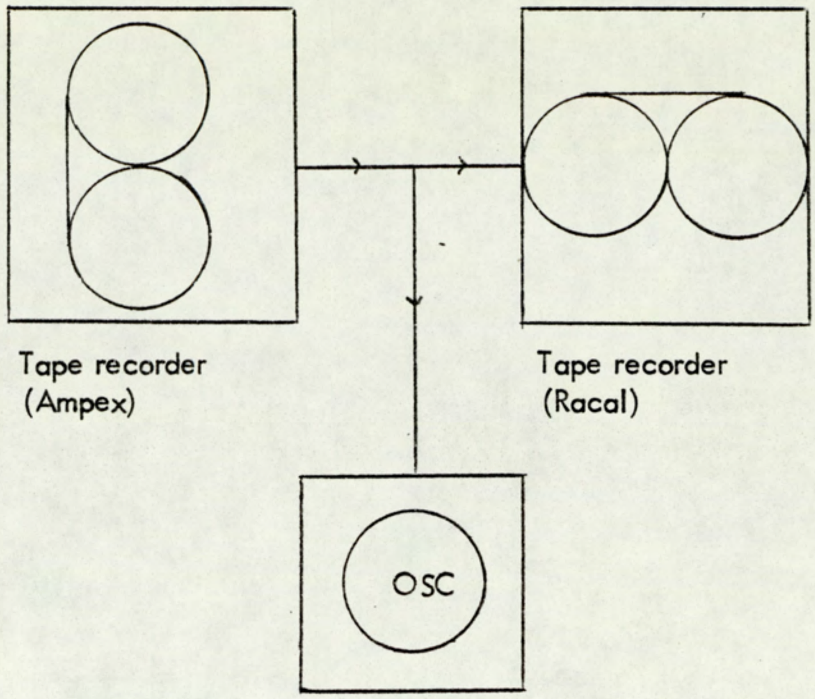

Fig. 9.a. Stage (2) frequency reduction.

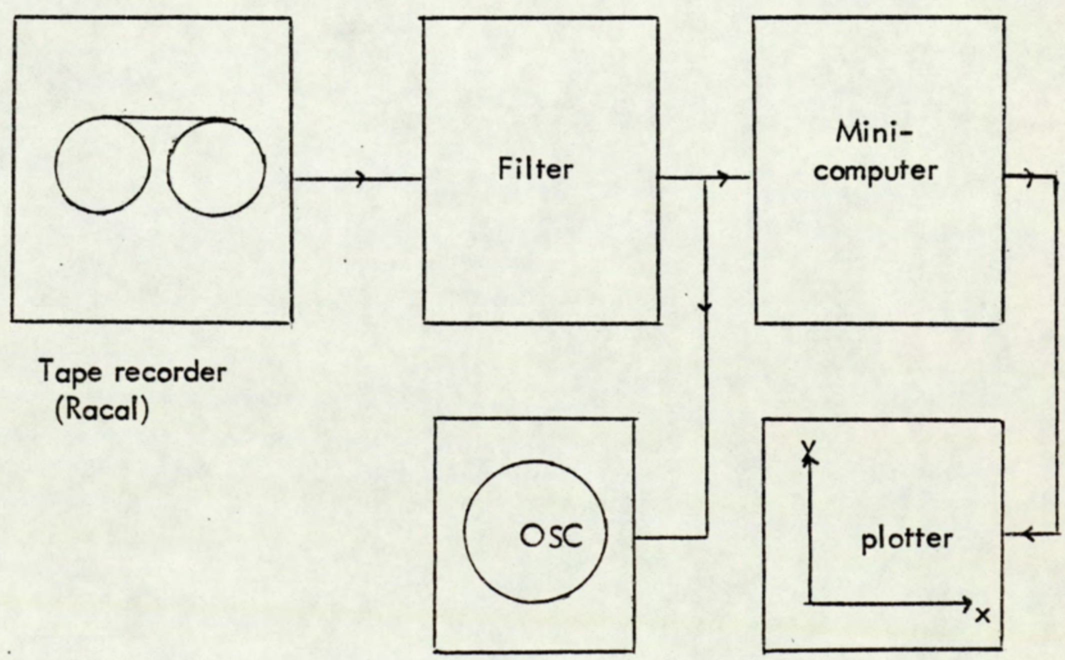

Fig. 9.b. Stage (3) signal analysis.

Fig. 9. Data analysis.

Fig. 10. The on-line minicomputer.

CHAPTER 4

EXPERIMENTAL WORK

4.1 Introduction

The fundamentals and theory of acoustic emission have been discussed in the previous chapter, and it is aimed in this chapter to study the acoustic emission characteristics from different types of metals and the factors affecting these characteristics.

In order to fulfil this requirement for the purpose of this study, the following programme of experiments was carried out:

a) Tensile test, notched tensile test and three-point bending test were to expose plastic deformation on flat and round specimens of different steels, Aluminium, Brass and Copper.

b) The set-up of instrumentation described in the previous chapter was employed simultaneously to measure acoustic emissions counts and recording acoustic emission pulses, time, load and displacements.

4.2 Preparation of the Steels

Different types of steels were used in this experimental programme together with non-ferrous metals, Aluminium, Copper and Brass. The chemical compositions of steels used are shown in table (1.a.) and the chemical composition of non-ferrous metals are shown in table (1.b.). The steels were classified as follows:-

a) Steels of group (A) of medium carbon steels and were divided into two types: A1 and A2. Type A1 was received in the form of strips and type A2 was received in the form of block. Steel A2 was a plain carbon steel.Bs1760 B were heat-treated for 5 hours at 900^{o}C and furnace cooled.

b) Steel (B), a low carbon steel, was received as strips.

The steels above, received in the form of strips, were used to produce tensile test specimens. For this purpose it was intended to aim for large deformation. Therefore, some of these steels were heat-treated to adjust the microstructure and to improve the ductility.

The different heat treatment procedures employed are shown below:-

i) The steels were heated at 900^{o}C for ½hr. then <u>furnace cooled</u>.

ii) The steels were heated at 1100^{o}C for ½hr. then <u>furnace cooled</u>.

iii) The steels were heated at 900^{o}C for ½hr. then <u>air cooled</u>.

These heat treatments produced very similar microstructures.

c) Steels of Group (c) were produced by melting, then suction casting into rods of 25mm diameter. The procedure of production is as follows:-

1.5Kg of Japanese electrolytic iron contained in alumina crucible Fig. (11) were melted under Argon gas to prevent oxidation. The contents were heated in an induction furnace up to 1600°C super heat and were held at this temperature. At this stage the first sample was taken to be analysed later for oxygen level.

The next step was the addition of ferric oxide (Fe_2O_3) and ferrous sulphide (FeS). The purpose of this addition was to adjust the required oxygen and sulphur levels. At this stage the second sample was taken.

Then a deoxidising alloy was added. This deoxidising alloy was prepared at three different proportions of Mn, Al and Si. The proportions of the three elements were varied for each melt and were used with three different percentages of sulphur 0.02%, 0.1% and 0.2% to give nine different compositions of steel (C).

Each melt was sucked into a 25mm diameter silicon tube and was left to air cool. The rods obtained were hot rolled at 1050°C to reduce their diameter.

These steels were analysed on the Quantitative Electron Microscope (Q.T.M.) and the quantities of sulphides and oxides were measured.

4.3 Preparation of Specimens

The flat tensile specimens were machined from flat strips of steels A1 and B. Examples of these specimens are shown in Fig. (12). The specimens' dimensions are as follows:-

Specimen width = 12.6mm

Specimen thickness = 4.98mm

Gauge length = 75mm

Two notched flat specimens were machined from flat strips of steel (B). These specimens had two-sided notches. Their dimensions are as follows:

Specimen width = 12.6mm

Specimen thickness = 4.98mm

Gauge length = 65.0mm

Notch depth = 3mm

Fig. (13) shows the notch shape.

Flat and tensile specimens (unnotched) with different gauge lengths were machined from flat strips of mild steel (steel B).

These specimens are shown in Fig. (14). The dimensions of these specimens are as follows:-

Specimen width = 12.6mm

Specimen thickness = 4.98mm

and gauge length Lo = 110mm, 370mm, and 620mm.

Round notched tensile specimens were machined from steel (C). These specimens had shorter gauge length than that in the flat specimens. Notches of varying root radii (three types of notches) were machined in these specimens. The dimensions of these specimens are as follows:-

Specimen diameter (D) = 10mm

Distance between the ends of the two notches (d) = 5mm

Gauge length = 25mm

The notch root radii = 1.00mm, 0.26mm, and 0.16mm.

Fig. (15) shows the round specimen and the three types of notches.

The three-point bending test specimens were machined according to the dimensions shown in Fig. (16). These specimens machined were from steel (A2) (Bs1760B). Three different types of notches were machined in these specimens. The dimensions are as follows:-

Specimen dimensions = 150mm x 20mm x 25mm

Notch root radii = 0.127mm, 12.7mm, and 25.4mm.

Notch depth = 8mm for the three notches.

The properties of steel (A2) were measured by tensile test and came out as follows:-

Tensile strength = 734MN/m^2

Yield stress = 360MN/m^2

Elongation = 12%

Reduction in area = 10%.

4.4 The Tensile Test

The tensile test for both flat and round specimens was carried out on a Mand Precision Tensile Machine, with a maximum load capacity of 10,000Kgf. The ranges of loads used were 0-10,000Kgf. for the flat specimens and 0-2,500Kgf. for the round notched tensile specimens.

The cross-head speed used for the flat tensile specimens was low gear 400 r.p.m. (i.e. 0.84mm/min.).
The cross-head speed used for the round tensile specimens was low gear 100 r.p.m. (i.e. 0.2mm/min.).

The specimen ends were adjusted to be in the centre of the grips. The transducer was attached on the centre of the gauge length in the case of the flat specimens as shown in Fig. (17). For the round specimens the transducer was attached to the grip due to the difficulties of fixing the transducer on the short gauge length. In both cases the transducer was fixed onto the specimen or onto the grip by using insulation tape. A thin layer of a vacuum s silicon grease was used between the specimen and the transducer. The transducer was connected to the pre-amplifier and then to the Counter (Dunegan/Endevco). The total gain used for most of the tests was 84.5dB. The output of the counter was recorded on an YY-T plotter as a number of counts. Acoustic emission signals, from the A.C. output of the counter, recorded on a magnetic tape recorder at a speed of 15.24 meter/sec.

Recording the acoustic emission signals started from the beginning of the test until the fracture in most of the tests. Fig. (18) shows the loading machine, the monitoring and the recording systems.

4.5 Long Gauge Length Tensile Test

Six flat unnotched tensile specimens were used. They have the same thickness and width but differ in the gauge length only. These specimens were machined from steel (B) and each two specimens have identical gauge length.

The cross-head speed was low gear 400 r.p.m. (0.84mm/min.). The monitoring system gain was 84.5dB and the load range used was 10,000Kgf. The tests were carried out using the same procedure as in the previous section.

4.6 Three-point Bending Test

A universal Instron 1197 Machine 50-ton capacity was used for this test. Seven specimens were used, and each two had the same notch radius and one plain specimen (free of notch).

A stress-coat was used to paint one side of the specimen to enable the plastic deformation at the notch tip to be seen. The cross-head speed was 0.1mm/min. An electronic transducer was used to measure the displacement of the specimen.

Two transducers were used for these tests. Both were attached to the long side of the specimen. One transducer was connected to the pre-amplifier and then to the counter. The output of the counter recorded on Y.Y-T plotter as number of counts. The other transducer was connected to the second pre-amplifier then to the tape recorder to record the acoustic emission signals. Fig. (19) shows the three-point bending test specimen with the transducer attached to it.

The acoustic emission monitoring system gain was 68dB. The gain increased to 76dB for large notch radius to 78dB for the plain specimen.

The acoustic emission signals were recorded at a gain of 60dB.

4.7 Measurements

Measurements were carried out at several stages during the experimental work. They were taken before, during and after all the above tests.

Those measurements before the tests included: parameters characterising the steels i.e. the chemical composition which were obtained from the chemical analysis and samples of each type of steel, and the changes exerted on their microstructure by heat treatment such as the effects of the dimensions of the specimens, and the carbon content.

Also, measurements of the notch geometry such as root radius, depth and diameter at the notch section were taken. These measurements were obtained by a projecting the notched area of the specimen on the screen of projection microscope at a magnification of 50X. This projection was drawn on tracing paper from which the dimensions of the notch geometry were measured and calculated.

Measurements taken during the mechanical tests included the load and time in the case of the flat tensile specimens, load time and extension in the case of the round notched tensile specimens. The load-acoustic emission counts relationships with time were plotted directly on a two-pen YY-T plotter. Also load - extension was plotted on X-Y plotter but in this case an electronic gauge was fixed on the specimen to measure its extension.

In the case of three-point bending tests, the load displacement was recorded in the same manner above on X-Y plotter while load and acoustic emission counts were plotted against time on a two-pen YY-T plotter.

It is worth mentioning that the set-up of the instrumentation described in the previous chapter was used simultaneously with the set-up of the test to measure and record the parameters of acoustic emission i.e. acoustic emission counts against time, amplitude and frequency.

Fast Fourior transformation analysis was used to analyse the acoustic emission signals. The analysis was carried out on signals from elastic, pre-yielding, and plastic (near fracture or at fracture) regions. The program used for this purpose is listed in the Appendix.

TABLE 1(a)

CHEMICAL COMPOSITION OF STEELS

	%C	Mn	Si	S	P	Ni	Cr	Mo	Al	W
A1	0.67	1.1	0.31	0.016	0.019	Trace	0.67			0.38
A2	0.54	1.02	0.85	0.03	0.013	0.02	0.01	0.02	0.023	
B	0.14 0.15	0.53	0.05	0.025	0.008					
C10	0.01	0.44	0.26	0.037						0.01
C11	0.03	0.41	0.22	0.10						0.005
C12	0.06	0.47	0.44	0.19						0.009
C20	0.01	0.98	0.38	0.03						0.01
C21	0.03	0.99	0.33	0.10						0.048
C22	0.07	0.97	0.26	0.19						0.008
C30	0.02	1.8	0.32	0.022						0.005
C31	0.03	1.65	0.44	0.089						0.012
C32	0.06	1.79	0.43	0.17						0.007

TABLE 1(b)

CHEMICAL COMPOSITION OF NON-FERROUS METALS

Copper	Commercially pure
Brass	56-60% Copper 2-3.5% Lead Zinc
Aluminium	1% Copper 1.5% Magnesium 1.0% Manganese 0.6% Iron 0.1% Zinc 0.5% Chrome Aluminium

FURNACE ASSEMBLY

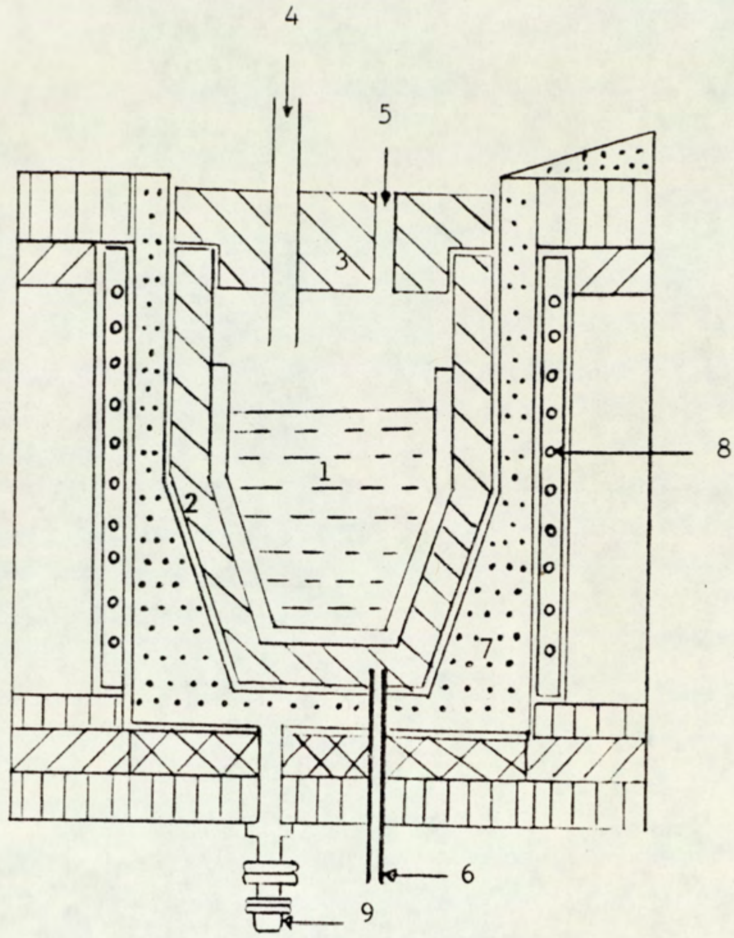

1) Iron Melt Contained in Alumina Crucible
2) Graphite Susceptor
3) Graphite Suscepter Lid
4) Argon Inlet Tube
5) Thermocouple and Sampling Hole
6) Thermocouple
7) Furnace Lining
8) Water Cooled Induction Coil
9) Earth Leakage Spider

FIG a

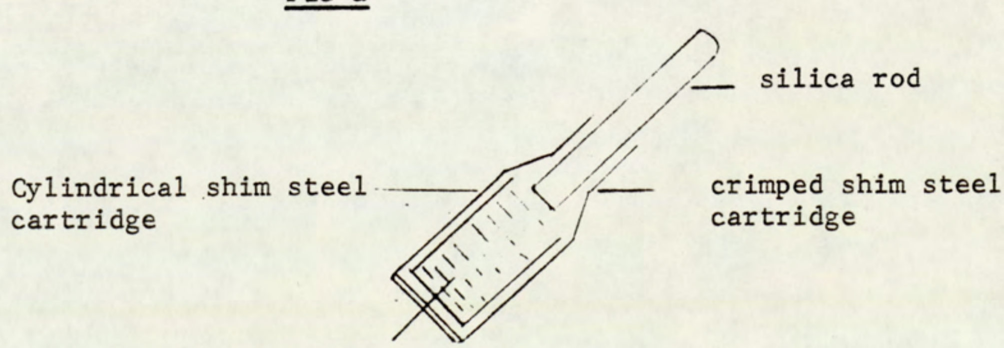

Fig. b.

Fig. 11. Induction furnace.

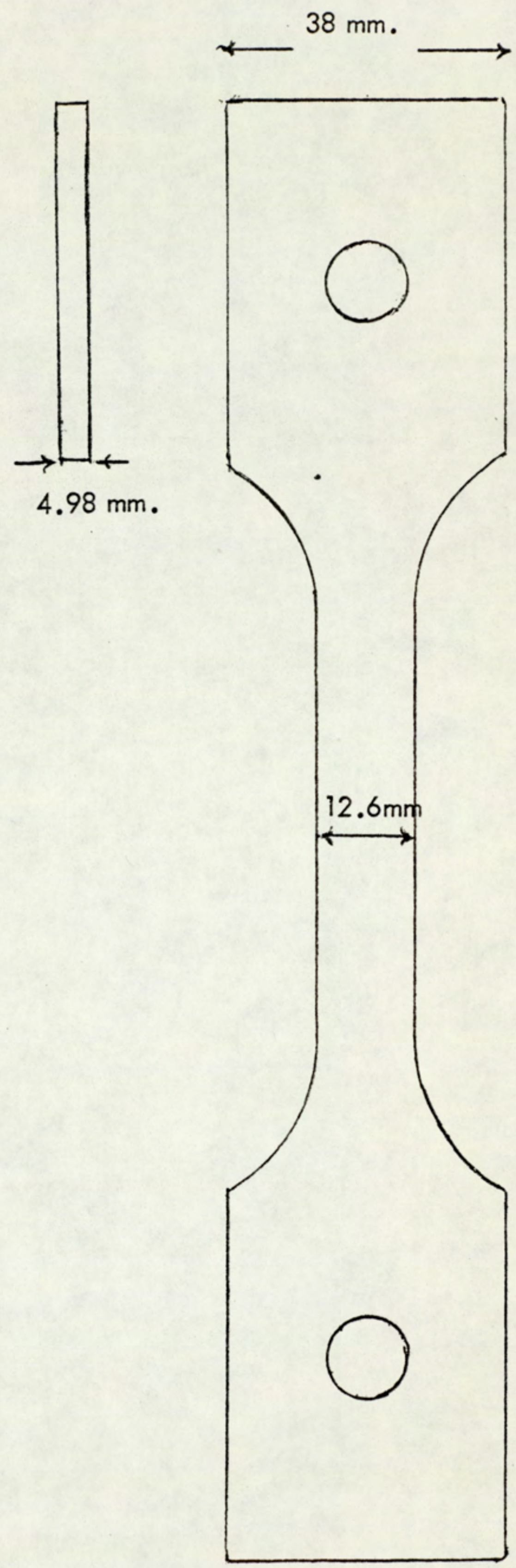

Fig. 12. Flat tensile specimen.

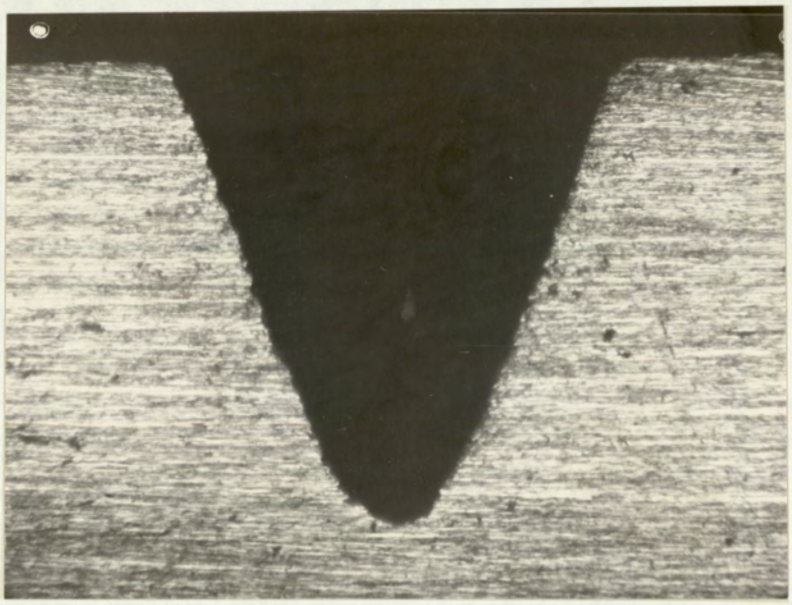

Fig. 13. Notch shape of flat specimen.

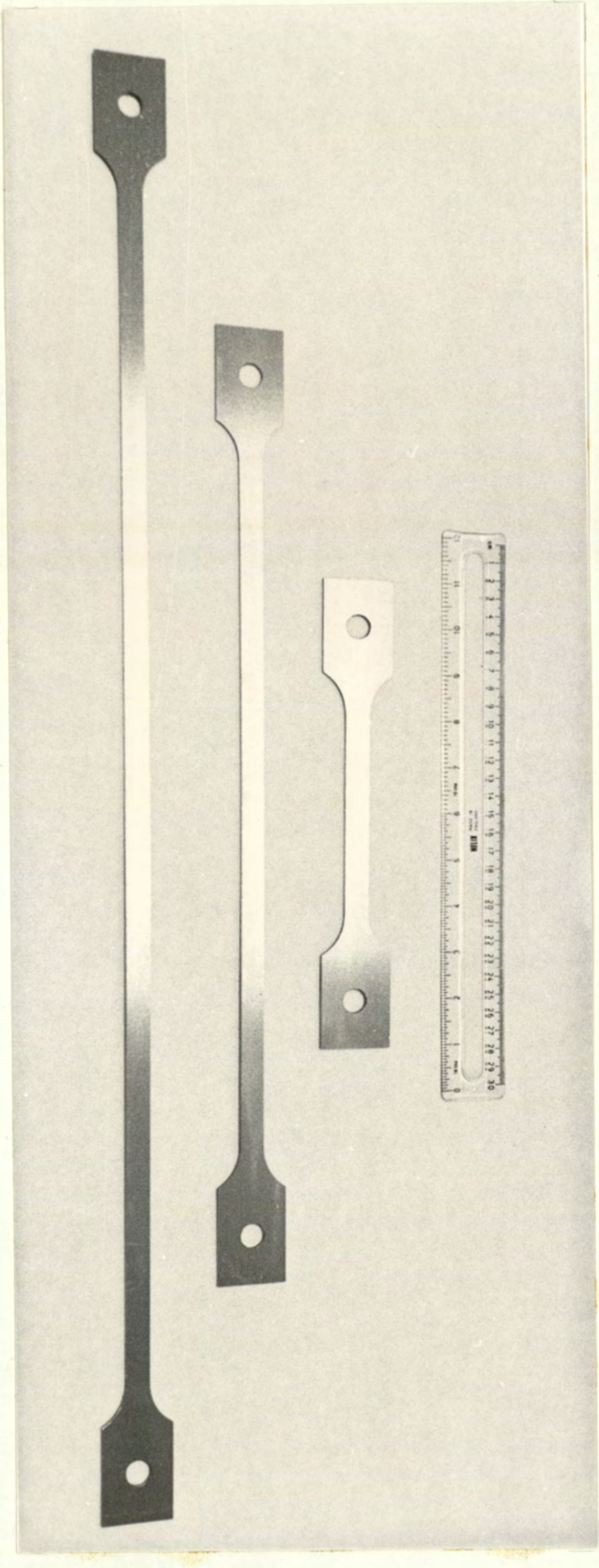

Fig. 14. Long flat tensile test specimens.

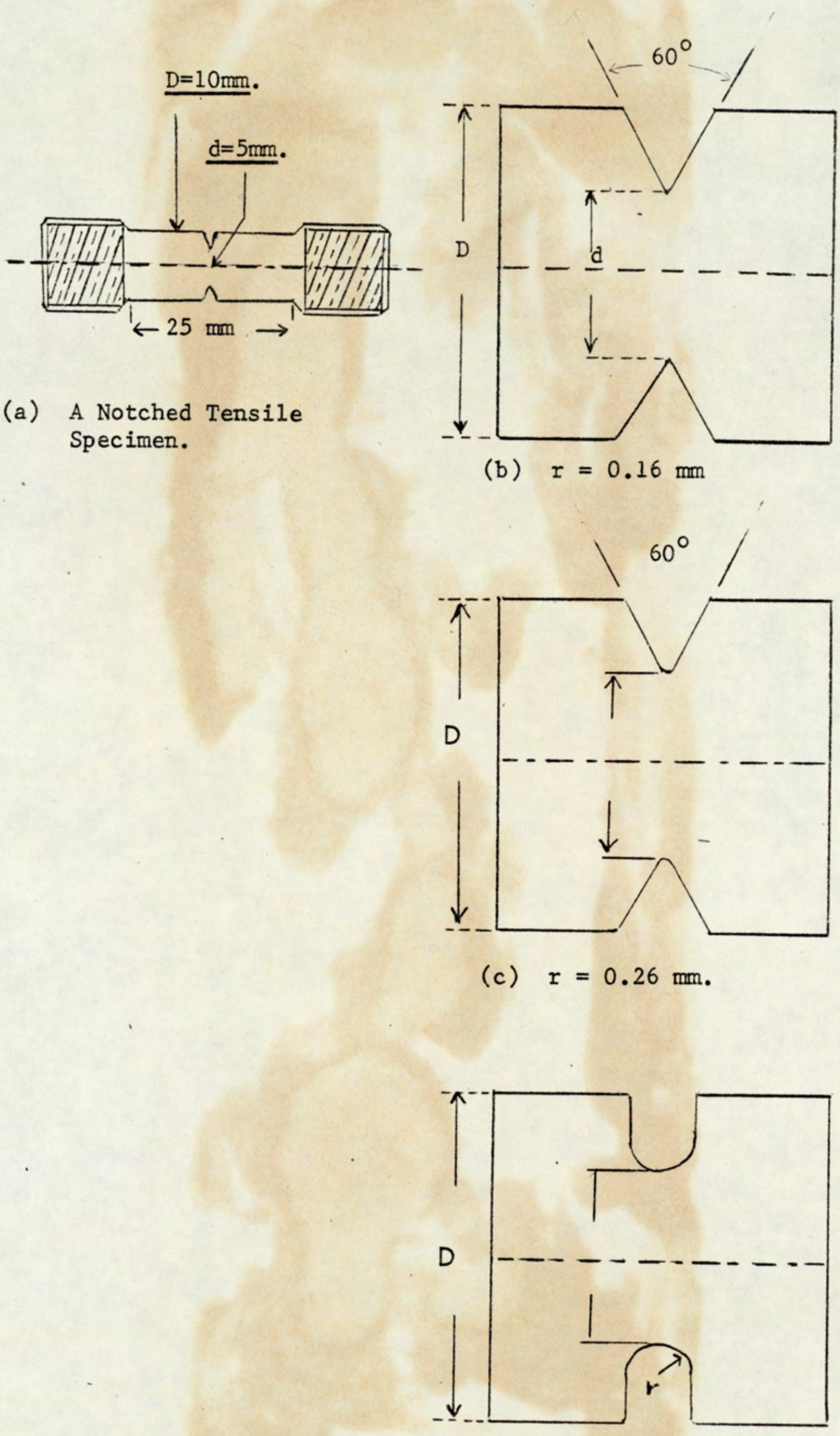

(a) A Notched Tensile Specimen.

(b) r = 0.16 mm

(c) r = 0.26 mm.

(d) r = 1.00 mm

Fig. 15. Round specimen with the three types of notches.

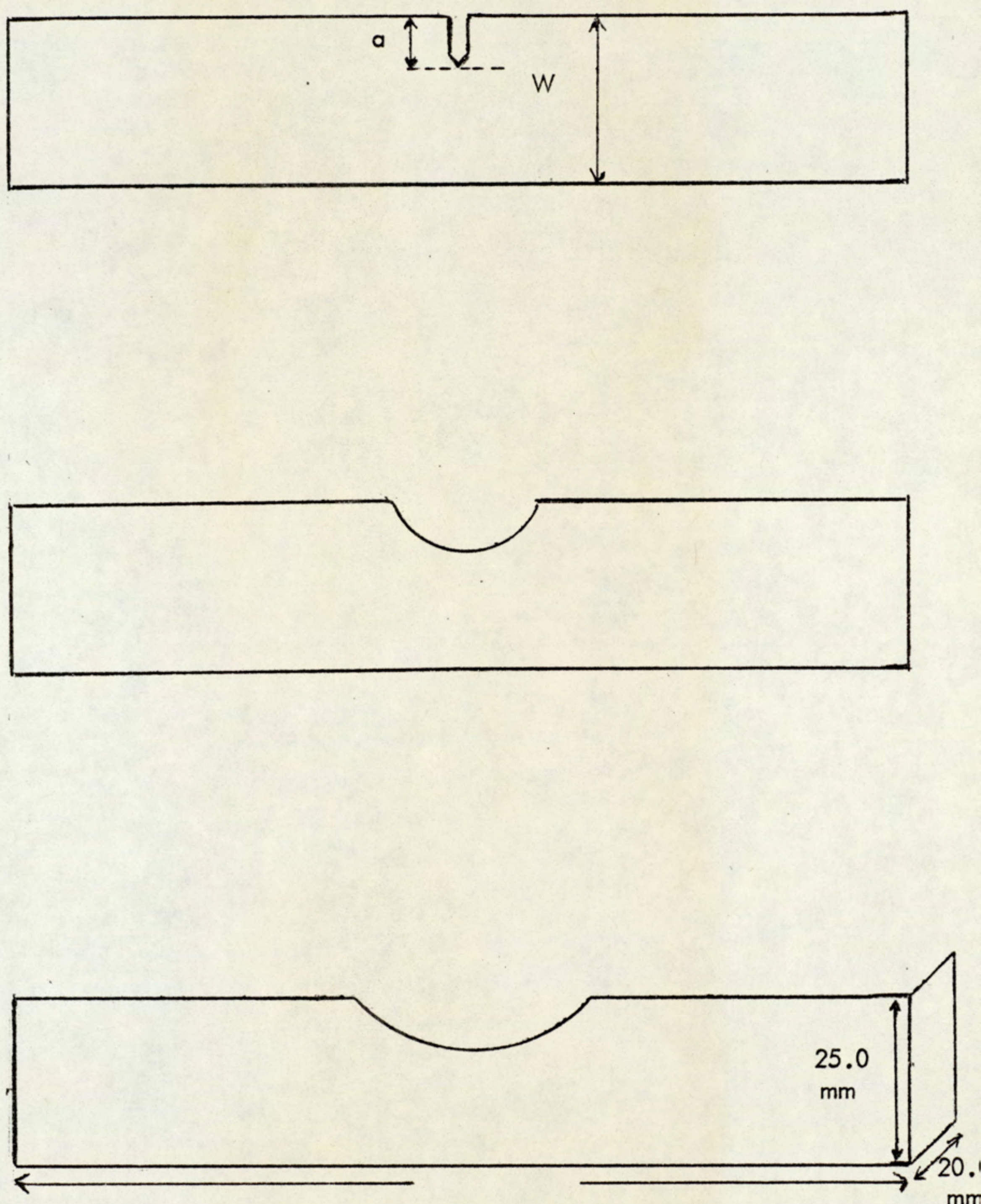

Fig. 16. Three-point bending specimen.

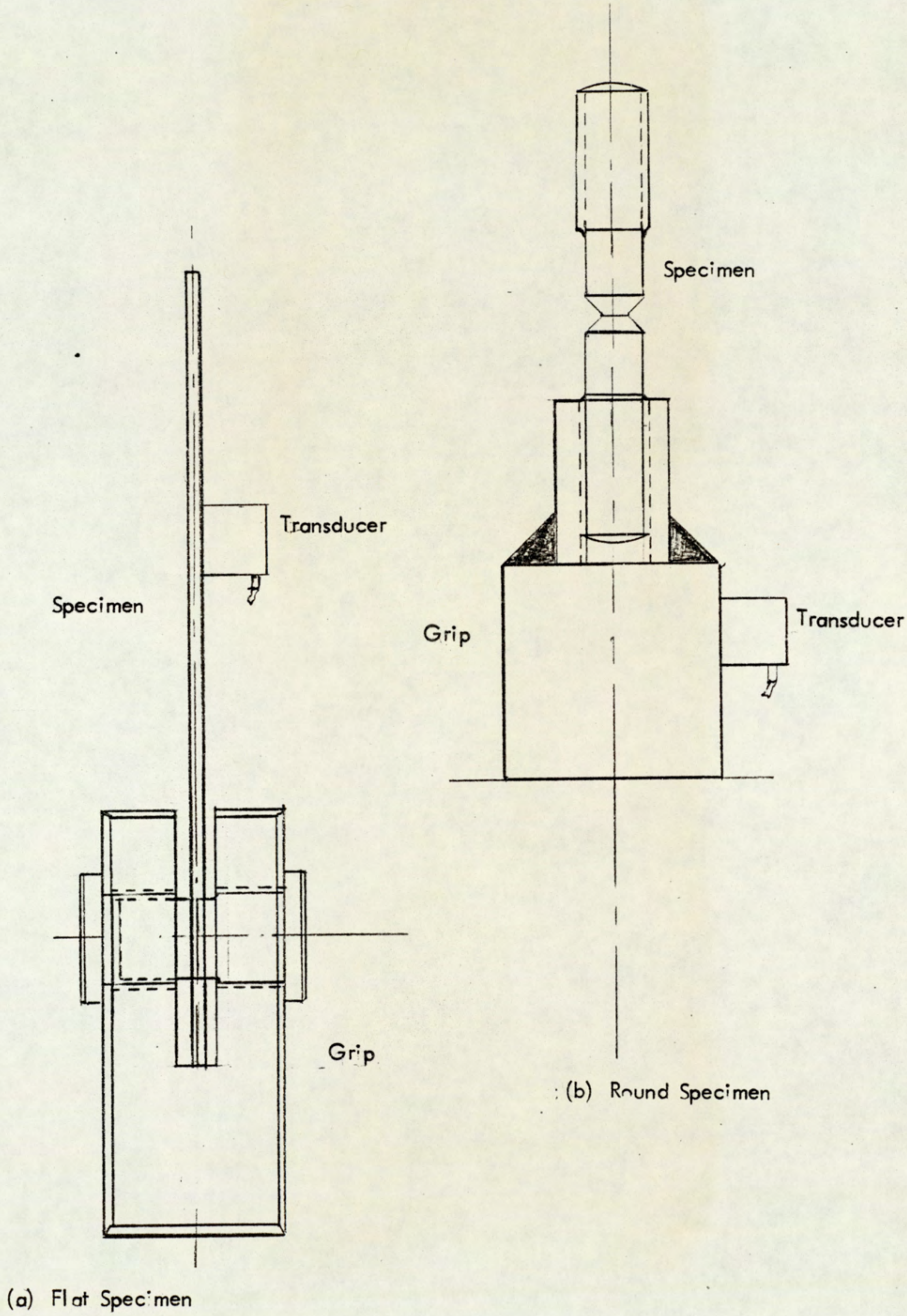

Fig. 17 Fixing method of the Transducer

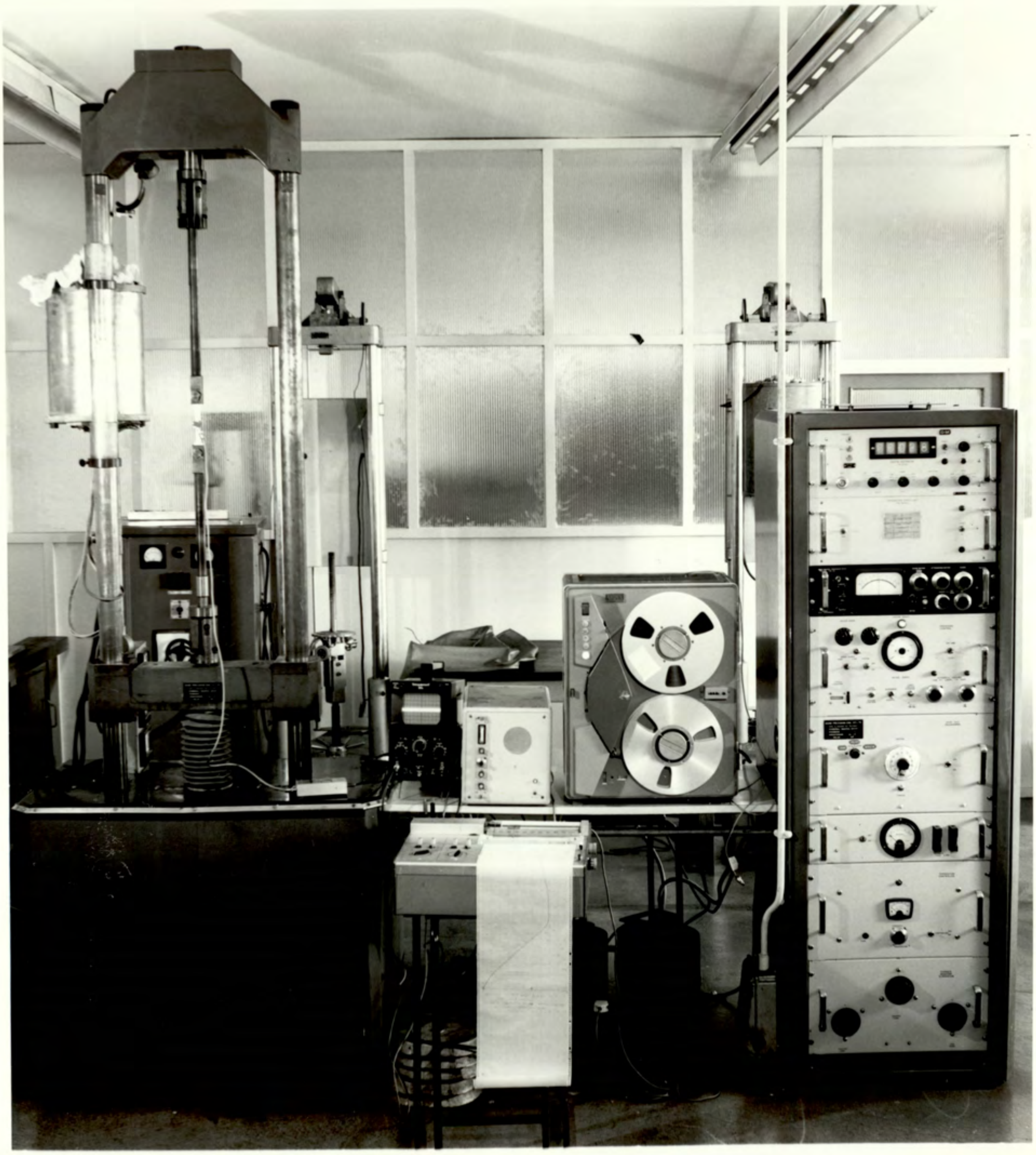

Fig. 18. Complete set-up of the tensile test.

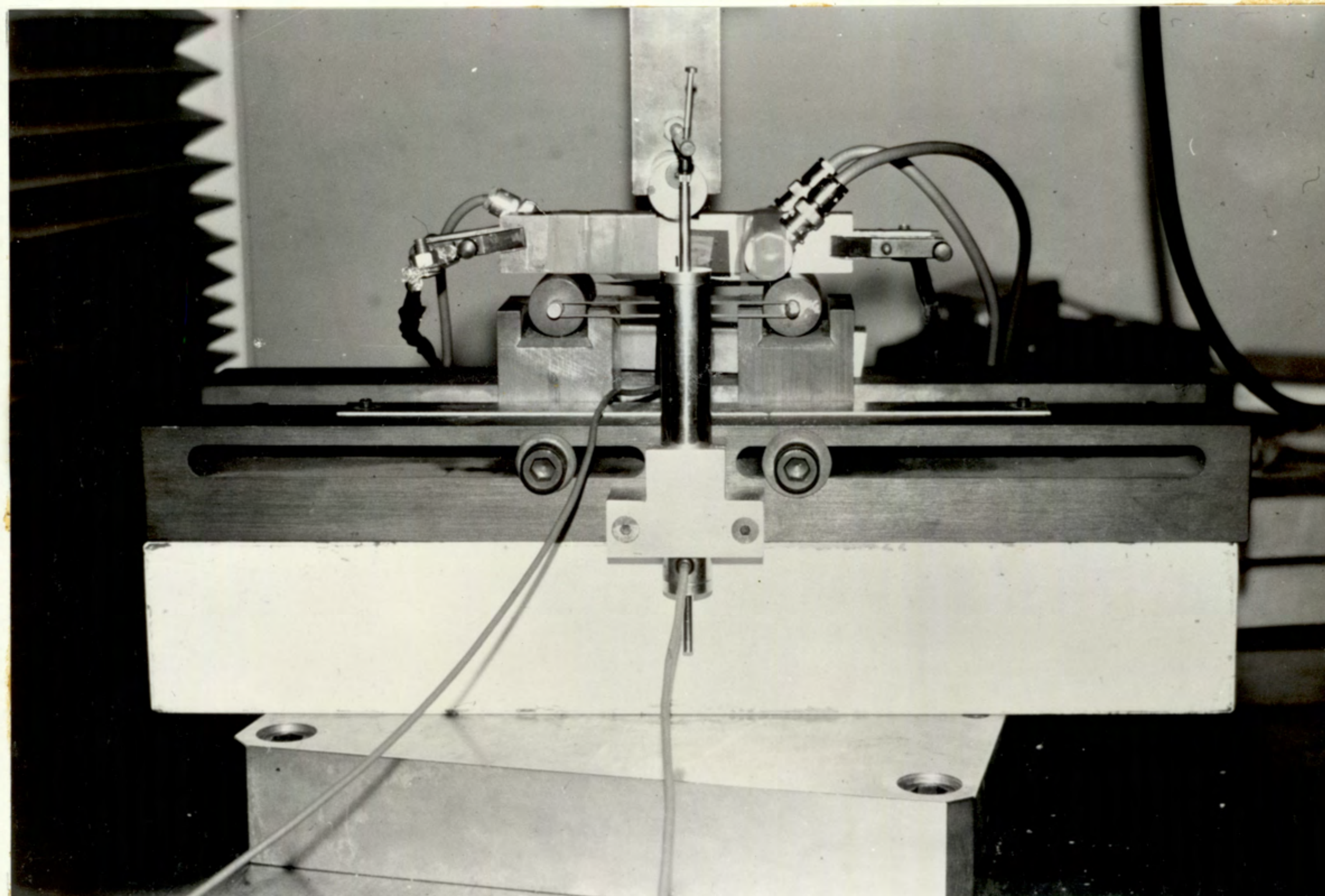

Fig. 19. Three-point bending test setup.

CHAPTER 5

RESULTS

Different parameters describing the properties of steel, the plastic deformation and acoustic emission properties were measured through the experiments in the previous chapter and the results of these measurements are presented in this chapter as follows.

5.1. Properties of Metals Used

The results of the chemical analysis of the steels and non-ferrous metals (Brass, Copper, and Aluminium) are shown in tables (1a, 1b). These analyses showed that all types of steels used were of low and medium carbon content ranging from 0.006%C to 0.67%C normal commercial steels.

Some changes in the microstructure were brought about through annealing which improved the ductility.

5.2. Flat Tensile Test

The results of the test of 0.086%C steel are shown in Fig. (20a, b). These specimens were loaded to 250Kgf. and kept at that load level for three days. The acoustic emission activity started after the load level was above the 250Kgf. This is shown very clearly in Figs. (20a, b) and the sudden increase takes place just prior to yielding. Then smaller jumps of acoustic emission counts were recorded after the yield point followed by a steady level until the fracture.

Fig. (21a, b) showed the results of the tests of 0.15%C steel. The results of two specimens which were tested showed that the number of acoustic emissions emitted is higher than that emitted from 0.85%C steel.

The results of the tests of medium carbon steel (0.67%C) are shown in Fig. (22,a, b). The acoustic emission activity startedto increase with the beginning of the test. After the yield point this increase takes the form of small steps until fracture.

Fig. (22, a.1) and Fig. (22, b.1) show the acoustic emission signals generated from the 0.67%C steel specimens. These signals are of long duration in the elastic region and short duration at yield point. The acoustic emission signals have higher amplitude at the elastic region and prior to fracture than in the pre-yielding region. The predominant frequency at the elastic region is between 106-135KHz and at the pre-yielding region is between 210-230KHz. The predominant frequency range at the region prior to fracture is between 100-130KHz. These are shown in Fig. (22, a.2) and Fig. (22, b.2).

The number of acoustic emission counts generated from 0.67%C steel is higher than that generated from 0.15%C and 0.086%C steels. These are shown in Fig. (20,a, b), Fig. (21, a, b) and Fig. (22, a, b).

The results of the tensile test of the two-sided notched specimens (mild steel 0.15%C steel) are shown in Fig. (23a, b). Acoustic emission activity started with a sharp increase until the yield point and after that there was no increase in the emission. Before the fracture the emissions started to increase in the form of steps in the fracture. The acoustic emission pulses from the three regions (elastic, pre-yielding and fracture) are shown in Fig. (23, a.1) and Fig. (23, b.1). These pulses have higher amplitude at elastic region, pre-fracture and fracture region than that at the pre-yielding region. Also the pulses at elastic region and fracture region have longer time duration.

The predominant frequency range in the elastic region is between 100-137KHz, while in the pre-yielding region the predominant frequency range is between 135-230KHz with central peak at about 224KHz. The frequency range at fracture is between 131-137KHz. These are shown in Fig. (23, a.2) and Fig. (23, b.2).

5.3. Long Flat Tensile Test Specimens

Three different gauge lengths (110mm, 370mm, and 620mm) were used. These are shown in Fig. (14).

The results of the test of short gauge length (L_o=110mm) specimens are shown in Fig. (24a, b). Both Figs. (24a, 24b) showed that the acoustic emission rate has a maximum peak before the yield, and also there is a large number of counts emitted at the beginning of the test.

The acoustic emission pulses generated from the elastic, yielding and fracture regions are shown in Fig. (24, a.1) and Fig. (24, b.1). These figures showed the pulses' shape and their amplitudes at different regions.

The predominant frequency range at the elastic region is between 118-228KHz. The frequency range at the pre-yielding is between 138-214KHz and at pre-fracture is between 133-142KHz with a central frequency of 141.8KHz.

The results of the tests of the medium gauge length (Lo=370mm) specimens are shown in Fig. (25a, b). The acoustic emission started after about 0.5min. from the beginning of the test. Also the emissions started with steps until the yielding region, then no emission was observed until fracture.

Fig. (25, a.1) and Fig. (24, b.1) showed the acoustic emission pulses' shapes. In Fig. (25, a.1) the signal was analysed from the plastic region and not from the fracture region. Both figures showed that the amplitude of the signals at the plastic region is higher than the amplitude of the signals at the yielding region.

The predominant frequency range in the elastic region is between 138-140KHz, while in the pre-yielding region the range is between 206-211KHz. The frequency range in the plastic region is between 138-225KHz, while at fracture the frequency range is between 98-140KHz. These are shown in Fig. (25, a.2) and Fig. (25, b.2).

The results of the tests of the longer gauge length (Lo=620mm) specimens are shown in Fig. (26a, b). The acoustic emission pulses are shown in Fig. (26, a.1) and Fig. (26, b.1.). The predominant frequency range in the elastic region is between 131-143KHz, while in the pre-yielding region the frequency range is between 100-224KHz with central peak at about 211KHz. The frequency range at fracture is between 100-131KHz.

5.4. Results of the Non-ferrous Specimens Tests

A flat tensile test specimen from each of Aluminium, Copper and Brass has been used.

Fig. (27) shows the results of the tensile tests of aluminium specimens. These figures (27a, 27b) showed the increase of acoustic emission counts sharply in the elastic region and after the yield point only a slight increase took place until fracture. The acoustic emission rate has a wide peak prior to the yield point. Acoustic emission signals generated from this test are shown in Fig. (27, a.1.)and Fig. (27, b.1.).

The predominant frequency range range of the acoustic emission signal in the elastic region is between 131-230KHz with a central frequency of about 132KHz, while near the yield point the frequency range is between 72-

230KHz, with the highest peak at 230KHz. Near the fracture the frequency range is between 72-230KHz with the highest peak at 135KHz.

The results of the tests of the copper specimens are shown in Fig. (28). The acoustic emission counts started in the early stage of the test. The increase took place in large jumps until the yield, when the increase took the form of small jumps until the fracture. The acoustic emission rate showed a sharp peak near the yield point and near the fracture the rate started to increase again. The acoustic emission signals are shown in Fig. (28, a.1.) and Fig. (28, b.1.).

The signals prior to the yield point, as shown in Fig. (28, a.1.), consisted of many pulses of short-time duration.

The predominant frequency range in the elastic region is between 130-136KHz while the frequency range in the pre-yielding region is 202KHz as a single peak as shown in Fig. (28, a.2) and 228KHz as a single peak as shown in Fig. (28, b.2). At the region near the fracture the frequency range is between 132-197KHz.

The last metal in this test is the Brass. The results of the test are shown in Fig. (29). From Figs. (29a, b) the number of acoustic emission counts is small compared with that generated from copper.

The acoustic emission signals are shown in Fig. (29, a.1.) and Fig. (29, b.1.) which represents the elastic, pre-yielding, and plastic regions respectively.

The predominant frequency range in the elastic region is about 140KHz and at the pre-yielding is between 205-230KHz. Prior to the fracture the frequency range is about 136KHz and 82KHz at fracture.

5.5. Tensile Test of Round Specimens

Nine different compositions of steel (C) were used. The chemical composition of the nine types of steel (C) are shown in table (1.a.).

The figures from 30 to 56 show the relationships between the load, acoustic emission counts and acoustic emission counts rate against time for the nine types of steel (C).

There are three curves for each type of root radii r=1.00mm, r=0.26mm, and r=0.16mm comparing each set of three figures for one type of steel together.

The values of the geometry of the different sizes of the notches such as the root radii, depths and elastic stress concentration factors are presented in tables (2-10).

The acoustic emission counts were found to be higher from specimens of sharp notches than those from specimens of large notches. Also the count rate showed a maximum increase prior to the yield point for most of the tests carried out.

These types of steel (C) were analysed on the Quantitative Electron Microscope (Q.T.M.) and the quantitites of sulphides and oxides were measured. These quantities are shown in table (11).

5.6. Three-point Bending Tests

The results of the three-point bending test are shown in Figures 57, 58, 59 and 60. Seven specimens were used in this test.

From these figures, the number of acoustic emission counts recorded in this group of tests is smaller than that recorded from the tensile tests.

Specimens of sharp notches emitted a higher number of acoustic emission counts than that from specimens of large notches. This is clearly shown in Figs. (57, 58, and 59).

The predominant frequency range in the elastic region is between 130-230KHz with central peak at about 218KHz, while in the pre-yielding region the frequency range is between 200-250KHz with central peak at about 235KHz. Prior to fracture the frequency range is between 200-251KHz with central peak at about 247KHz. These are shown in Figs. (57a.2, 57b.2), (58a.2, 58b.2), (59a.2), (59b.2).

A test was carried out on a specimen of notch root radius r = 25.4mm at gain of 68dB and the result showed that no acoustic emission counts recorded from this test. This is shown in Fig. (59a).

Fig. (60) shows the test results of the plain specimen (free of notch). Acoustic emission started to increase slowly prior to yield point. The rapid increase in acoustic emission takes place prior to the fracture.

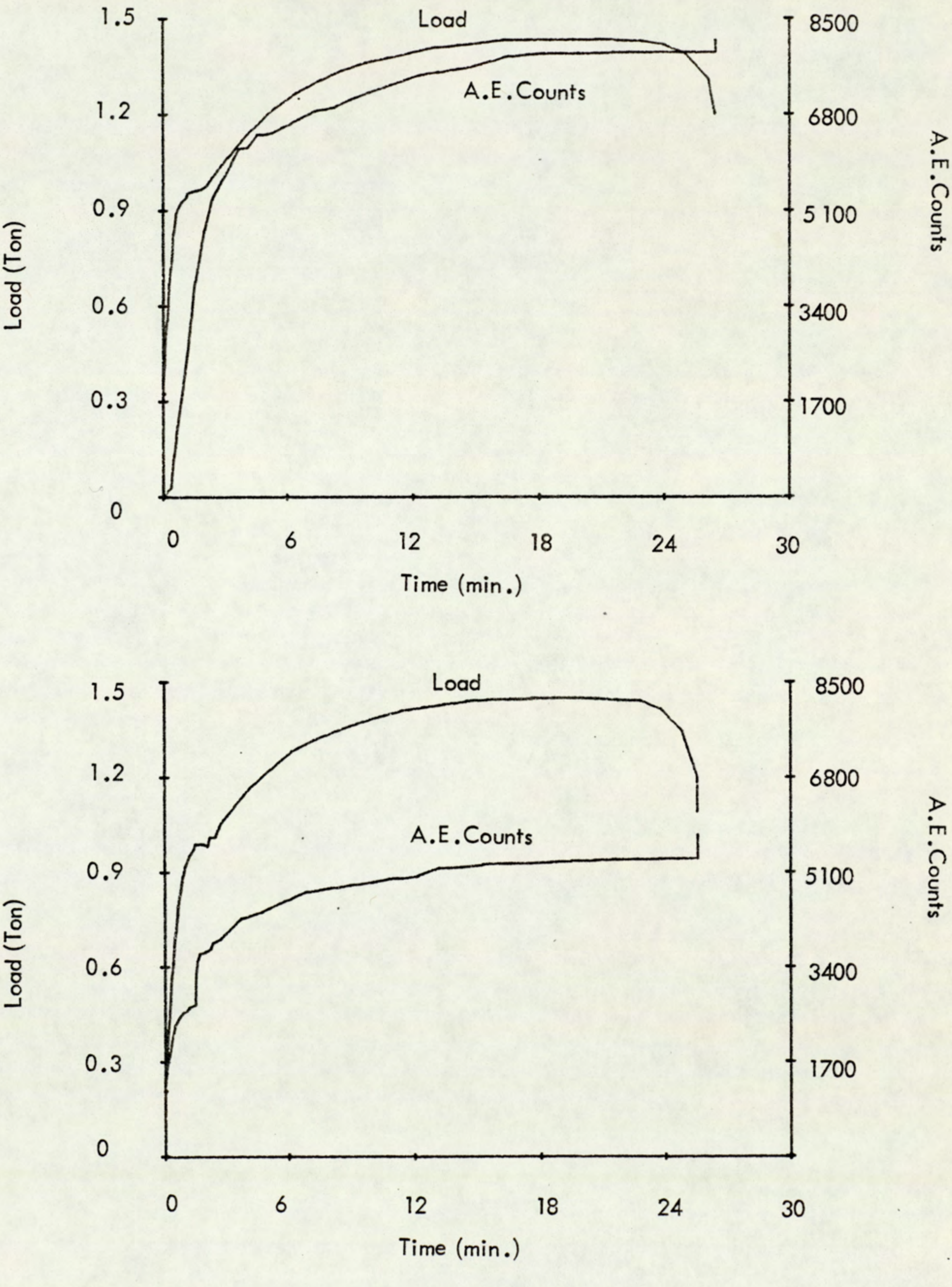

Fig. 20. Tensile test of 0.086%C steel.

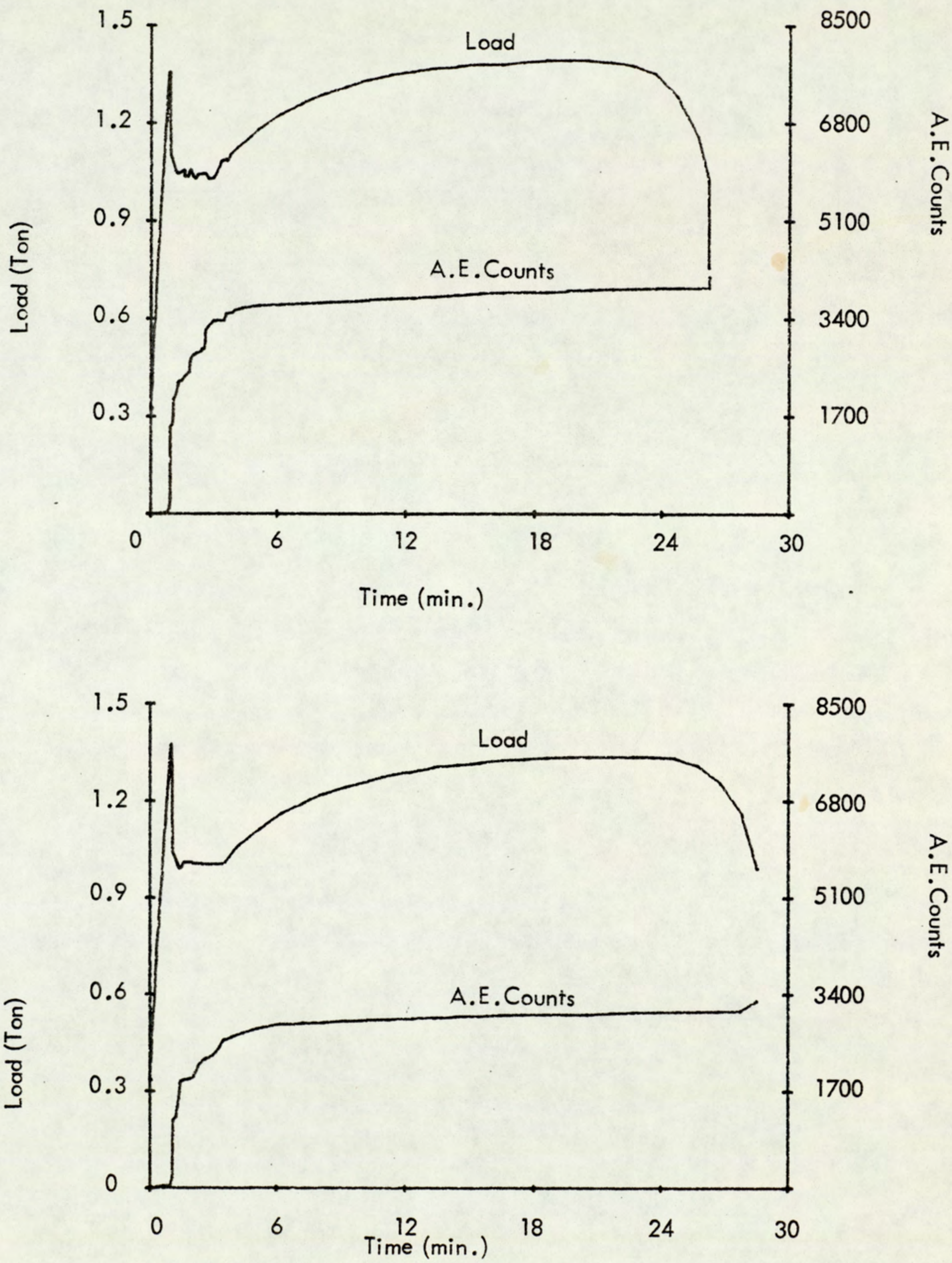

Fig. 21. Tensile test of 0.15%C steel.

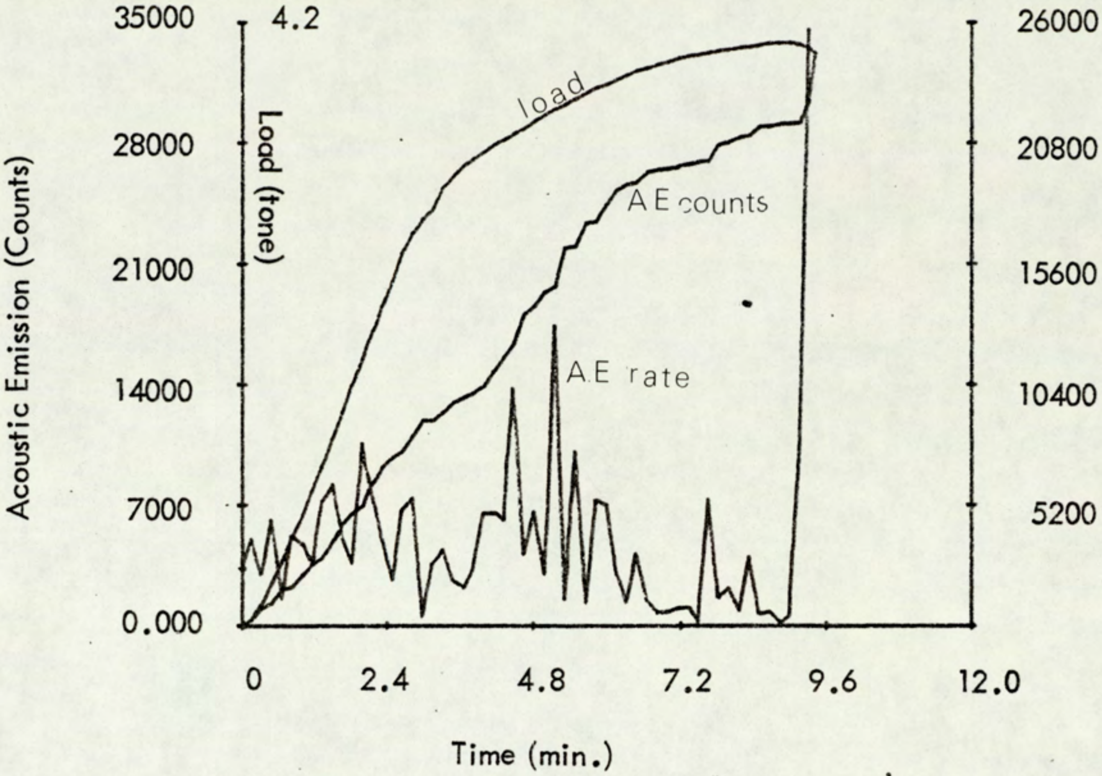

Fig. 22.a.

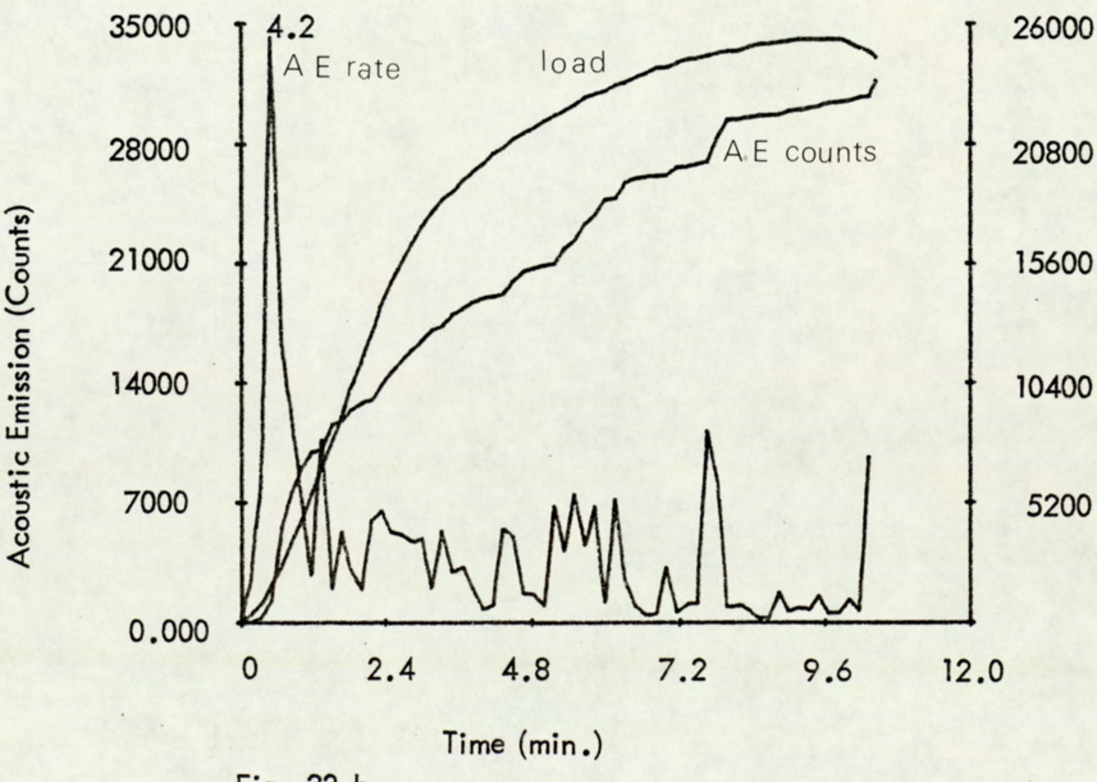

Fig. 22.b.

Fig. 22. Tensile tests of flat specimens of steel (0.67%C)

a. At elastic

b. At pre yielding

c. At fracture

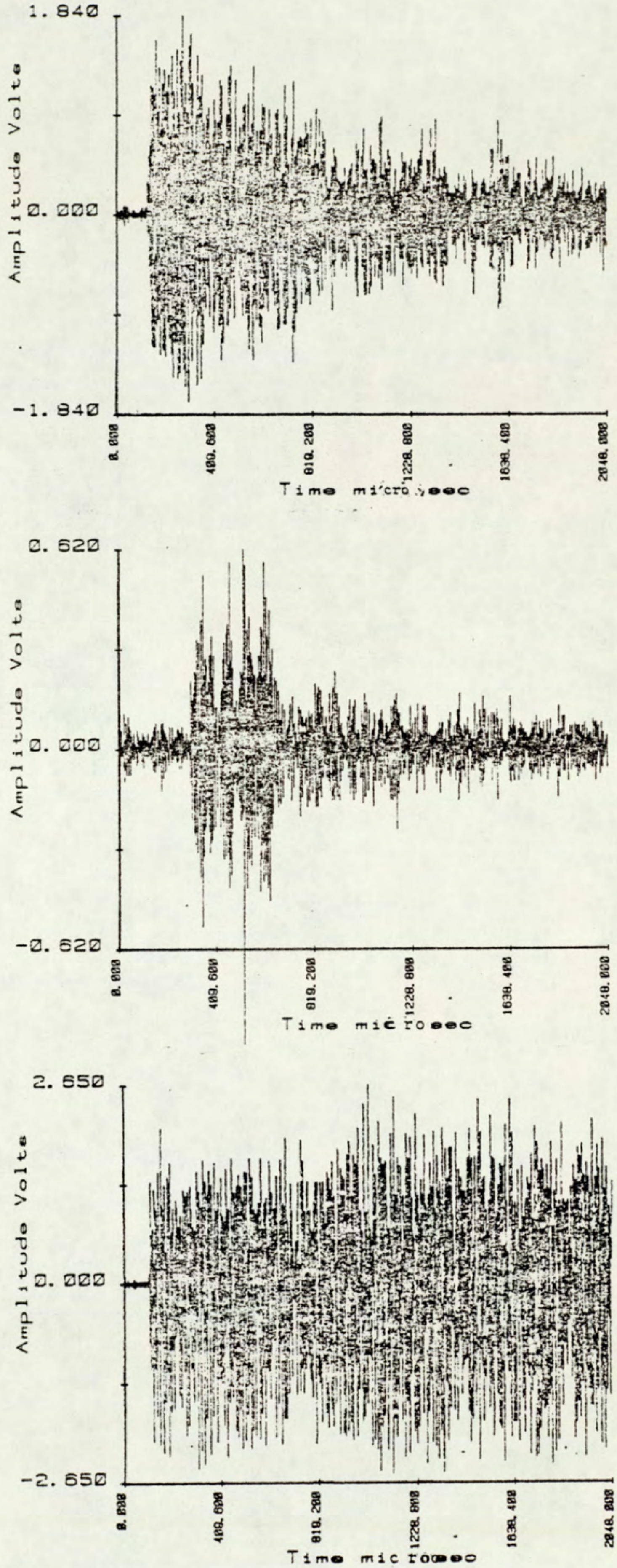

Fig. 22.a.1. Acoustic emission pulses from the tensile tests of 0.67%C steel flat specimen.

a. At elastic

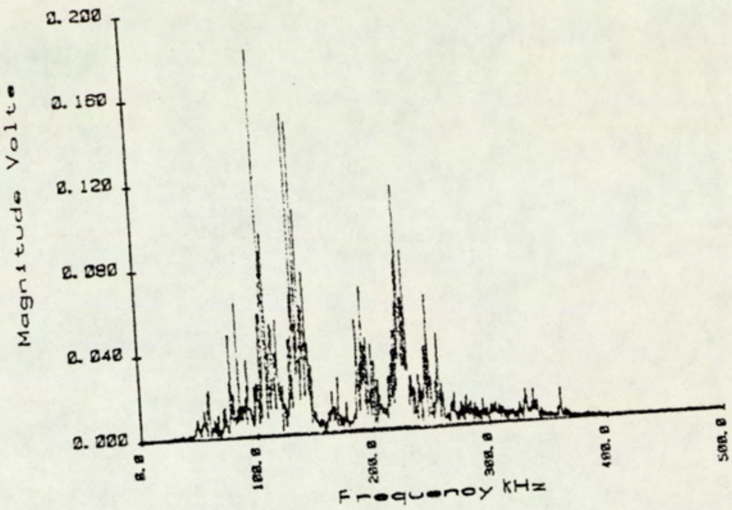

b. At pre yielding

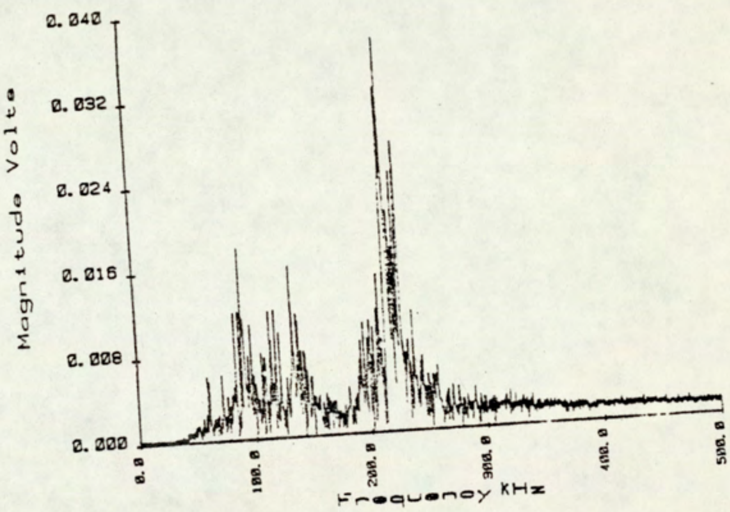

c. At fracture

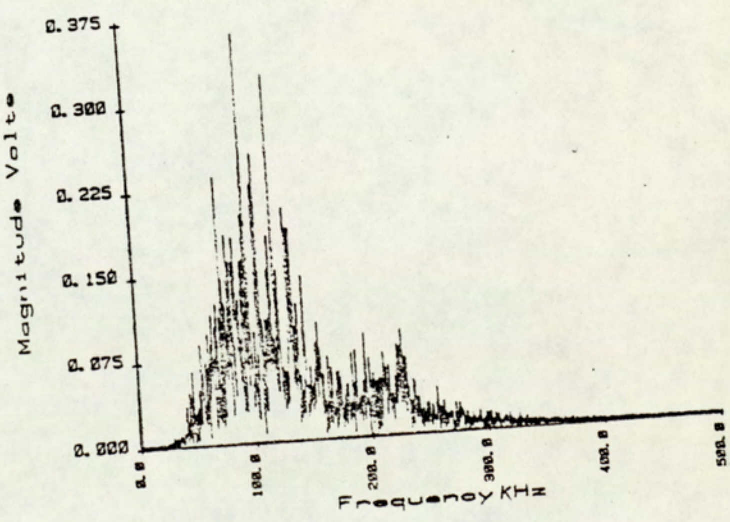

Fig. 22.a.2. F.F.T. spectrum analysis of the A.E. signals from the flat steel specimen (0.67%C).

a. At elastic

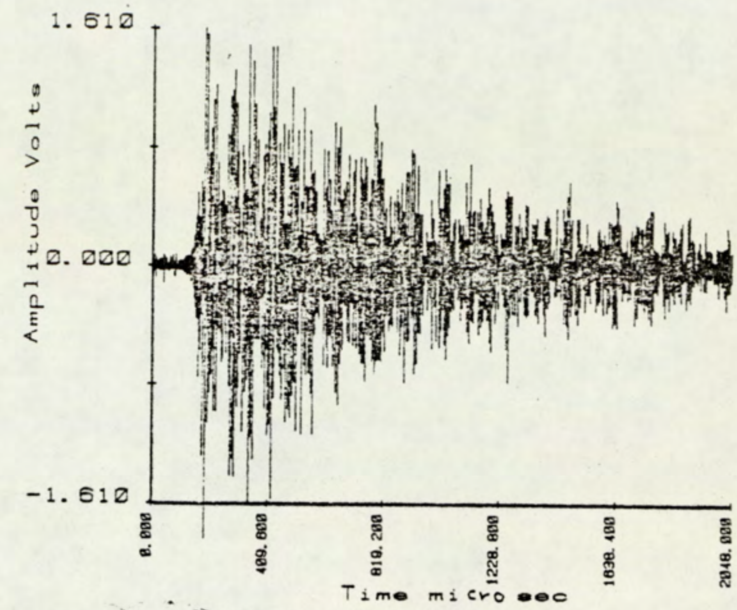

b. At pre yielding

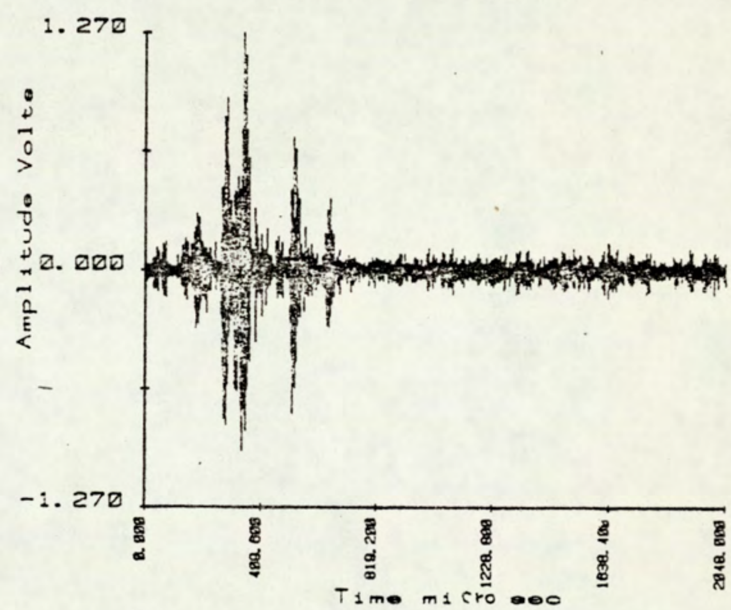

c. At fracture

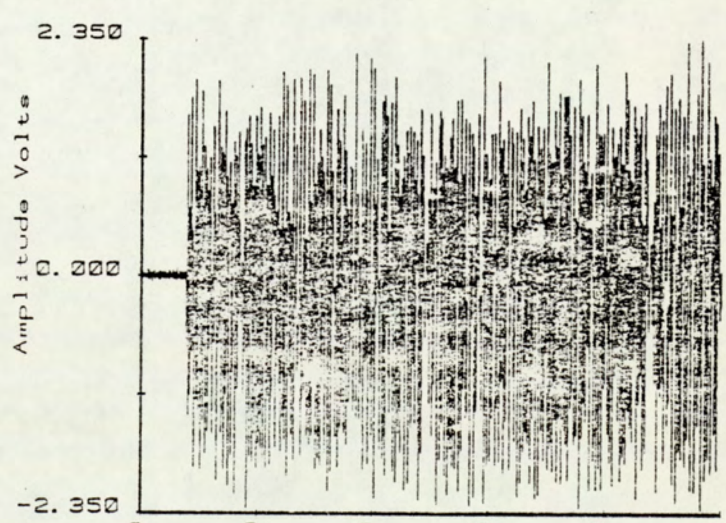

Fig. 22.b.1. Acoustic emission pulses generated from the tensile test of 0.67%C steel flat specimen.

a. At elastic

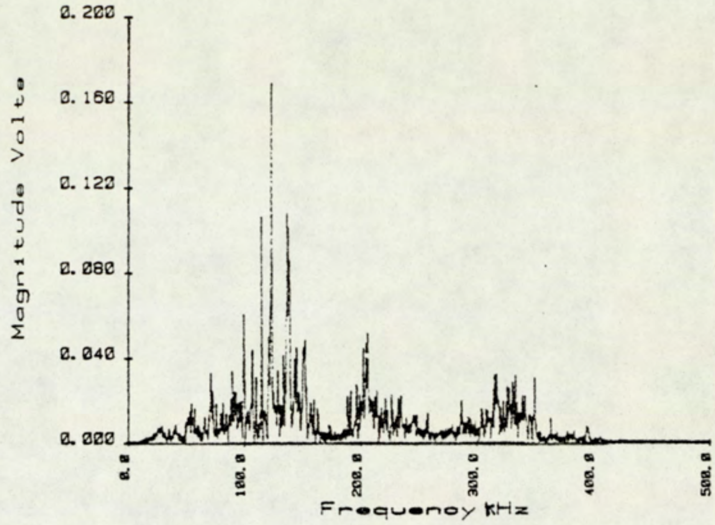

b. At pre yielding

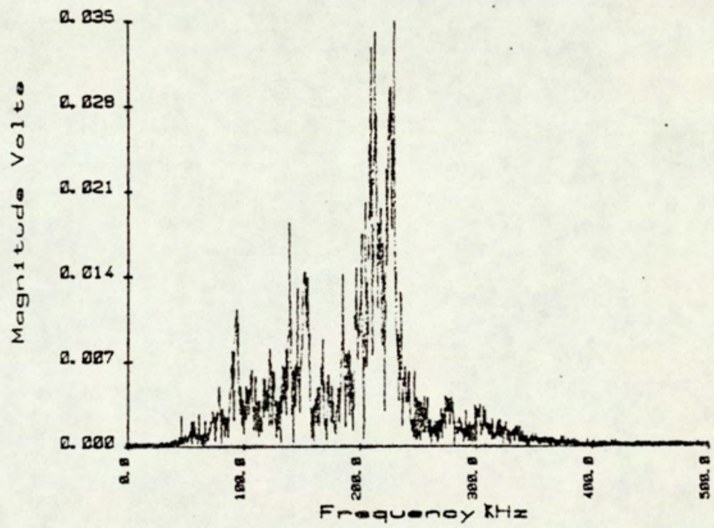

c. At fracture

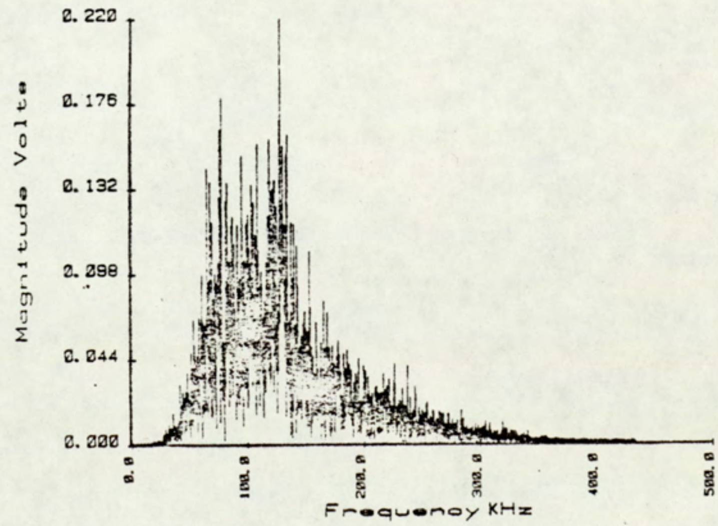

Fig. 22.b.2. F.F.T. spectrum analysis of A.E. signals from flat steel specimen (0.67%C).

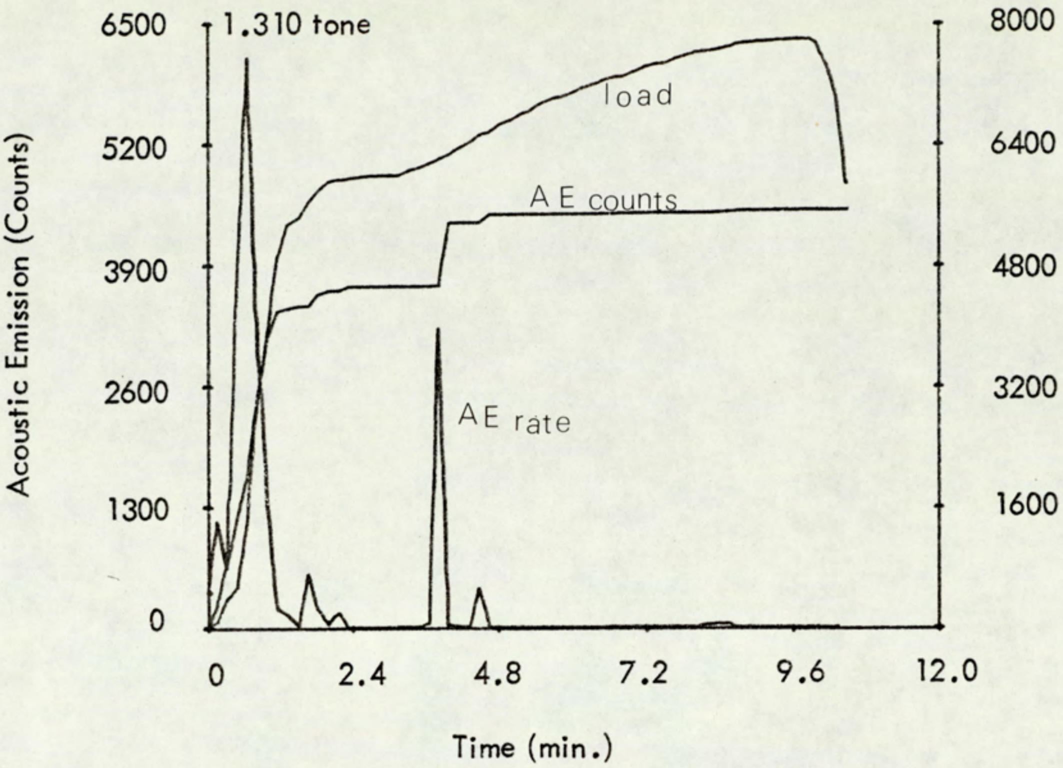

Fig. 23.a.

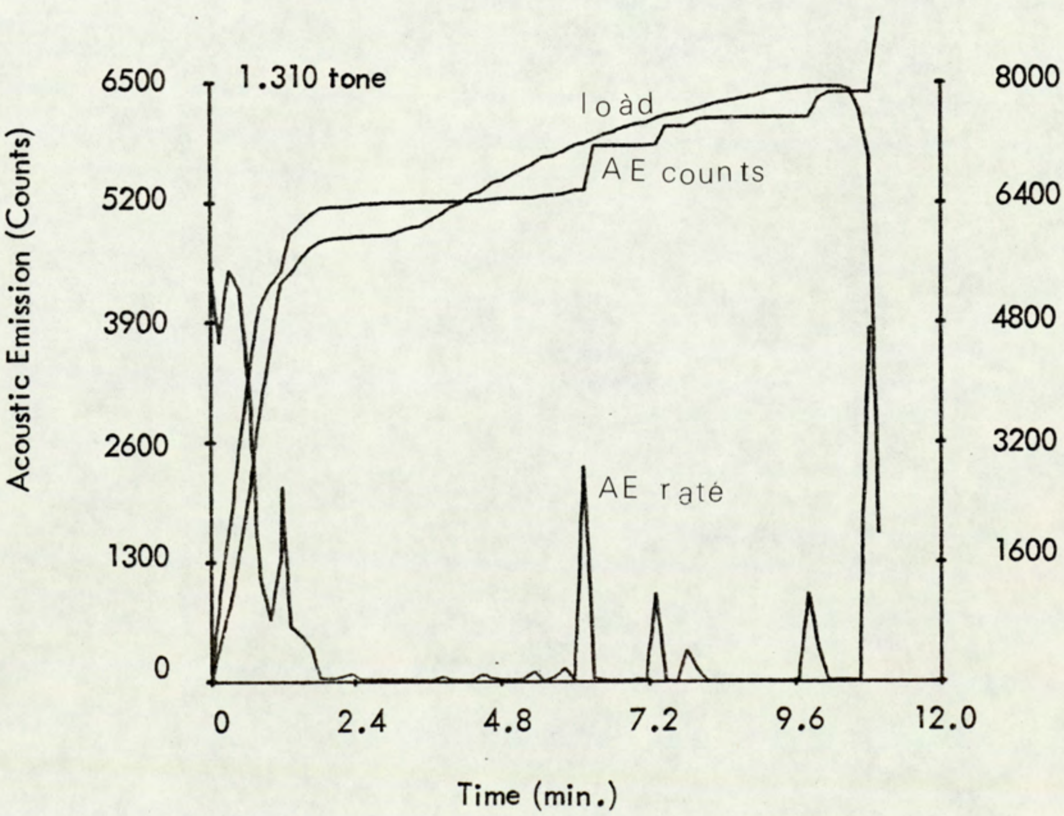

Fig. 23.b.

Fig. 23. Tensile tests of two-sided notched flat specimens of mild steel.

a. At elastic

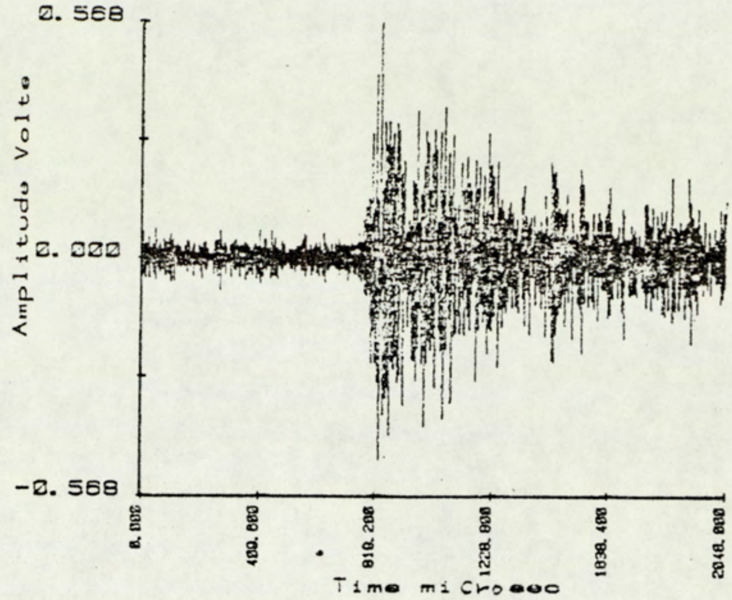

b. At pre yielding

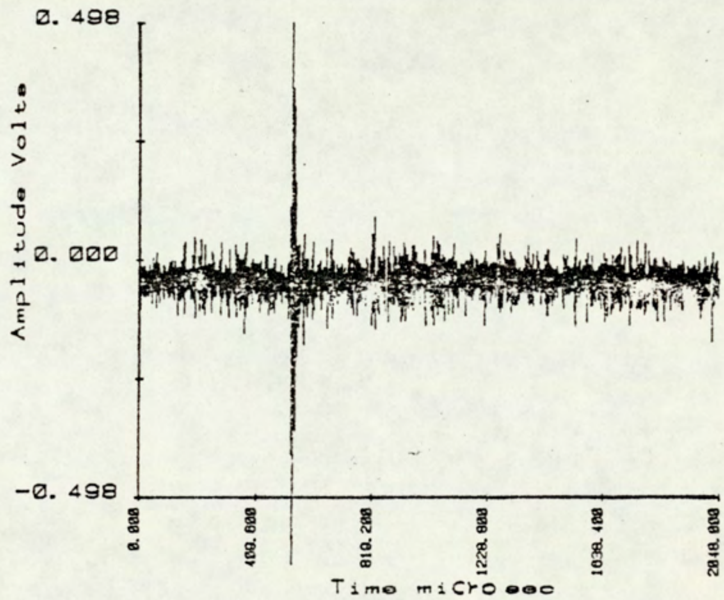

c. At fracture

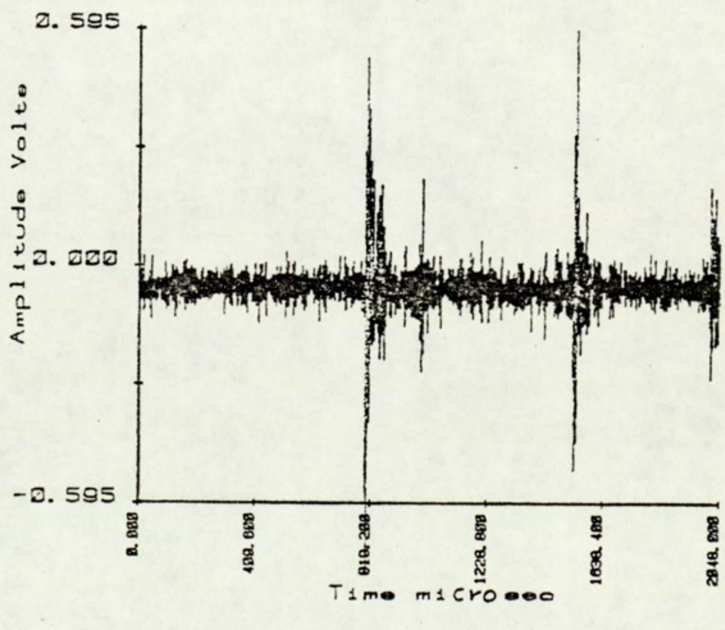

Fig. 23.a.1. Acoustic emission pulses generated from tensile test of two-sided notched specimen.

a. At elastic

b. At pre yielding

c. At fracture

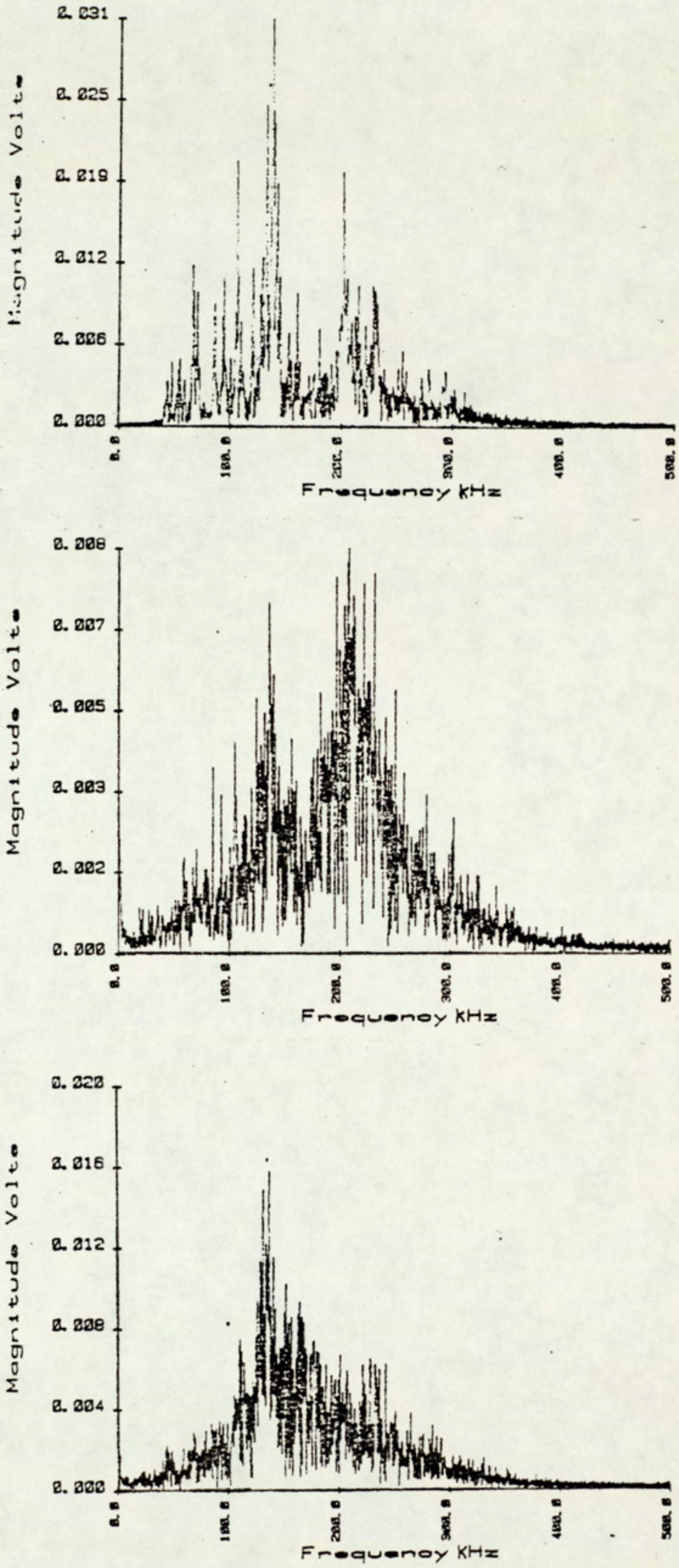

Fig. 23.a.2. F.F.T. spectrum analysis of A.E. signals from two-sided notched specimen.

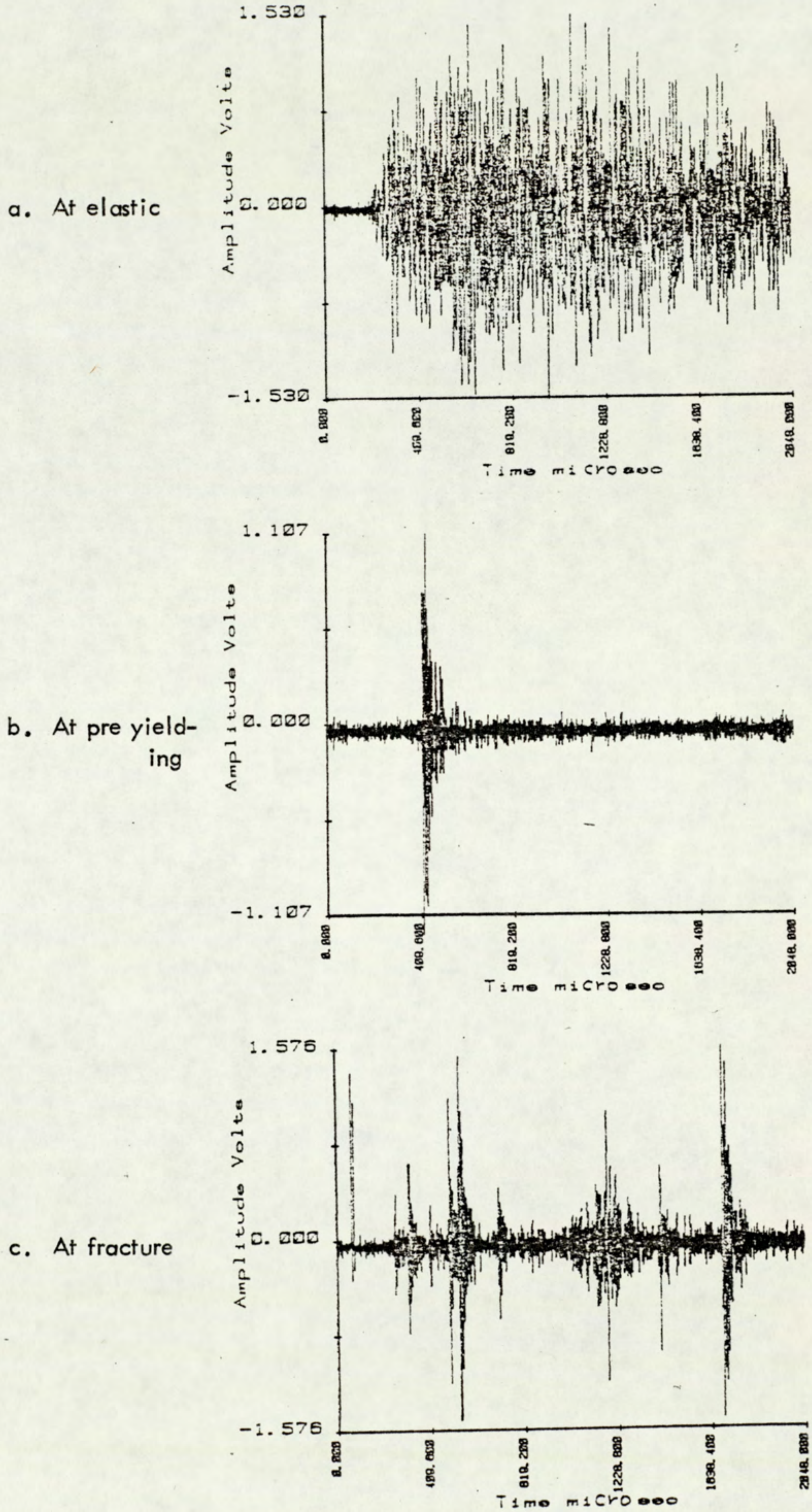

Fig. 23.b.1. Acoustic emission pulses generated from tensile test of two-sided notched specimen.

a. At elastic

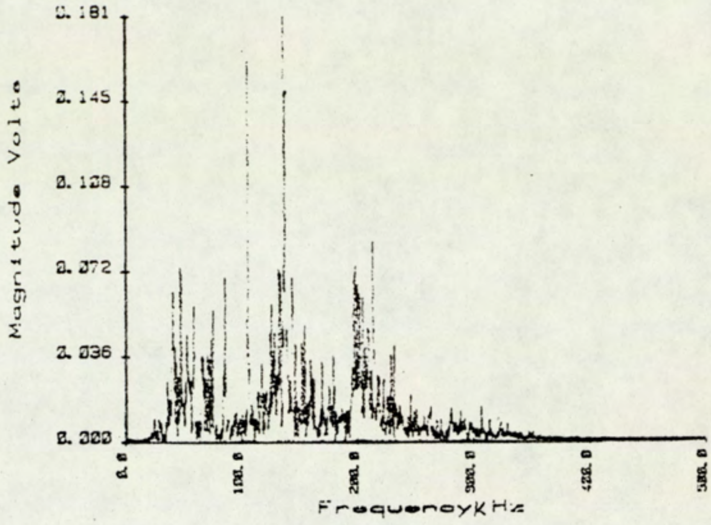

b. At pre yielding

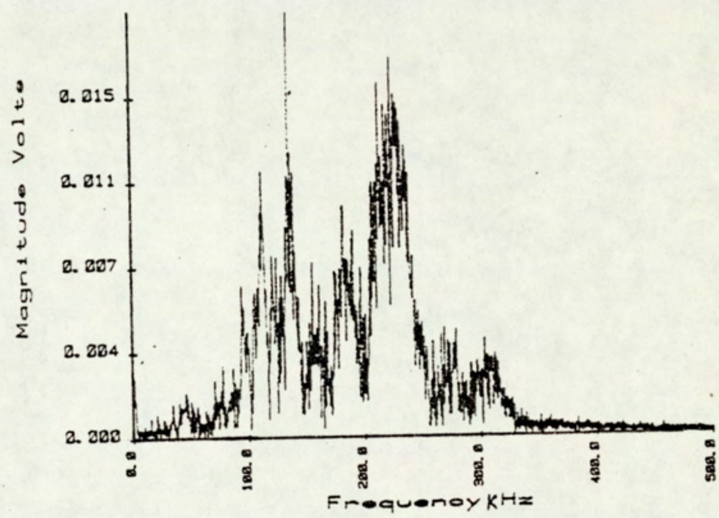

c. At fracture

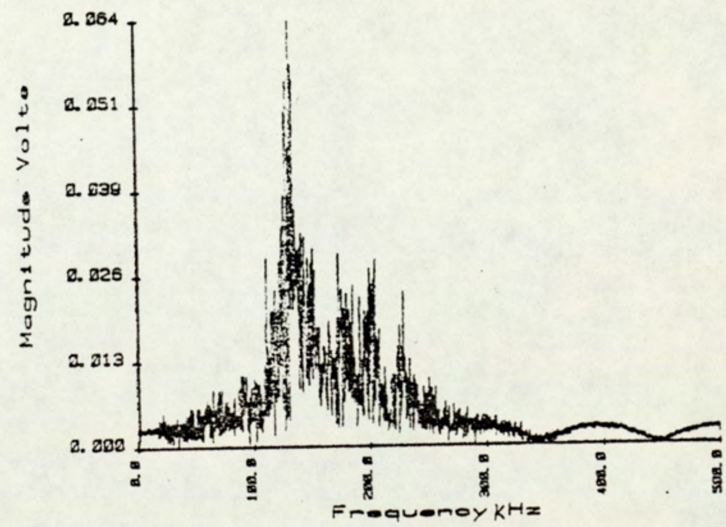

Fig. 23.b.2. F.F.T. spectrum analysis of A.E.signals from two-sided notched specimen.

Mild steel tensile specimen

Gauge length 110 mm

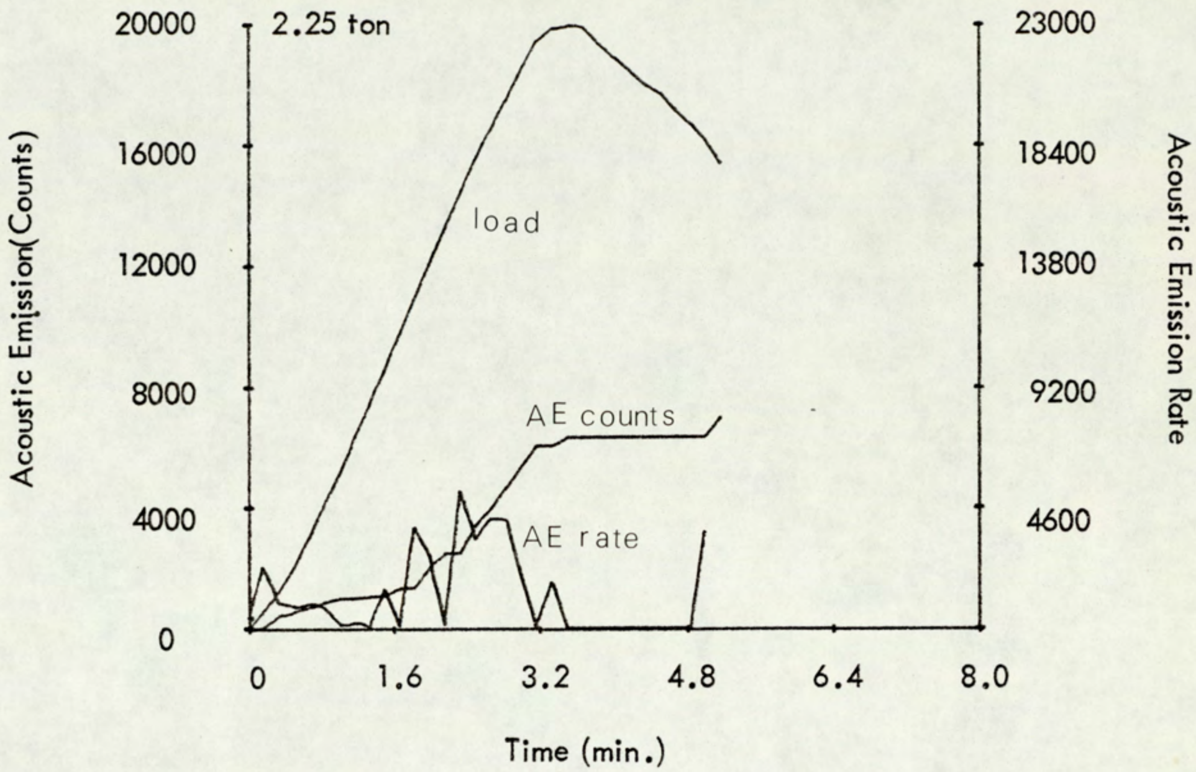

Fig. 24.a.

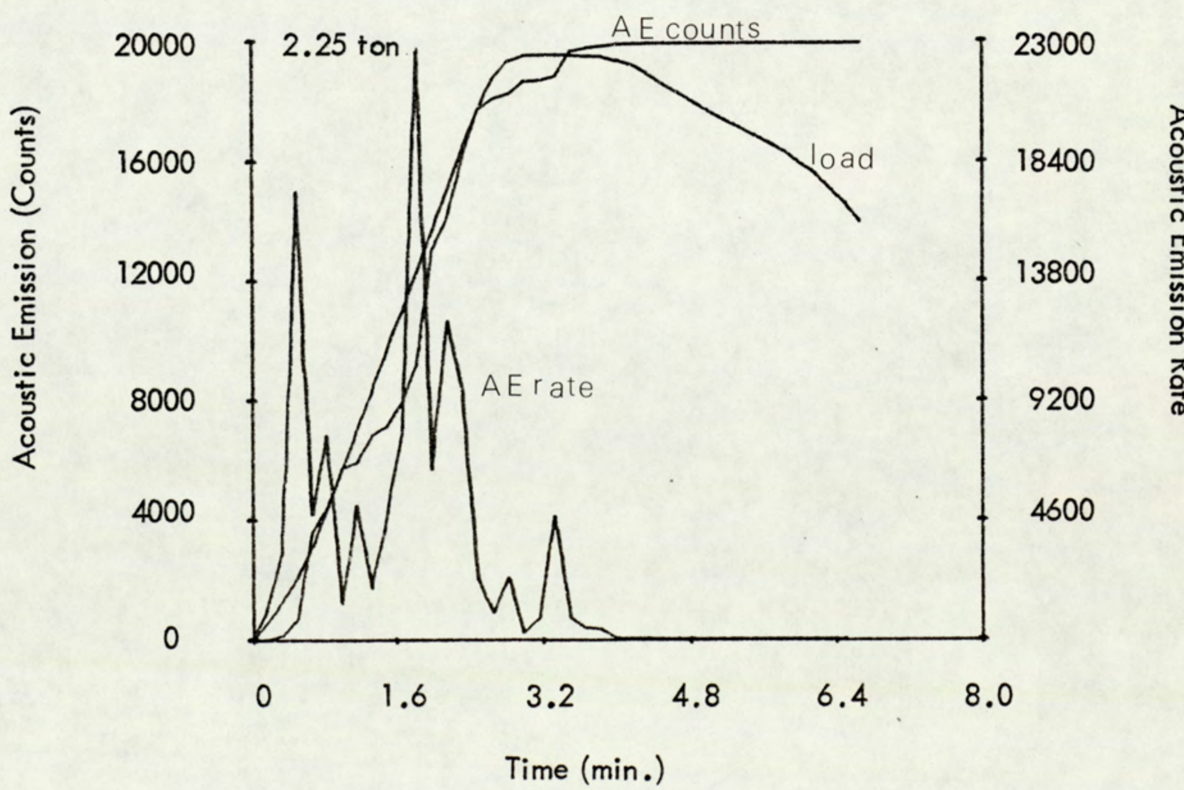

Fig. 24.b.

Fig. 24. Tensile tests of flat specimen of mild steel (gauge length = 110mm)

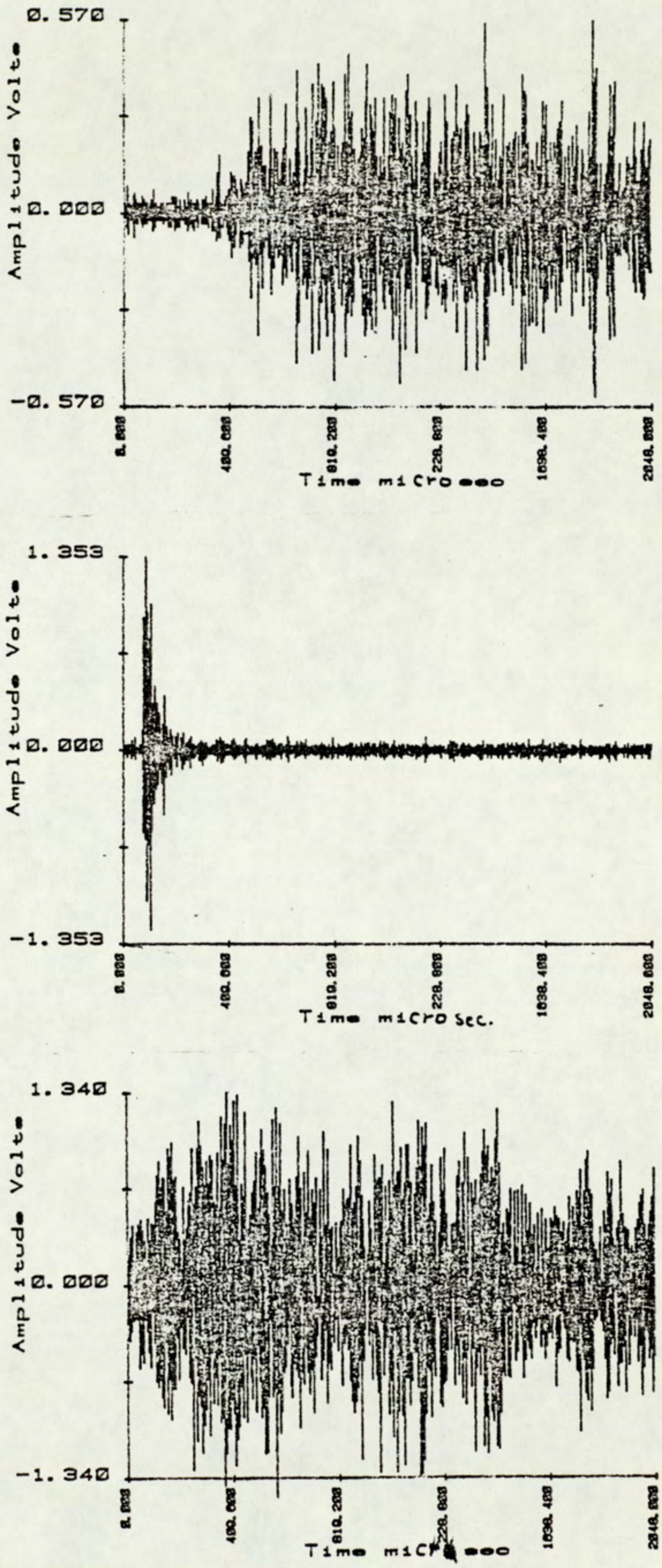

a. At elastic

b. At pre yielding

c. At near fracture

Fig. 24.a.1. Acoustic emission pulses generated from the tensile test of mild steel specimen (gauge length = 110mm)

a. At elastic

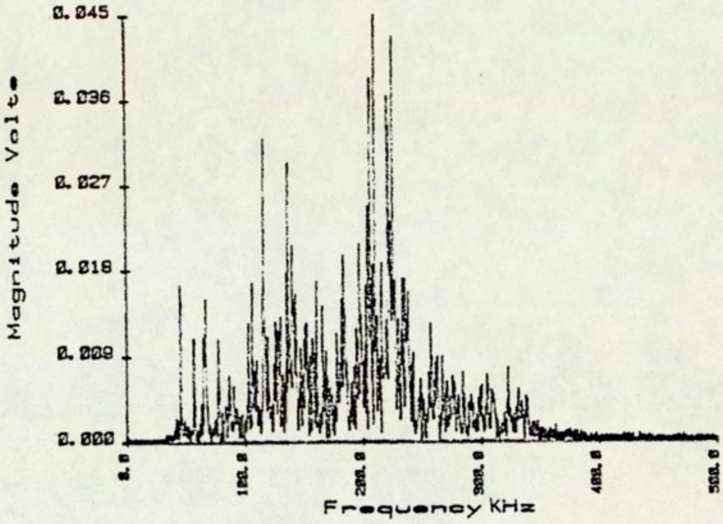

b. At pre yielding

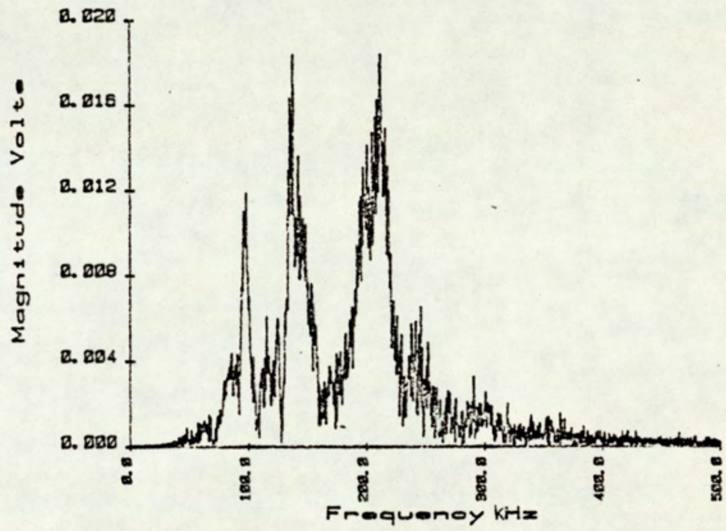

c. At near fracture

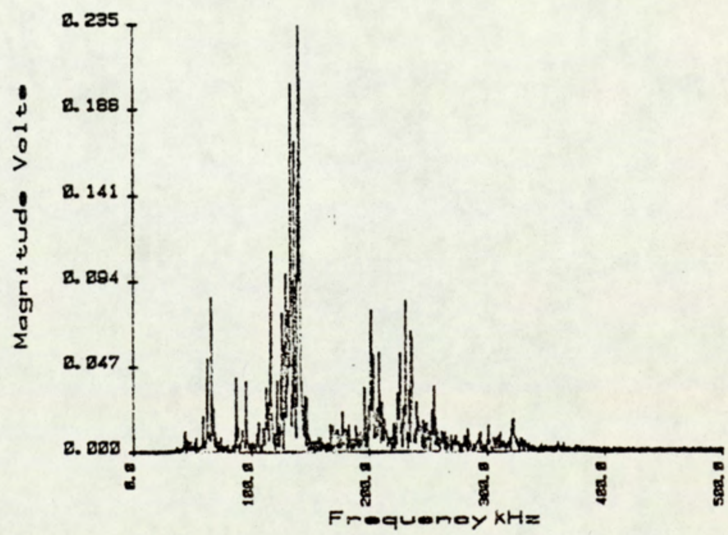

Fig. 24.a.2. F.F.T. spectrum analysis of A.E. signals from mild steel specimen (gauge length = 110mm)

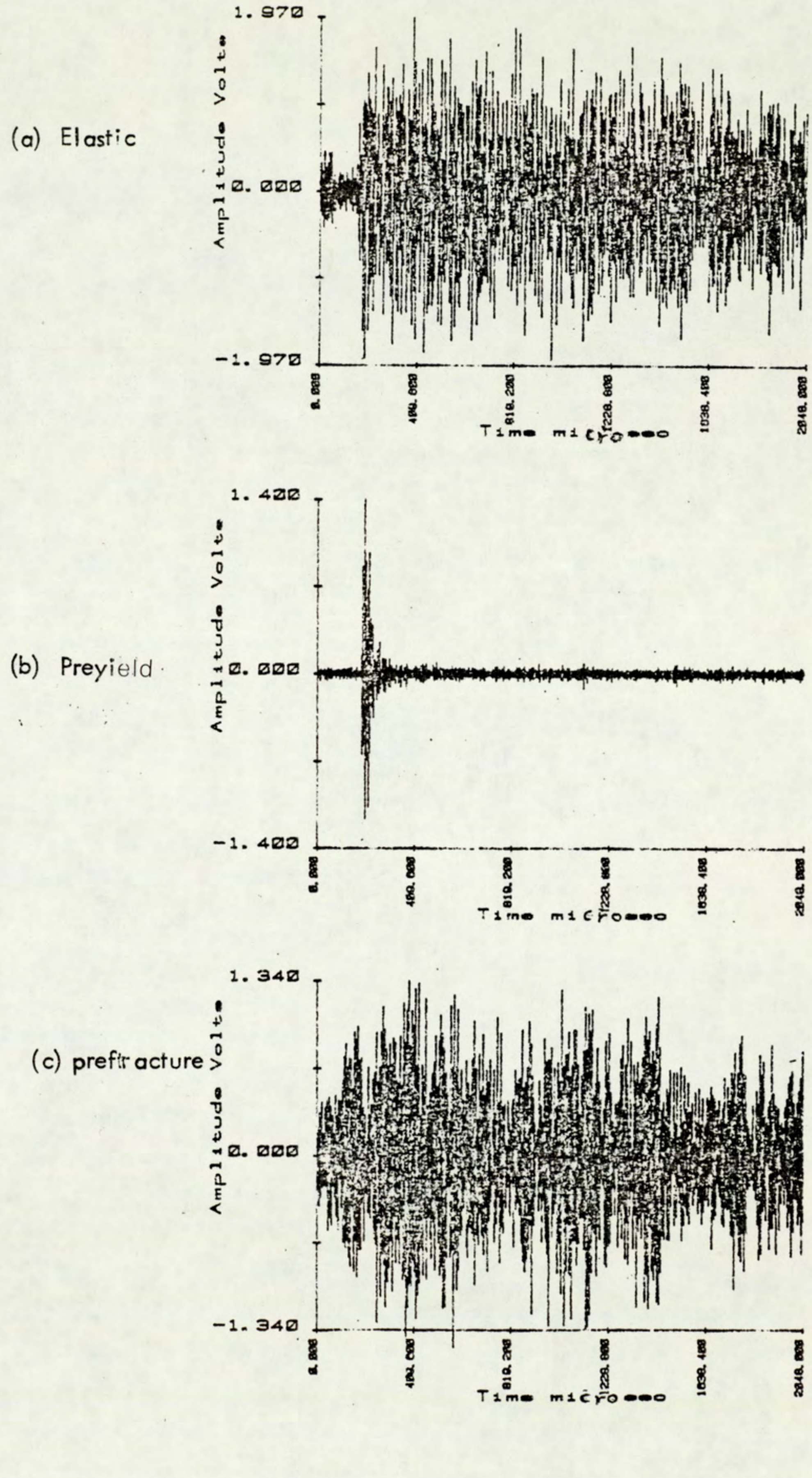

Fig. (24.b.1) A.E. pulses generated from the tensile test
gauge length = 110mm)

(a) Elastic

(b) Preyield

(c) Prefracture

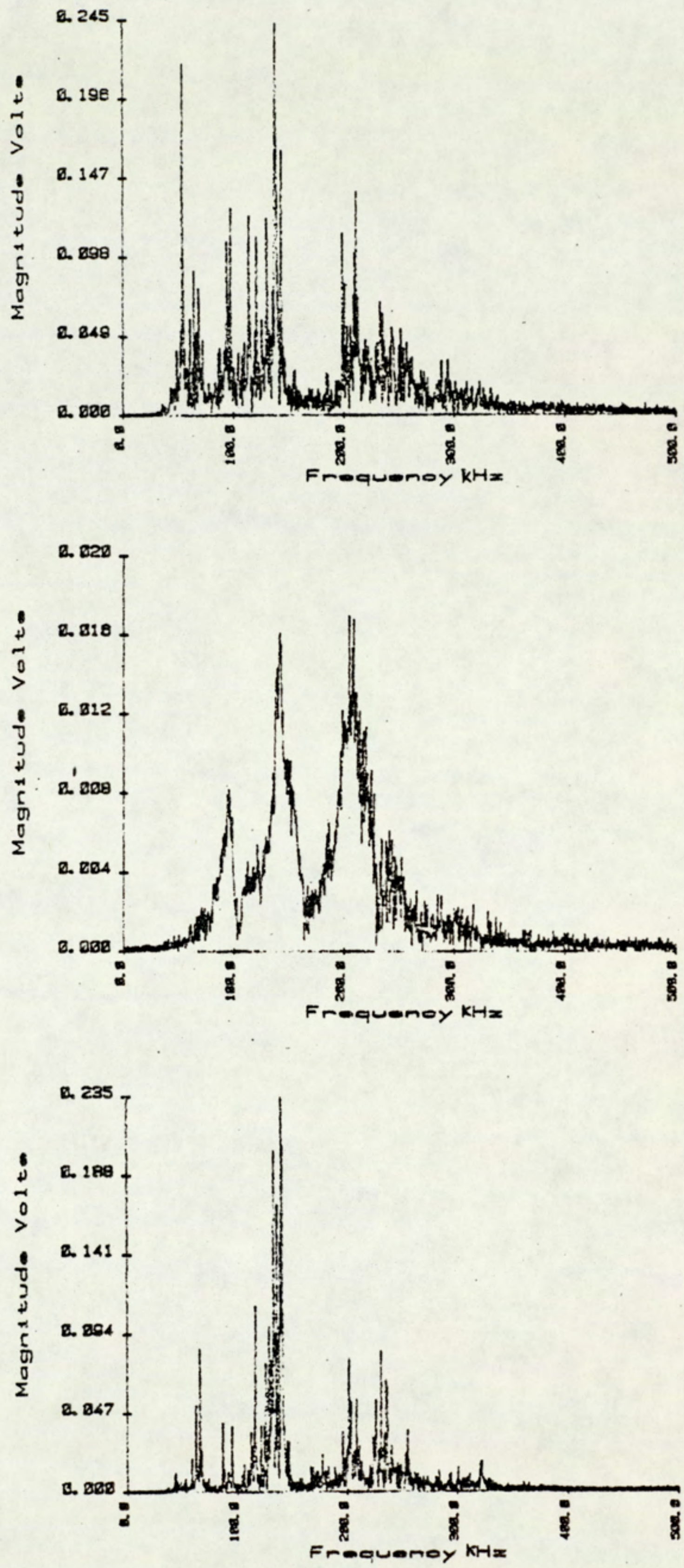

Fig. (24.b.2) F.F.T spectrum analysis of A.E. signals from mild steel (gauge length = 110mm)

Mild steel tensile specimen

Gauge length 370 mm

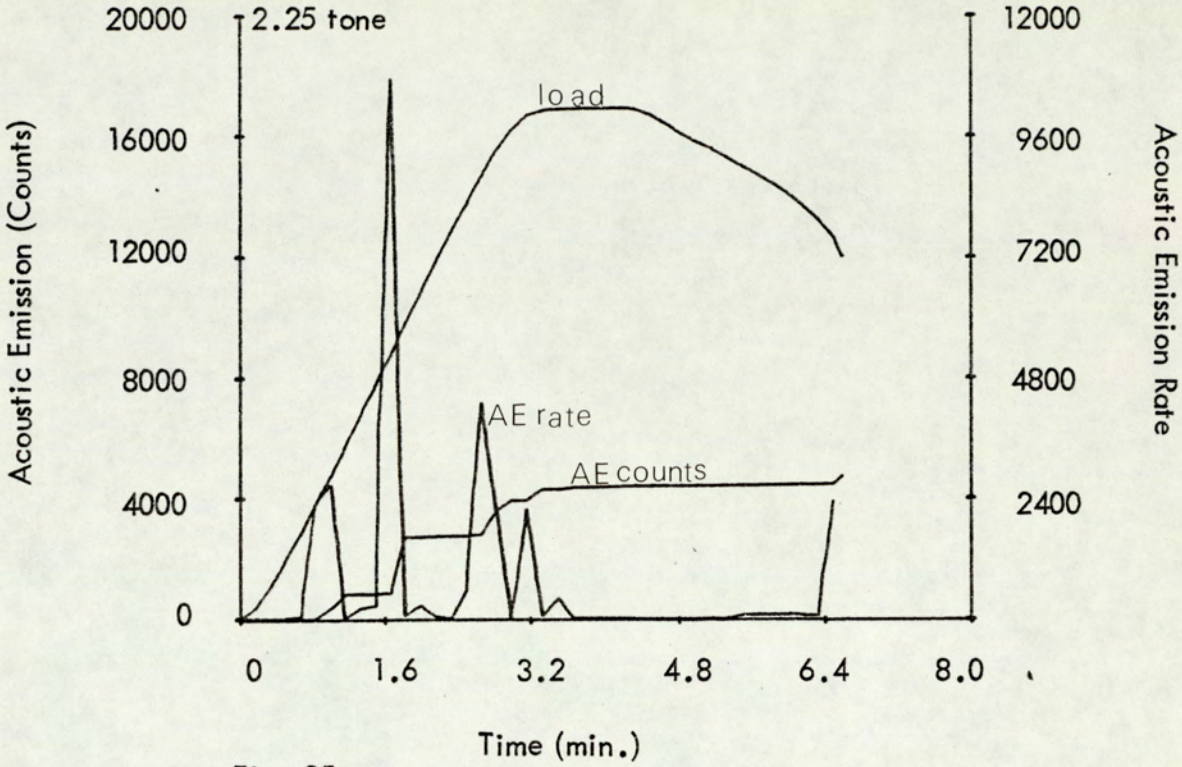

Fig. 25.a.

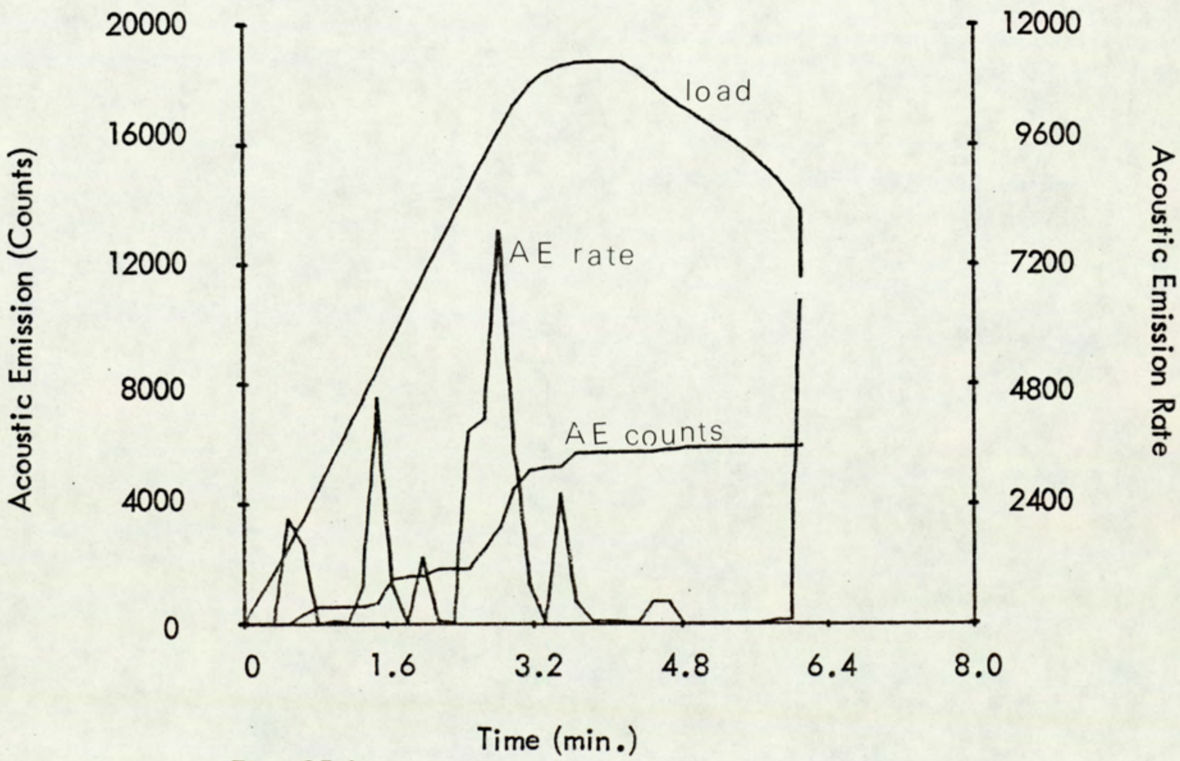

Fig. 25.b.

Fig. 25. Tensile tests of flat specimens of mild steel (gauge length = 370mm)

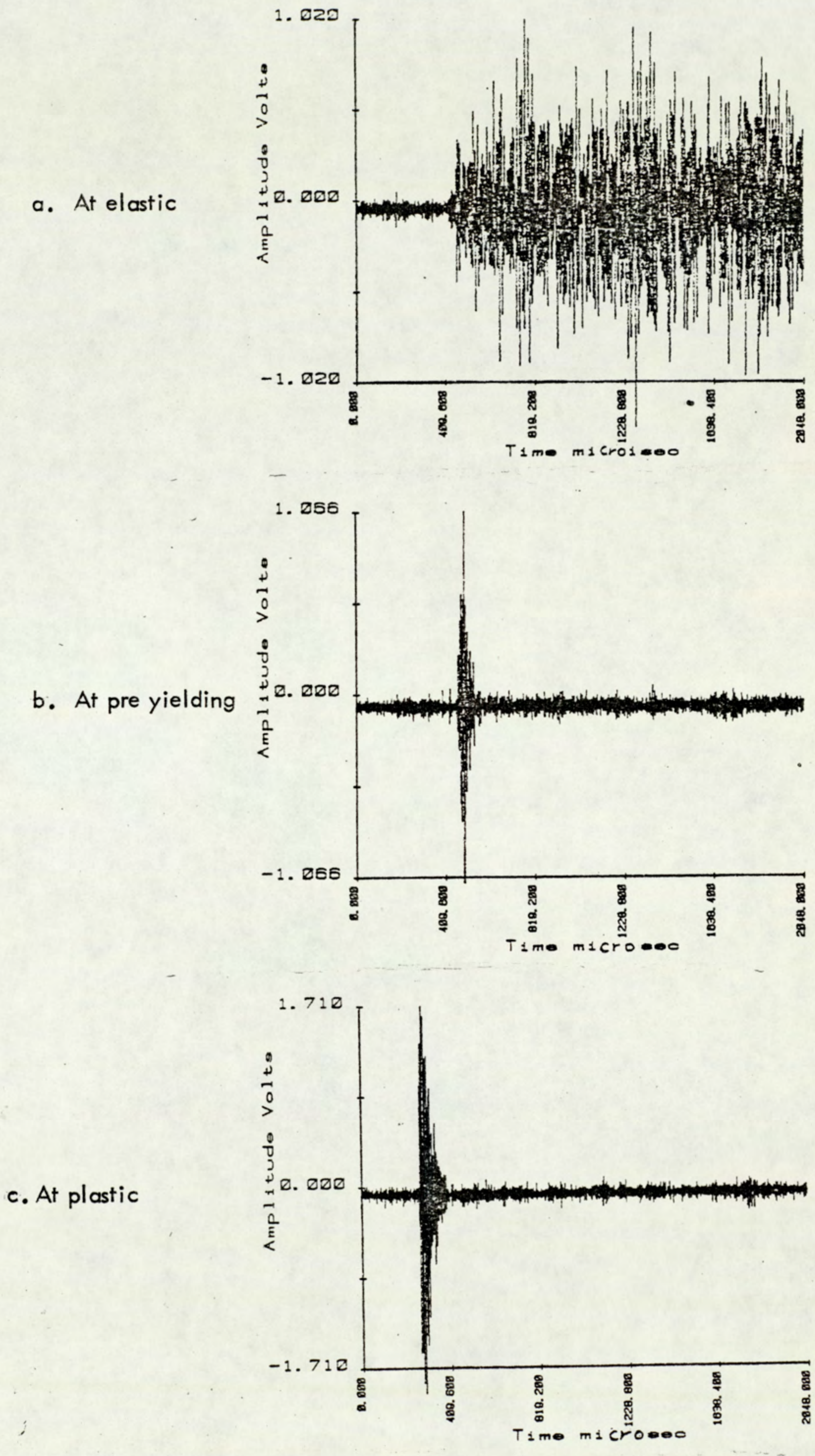

Fig. 25.a.1. Acoustic emission pulses generated from the tensile test of mild steel specimen (gauge length = 370mm).

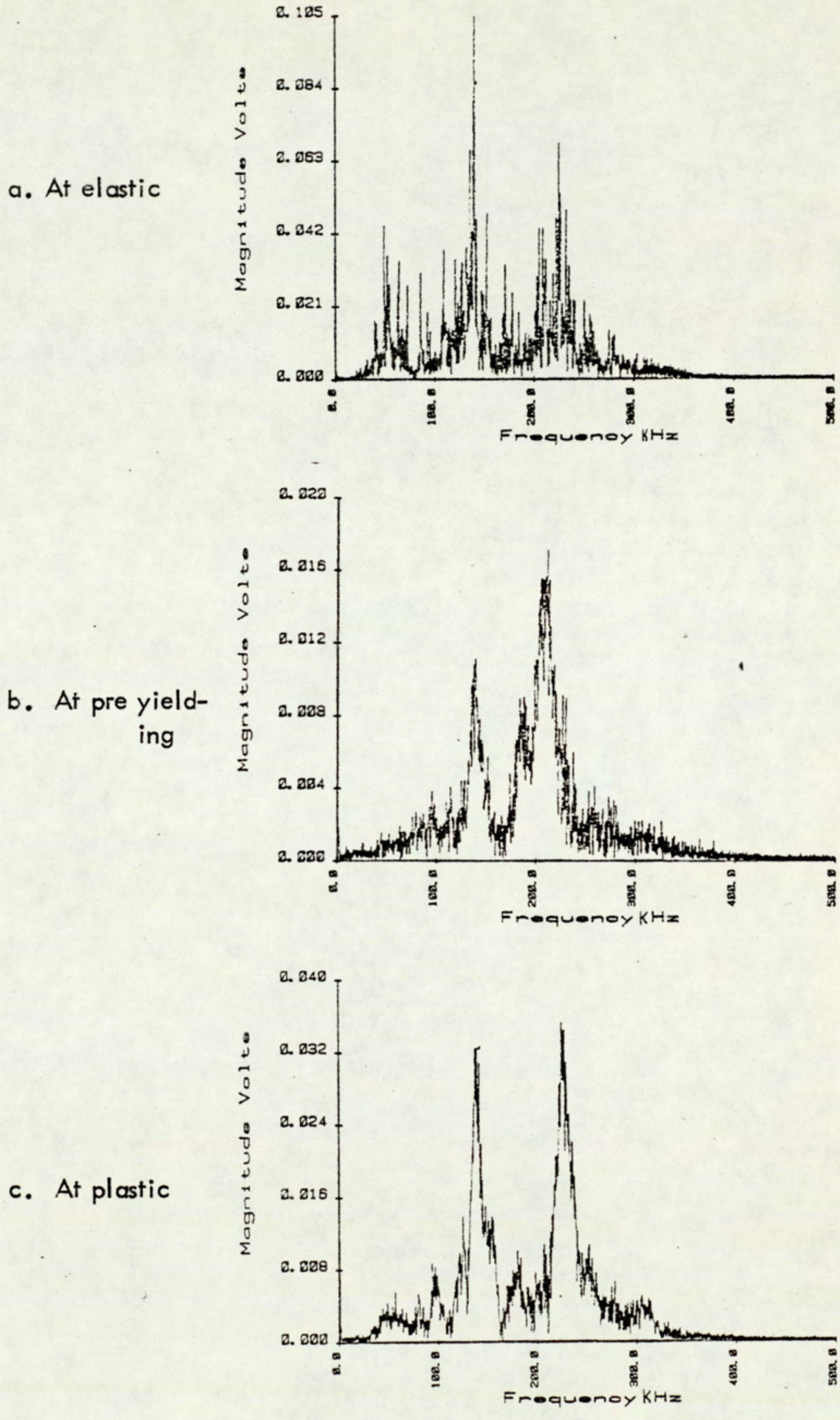

Fig. 25.a.2. F.F.T. spectrum analysis of A.E. signals from mild steel specimen (gauge length = 370mm).

a. At elastic

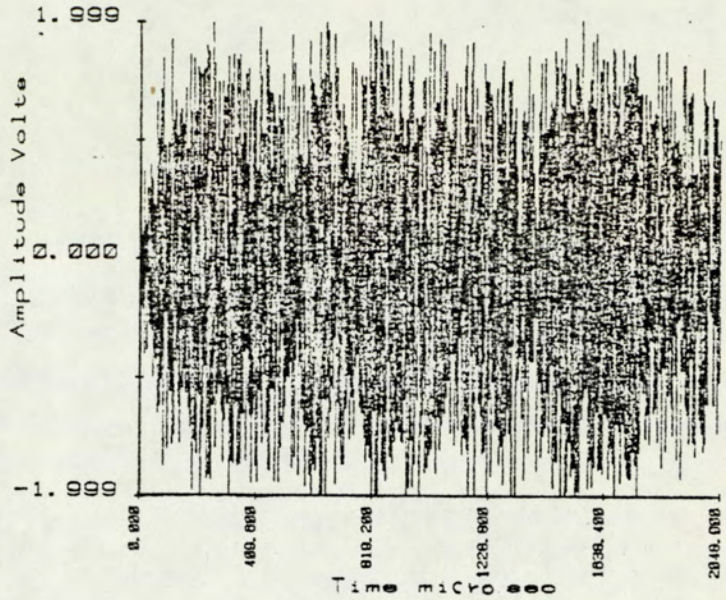

b. At pre yielding

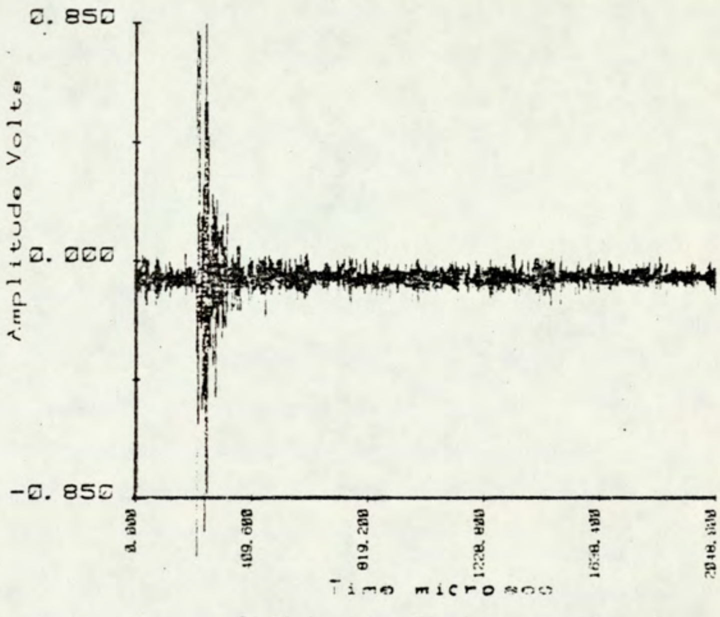

c. At plastic

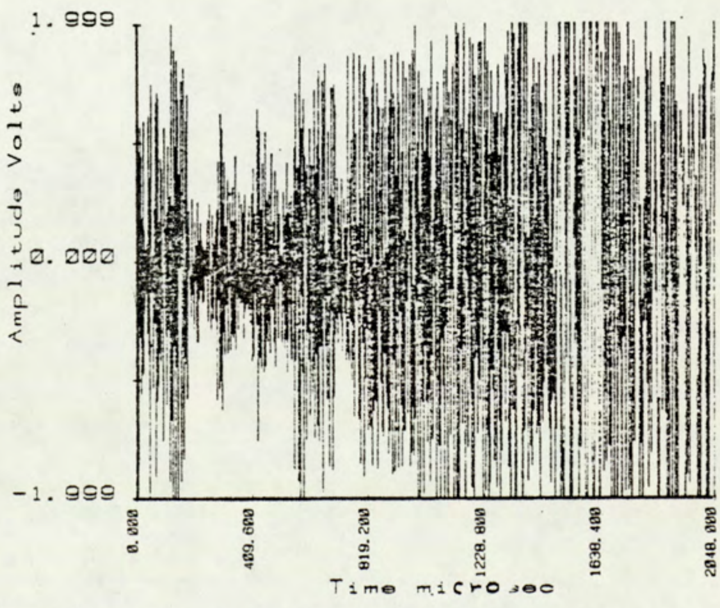

Fig. 25.b.1. A.E. pulses generated from tensile test of mild steel specimen (gauge length = 370mm).

a. At elastic

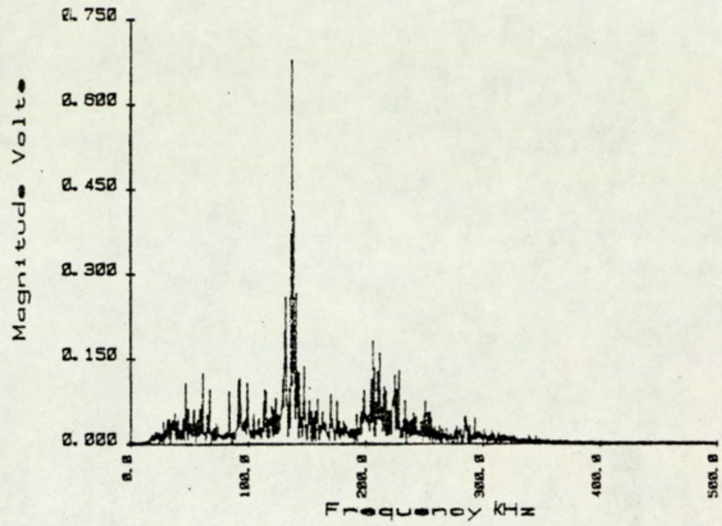

b. At pre yielding

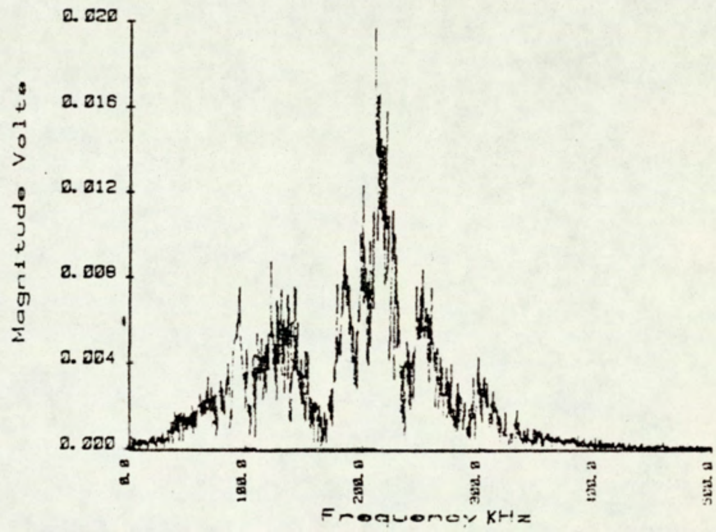

c. At plastic

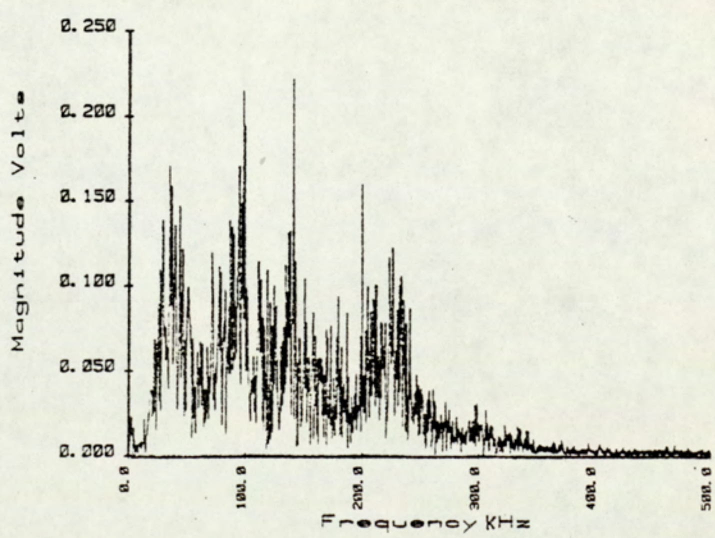

Fig. 25.b.2. F.F.T. spectrum analysis of A.E. signals from mild steel specimen (gauge length = 370mm).

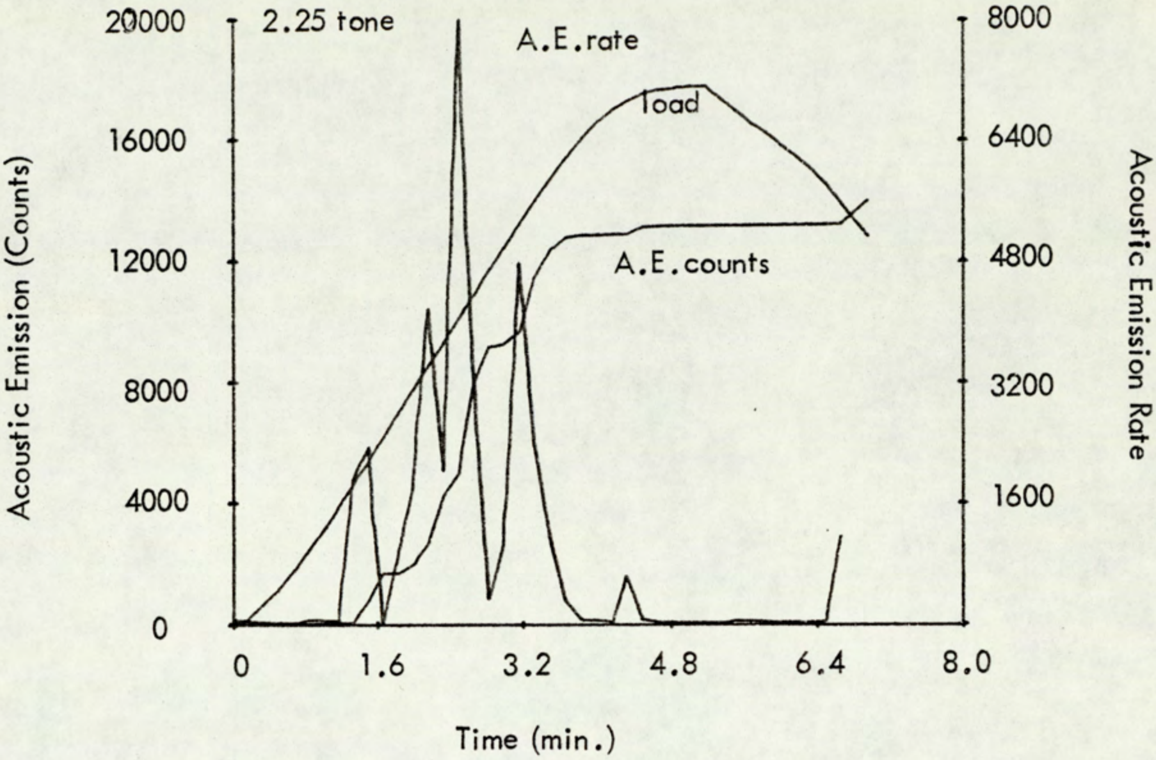

Fig. 26.a.

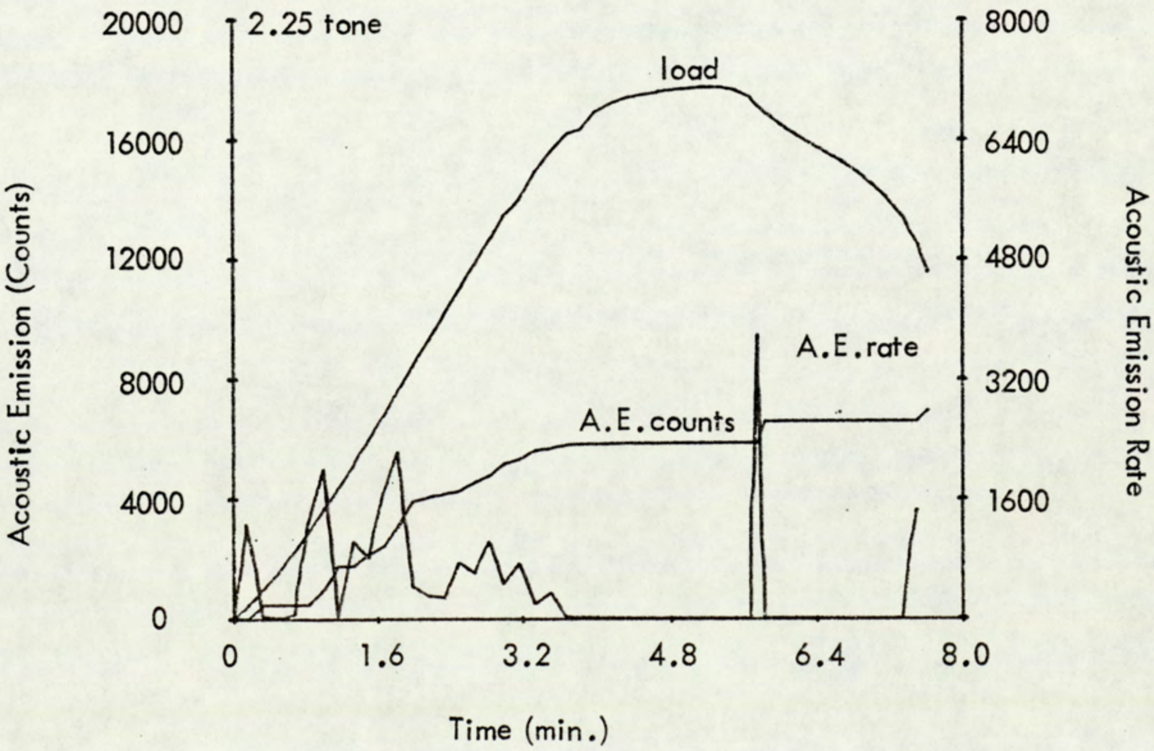

Fig. 26.b.

Fig. 26. Tensile tests of flat specimens of mild steel (gauge length = 620 mm)

a. At elastic

b. At pre yielding

c. At fracture

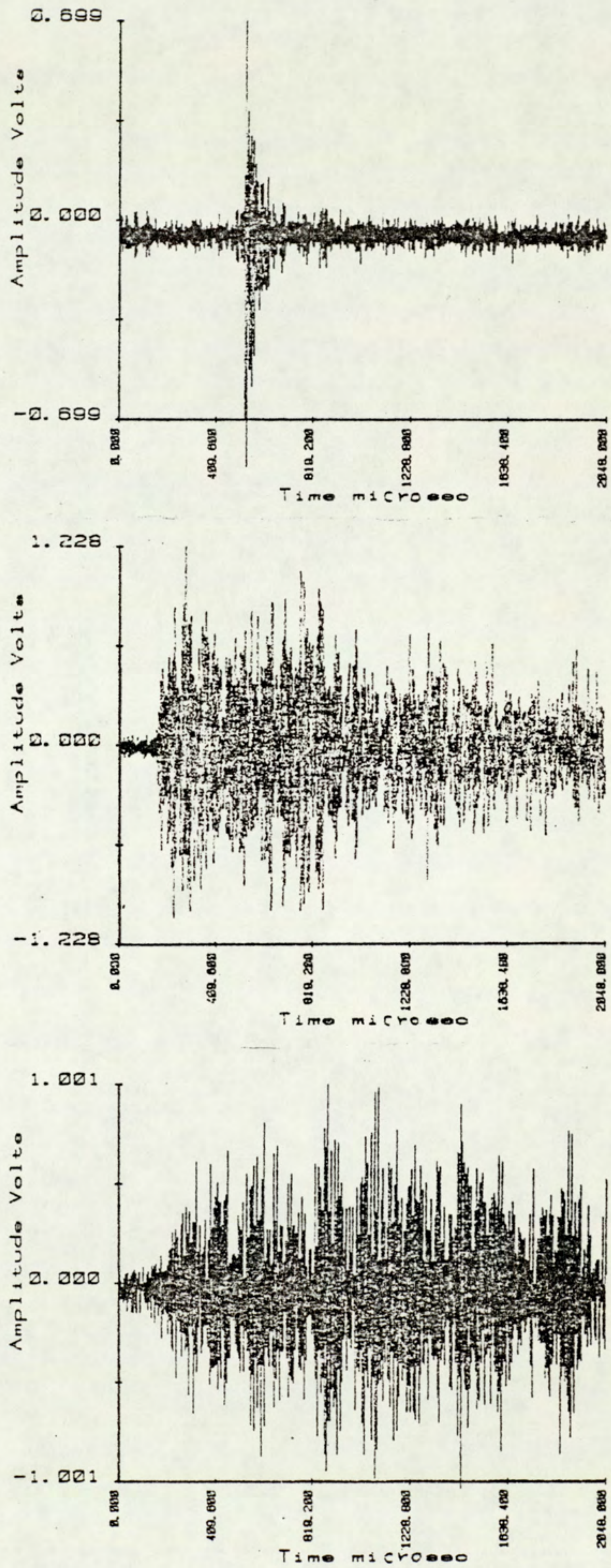

Fig. 26.a.1. A.E. pulses generated from tensile test of mild steel specimen (gauge l ength = 620mm).

a. At elastic

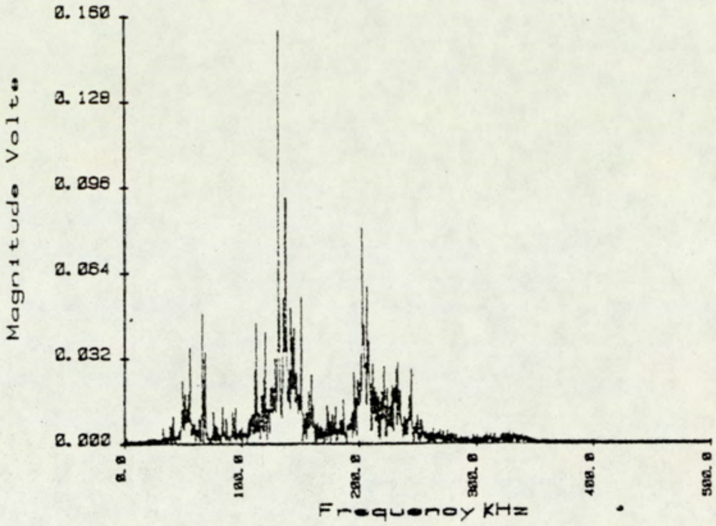

b. At pre yielding

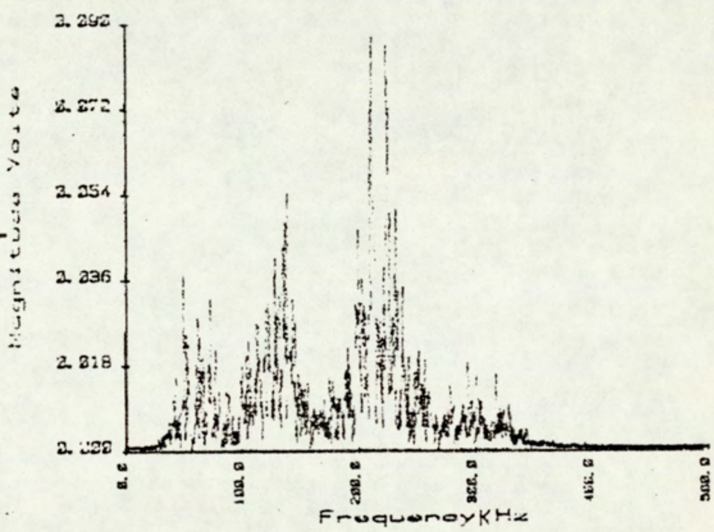

c. At fracture

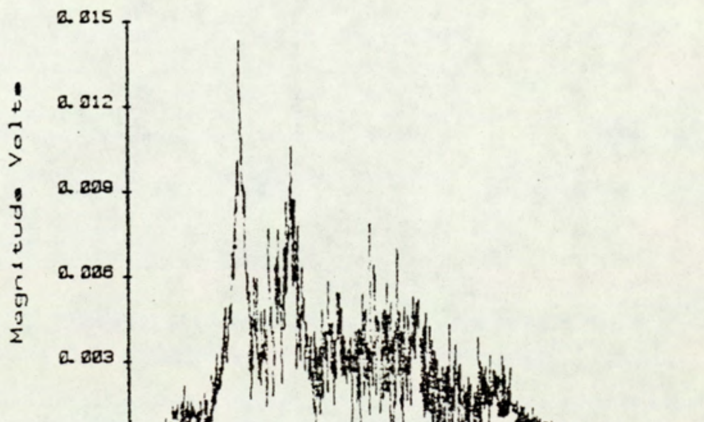

Fig. 26.a.2. F.F.T. spectrum analysis of the signals from mild steel specimen (gauge length = 620mm).

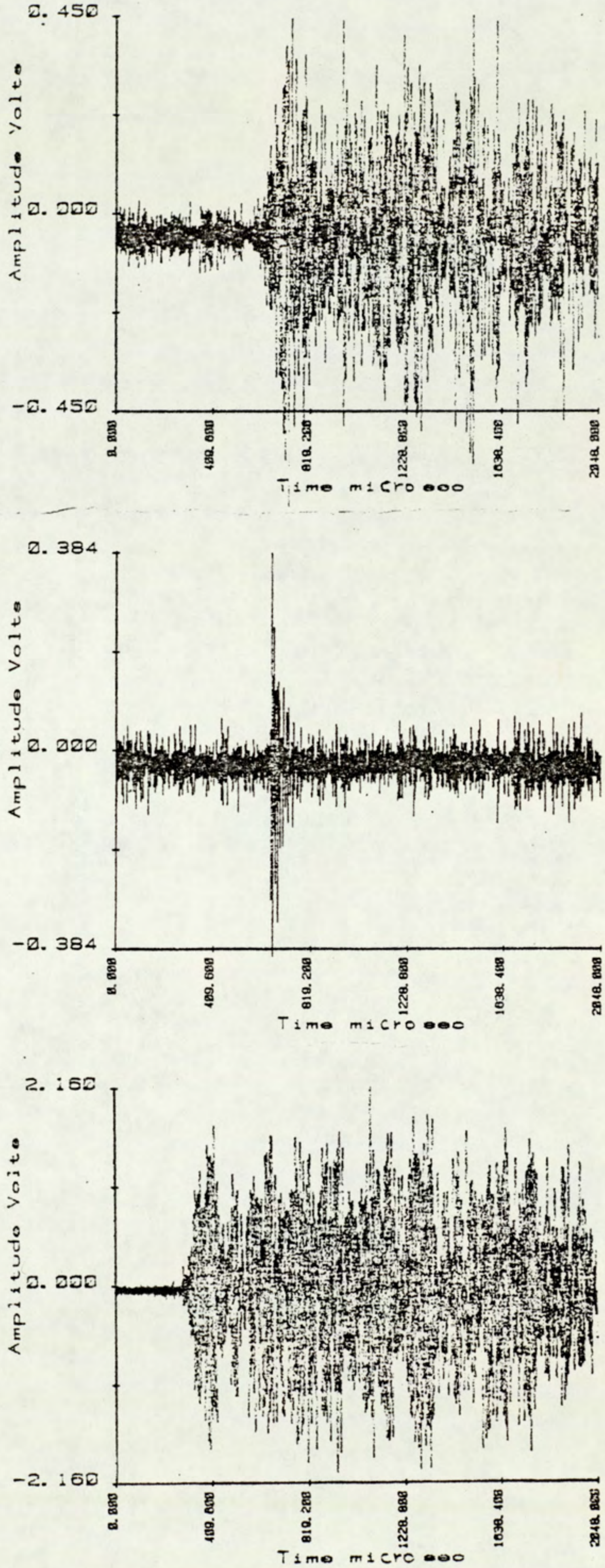

a. At elastic

b. At pre yielding

c. At fracture

Fig. 26.b.1. A.E. pulses generated from tensile test of mild steel specimen (gauge length = 620mm).

a. At elastic

b. At pre yield ing

c. At fracture

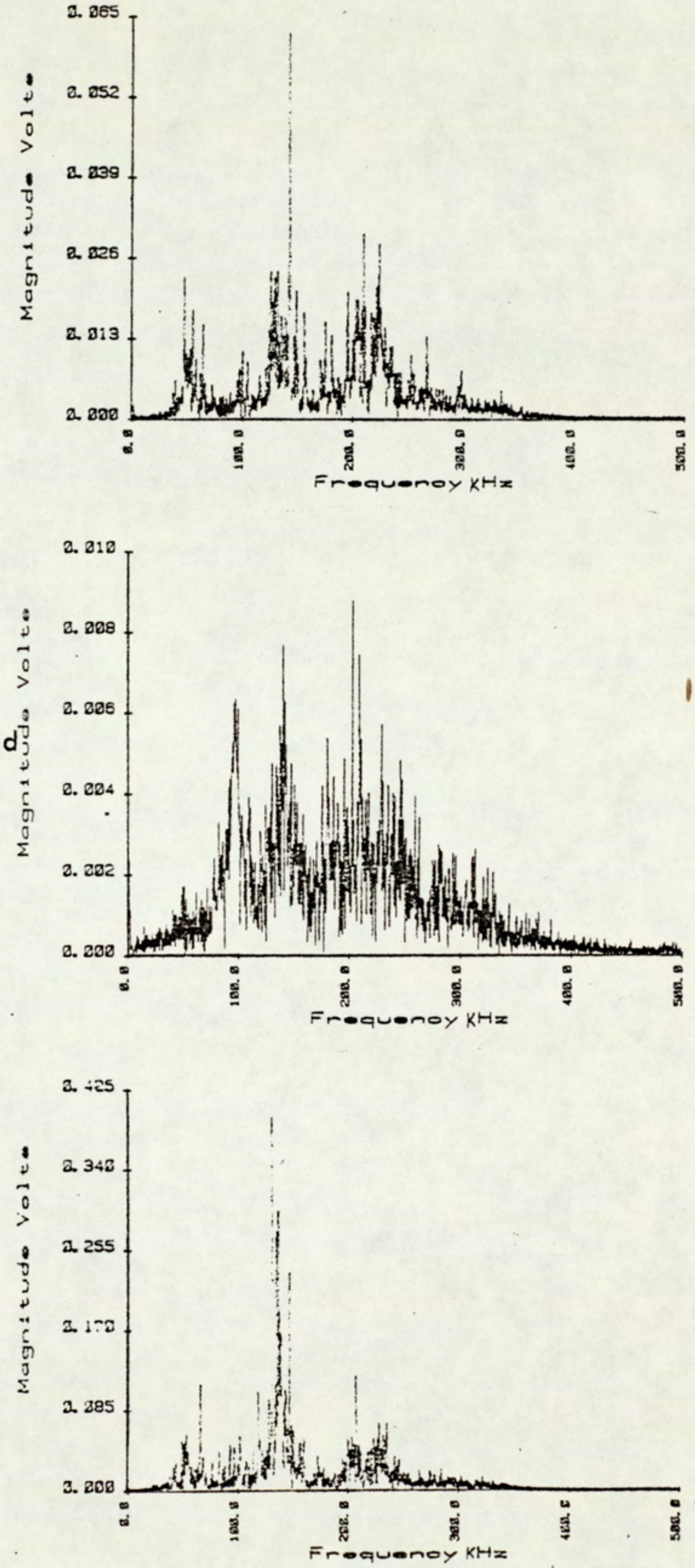

Fig. 26.b.2. F.F.T. spectrum analysis of the signals from mild steel specimen (gauge length = 620mm).

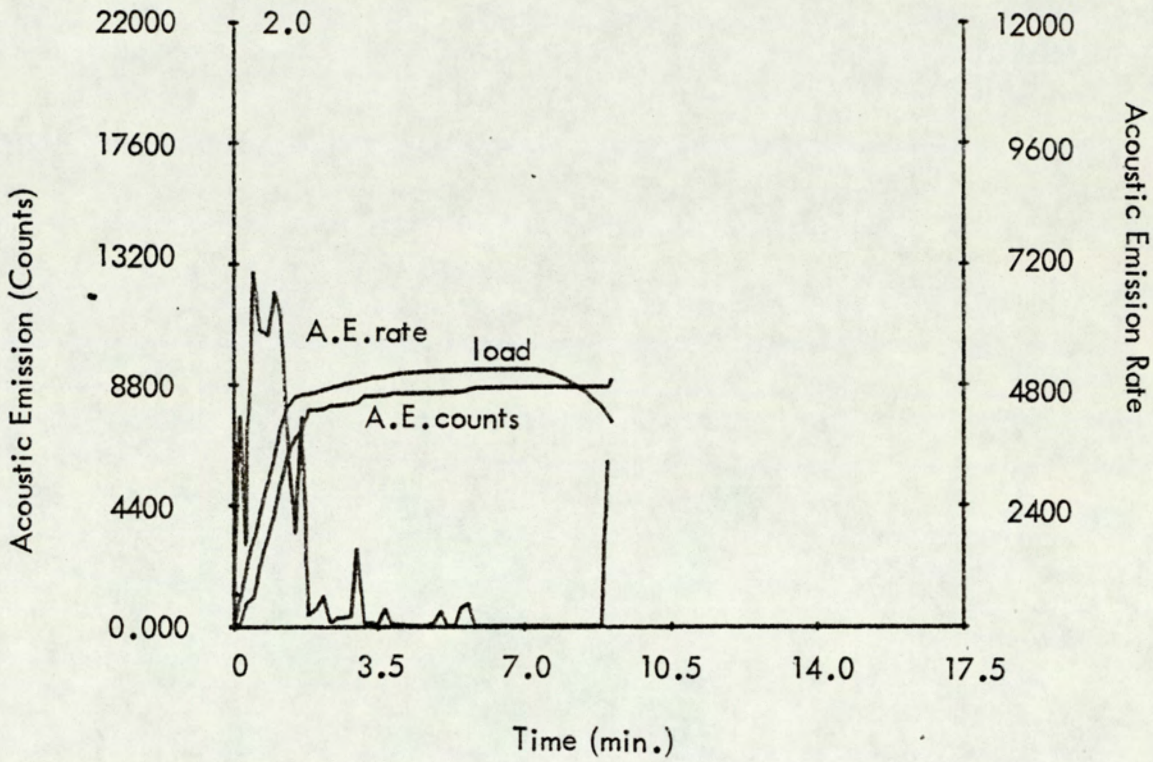

Fig. 27.a.

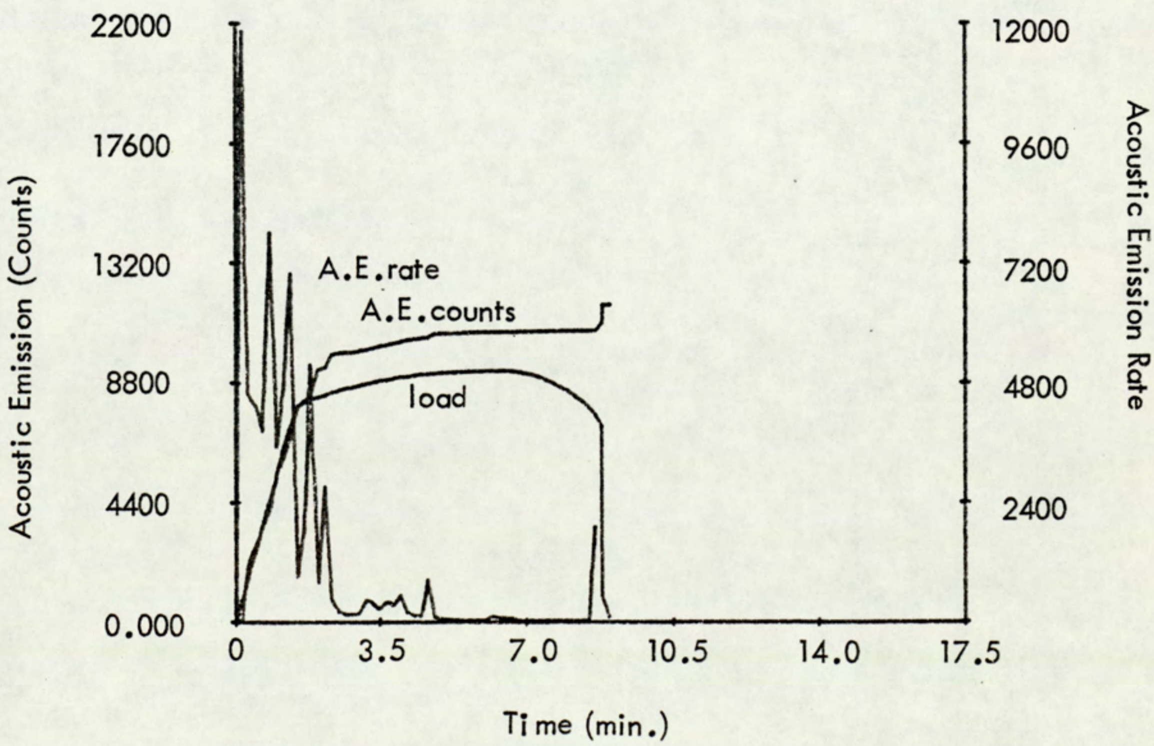

Fig. 27.b.

Fig. 27. Tensile tests of flat specimens of aluminium

a. At elastic

b. At pre yielding

c. At fracture

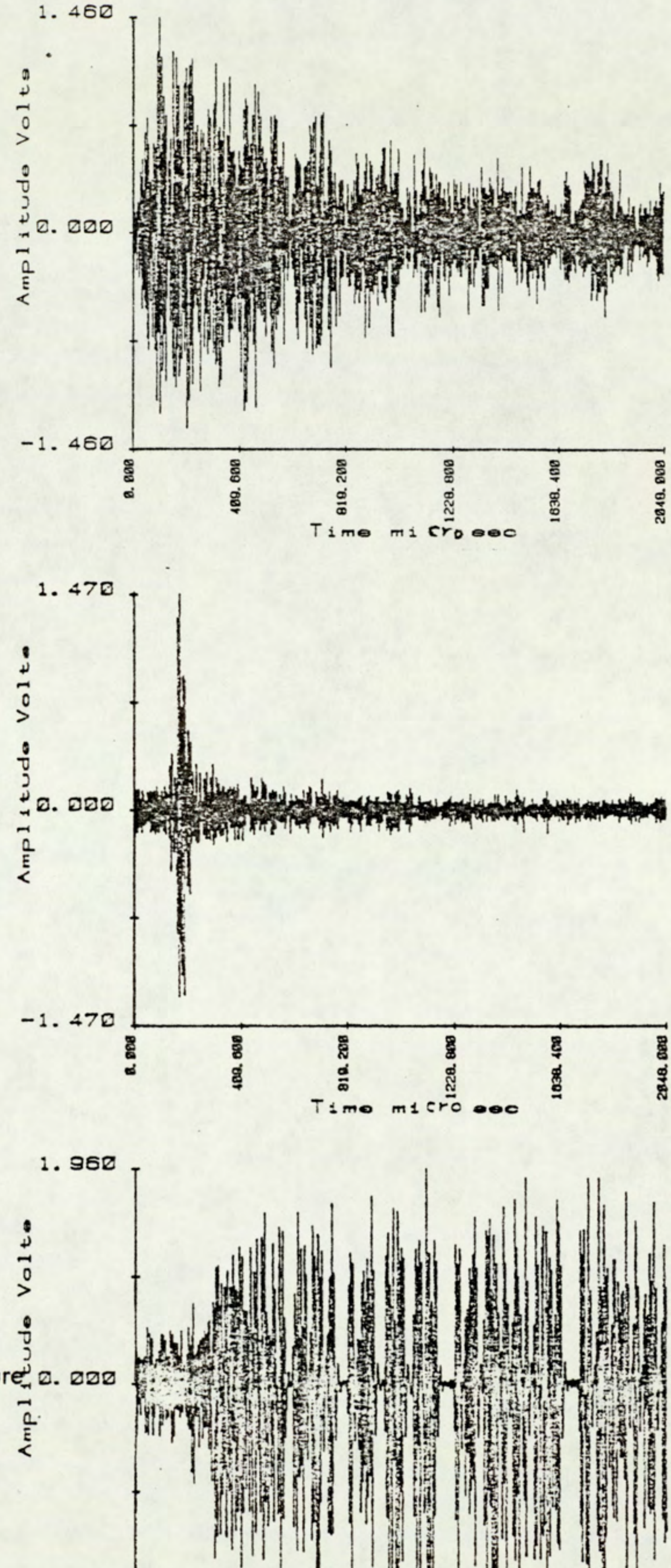

Fig. 27.a.1. A.E. pulses generated from tensile test specimen of aluminium.

a. At elastic

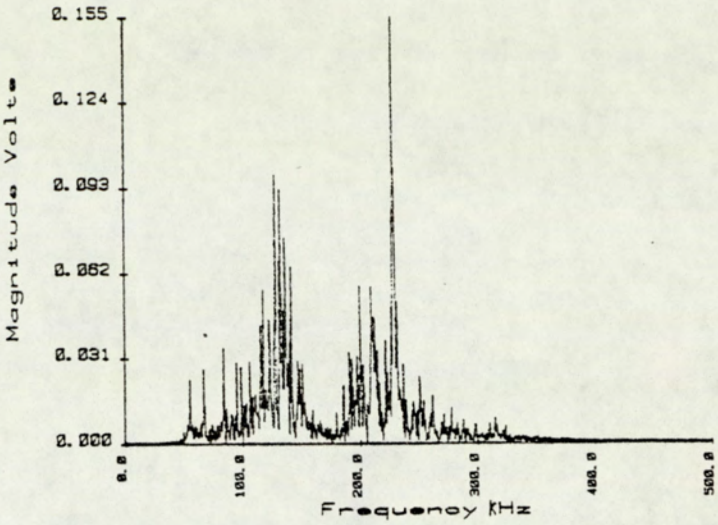

b. At pre yielding

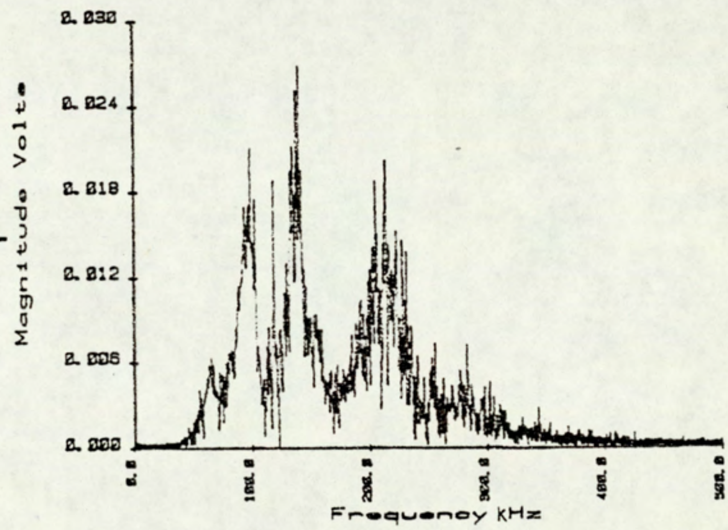

c. At fracture

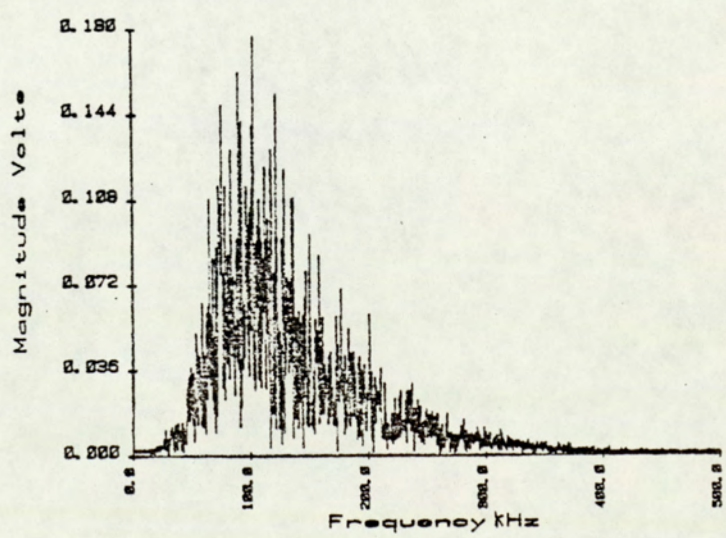

Fig. 27.a.2. F.F.T. spectrum analysis of the signals from aluminium specimen.

a. At elastic

b. At pre yielding

c. At fracture

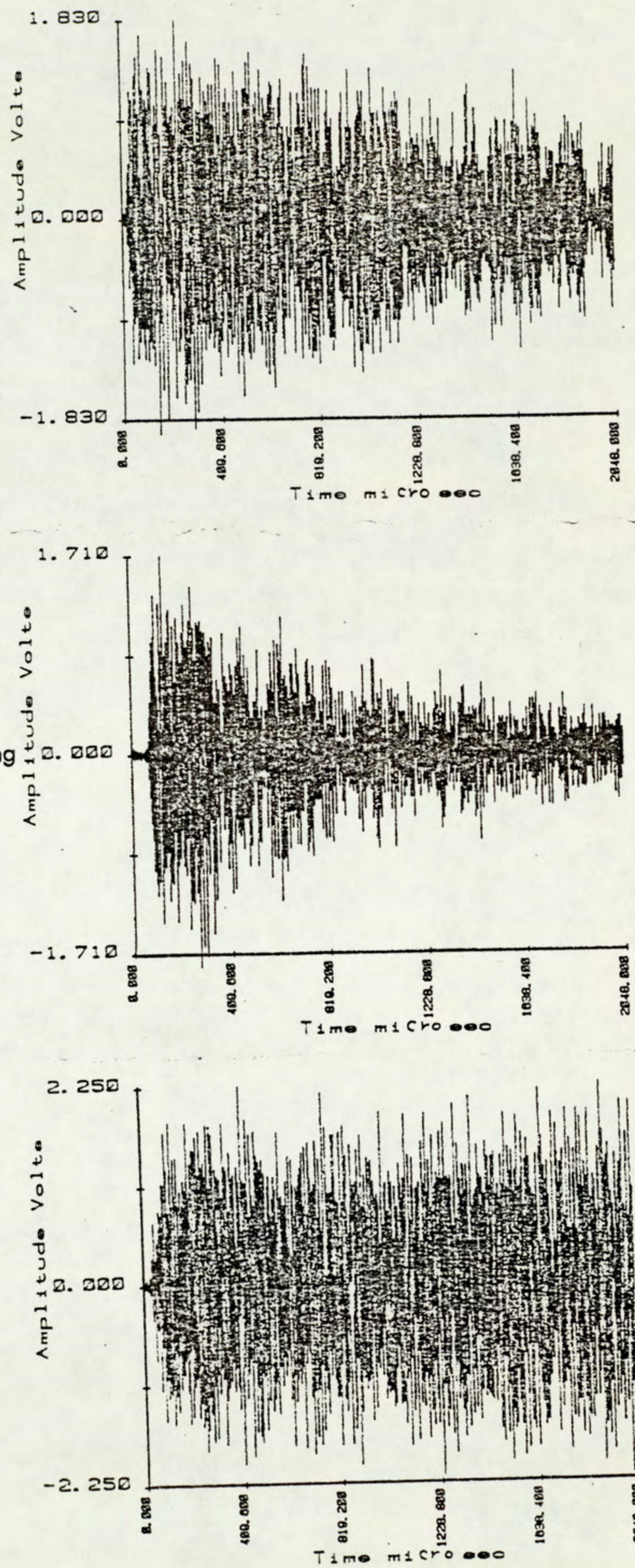

Fig. 27.b.1. A.E.pulses generated from tensile test specimen of aluminium.

a. At elastic

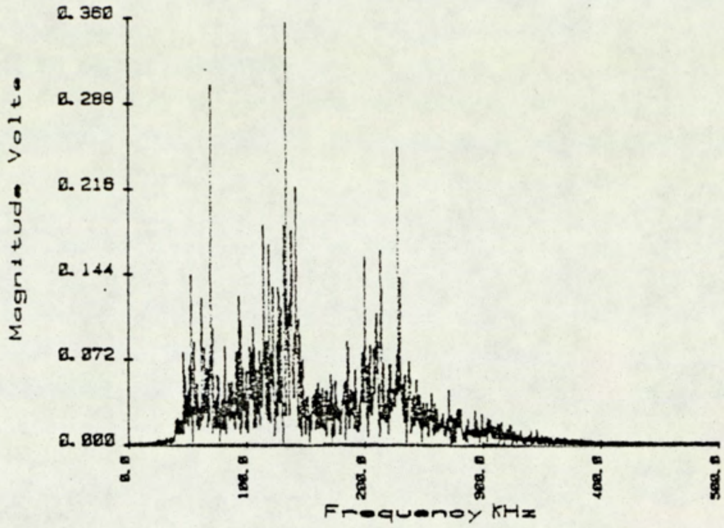

b. At pre yielding

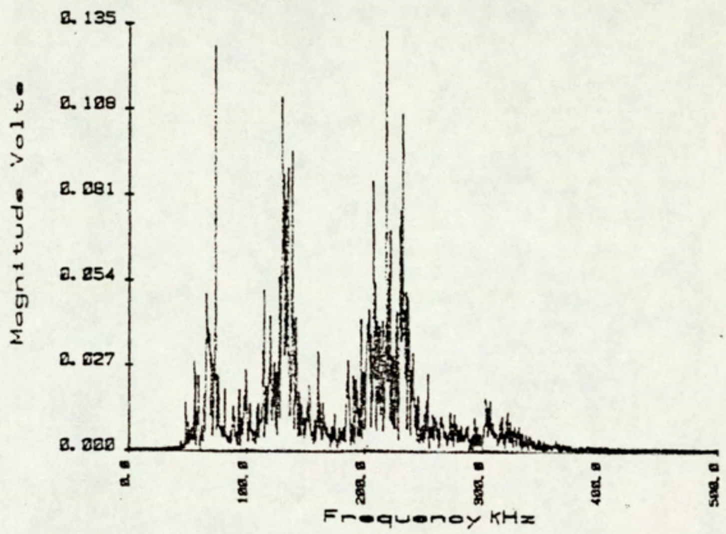

c. At fracture

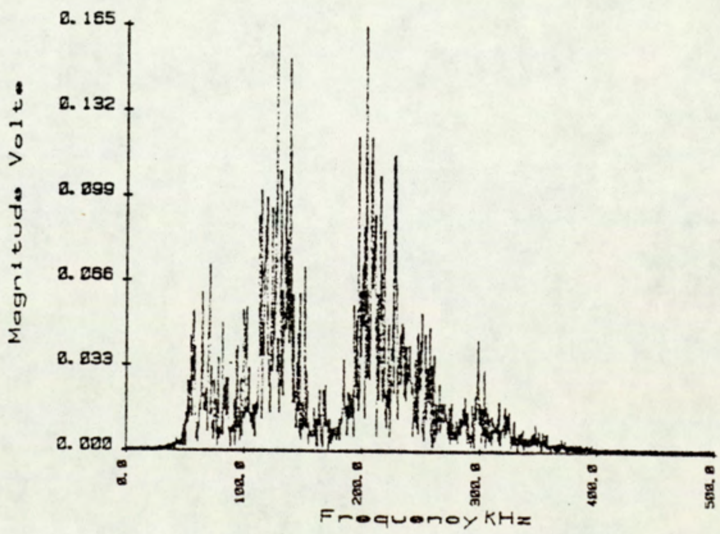

Fig. 27.b.2. F.F.T. spectrum analysis of the signals from aluminium specimen.

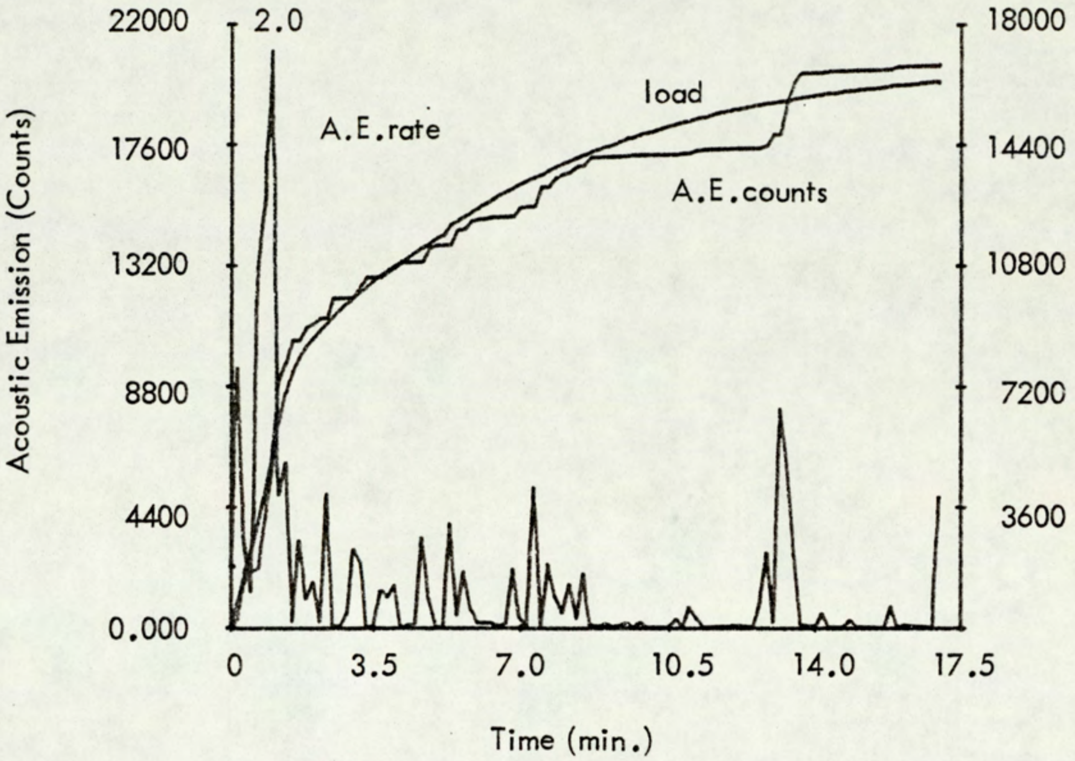

Fig. 28.a.

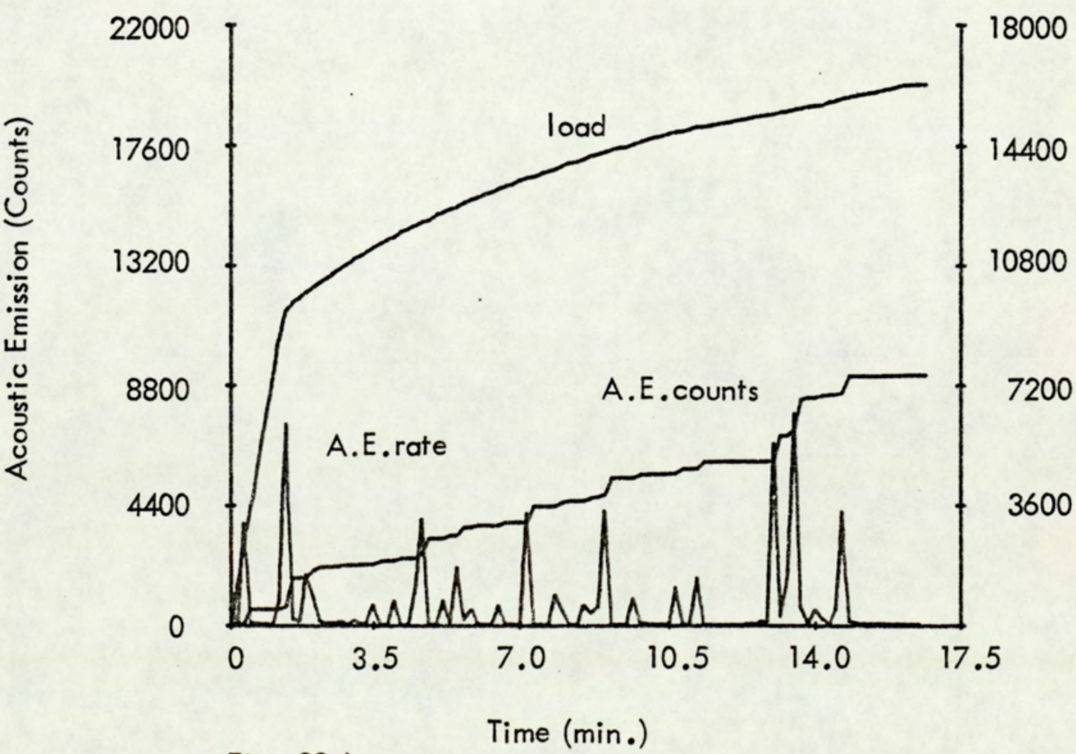

Fig. 28.b.

Fig. 28. Tensile tests of flat specimens of copper

a. At elastic

b. At pre yielding

c. At near fracture

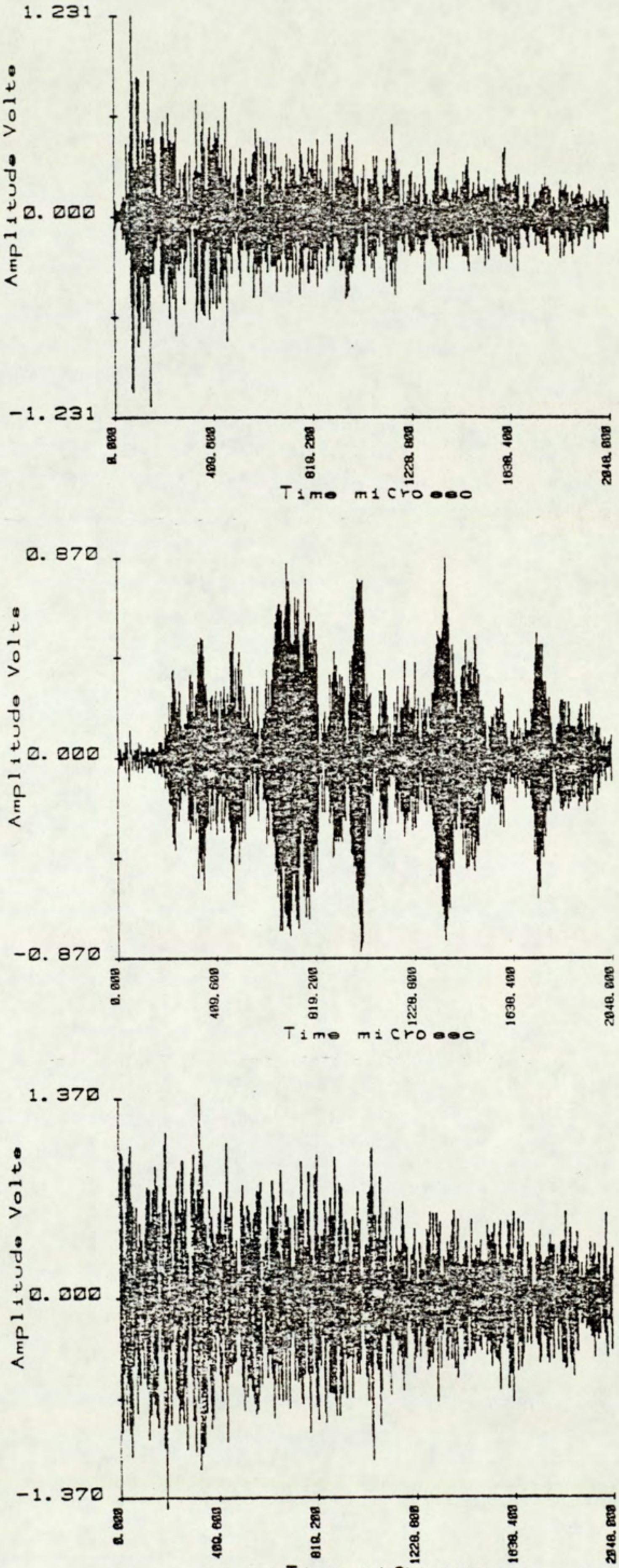

Fig. 28.a.1. A.E.pulses generated from tensile test specimen of copper.

a. At elastic

b. At pre yielding

c. At near fracture

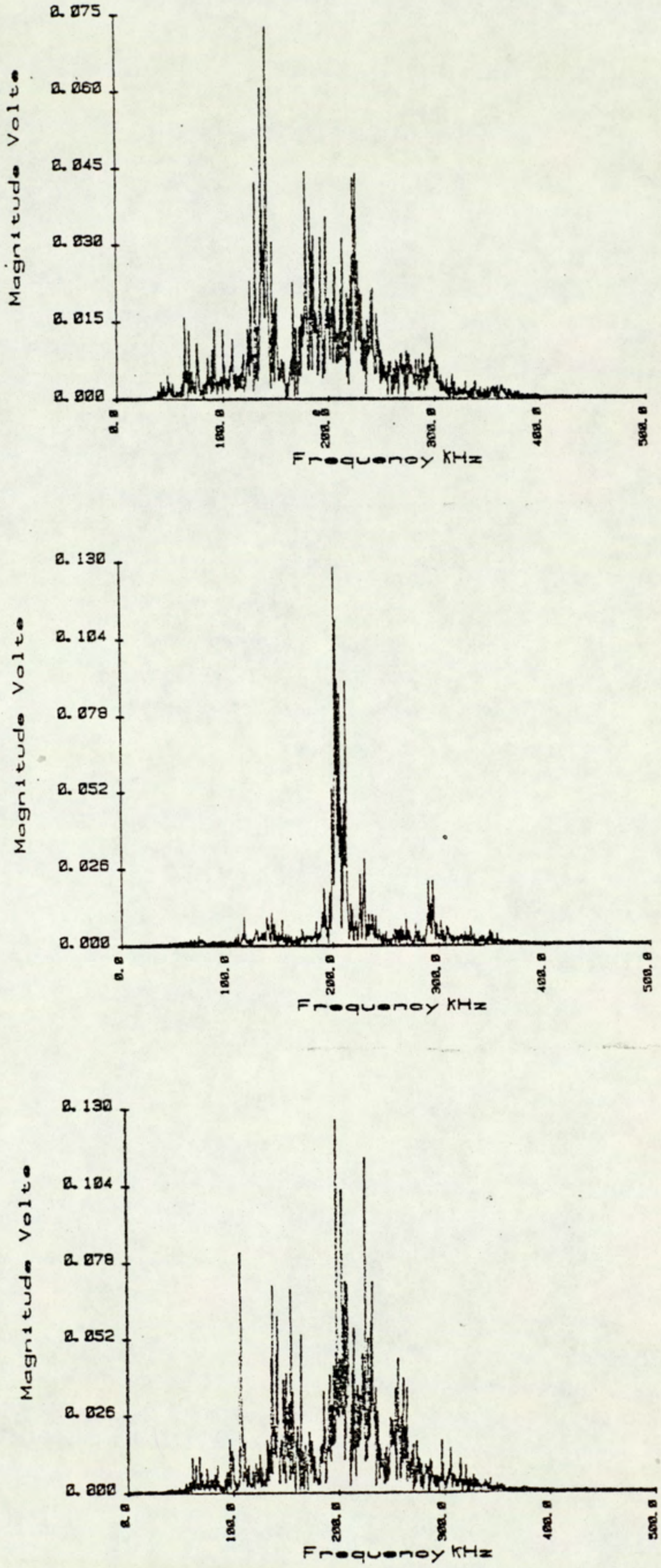

Fig. 28.a.2. F.F.T. spectrum analysis of the A.E. signal from copper specimen.

a. At elastic

b. At pre yielding

c. At fracture

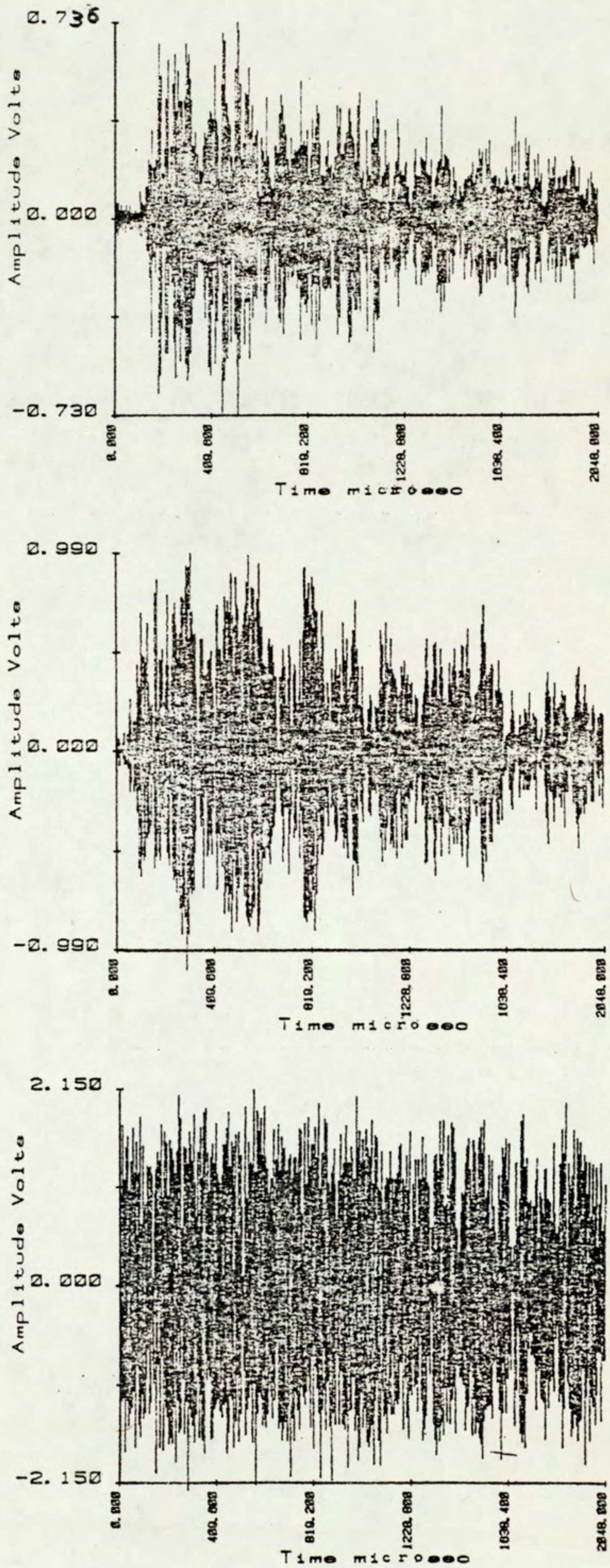

Fig. 28.b.1. A.E.pulses generated from tensile test specimen of copper.

a. At elastic

b. At pre yielding

c. At fracture

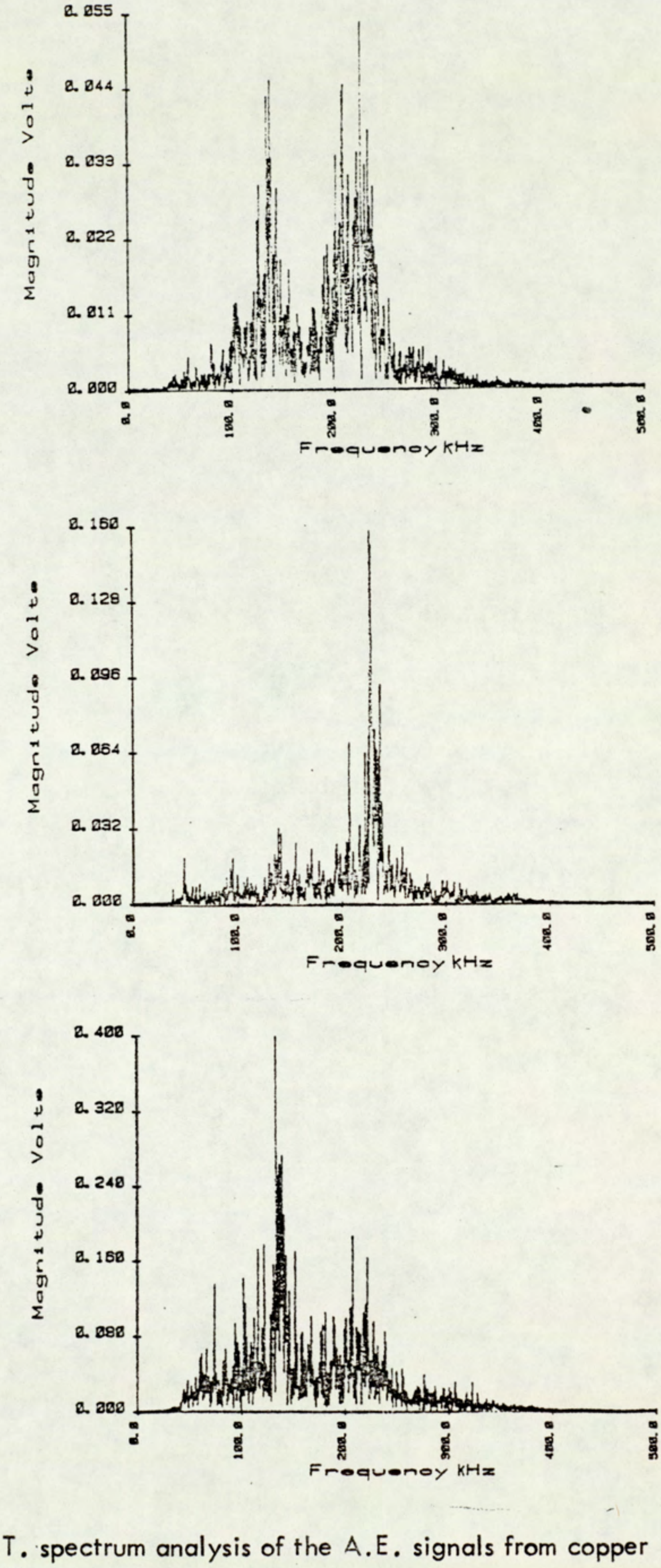

Fig. 28.b.2. F.F.T. spectrum analysis of the A.E. signals from copper specimen.

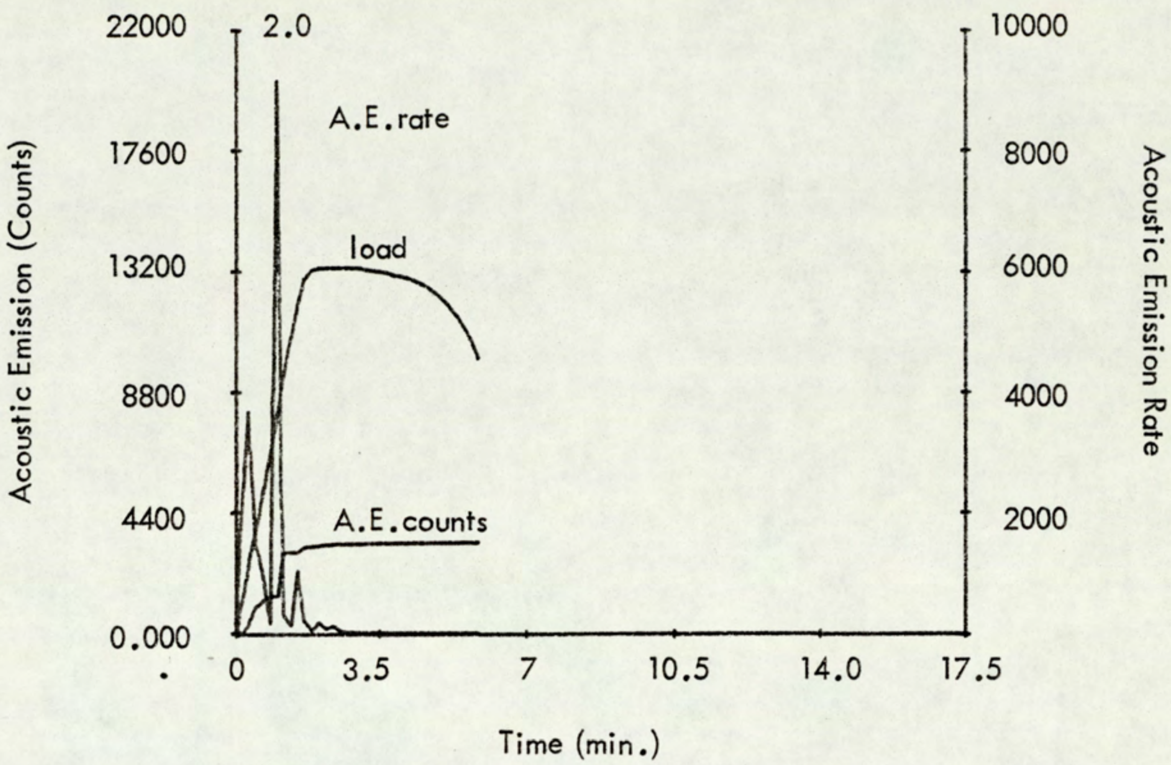

Fig. 29.a.

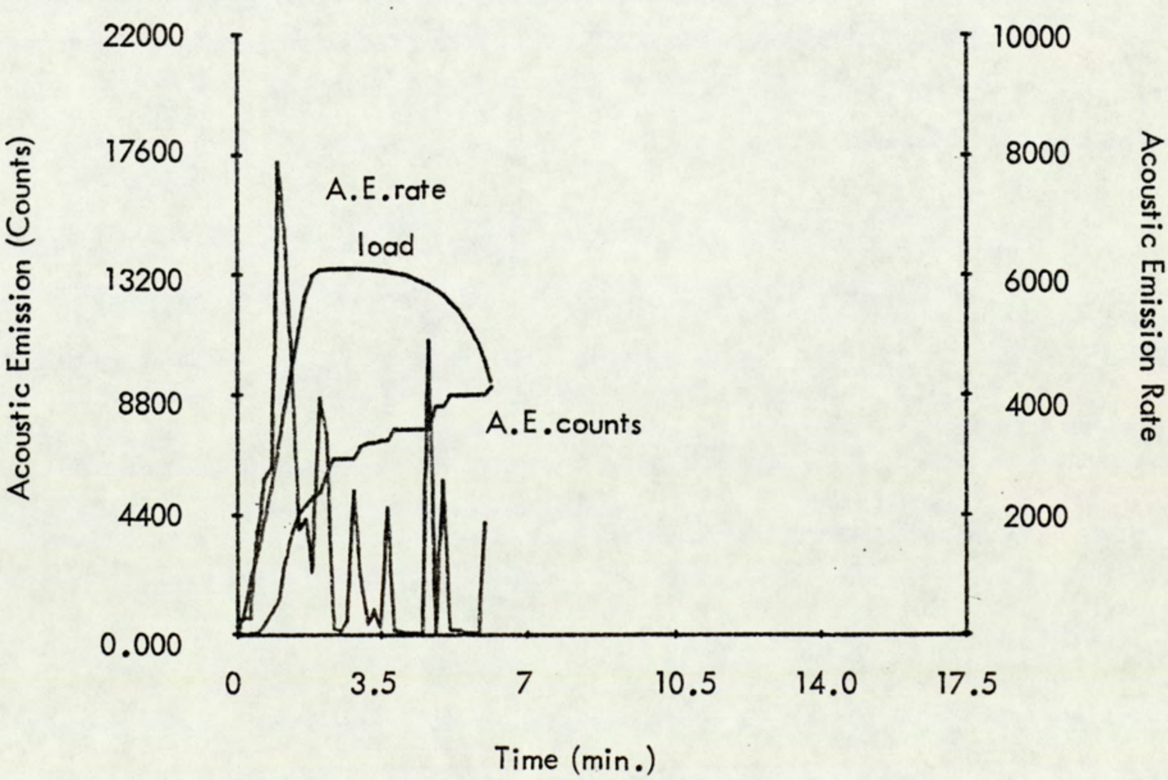

Fig. 29.b.

Fig. 29. Tensile tests of flat specimens of brass

a. At elastic

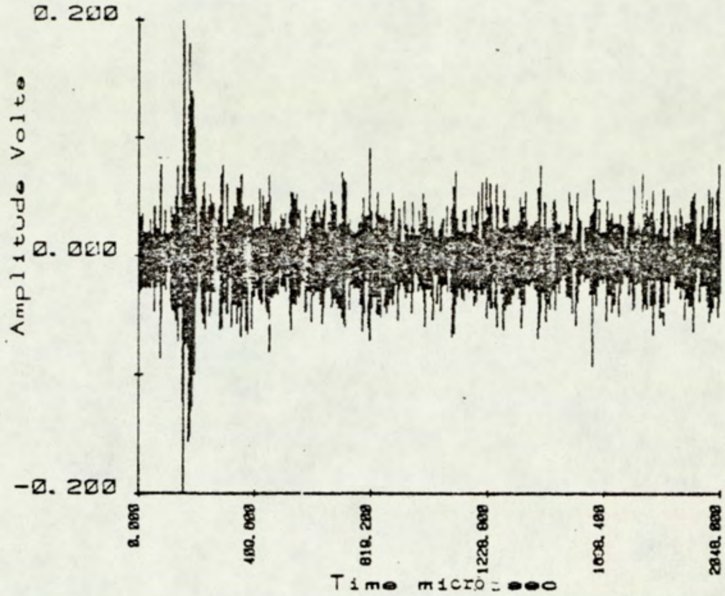

b. At pre yielding

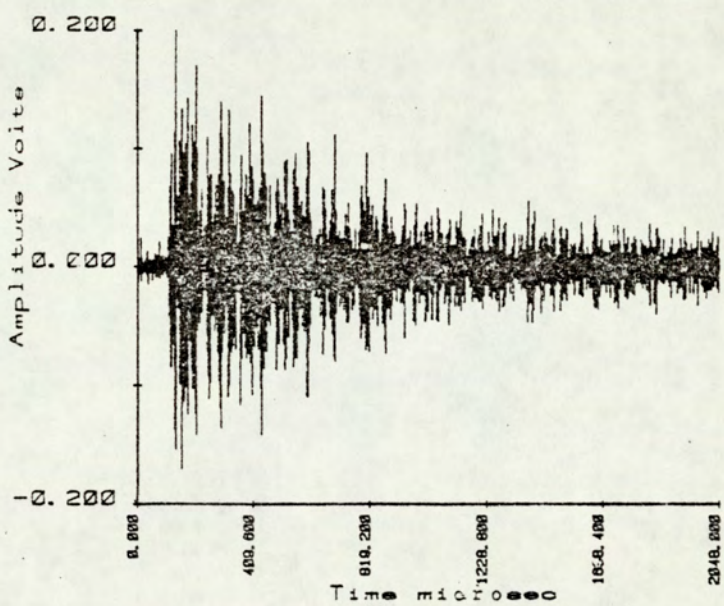

c. At fracture

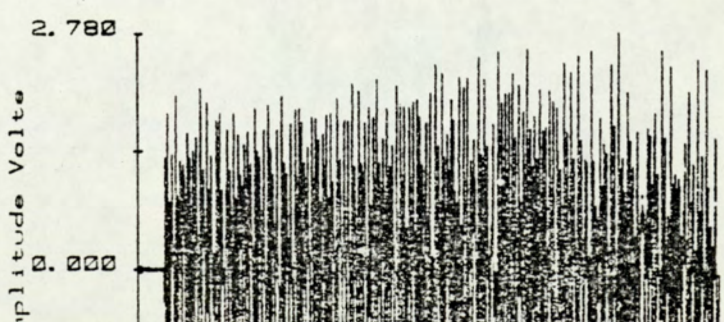

Fig. 29.a.1. A.E.pulses generated from tensile test of brass specimen.

a. At elastic

b. At pre yielding

c. At fracture

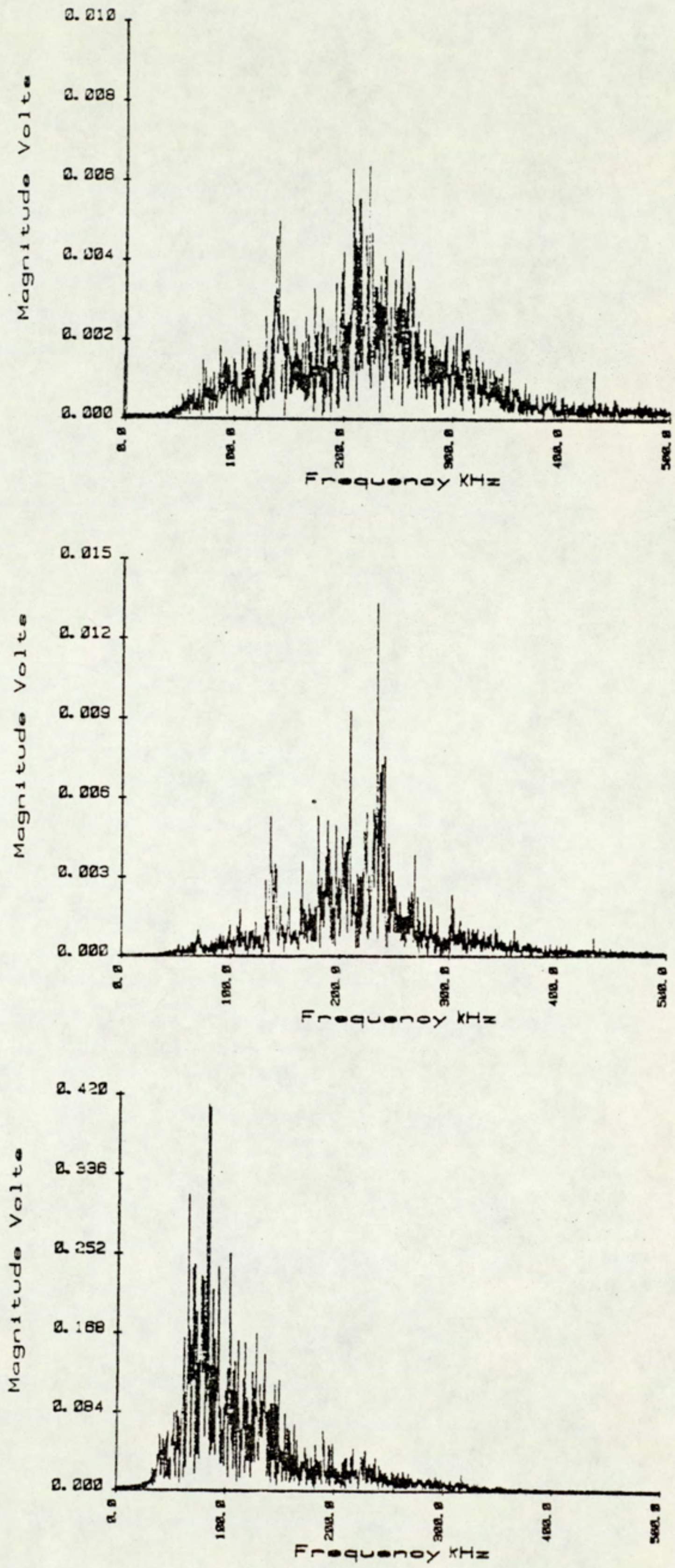

Fig. 29.a.2. F.F.T. spectrum analysis of the A.E. signals from brass specimen.

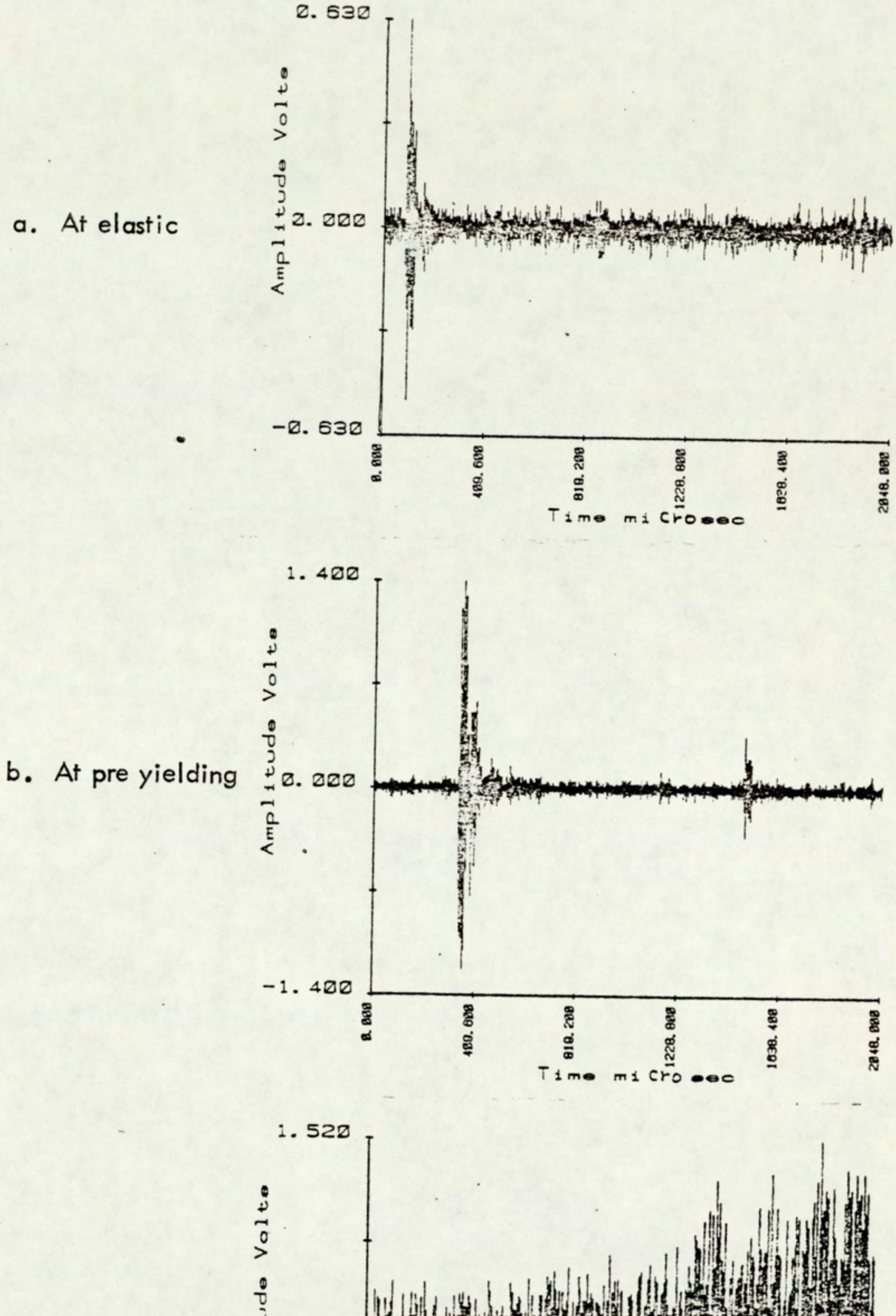

Fig. 29.b.1. A.E. pulses generated from tensile test of brass specimen.

a. At elastic

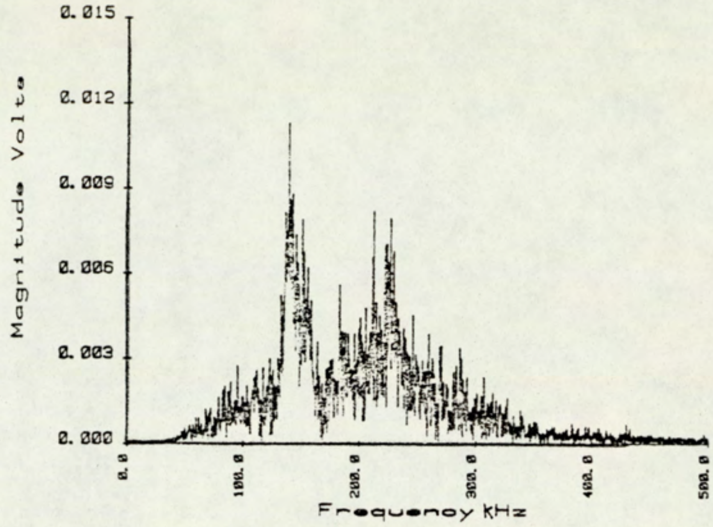

b. At pre yielding

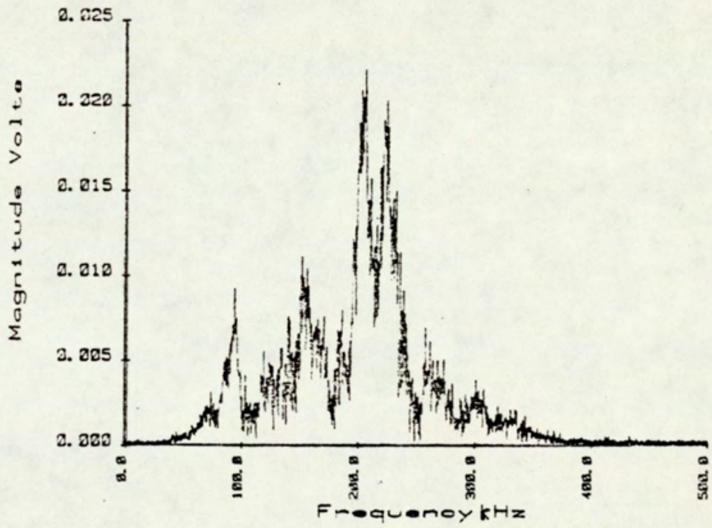

c. At near fracture

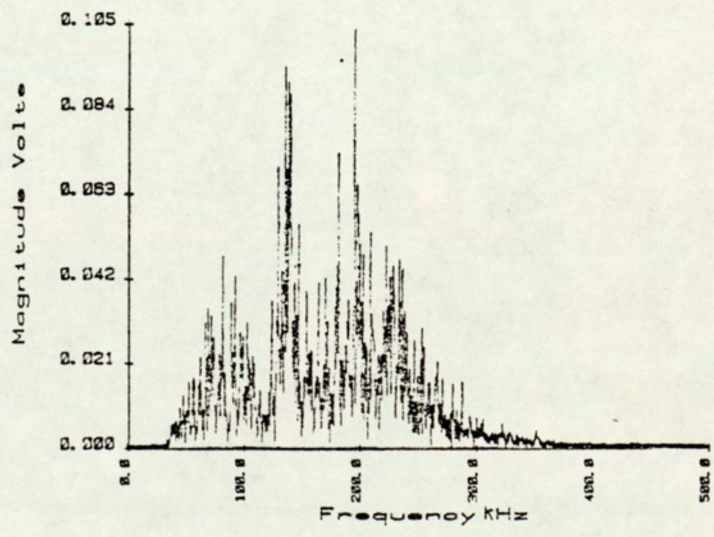

Fig. 29.b.2. F.F.T. spectrum analysis of the A.E.signals from brass specimen.

TABLE 2

Spec. Code	D (mm) ±0.01	d (mm)	r (mm)	d/D	r/D	K_t
101	9.98	5.00	1.02	0.501	0.102	1.835
102	10.00	5.00	1.02	0.500	0.102	1.835
103	9.99	5.08	1.02	0.509	0.102	1.840
104	10.03	5.12	0.26	0.510	0.026	3.15
105	10.01	5.08	0.26	0.507	0.026	3.15
106	10	5.04	0.26	0.504	0.026	3.10
107	9.99	5.04	0.16	0.505	0.016	3.95
108	9.99	5.04	0.16	0.505	0.016	3.95
109	10.00	5.00	0.16	0.500	0.016	3.90

TABLE 3

Spec. Code	D (mm) ±0.01	d (mm)	r (mm)	d/D	r/D	K_t
111	10.0	5.24	1.00	0.524	0.1	1.865
112	10.0	5.08	1.00	0.508	0.100	1.845
113	10.C	5.08	1.00	0.508	0.100	1.845
114	10.0	5.04	0.26	0.503	0.026	3.15
115	9.98	5.04	0.26	0.505	0.026	3.15
116	10.00	5.24	0.27	0.524	0.027	3.20
117	10.01	5.08	0.16	0.507	0.016	3.95
118	9.99	5.12	0.16	0.513	0.016	4.00
119	10.01	5.00	0.16	0.500	0.016	3.900

TABLE 4

Spec. Code	D (mm) ±0.01	d (mm)	r (mm)	d/D	r/D	K_t
121	10.0	5.04	1.00	0.504	0.100	1.84
122	9.98	5.00	1.00	0.501	0.100	1.840
123	10.04	4.96	1.00	0.494	0.100	1.835
124	10	5.00	0.26	0.500	0.026	3.10
125	9.98	5.04	0.26	0.505	0.026	3.15
126	9.98	5.08	0.26	0.509	0.026	3.15
127	10.02	5.08	0.16	0.507	0.016	3.95
128	10.02	5.16	0.16	0.515	0.016	4.00

TABLE 5

Spec. Code	D (mm) ±0.01	d (mm)	r (mm)	d/D	r/D	K_t
201	9.96	5.00	1.02	0.502	0.102	1.835
202	9.95	5.07	1.02	0.510	0.103	1.840
203	10.0	5.00	1.02	0.500	0.102	1.835
204	10.02	4.98	0.26	0.497	0.026	3.15
205	9.96	4.96	0.26	0.498	0.026	3.15
206	10.00	5.08	0.26	0.508	0.026	3.18
207	9.97	5.01	0.18	0.503	0.018	3.67
208	9.97	5.01	0.18	0.503	0.018	3.67
209	10.02	5.06	0.18	0.505	0.018	3.69

TABLE 6

Spec. Code	D (mm) ±0.01	d (mm)	r (mm)	d/D	r/D	K_t
211	10.0	5.12	1.00	0.512	0.100	1.85
212	9.97	5.08	1.00	0.510	0.100	1.85
213	10.00	5.04	1.00	0.504	0.100	1.845
214	9.99	5.00	0.26	0.501	0.026	3.10
215	10.01	5.12	0.26	0.511	0.026	3.15
216	9.99	5.04	0.26	0.505	0.026	3.10
217	9.94	5.08	0.16	0.511	0.016	4.00
218	10.00	5.00	0.16	0.500	0.016	3.95

TABLE 7

Spec. Code	D (mm) ±0.01	d (mm)	r (mm)	d/D	r/D	K_t
221	10.03	4.92	1.00	0.491	0.100	1.83
222	9.97	5.04	1.00	0.506	0.100	1.84
223	10.02	5.04	1.00	0.503	0.100	1.84
224	10.00	5.16	0.26	0.516	0.026	3.15
225	10.00	5.12	0.26	0.512	0.026	3.15
226	10.00	5.08	0.26	0.508	0.026	3.15
227	10.01	5.08	0.16	0.507	0.016	3.95
228	10.02	5.12	0.16	0.511	0.016	4.00
229	10.01	5.16	0.16	0.515	0.016	4.00

TABLE 8

Spec. Code	D (mm) ± 0.01	d (mm)	r (mm)	d/D	r/D	K_t
301	9.94	5.00	1.00	0.503	0.101	1.84
302	10.00	5.08	1.00	0.508	0.100	1.85
303	10.03	5.00	0.26	0.499	0.026	3.10
304	9.99	5.12	0.26	0.513	0.026	3.15
305	10.05	4.92	0.26	0.49	0.026	3.10
306	10.01	5.00	0.16	0.500	0.016	3.9
307	10.00	5.24	0.18	0.524	0.018	3.75
308	10.01	5.12	0.16	0.511	0.016	4.00

TABLE 9

Spec. Code	D (mm) ± 0.01	d (mm)	r (mm)	d/D	r/D	K_t
311	9.96	5.2	1.00	0.522	0.100	1.86
312	9 98	5.08	1.00	0.509	0.100	1.85
313	9.99	5.00	0.26	0.501	0.026	3.10
314	10.01	5.04	0.26	0.503	0.026	3.10
315	9.99	5.12	0.26	0.513	0.026	3.15
316	10.00	5.04	0.16	0.504	0.016	3.95
317	9.99	5.12	0.16	0.513	0.016	4.00

TABLE 10

Spec. Code	D (mm) ± 0.01	d (mm)	r (mm)	d/D	r/D	K_t
321	10.02	5.02	1.02	0.501	0.102	1.835
323	10.01	5.01	1.02	0.500	0.102	1.835
324	10	5.08	0.26	0.508	0.026	3.18
325	10.01	5.13	0.26	0.512	0.026	3.19
326	10.00	5.04	0.26	0.504	0.026	3.18
327	10.02	5.02	0.18	0.501	0.018	3.70
328	9.92	5.08	0.18	0.512	0.018	3.73
329	10.03	5.15	0.18	0.513	0.018	3.73

TABLE 11

STEEL (C)	SULPHIDES	OXIDES
C10	0.283	0.197
C11	0.503	0.236
C12	0.73	0.339
C20	0.226	0.054
C21	0.700	0.114
C22	0.993	0.18
C30	0.213	0.029
C31	0.380	0.048
C32	0.811	0.036

Fig. 30. Round specimens (C10)
r = 1.00mm

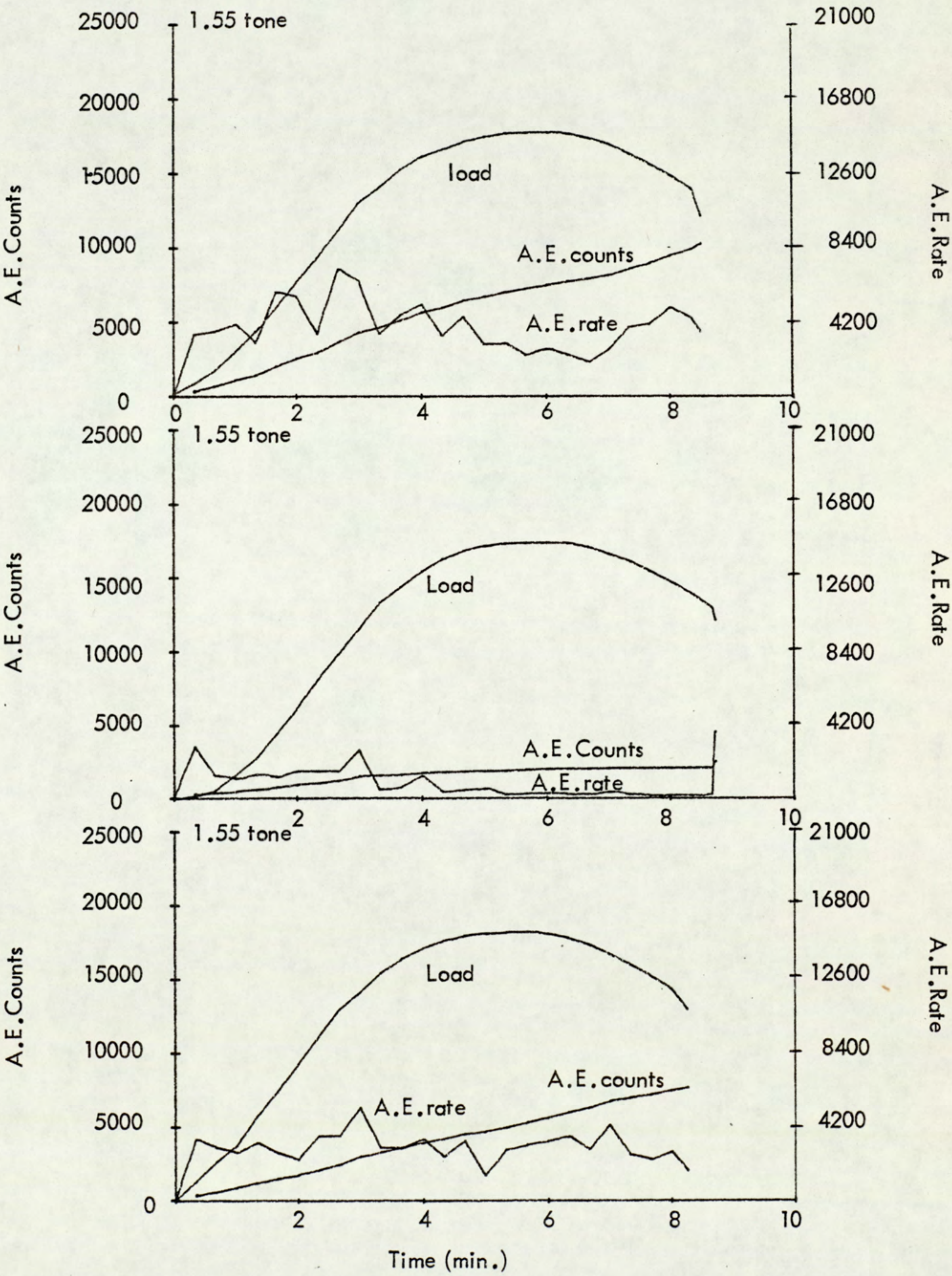

Fig. 31. round specimens (C10)

r = 0.26 mm

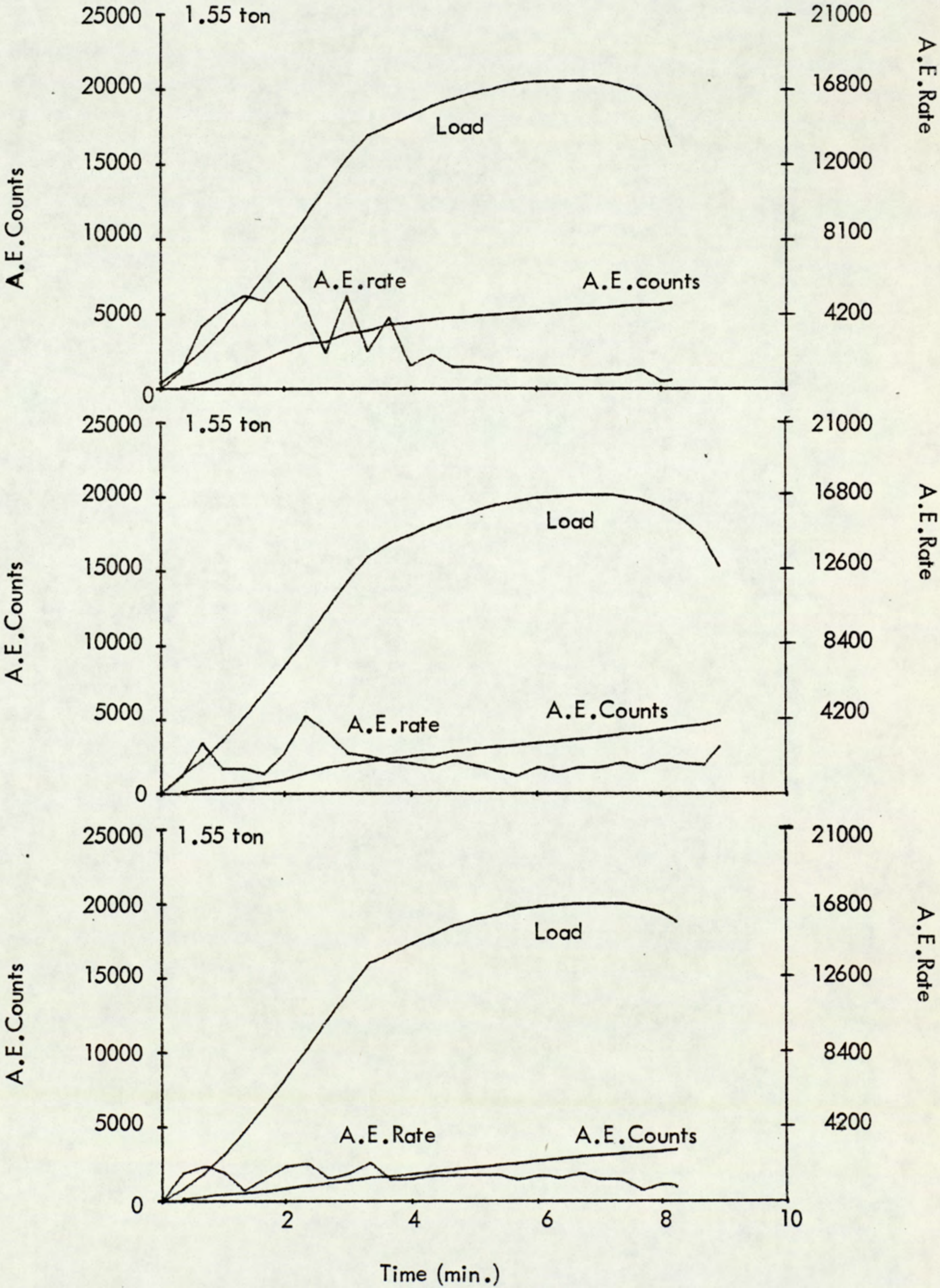

Fig. 32. round specimens (C10)

r = 0.16 mm

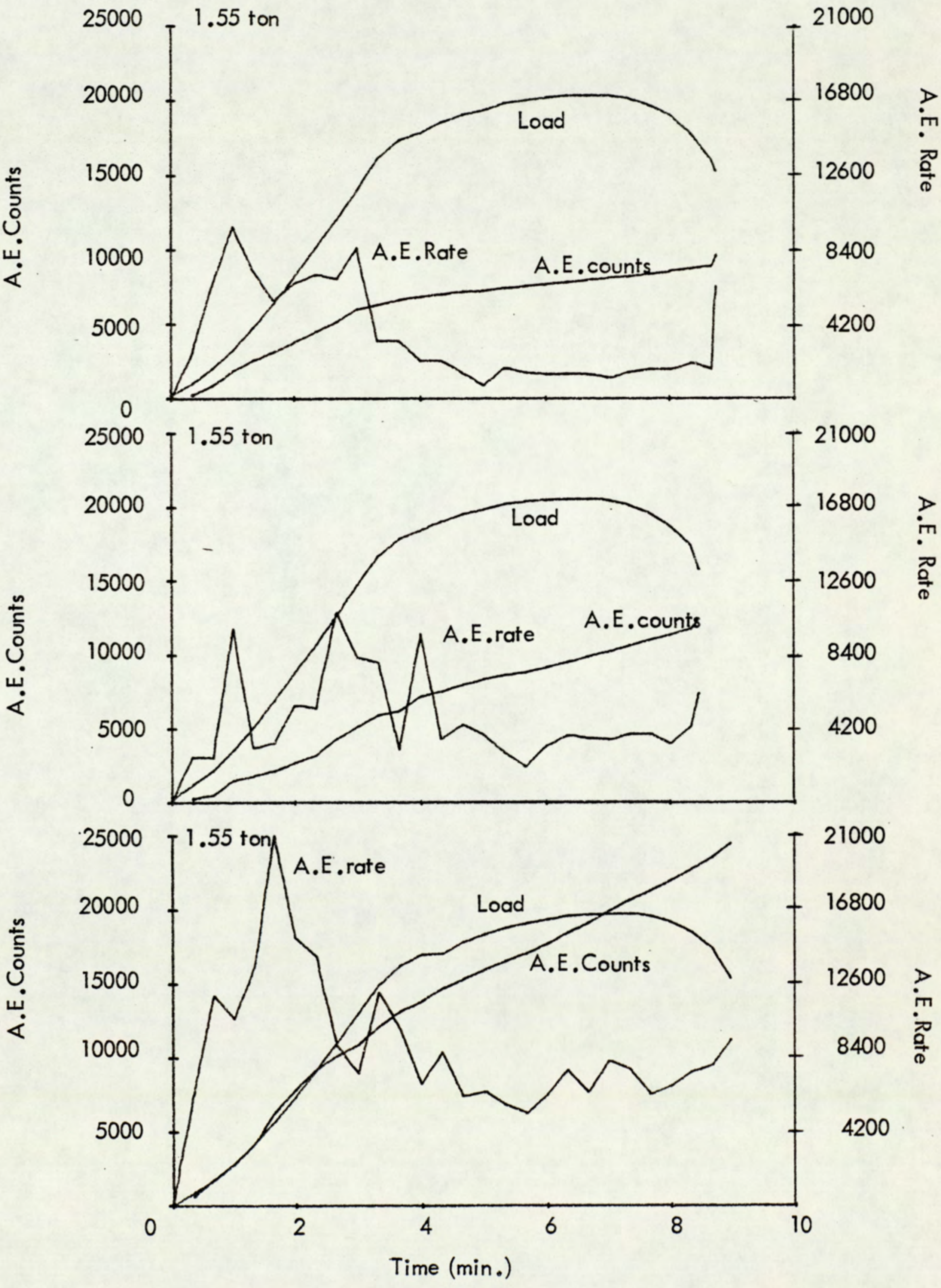

Fig. 33. round specimens (C11)

r = 1.00 mm

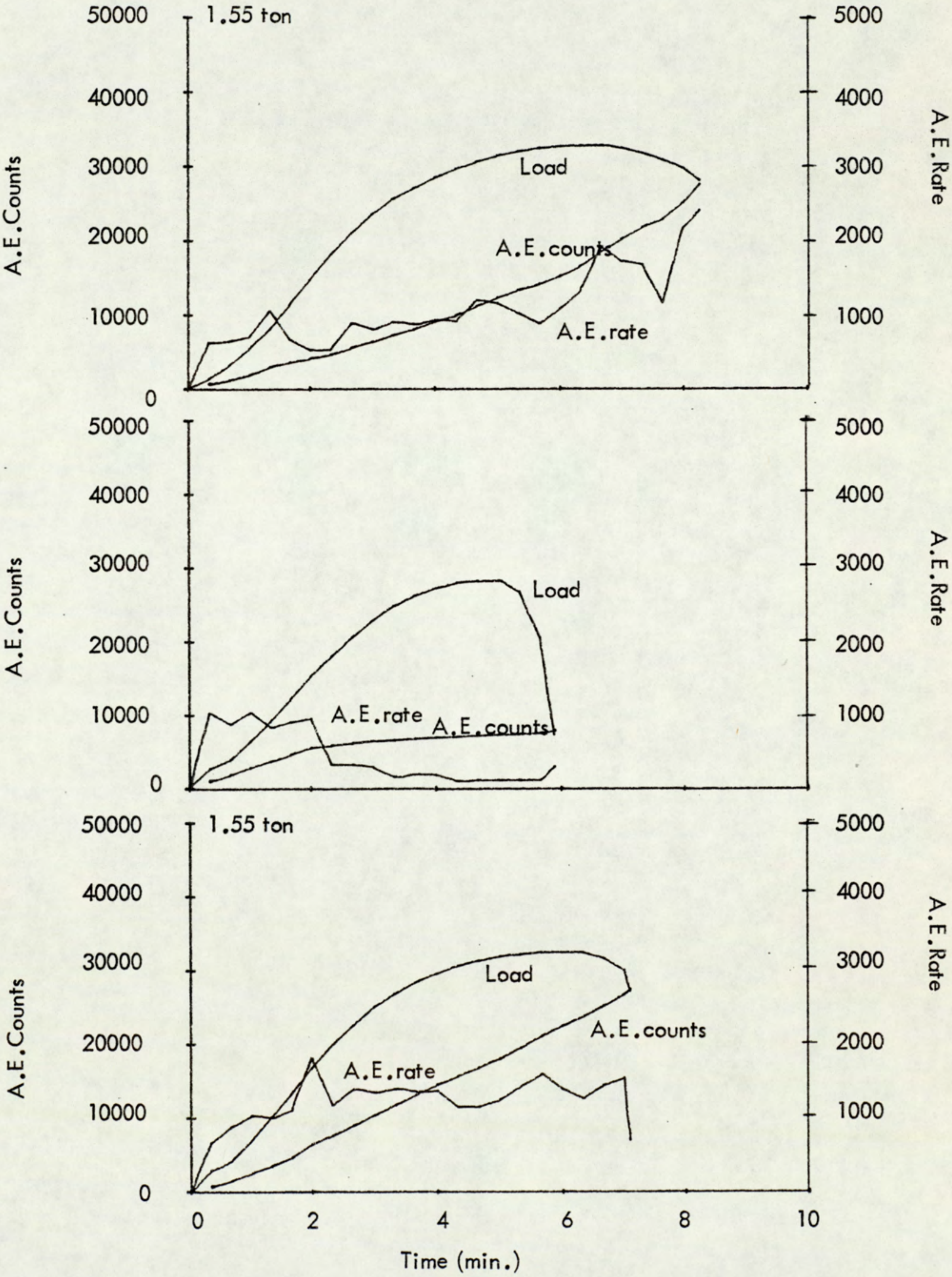

Fig. 34. round specimens (C11)

r = 0.26 mm

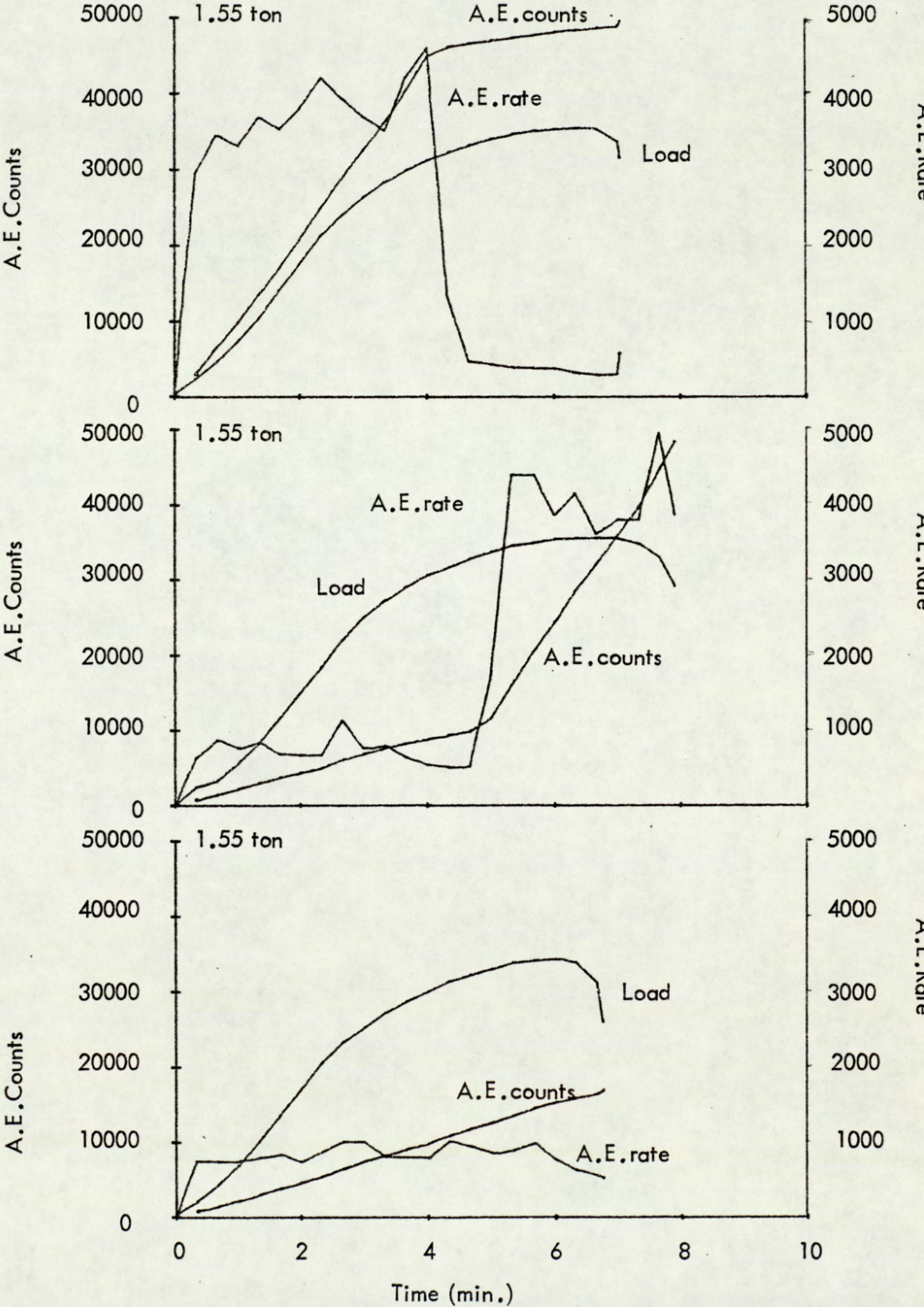

Fig. 35. round specimens (C11)

r = 0.16 mm

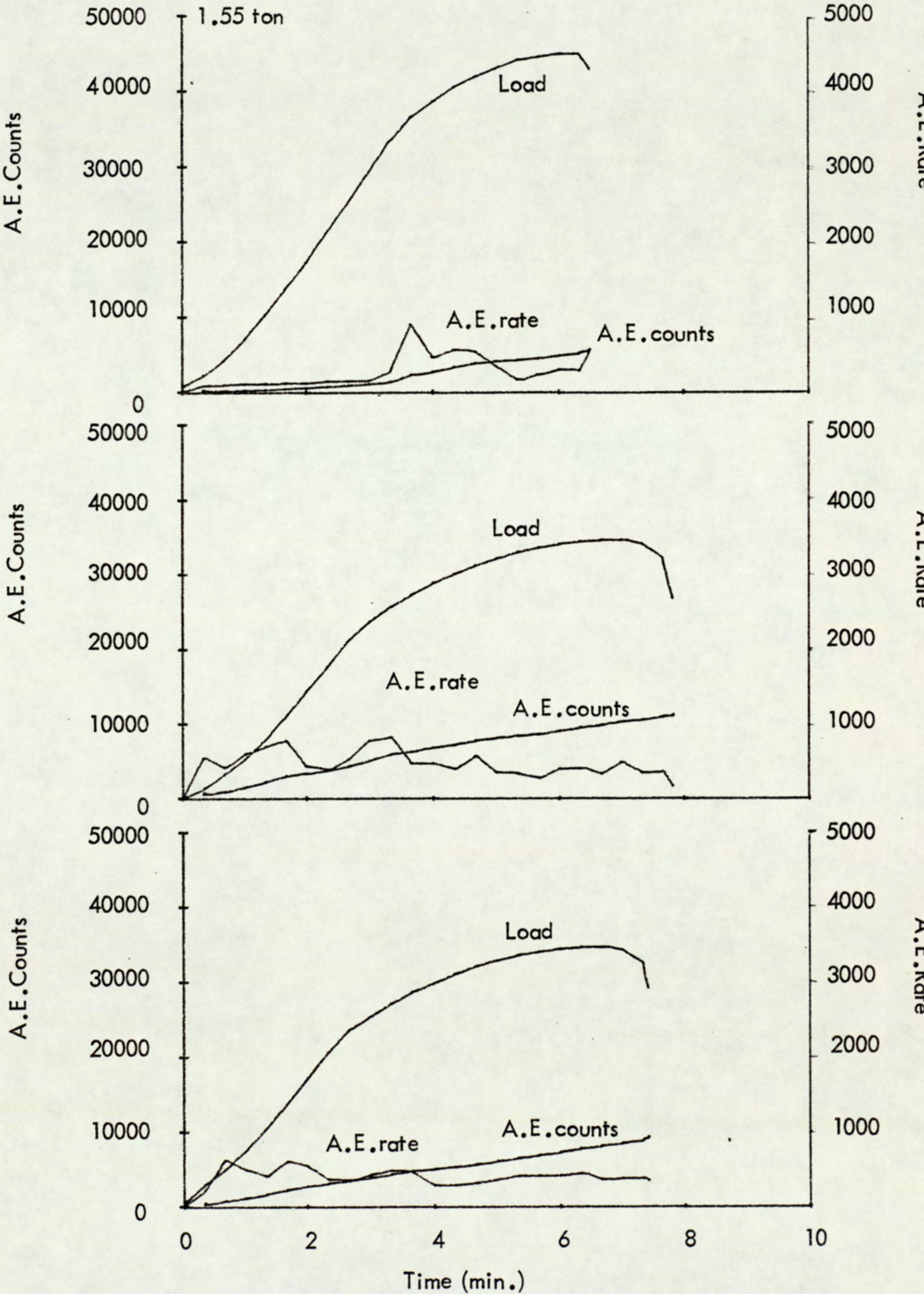

Fig. 36. round specimens (C12)

r = 1.00 mm

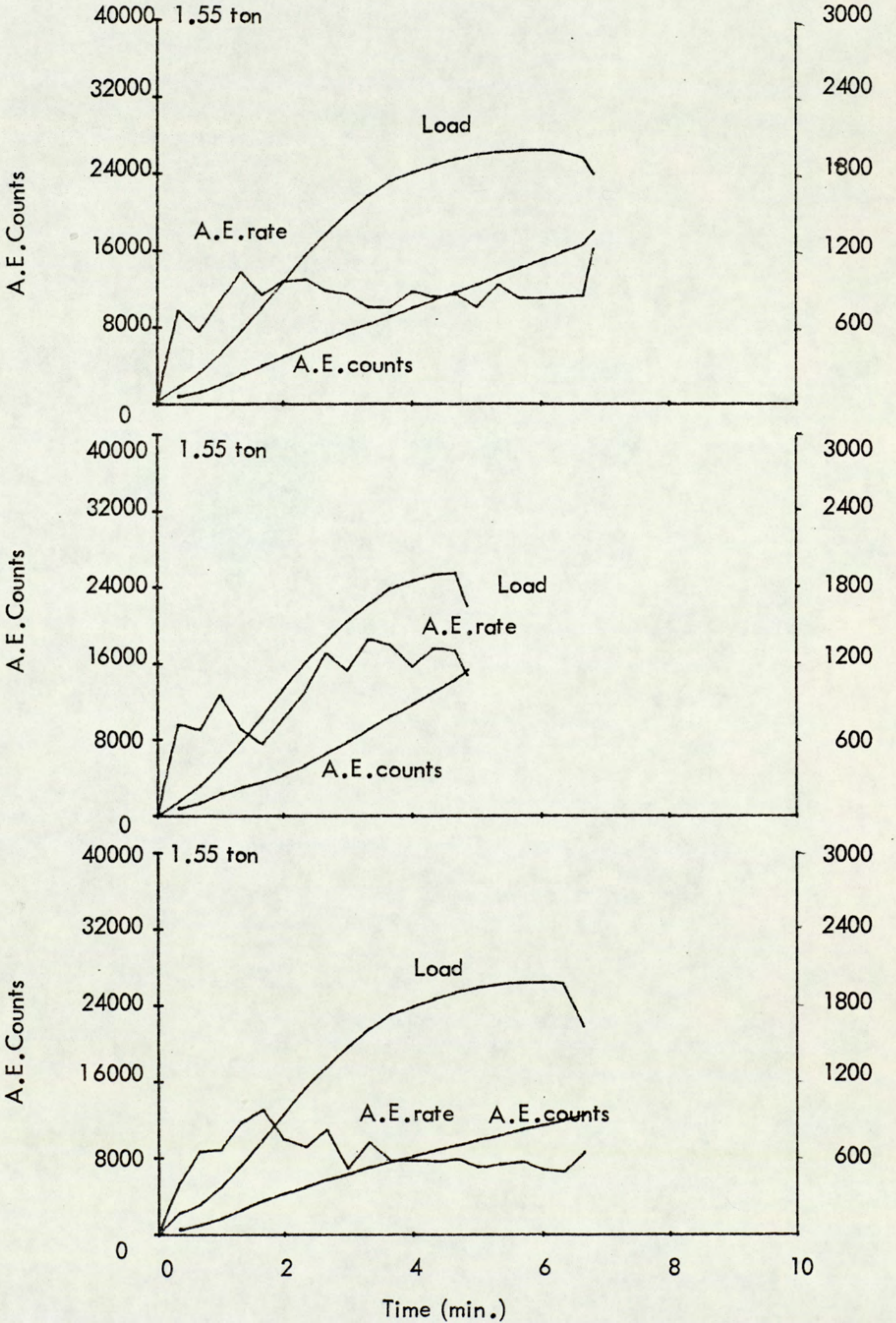

Fig. 37. round specimens (C12)

r = 0.26 mm

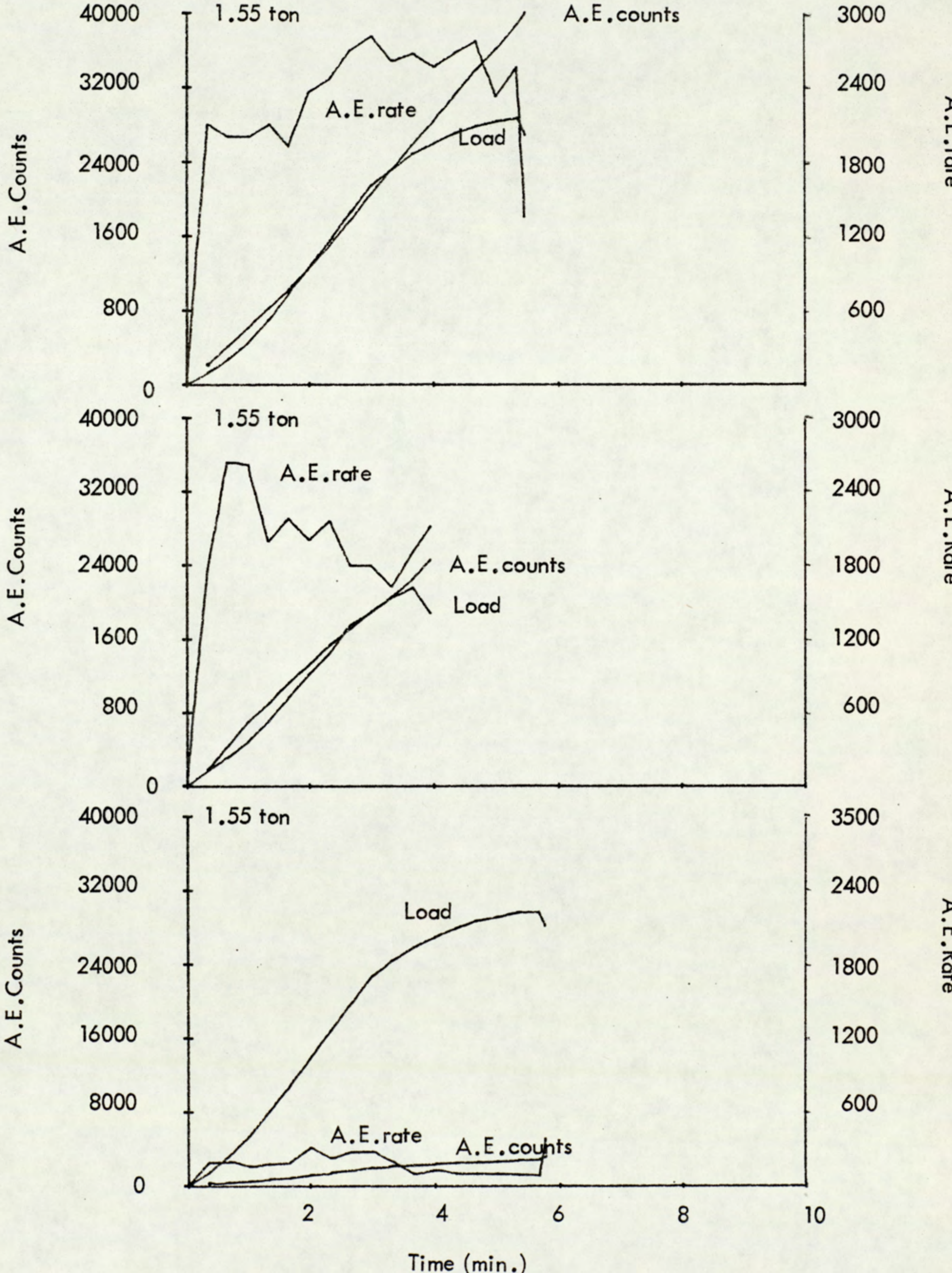

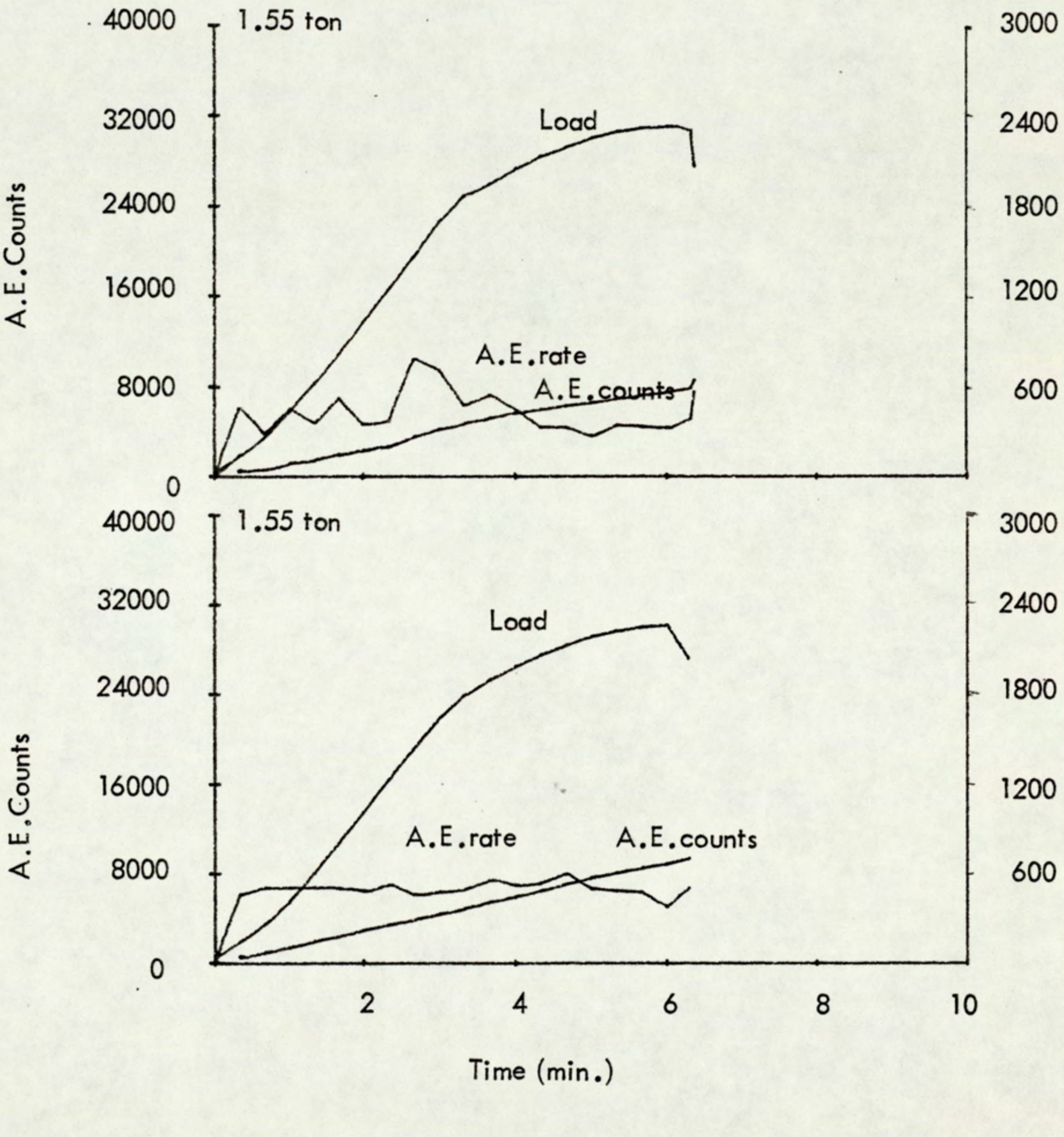

Fig. 38. round specimens (C12)

r = 0.16 mm

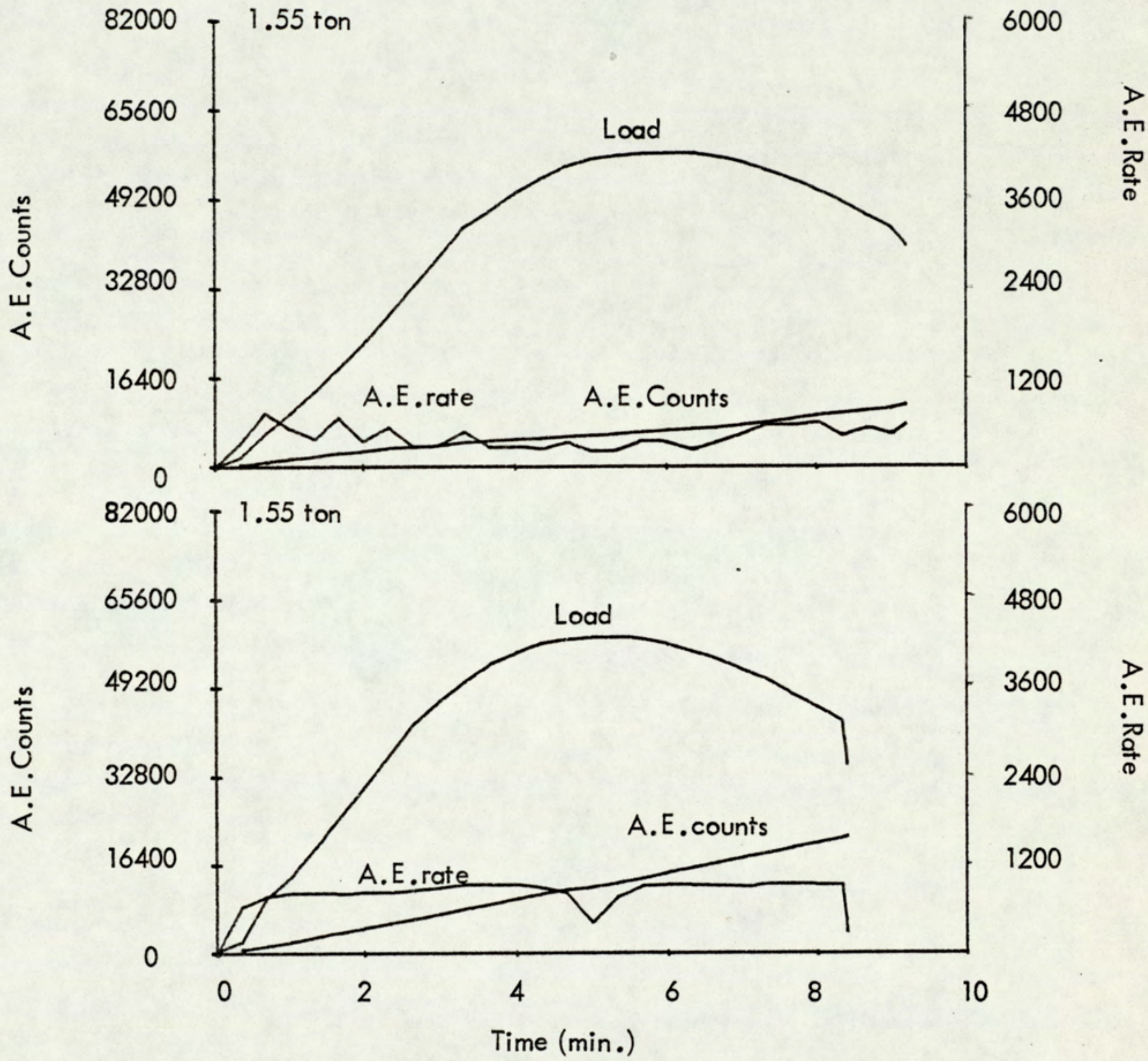

<u>Fig. 39.</u> round specimens (C20)

r = 1.00 mm

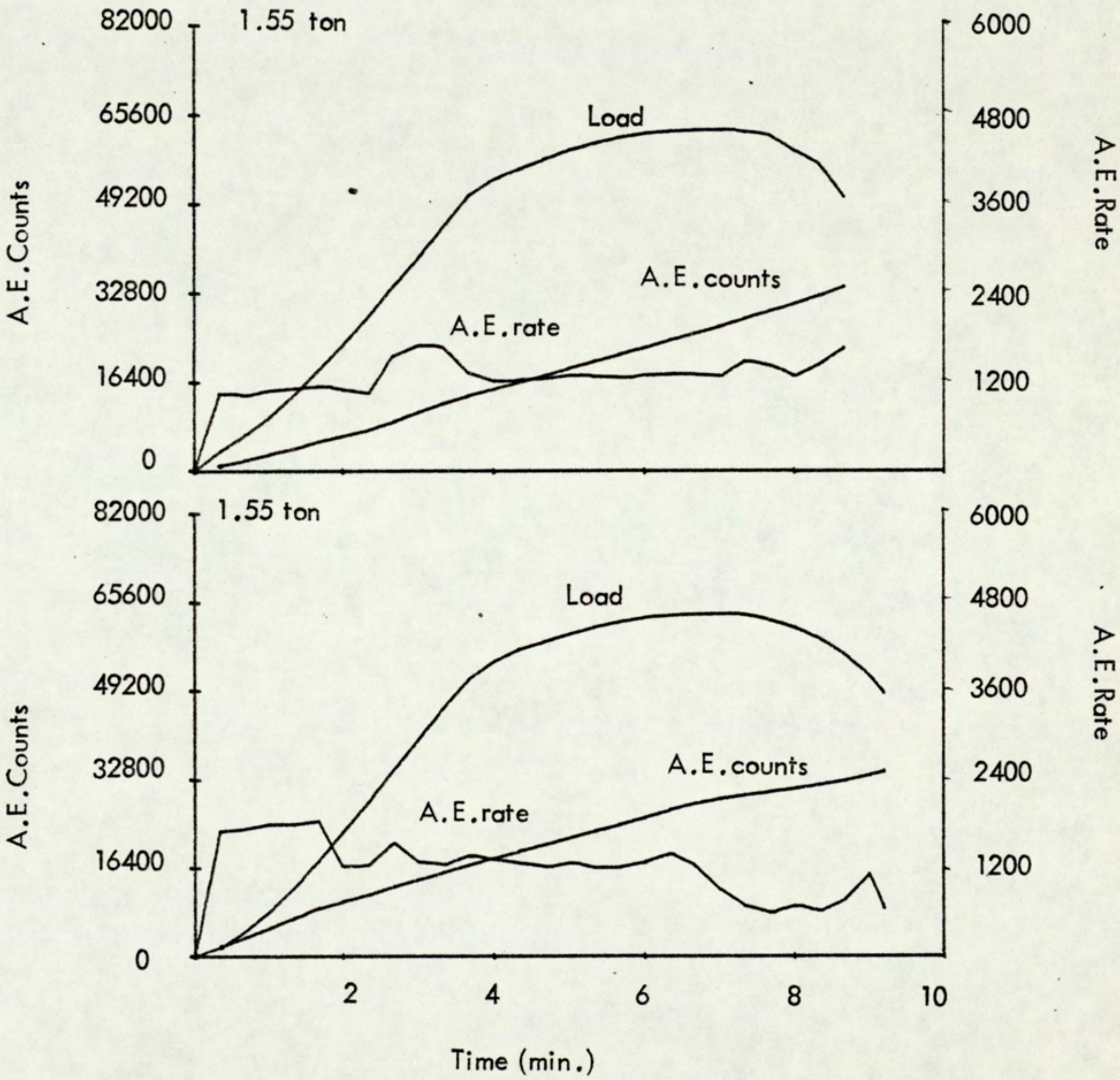

Fig. 40. round specimens (C20)

r = 0.26 mm

Fig. 41. round specimens (C20)

r = 0.16 mm

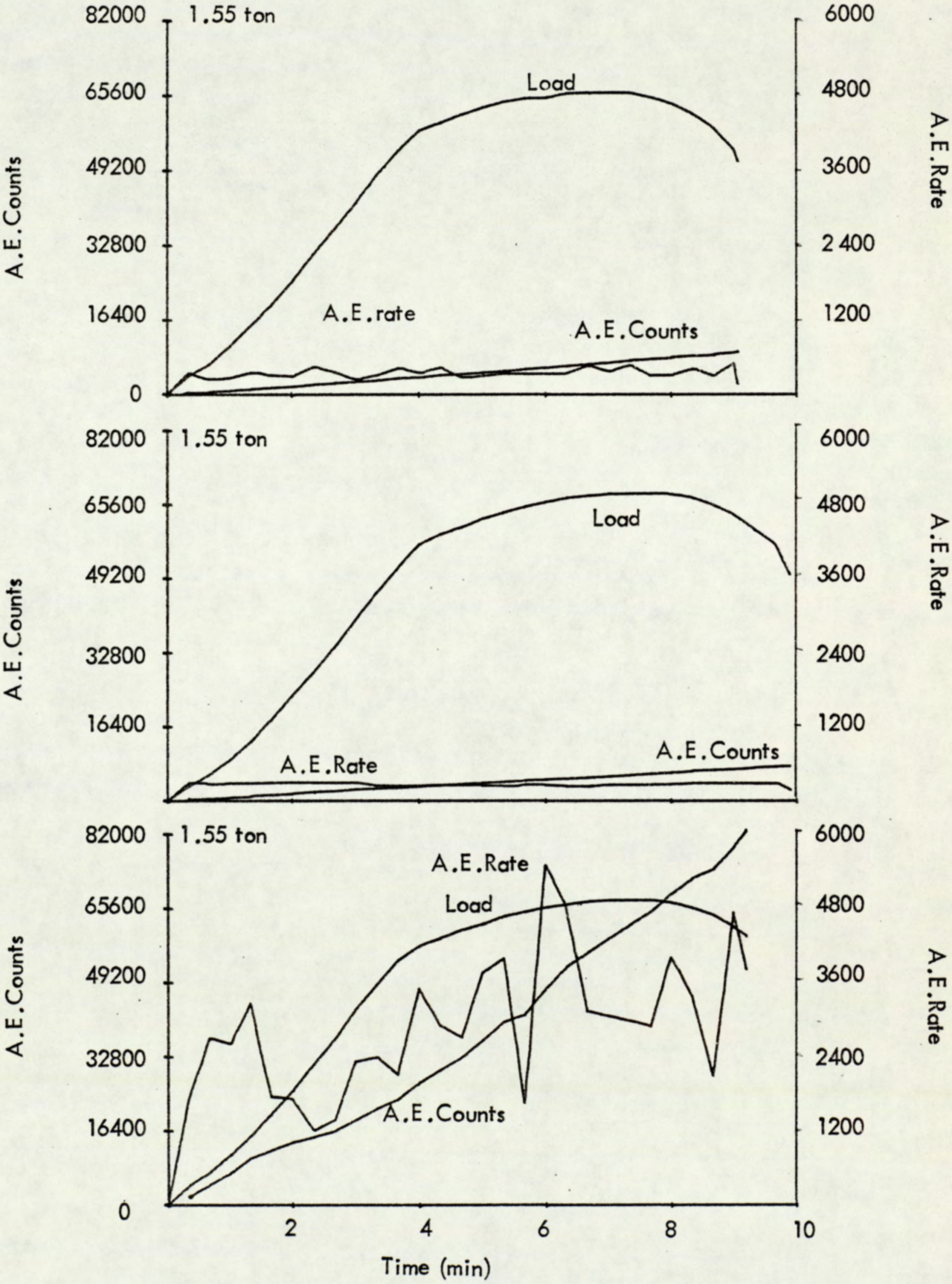

Fig. 42. round specimens (C21)

r = 1.00 mm

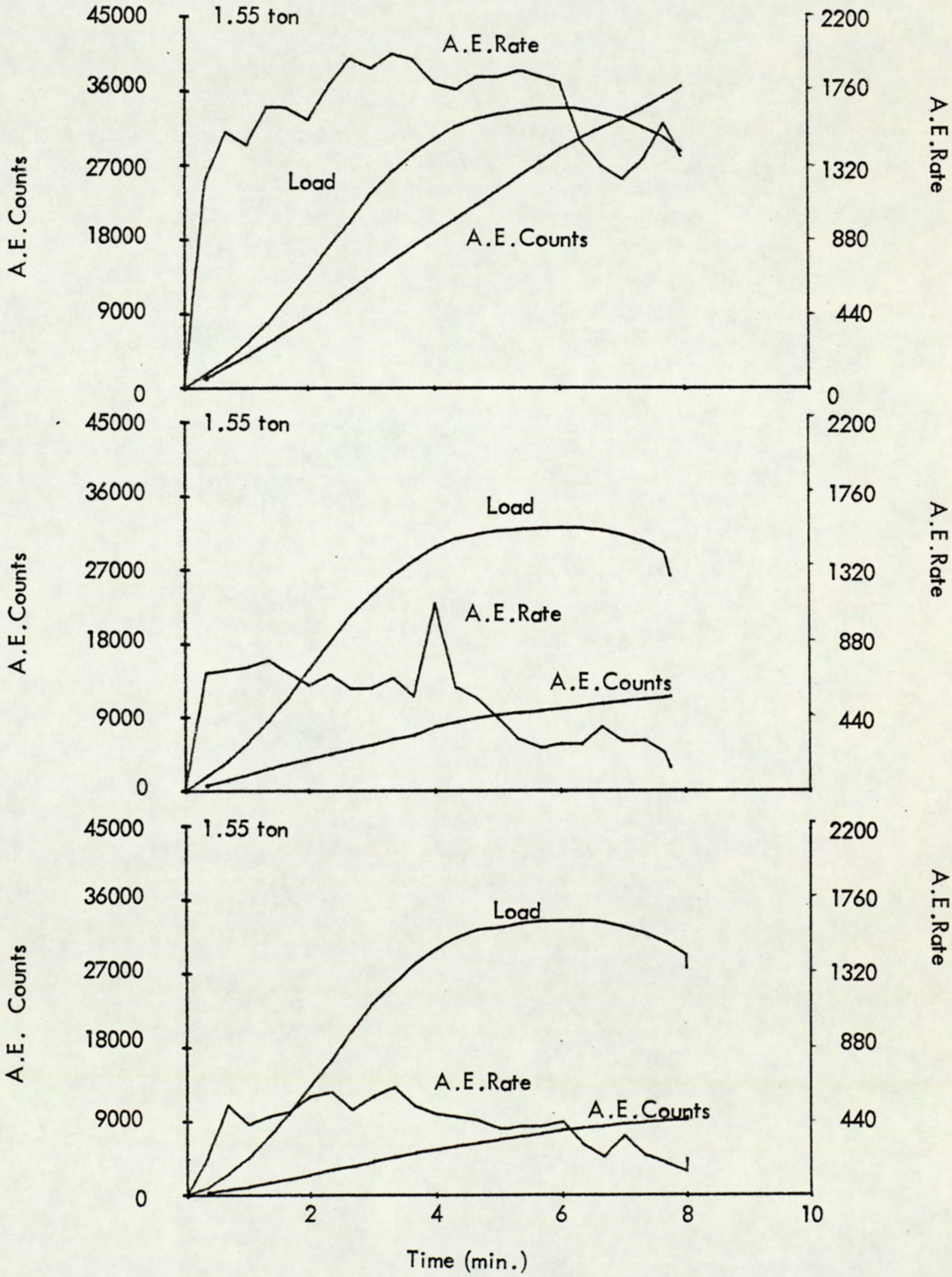

Fig. 43. round specimens (C21)

r = 0.26 mm

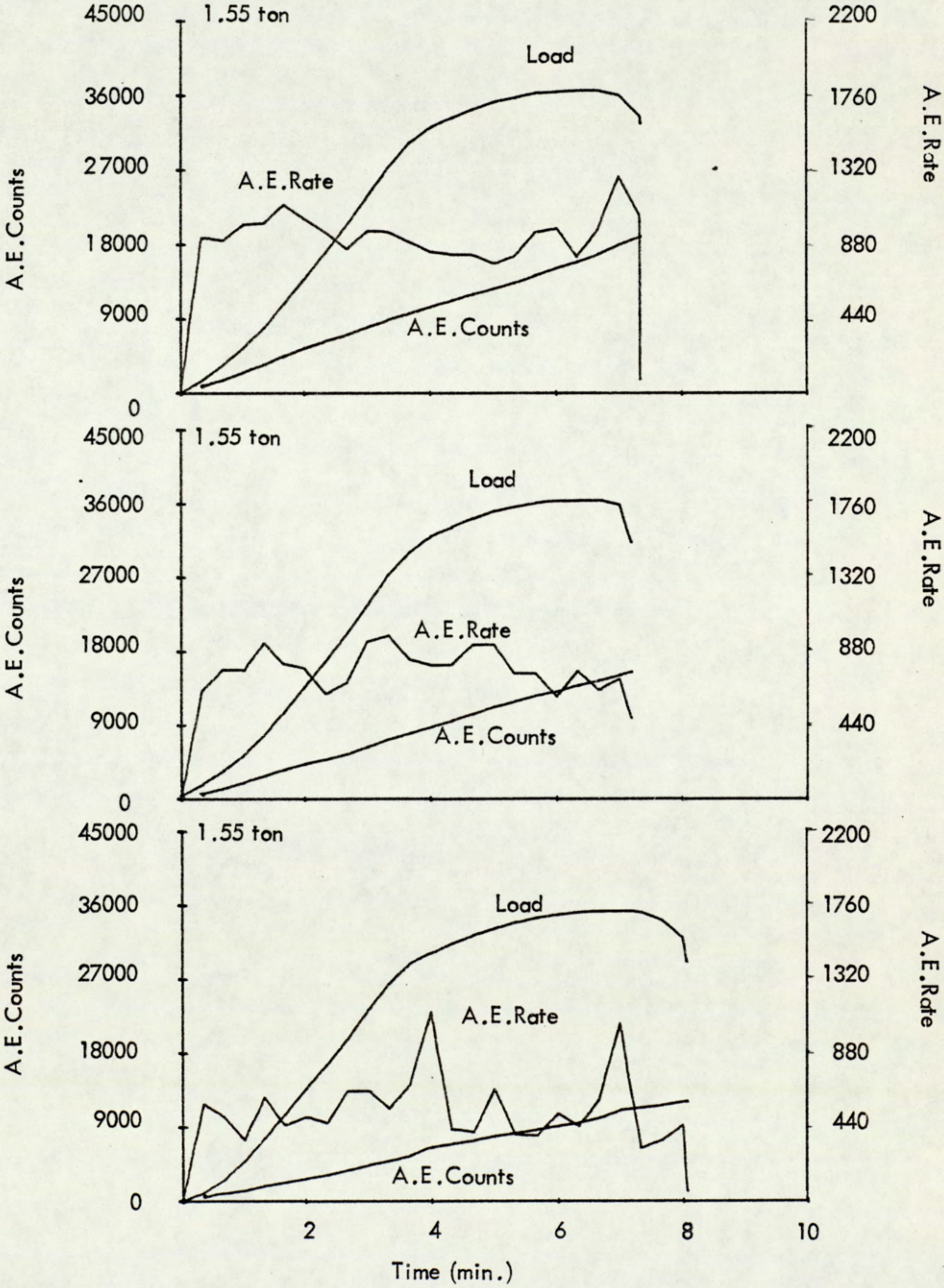

Fig. 44. round specimens (C21)

r = 0.16 mm

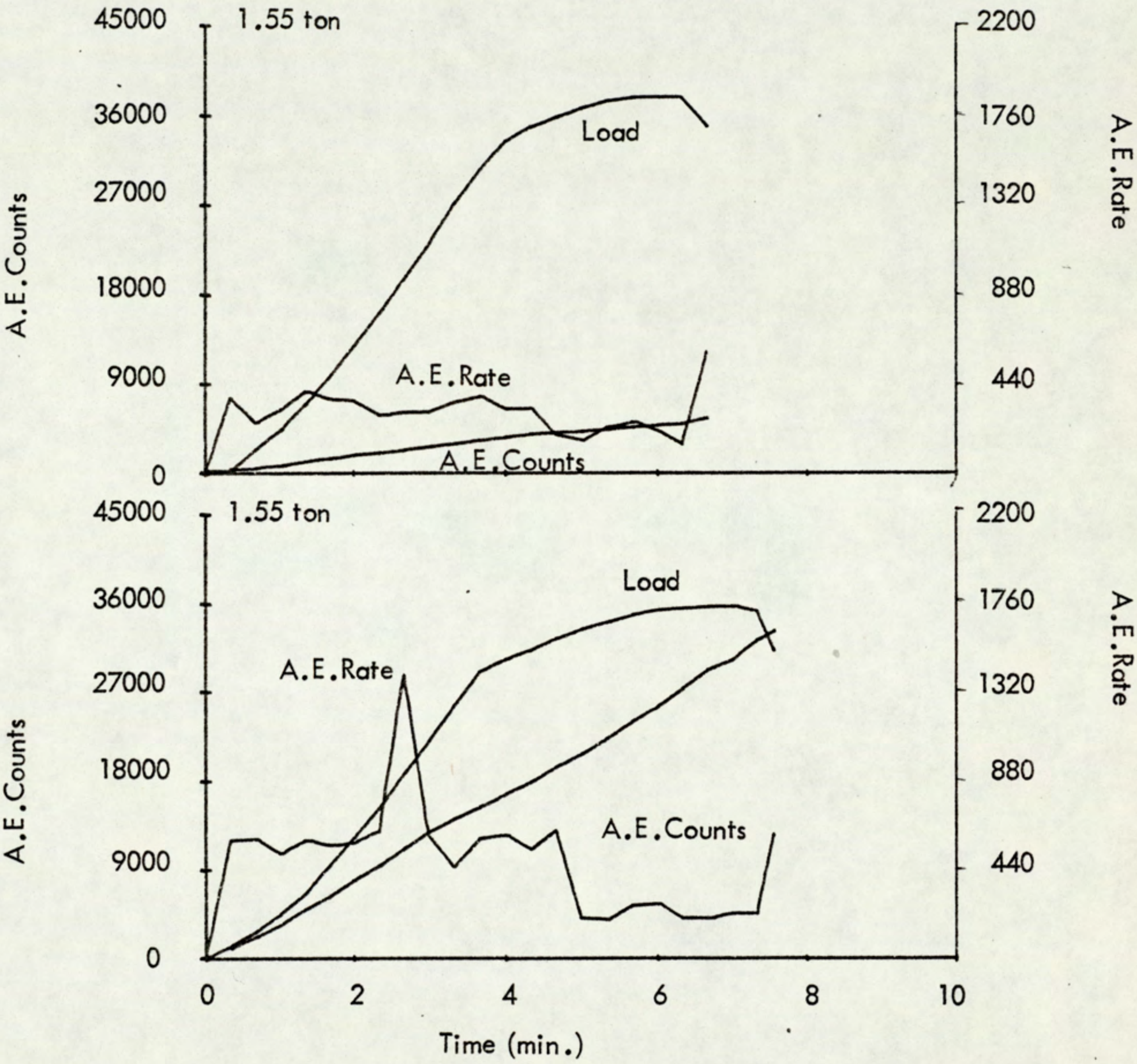

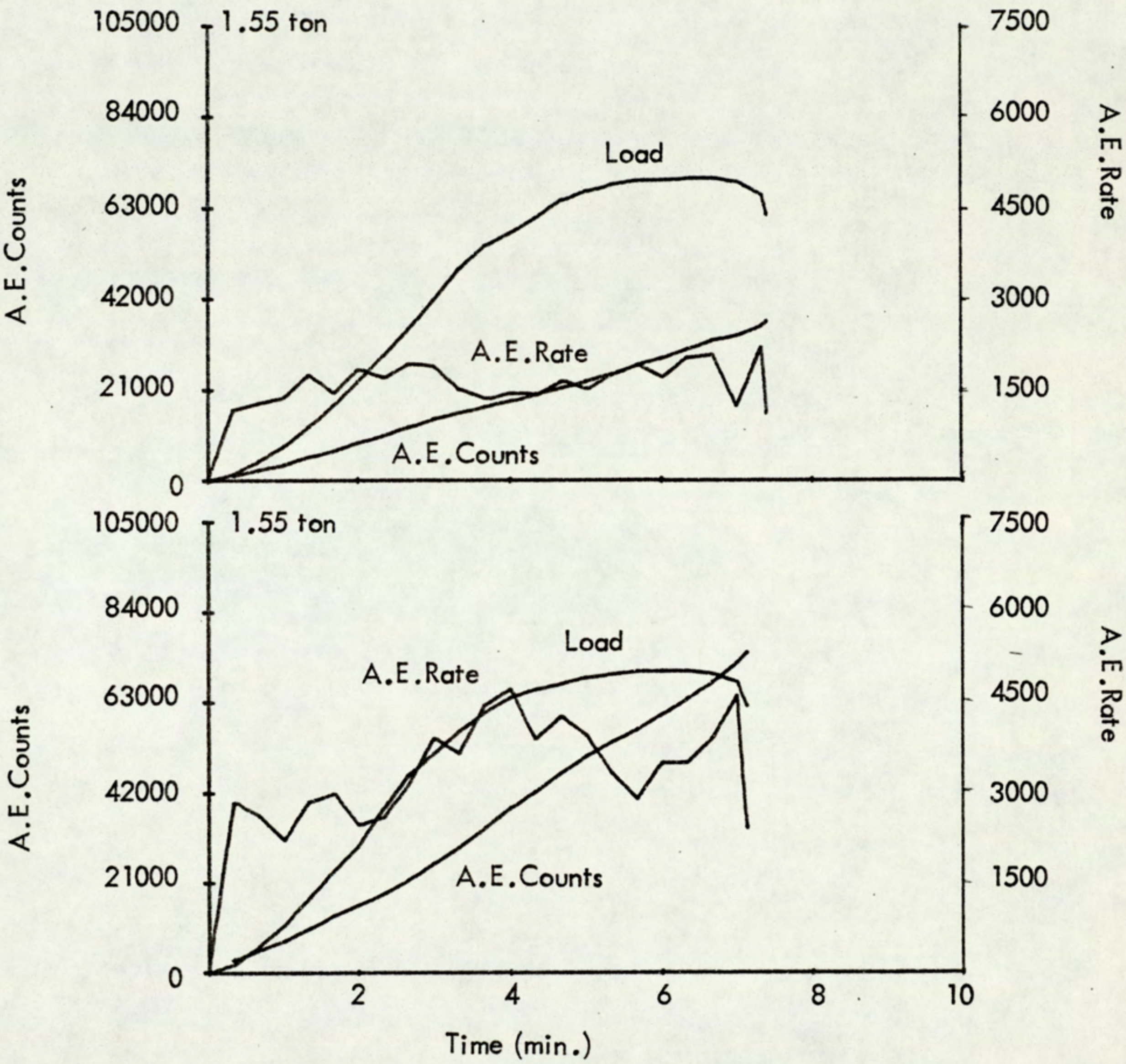

Fig. 45. round specimens (C22)

r = 1.00 mm

Fig. 46. round specimens (C22)

r = 0.26 mm

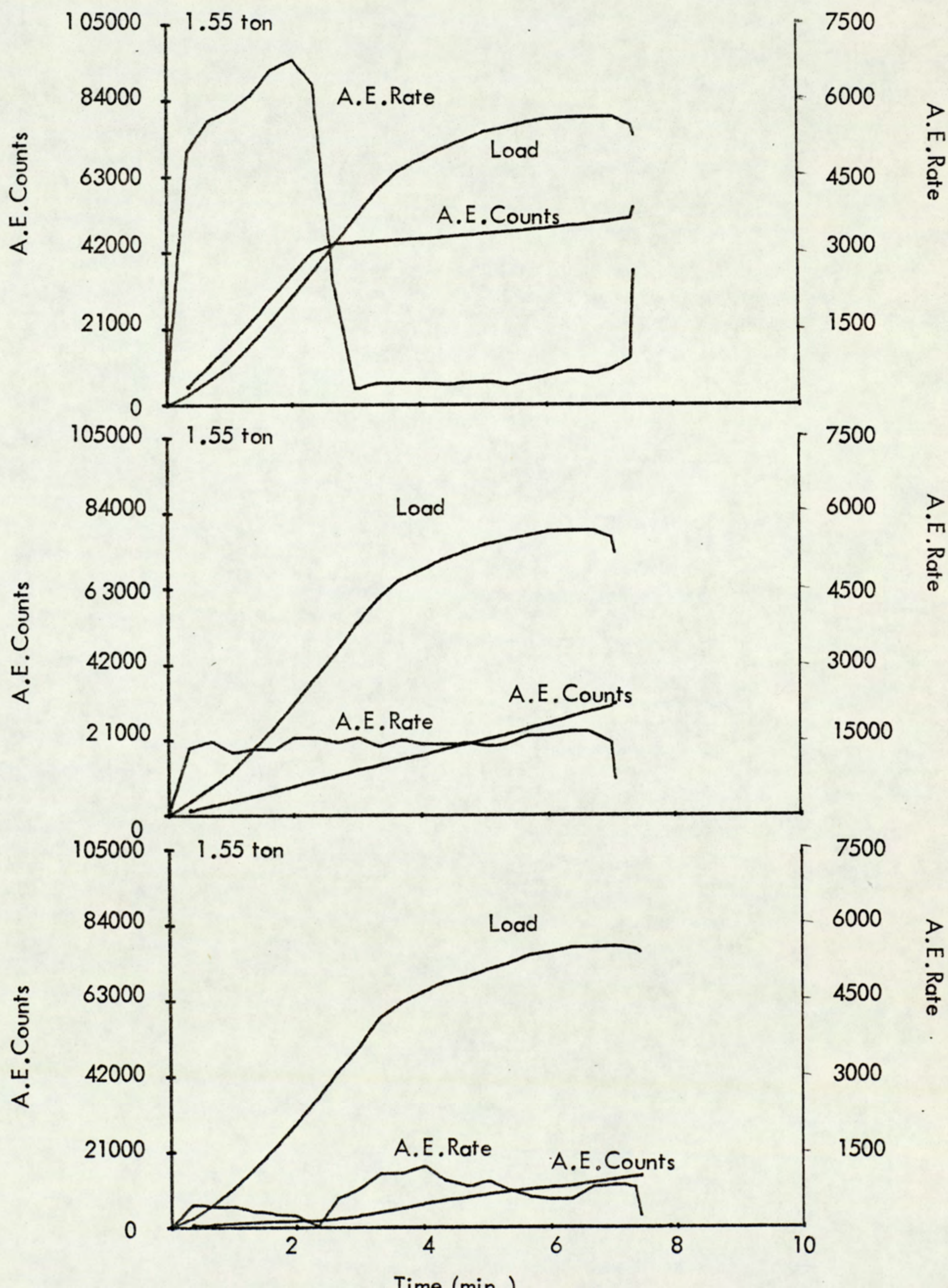

Fig. 47. round specimens (C22)

r = 0.16 mm

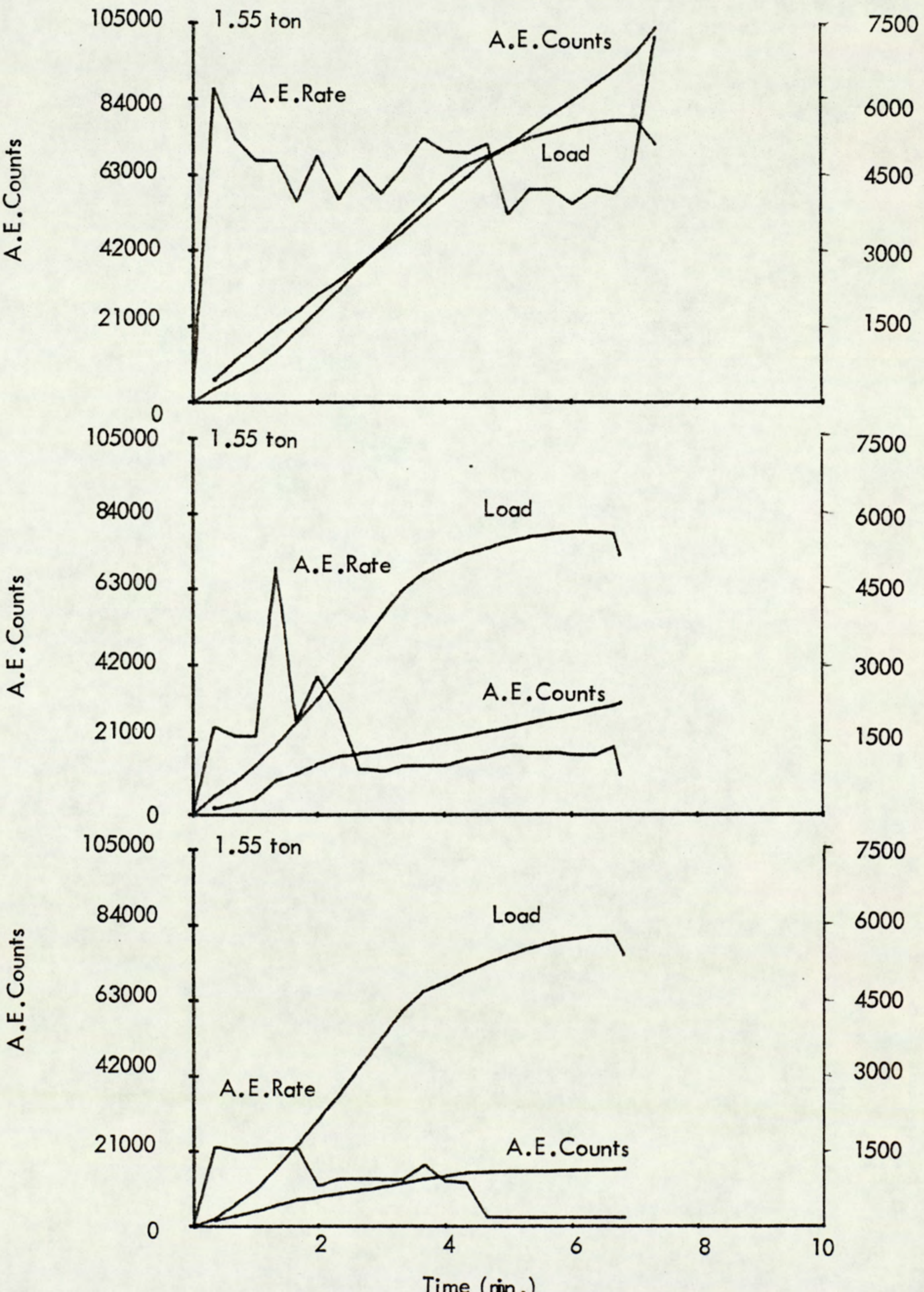

Fig. 48. round specimens (C30)

r = 1.00 mm

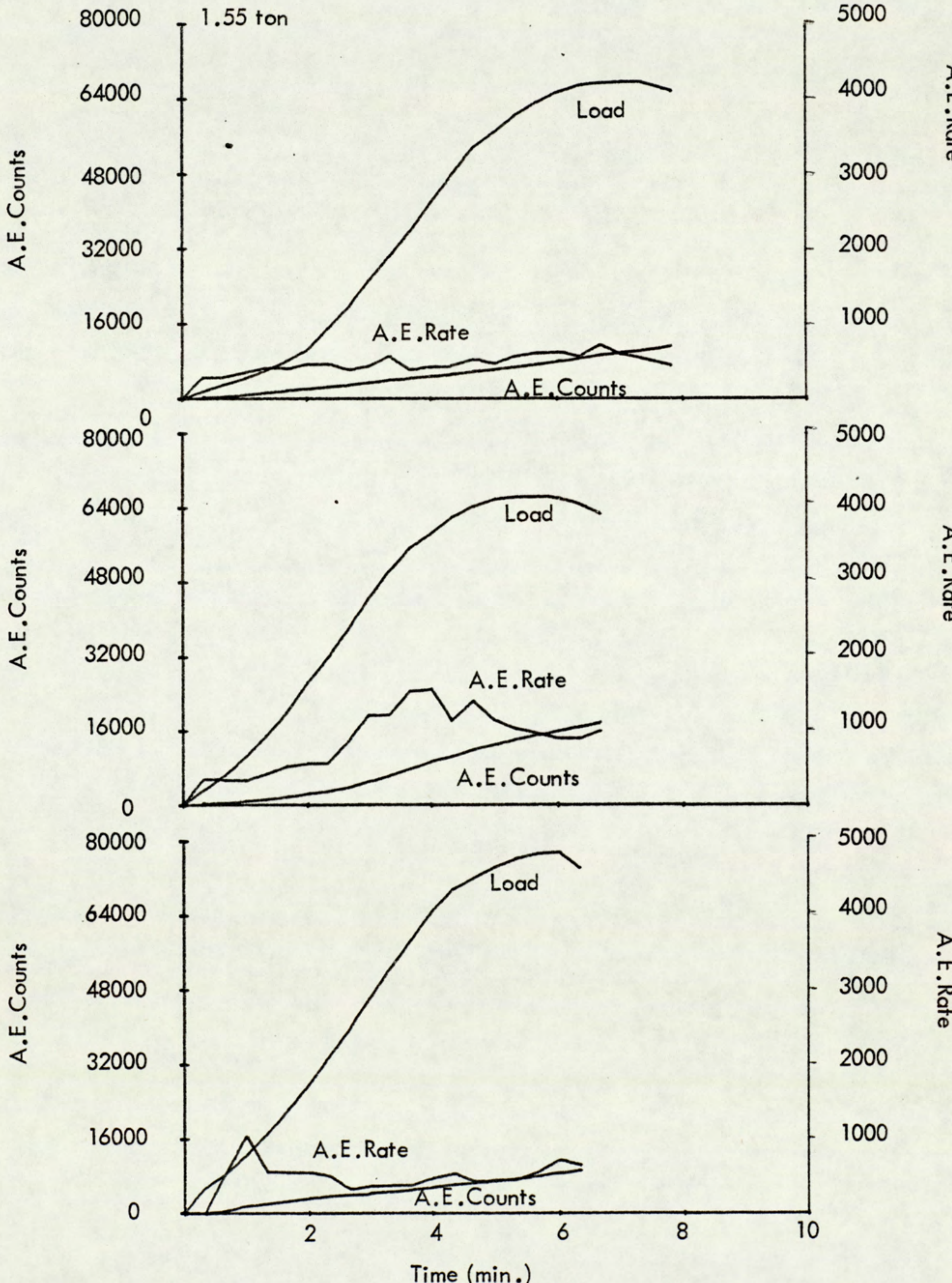

Fig. 49. round specimens (C30)

r = 0.26 mm

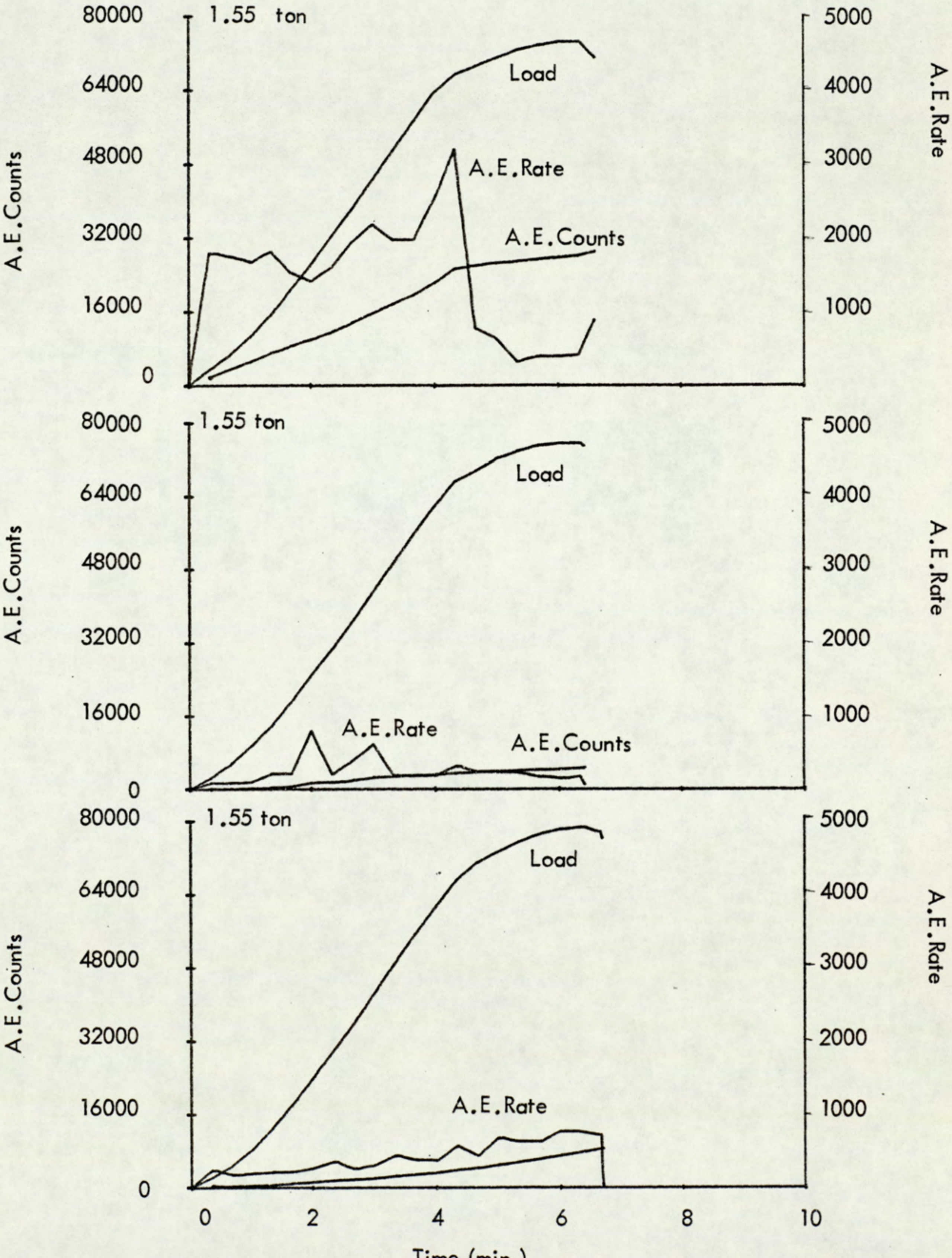

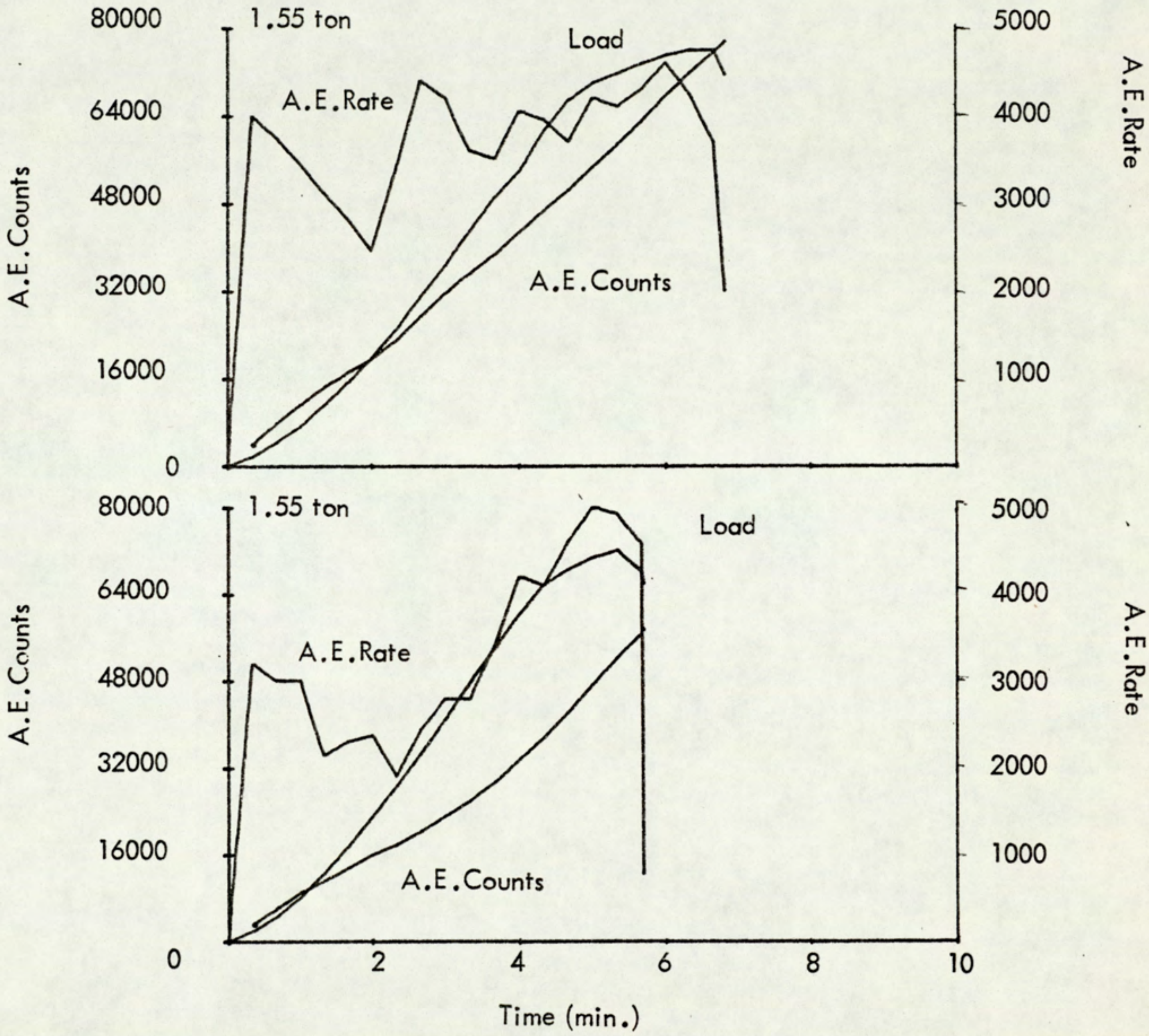

Fig. 50. round specimens (C30)

r = 0.16 mm

Fig. 51. round specimens (C31)

r = 1.00 mm

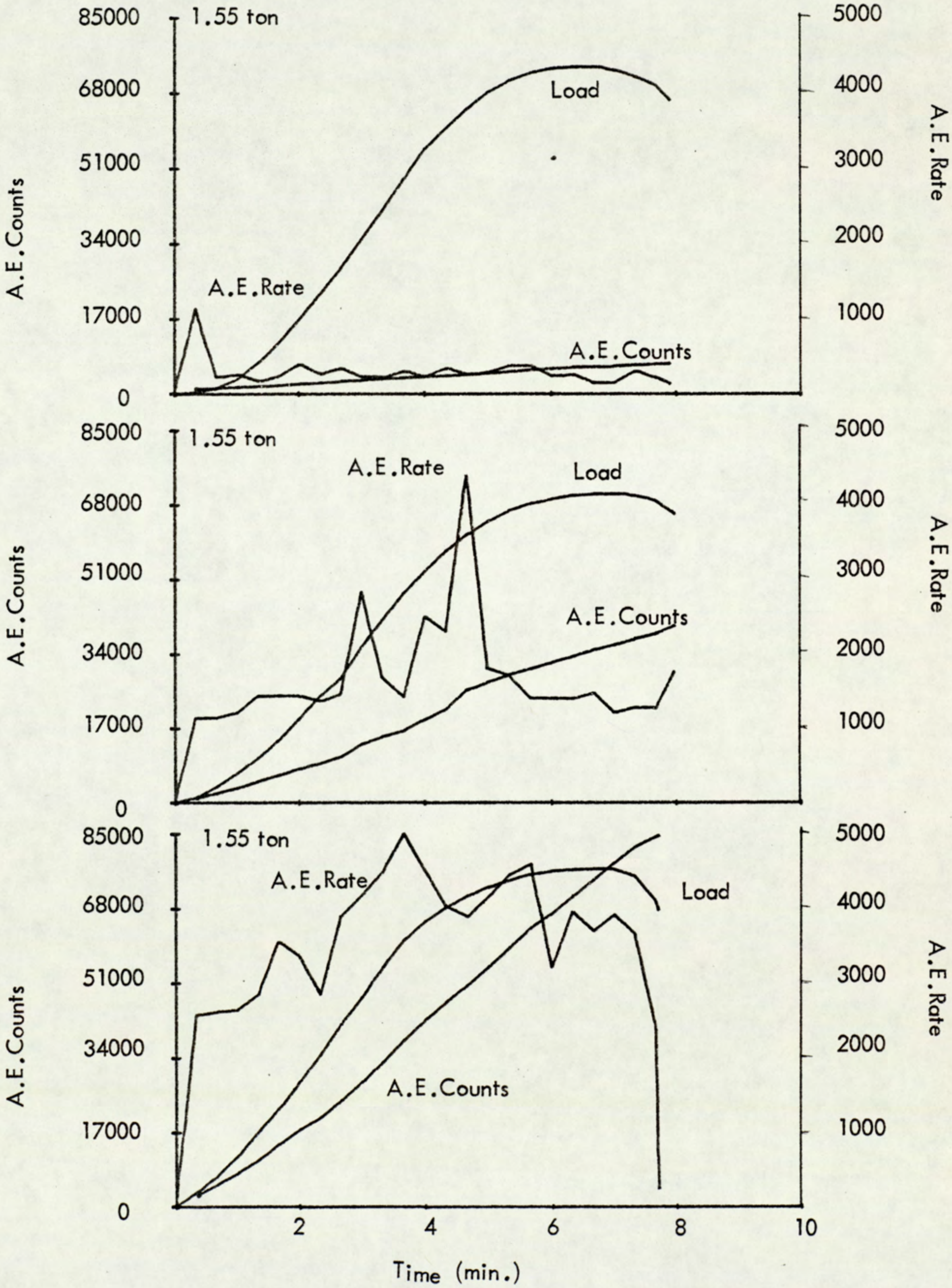

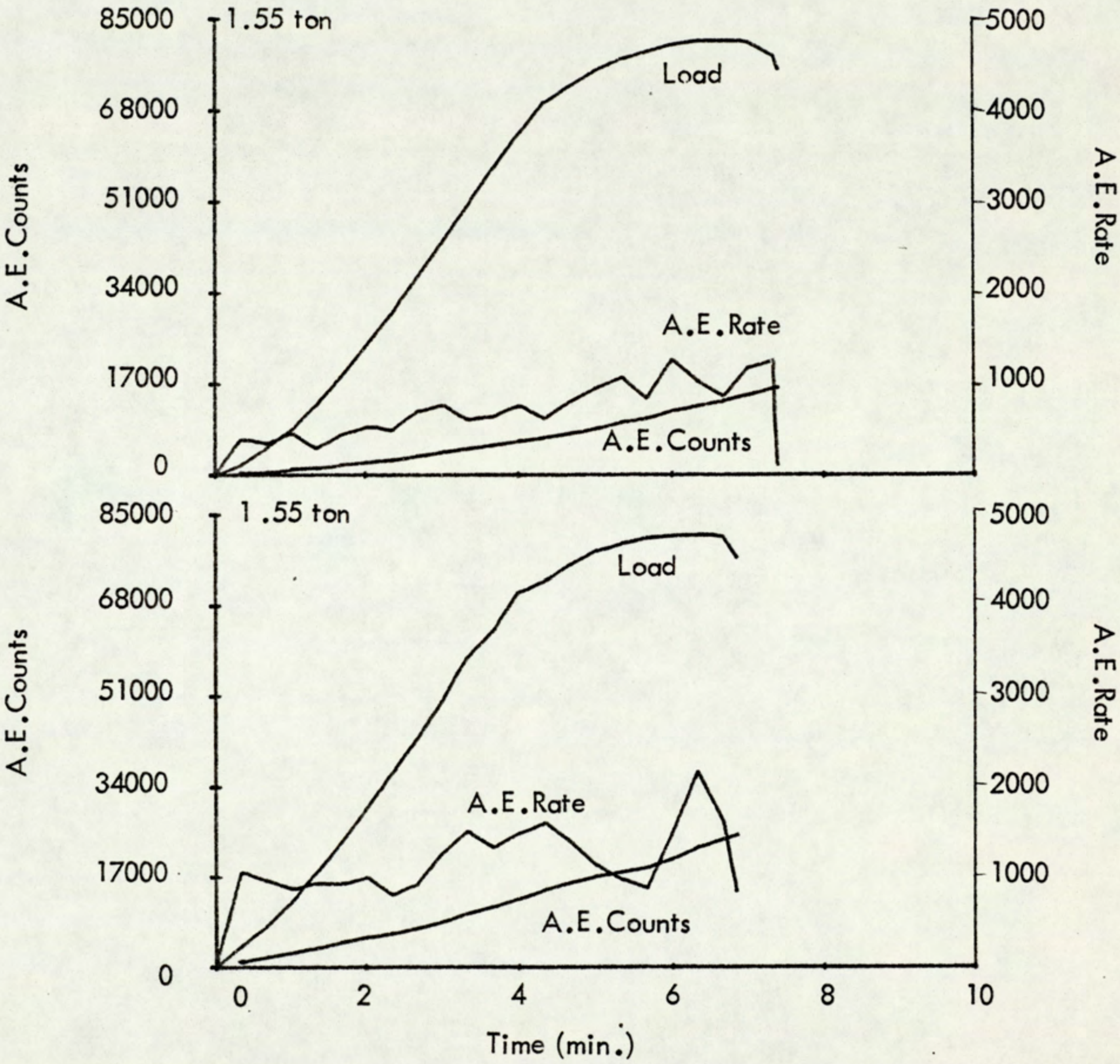

Fig. 52. round specimens (C31)

r = 0.26 mm

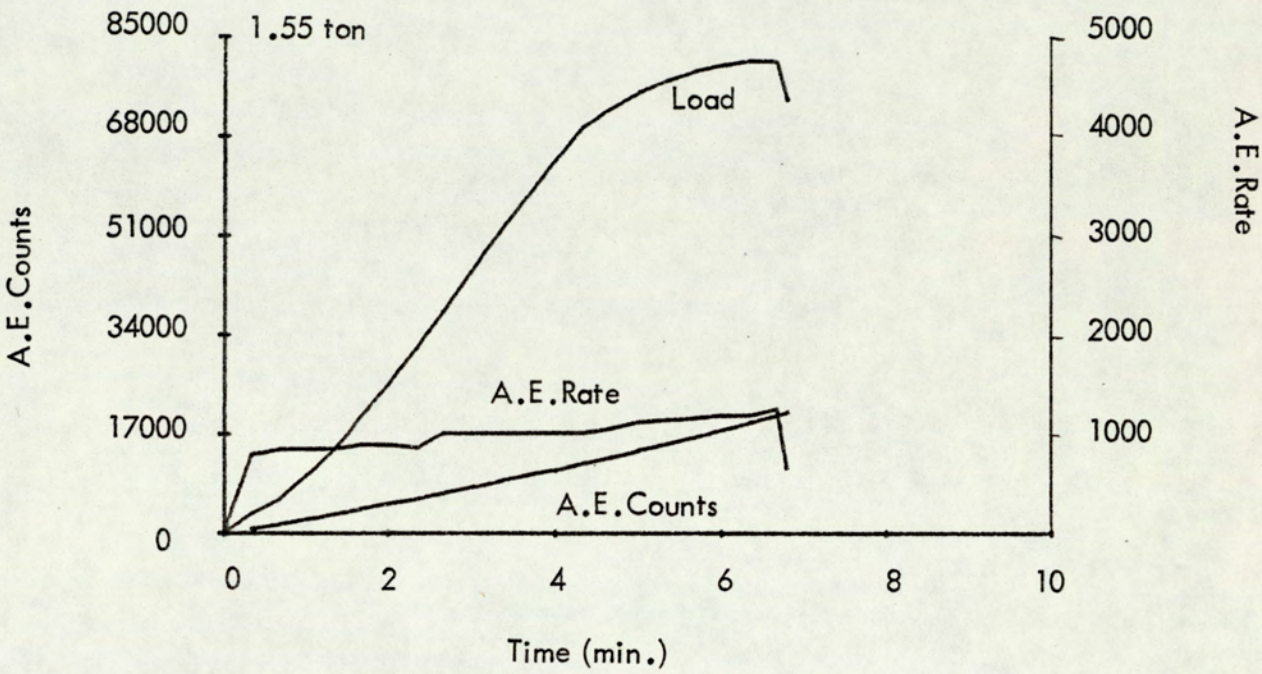

<u>Fig. 53.</u> round specimens (C31)

r = 0.16 mm

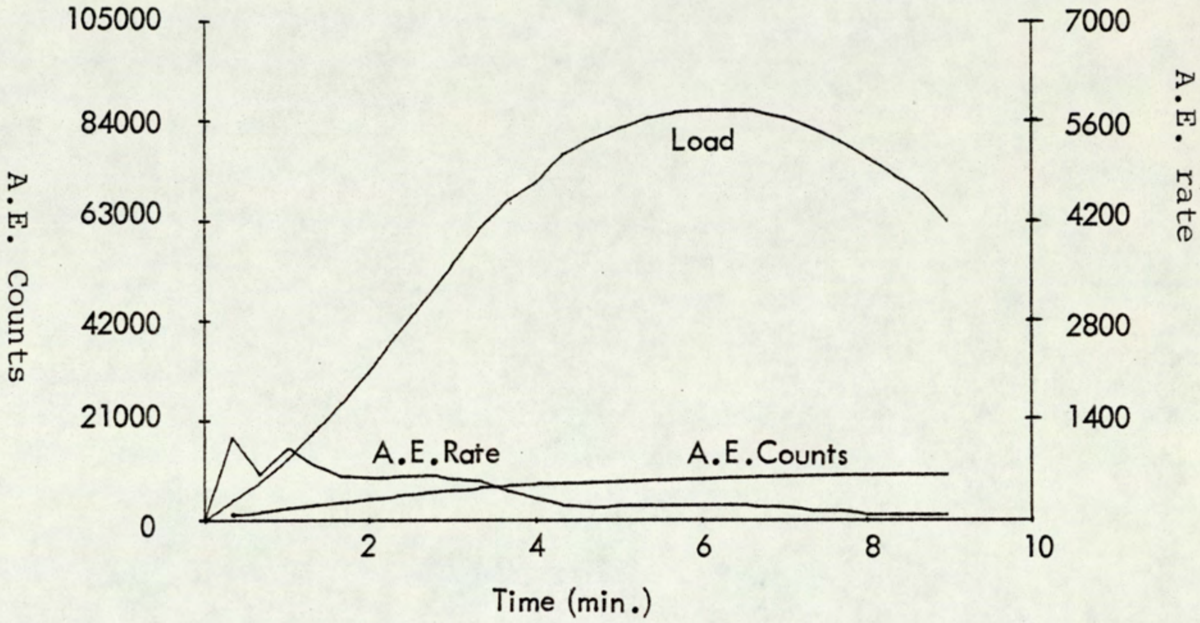

Fig. 54. round specimens (C32)

r = 1.00 mm

Fig. 55. round specimens (C32)

r = 0.26 mm

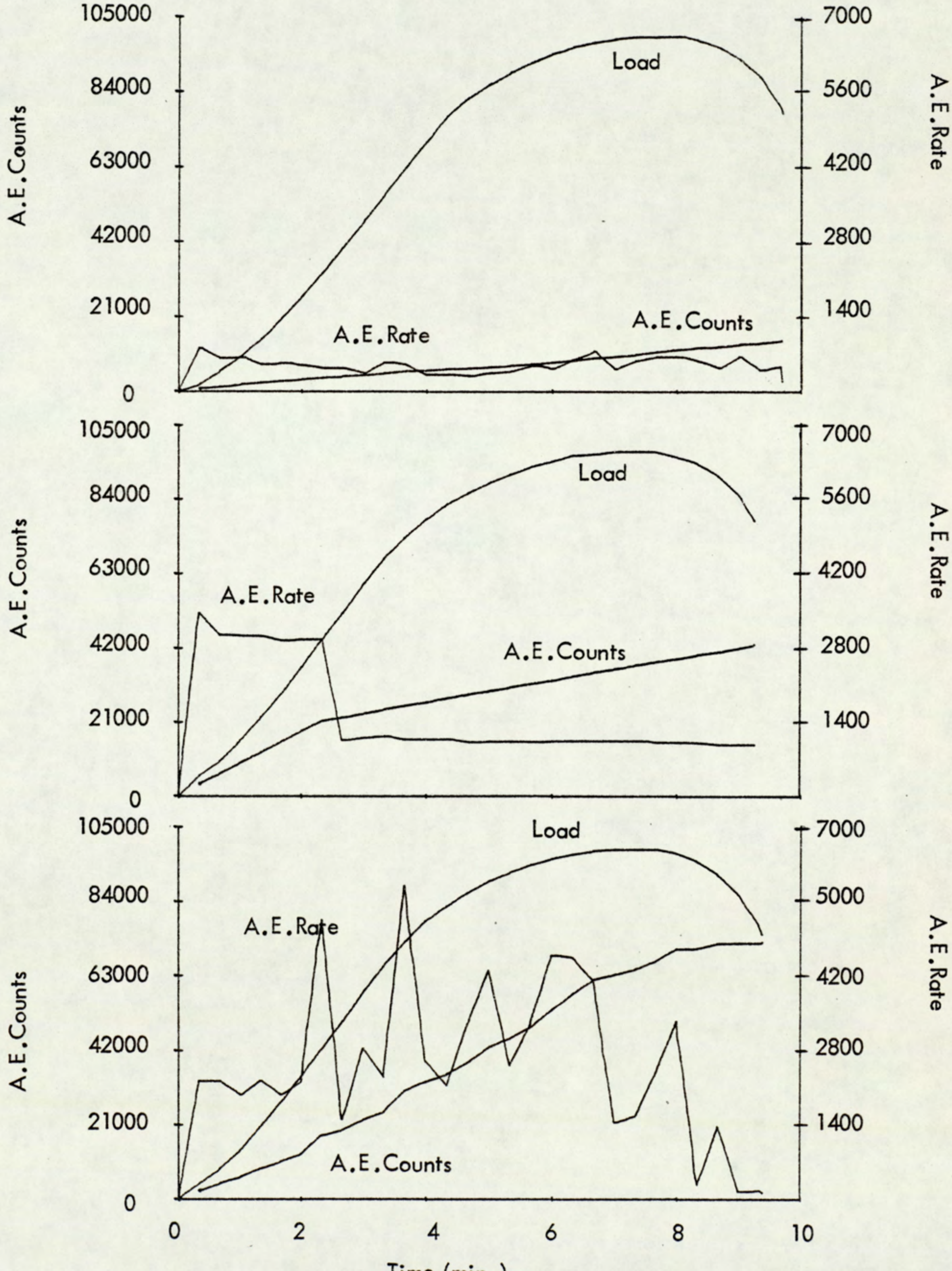

Fig. 56. round specimens (C32)

r = 0.16 mm

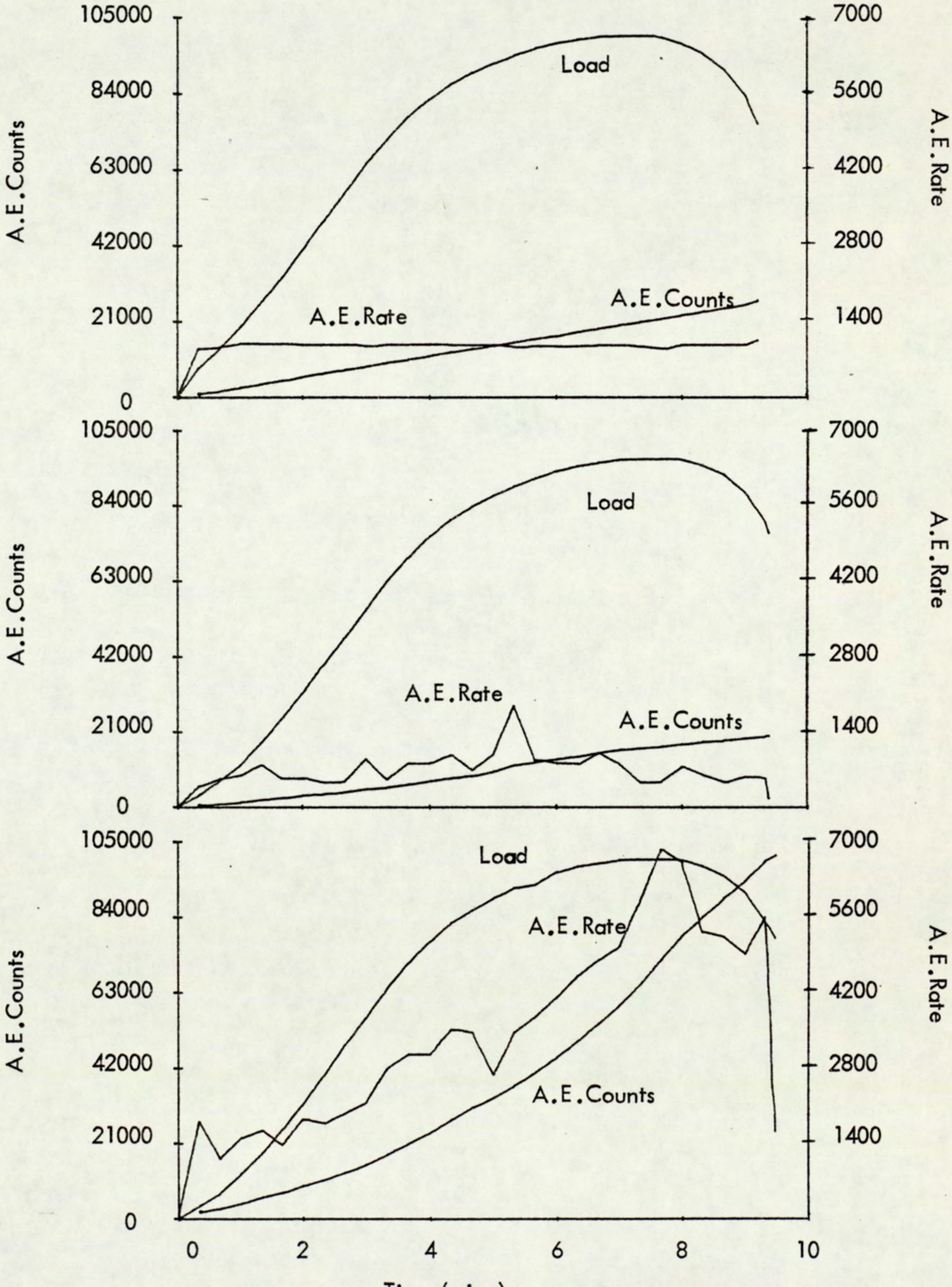

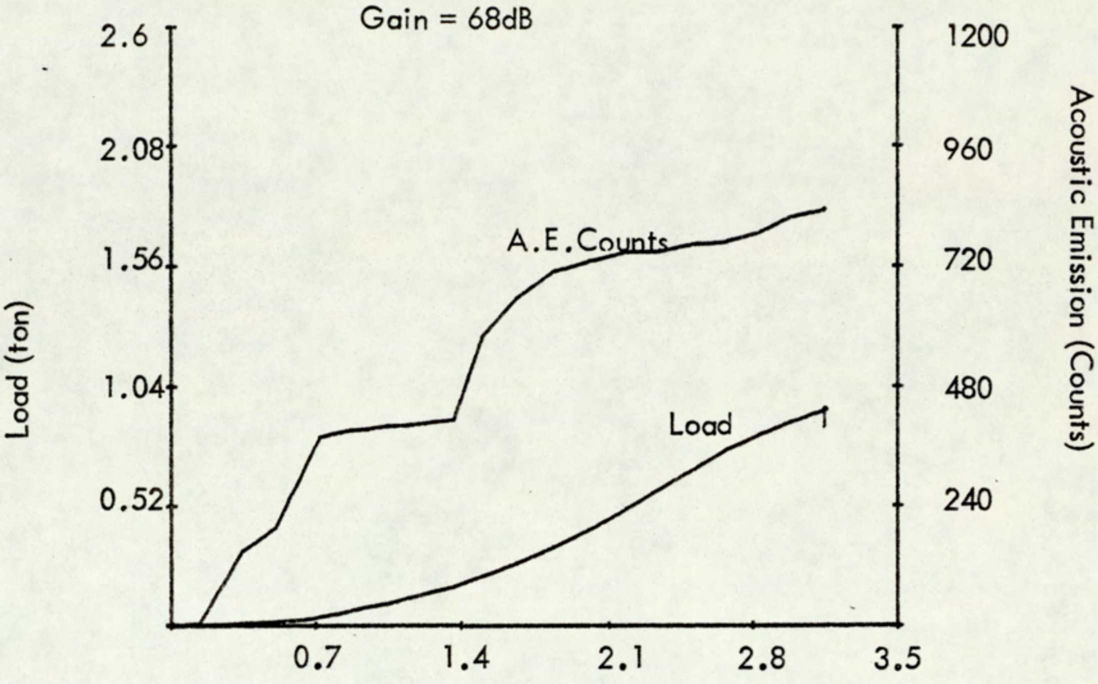

Fig. 57.a. Displacement (mm)

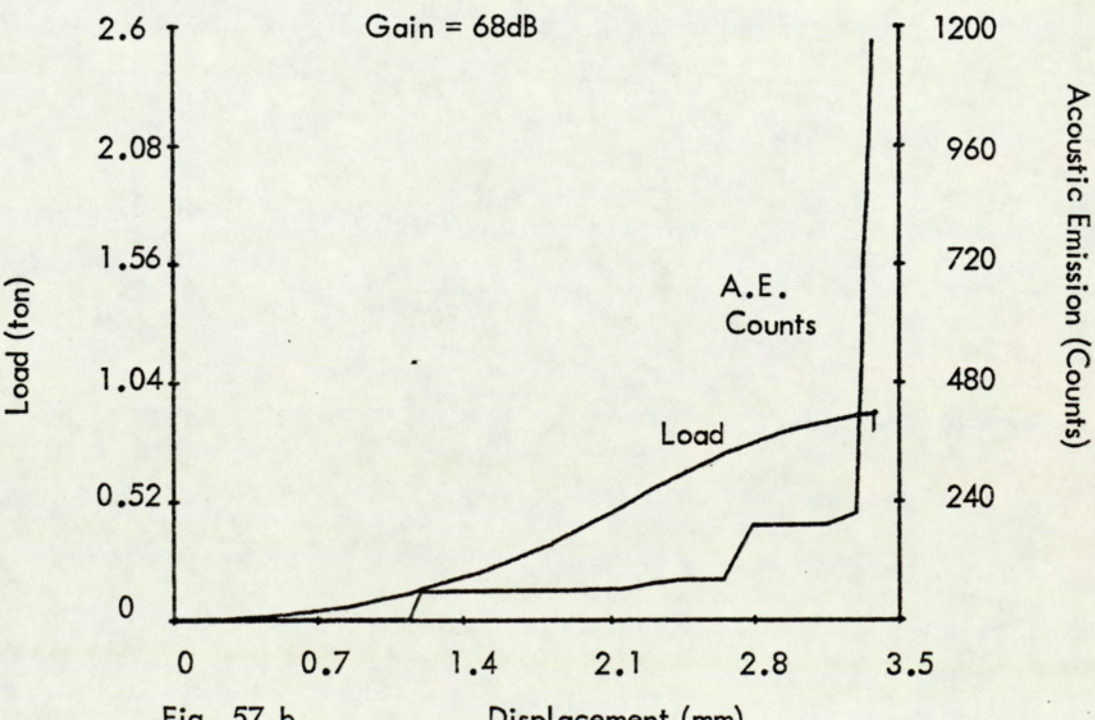

Fig. 57.b. Displacement (mm)

Fig. 57. Three-point bending tests (r = 0.127mm)

a. As elastic

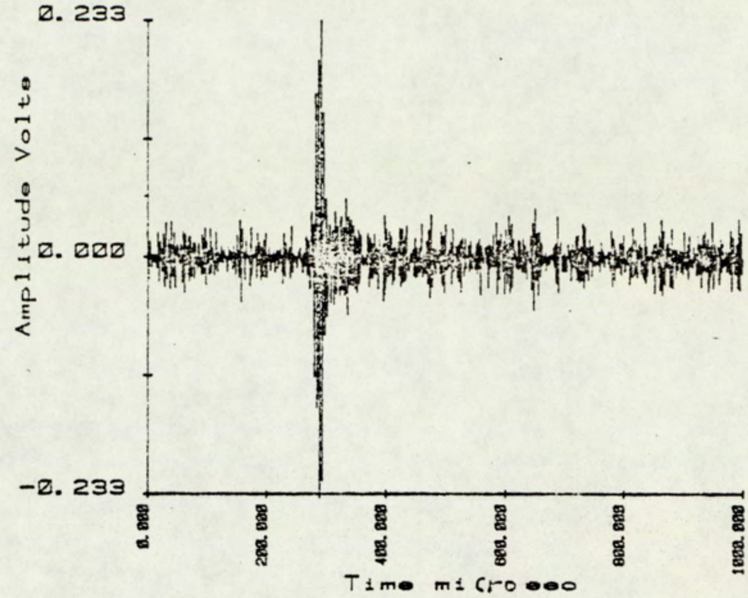

b. At pre yielding

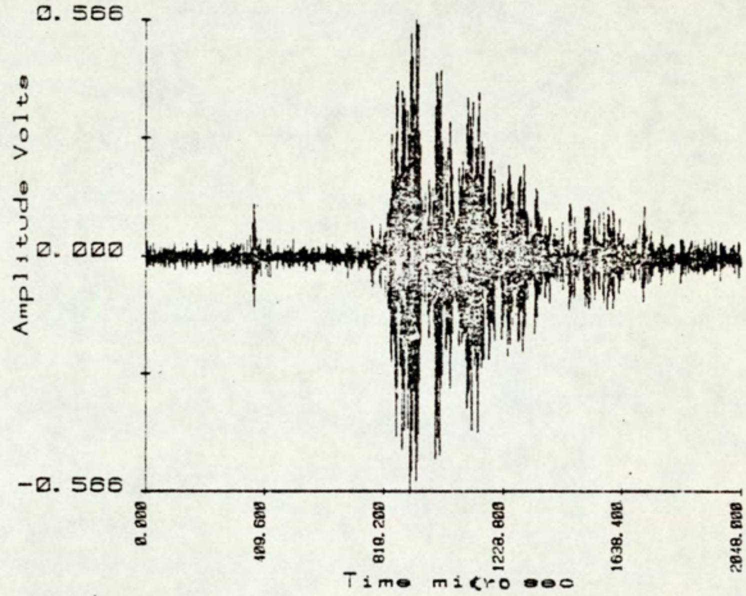

c. At fracture

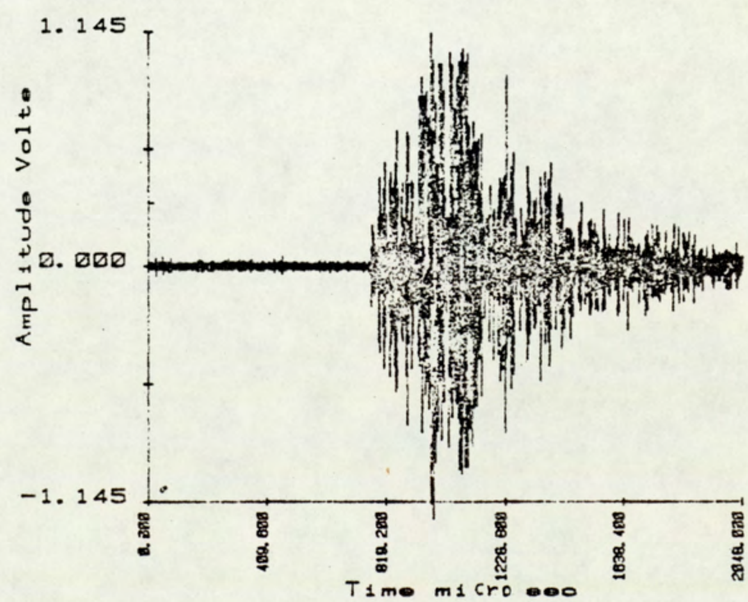

Fig. 57.a.1. A.E. pulses generated from a three-point bending test (r = 0.127mm)

a. At elastic

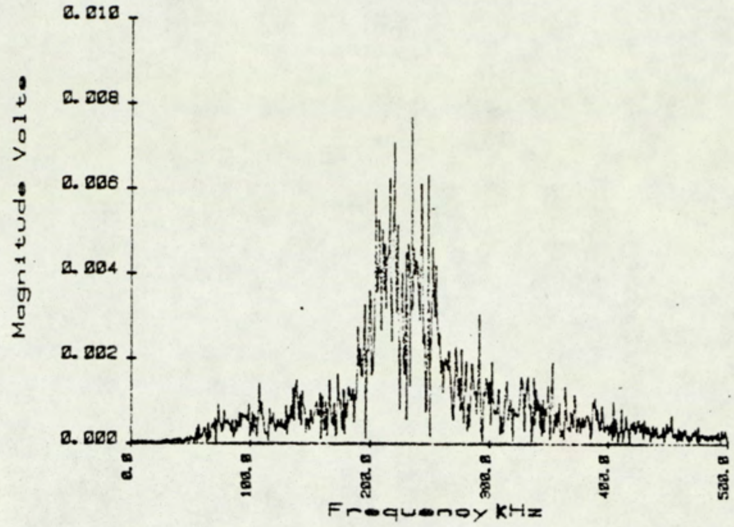

b. At pre yielding

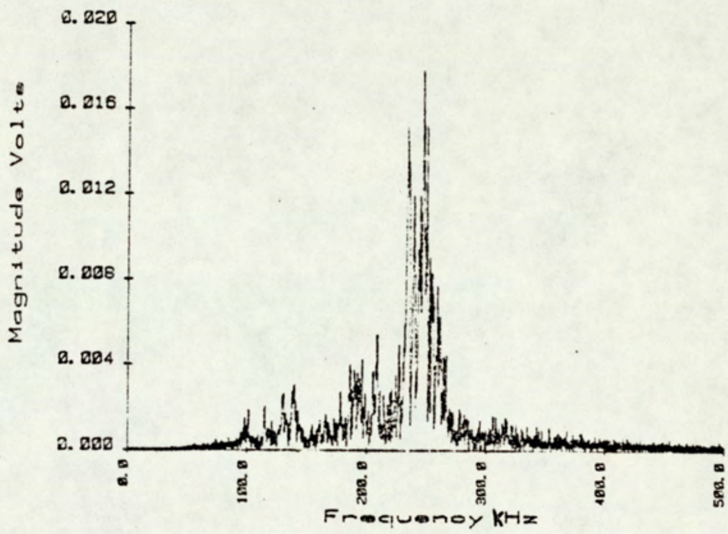

c. At fracture

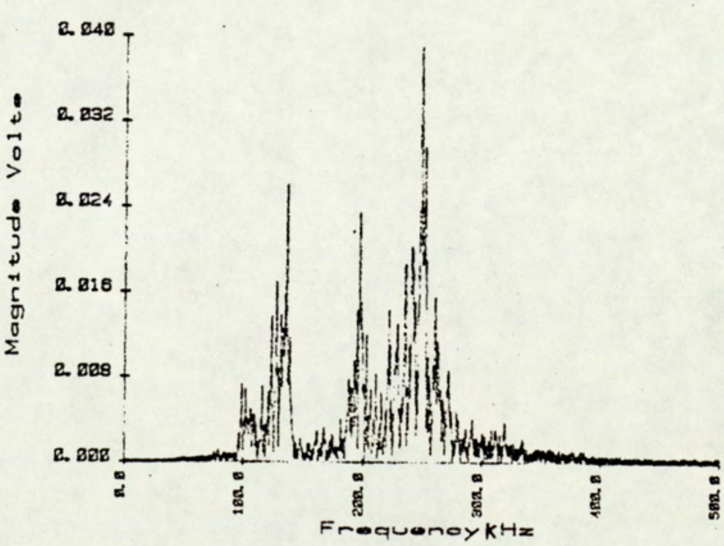

Fig. 57.a.2. F.F.T. spectrum analysis of the A.E. signals from three-point bending test

(r = 0.127mm)

a. At elastic

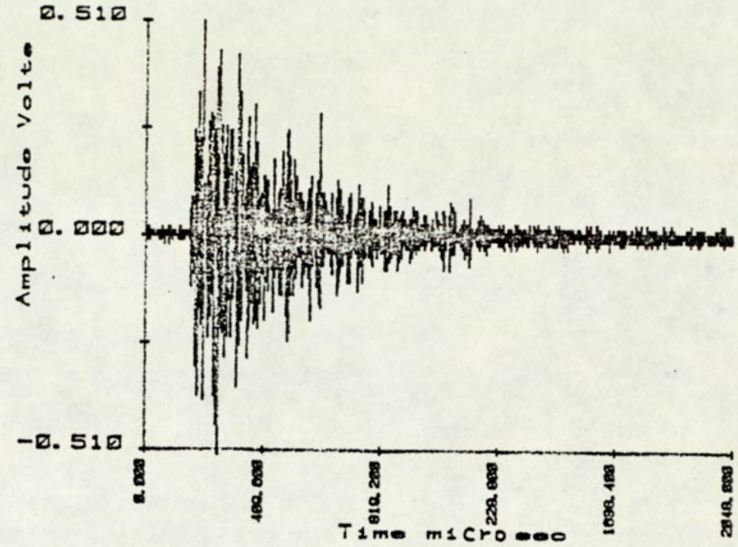

b. At pre yielding

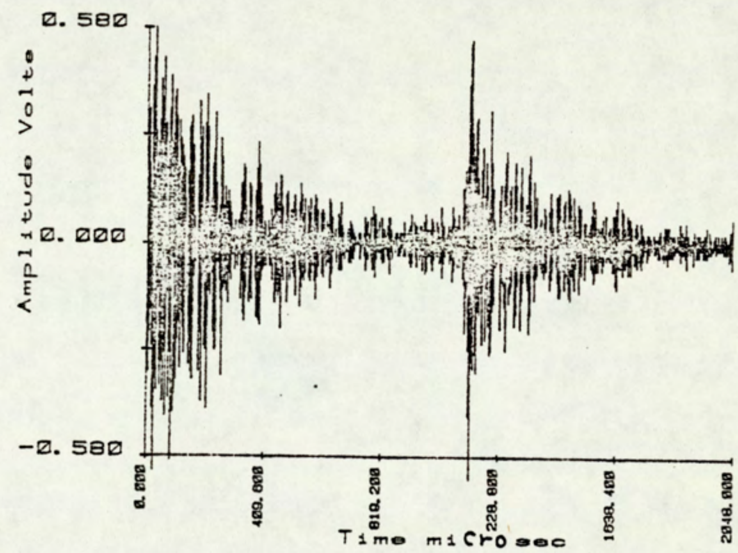

c. At fracture

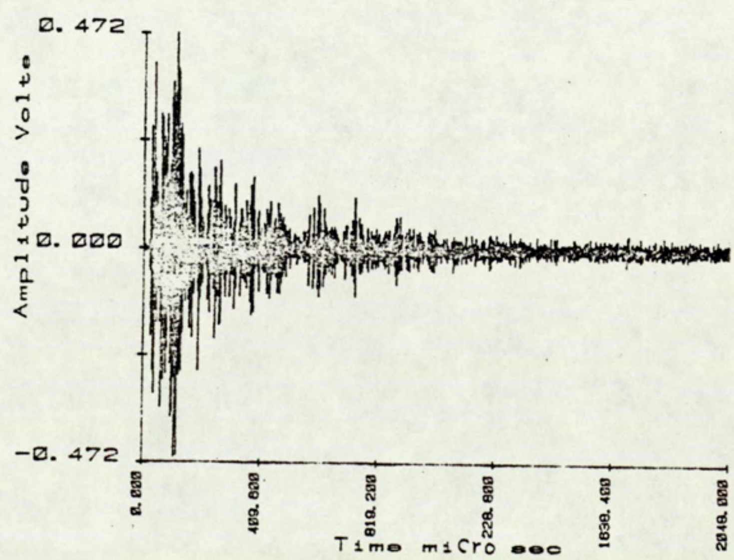

Fig. 57.b.1. A.E. pulses generated from a three-point bending test (r = 0.127mm)

a. At elastic

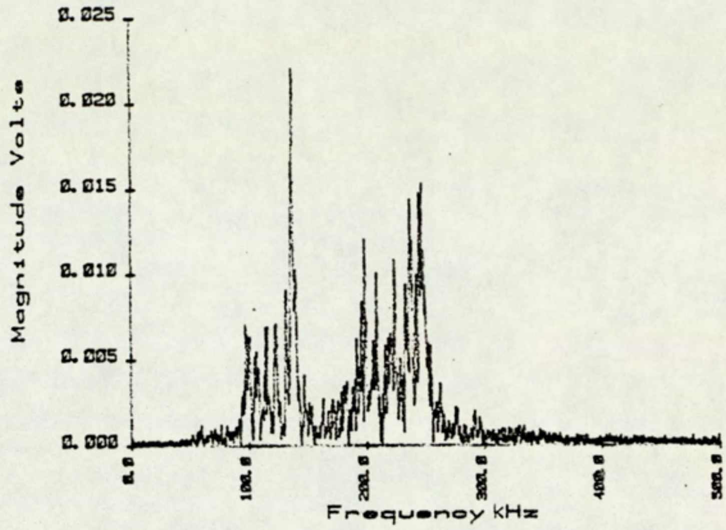

b. At pre yielding

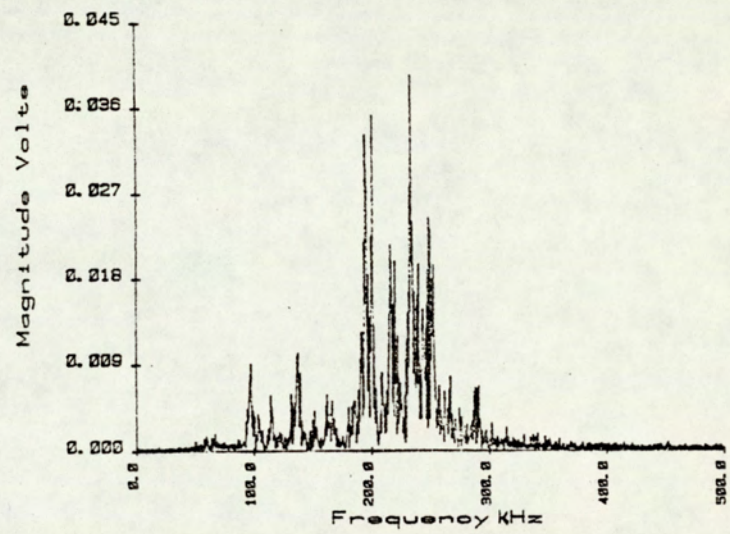

c. At fracture

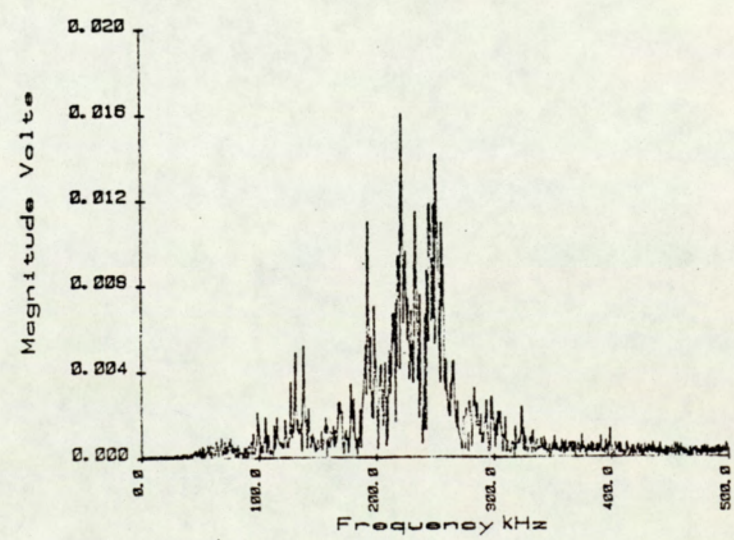

Fig. 57.b.2. F.F.T. spectrum analysis of the A.E. signals from three-point bending test (r = 0.127mm)

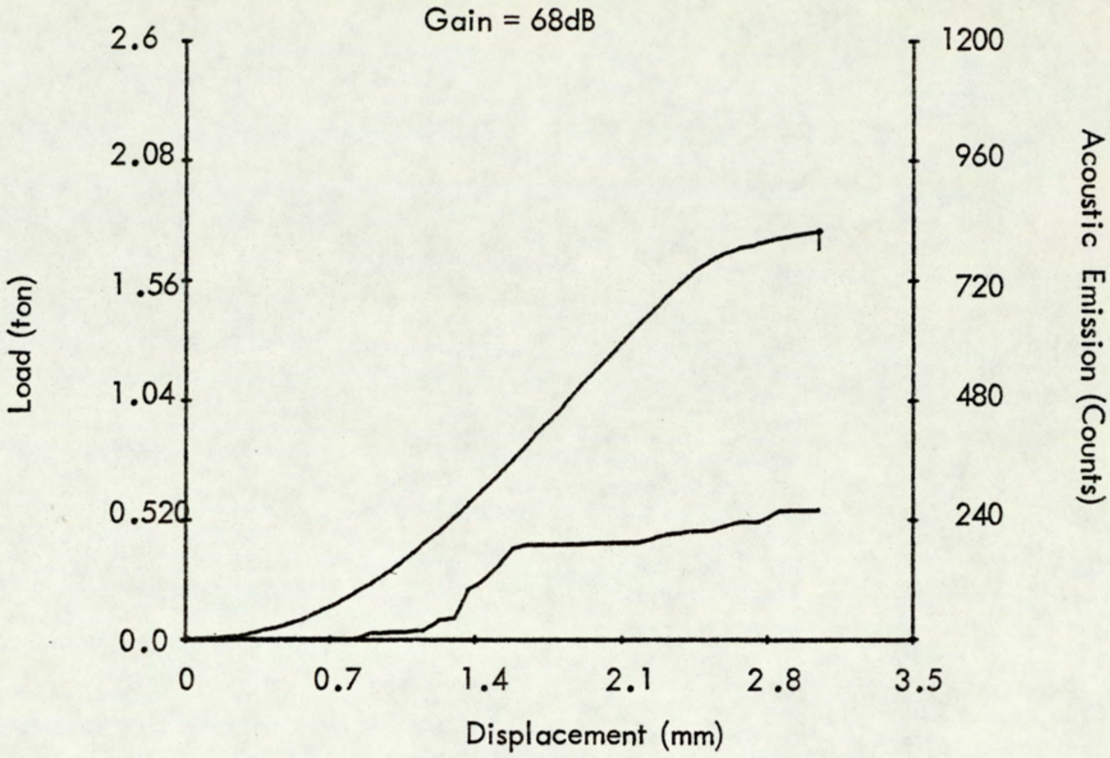

Fig. 58.a.

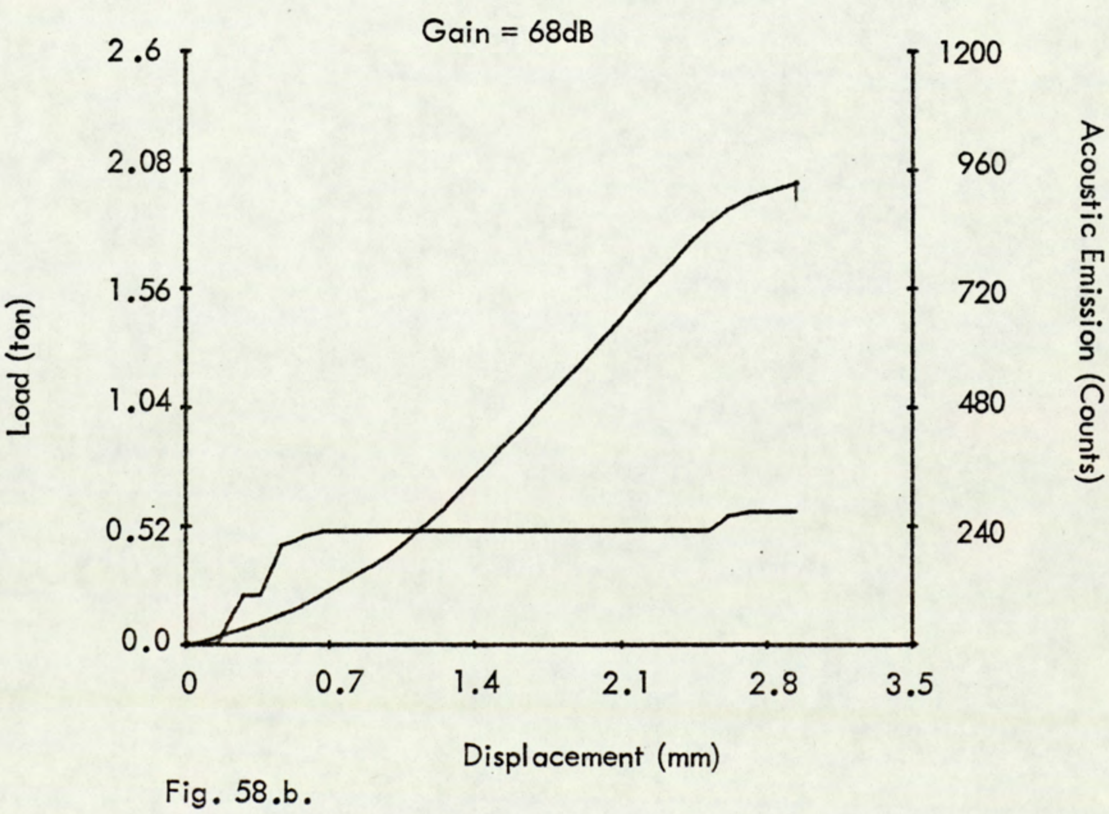

Fig. 58.b.

Fig. 58. Three-point bending tests (r = 12.7mm)

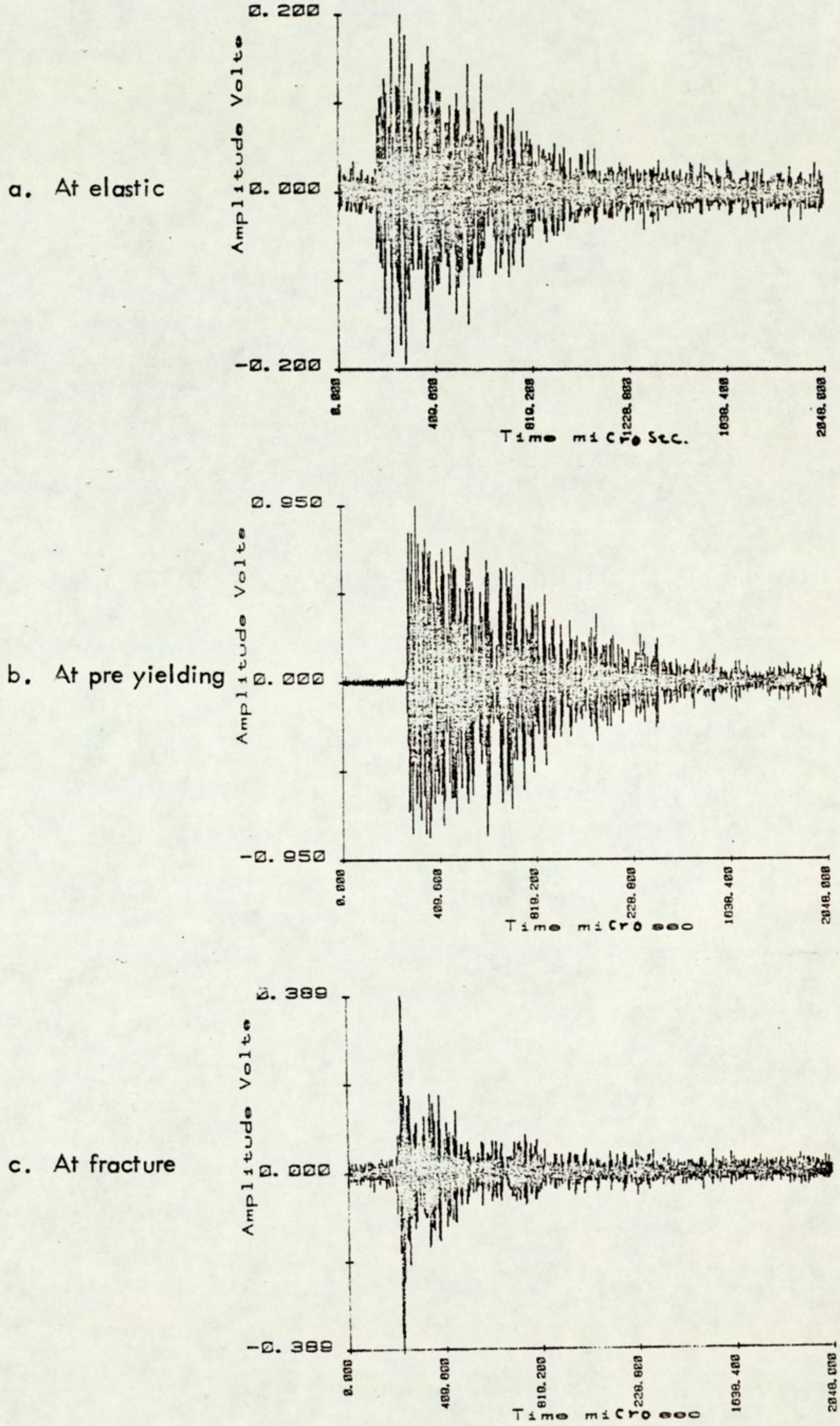

Fig. 58.a.1. A.E. pulses generated from three-point bending test (r = 12.7mm)

a. At elastic

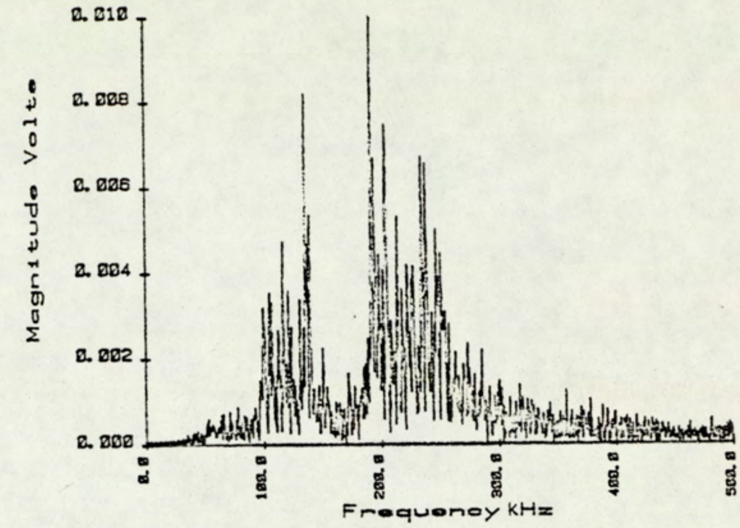

b. At pre yielding

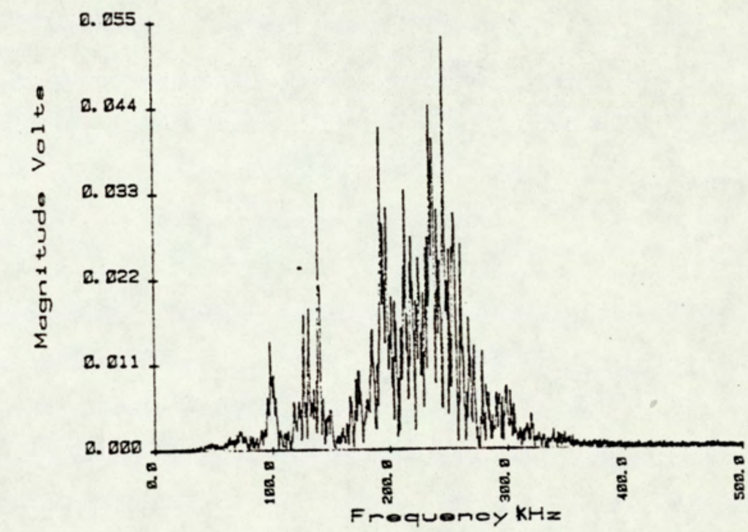

c. At fracture

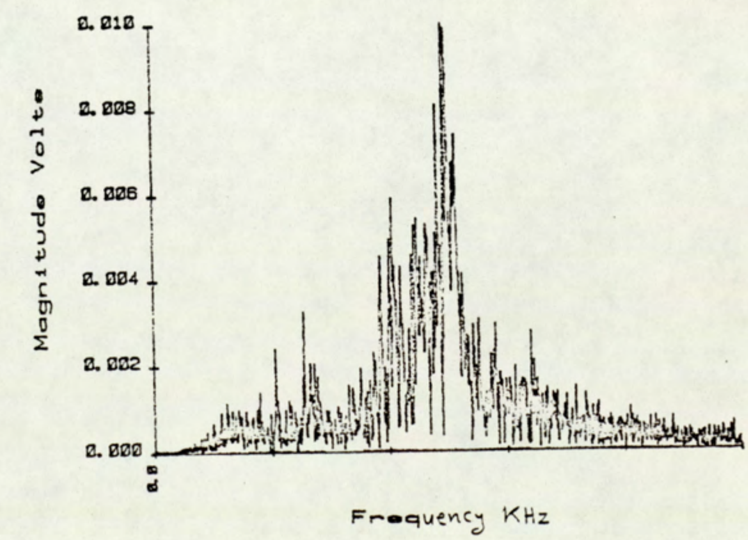

Fig. 58.a.2. F.F.T. spectrum analysis of the A.E.signals from three-point test

(r = 12.7mm)

a. At elastic

b. At pre yielding

c. At fracture

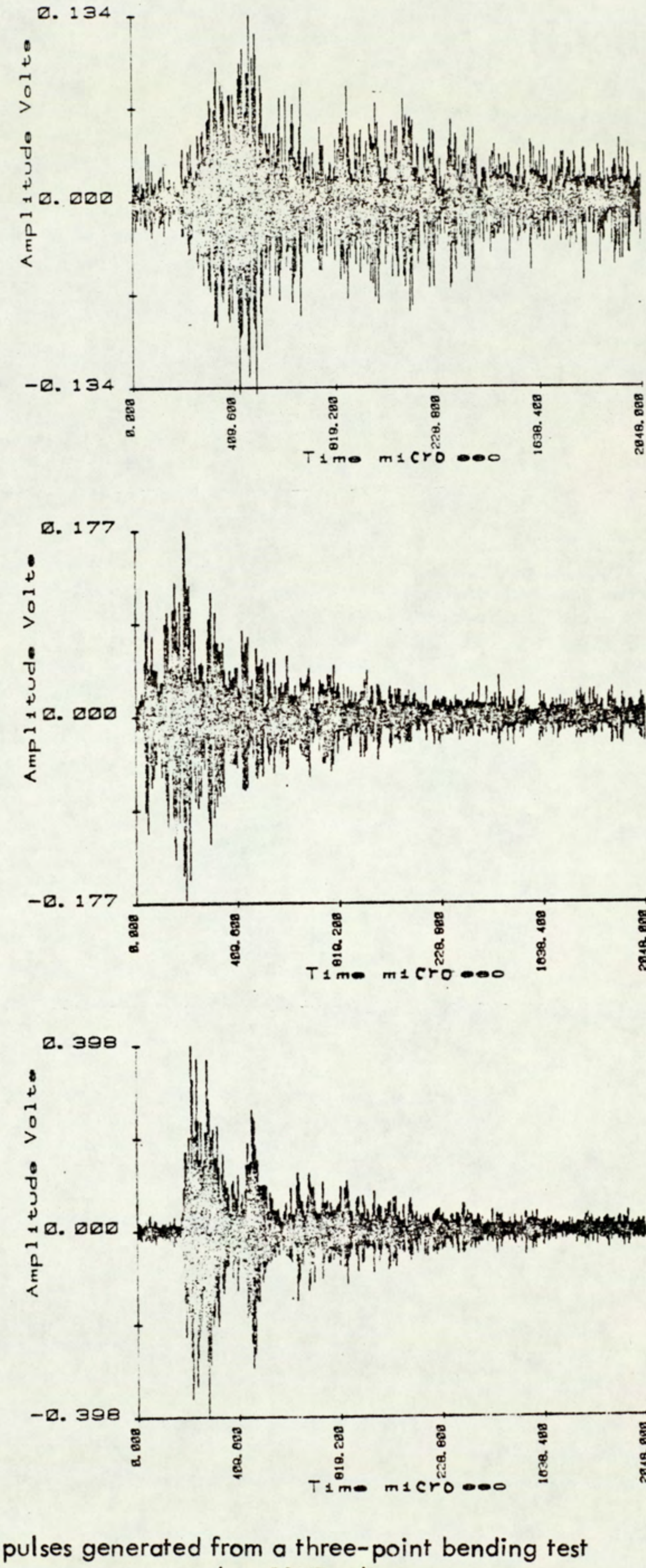

Fig. 58.b.1. A.E.pulses generated from a three-point bending test (r = 12.7mm)

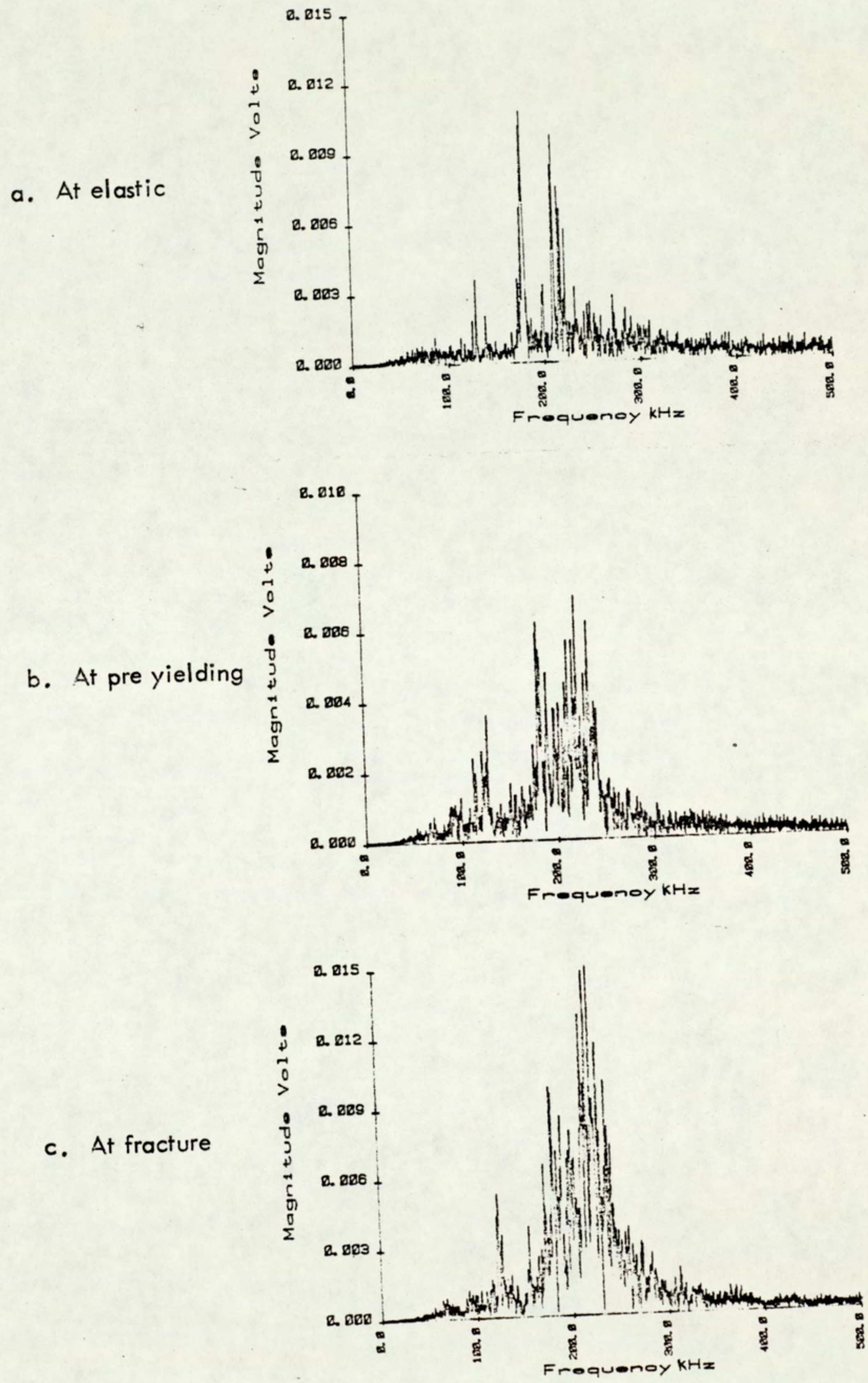

Fig. 58.b.2. F.F.T. spectrum analysis of the A.E.signals from three-point bending test
(r = 12.7mm)

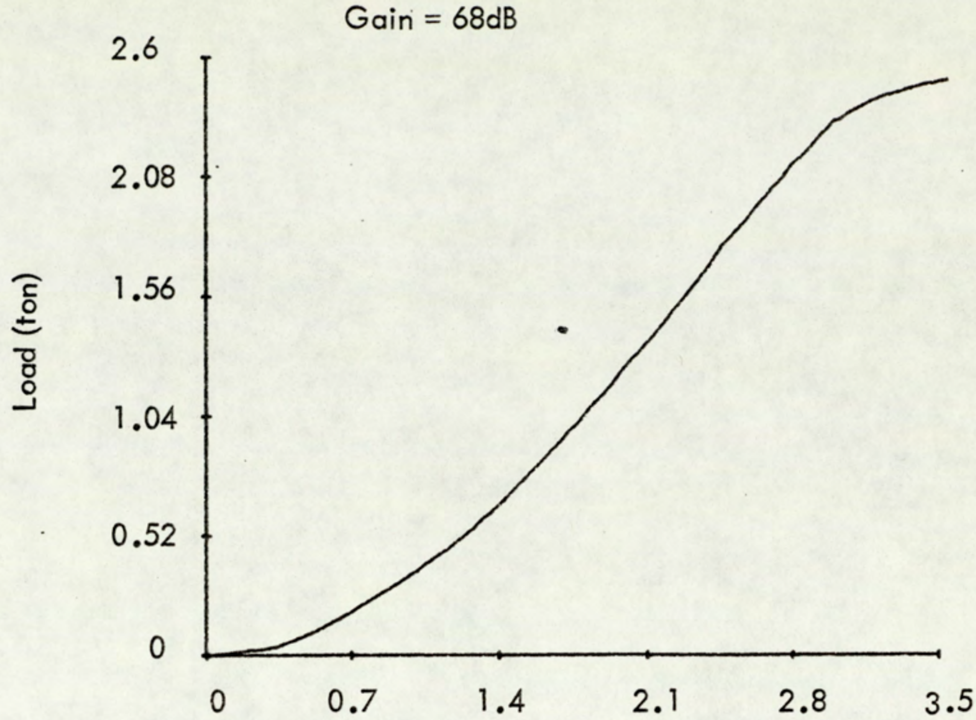

Fig. 59.a. Displacement (mm)

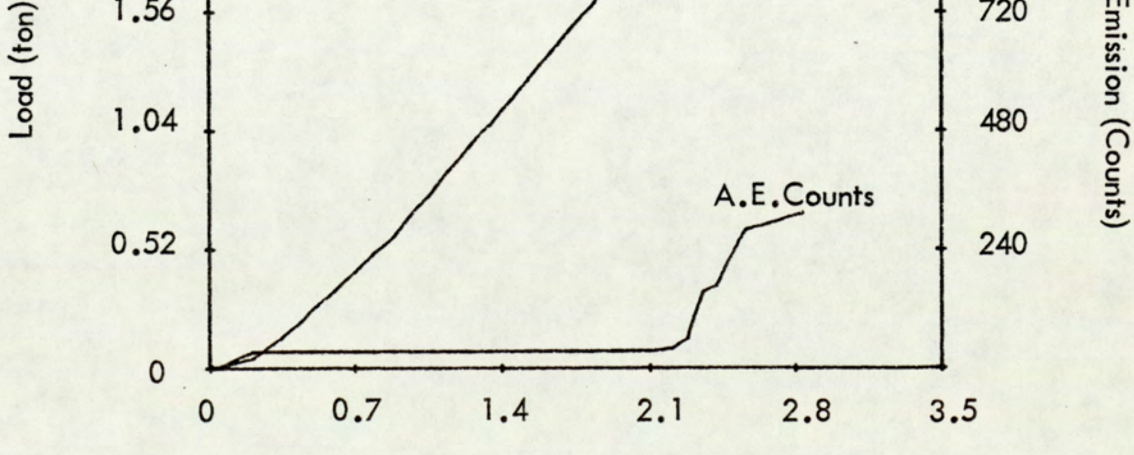

Fig. 59.b. Displacement (mm)

Fig. 59. Three-point bending test (r = 25.4mm)

a. At elastic

b. At pre yielding

c. At fracture

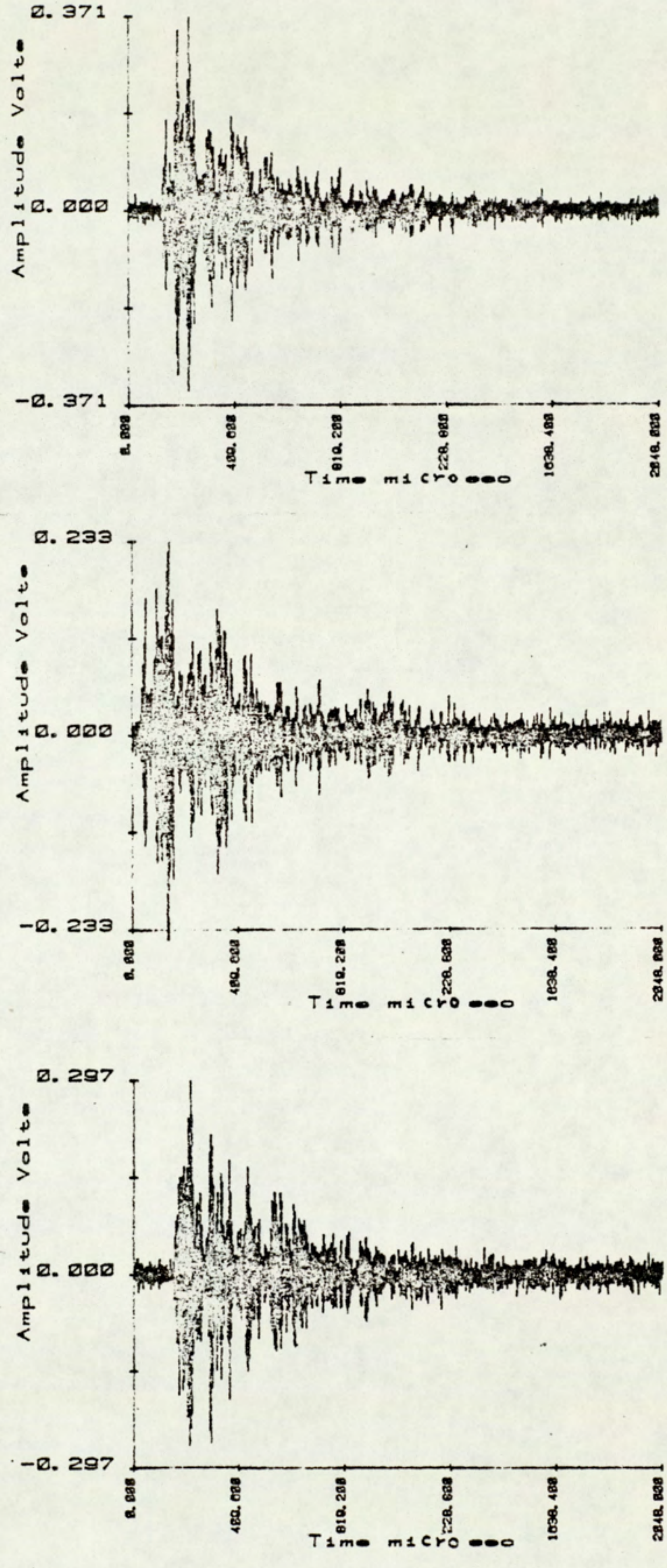

Fig. 59.b.1. A.E.pulses generated from a three-point bending test
(r = 25.4mm)

a. At elastic

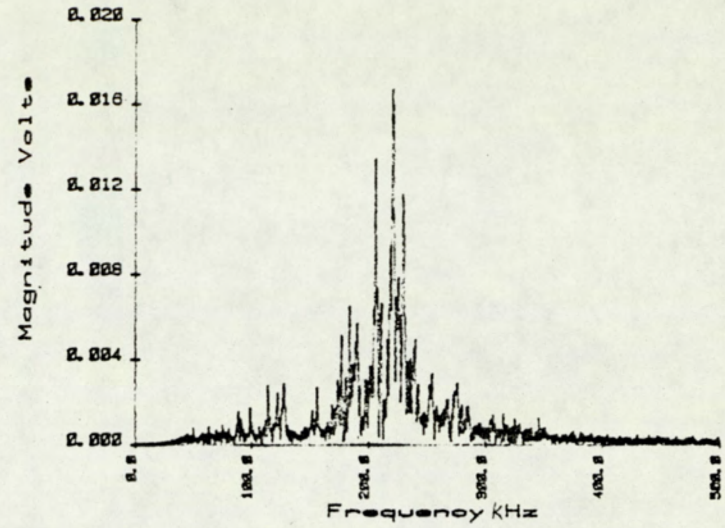

b. At pre yielding

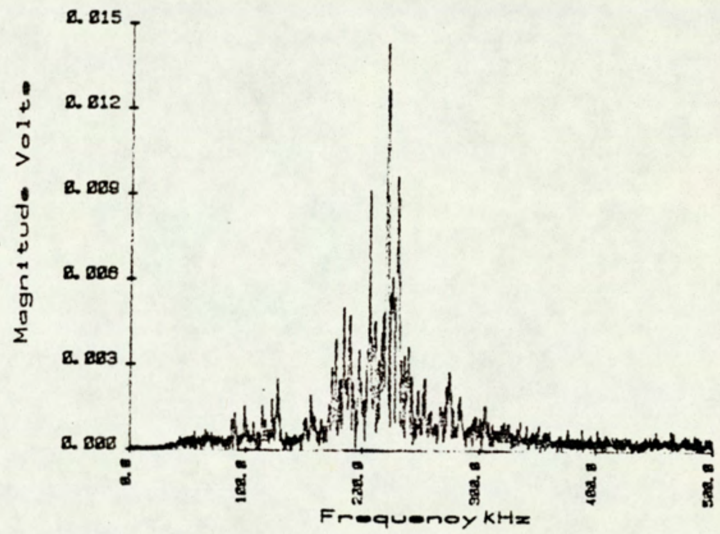

c. At fracture

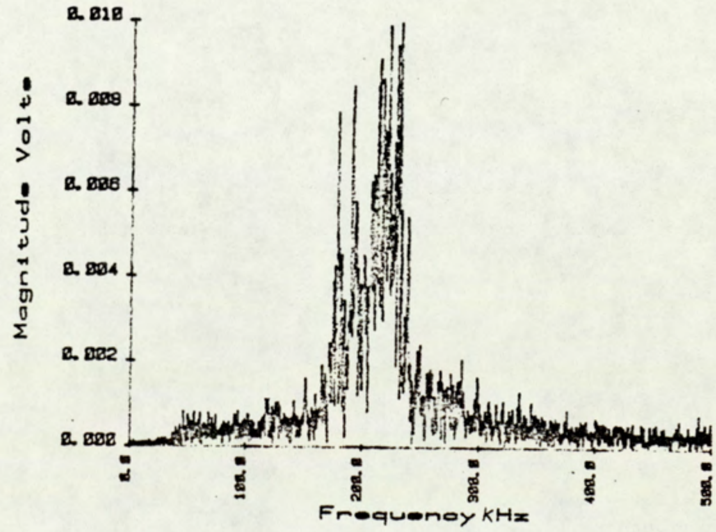

Fig. 59.b.2. F.F.T. spectrum analysis of the A.E. signals from three-point bending test

(r = 25.4mm)

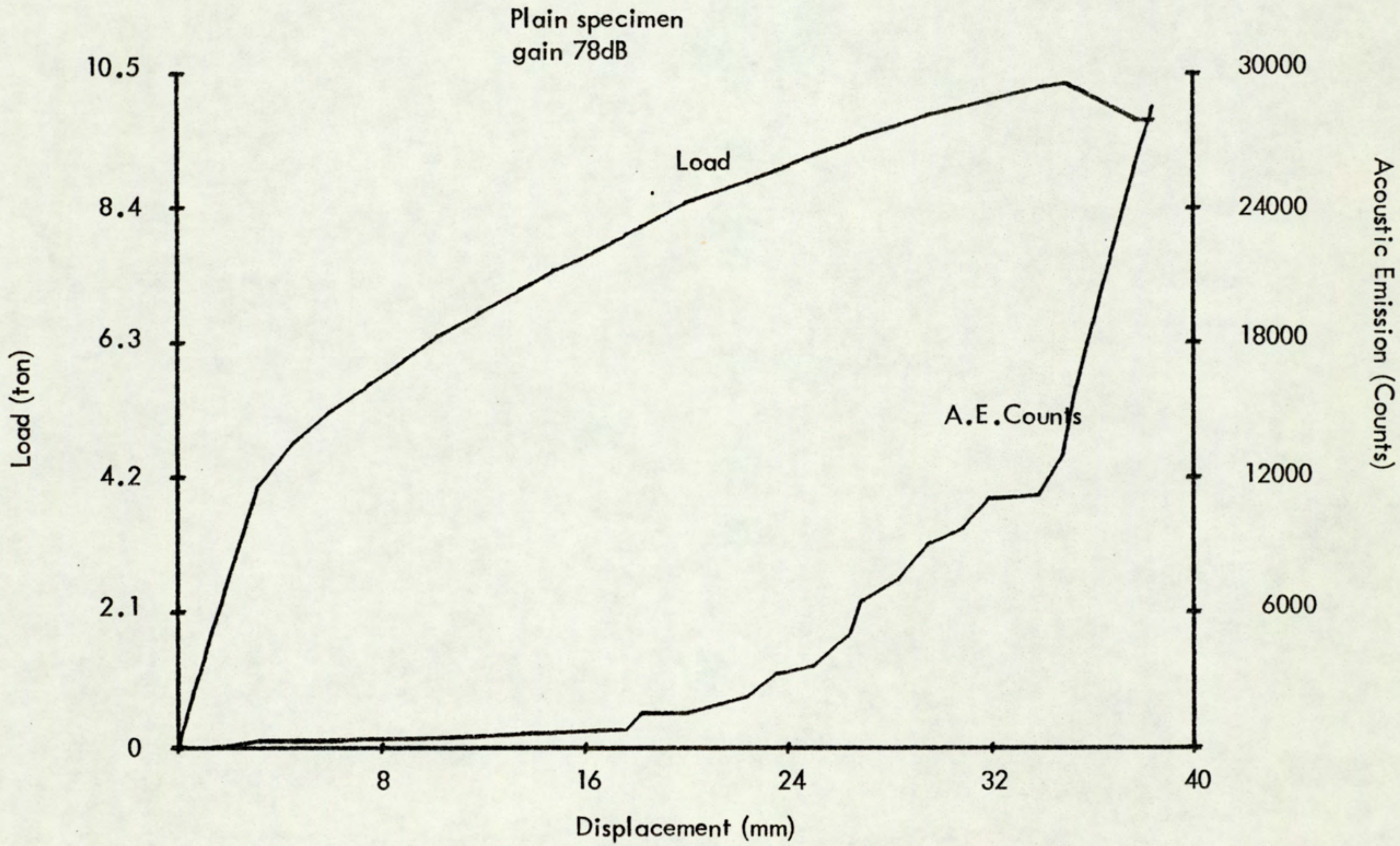

Fig. 60. Three-point bending test of plain specimen.

CHAPTER 6

DISCUSSION

The results presented in the previous chapter were analysed and discussed in detail in this chapter. The analysis presented below includes the relationships established between the different variables measured during the experiments i.e. load, displacement, acoustic emission, and time.

The discussion was presented in steps for each group of tests as follows:

(1) Acoustic emission from flat tensile test specimens; these included specimens of 0.086%C, 0.15%C, and 0.67%C steel. Also a two-sided notched specimen.

(2) Acoustic emission from long flat tensile test specimens.

(3) Acoustic emission from non-ferrous flat tensile test specimens, included specimens of Aluminium, Copper and Brass.

(4) Acoustic emission from notched round tensile test specimens.

(5) Acoustic emission from three-point bending test.

6.1. Acoustic Emission from Flat Tensile Test Specimens

The tensile tests of specimens of (0.086%C, 0.15%C, and 0.67%C) steels showed the following:

(a) The number of acoustic emission counts was higher for the medium carbon (0.67%C) compared with that generated from low carbon steel (0.086%C and 0.15%C). This can be justified by the fact that medium carbon steels contain more carbon and that the carbon atoms are interstitial, they resist dislocation movement. In general they resist deformation, therefore, a greater number of acoustic emission counts were generated. This is clear by comparing Fig. (20, Fig. (21) and Fig. (22).

(b) In the low carbon steel (0.086%C and 0.15%C), the number of acoustic emission counts increased at a rapid rate in the elastic region before yielding, then the rate decreased after yielding; hence the number of acoustic emission counts continued to increase at a slow rate until the fracture where the number of acoustic emission counts increased in the form of a jump. These are shown in Fig. (20) and Fig. (21).

For the 0.67%C steel, the acoustic emission counts increased less faster than those in the case of low carbon steel. This is because the higher carbon steel contained a high percentage of Pearlite. The interfaces between the Pearlite and the Ferrite act as a vibration absorber.

The number of acoustic counts for the 0.67%C steel increased slowly at the yielding and after the yield the increase took the form of jumps until fracture.

Fig. (22) shows the increase of acoustic emission counts after the yielding until the fracture where this increase in the low carbon steel is very small.

(c) Once the load is applied to the tensile specimen, elastic elongation of the specimen starts here, and the geometric dislocations start to move. At the same time more dislocations are generated, hence the density of dislocations continued to increase to a rapid rate during this elastic deformation. This produced acoustic emission counts and the number of these acoustic emission counts increased at a rapid rate.

Also some of these generated counts could be due to the slippage between the specimen and the grips holding it, at the start of the test. This slippage causes friction between the bolts in the grips and the specimen hole, which in turn produces more acoustic emission counts. This is why a rapid rate of increase of acoustic emission counts was found in the elastic region.

Other factors that cause this rapid rate of increase in the number of acoustic emission counts were the presence of oxides on the surface of the specimen hole. These oxides break with the increase in the friction and the pull. The defects due to the preparation of the specimens, such as uneven surface of the hold and the specimen also cause more acoustic emission counts.

Added to all this, the deformation is first observed in the region of the grips.

In general, the macro-activities such as friction, slippage were mainly responsible for generating this rapid increase in the number of acoustic emission counts.

Prior to the yield point, the acoustic emission rate has a maximum peak. This rate decreased rapidly at the yielding. The activities during yielding were micro, hence it was expected that the rate of increase drops. Analogous to this it was also expected that the rate of increase in the number of acoustic emission counts were going to drop further so that it became very slow during the later stages of deformation. But there was a small sudden increase in the number of acoustic emission counts near the fracture.

The tensile test of the two-sided notched specimens showed the same behaviour as above. This is shown in Fig. (23).

From the above discussion it was clear that there were three significant regions during the deformation which affects the acoustic counts. Three points could be located at the elastic, pre-yielding and the third at fracture.

This was well demonstrated when the number of counts were plotted against time on the same previously discussed curves. Fig. (23, a.2) and Fig. (23, b.2) show clearly the three regions (elastic, pre-yielding and fracture). F.F.T. spectrum of signals from the elastic, pre-yielding, and fracture showed that the predominant frequency in the elastic region is about 135-137KHz and frequency range in the pre-yielding region is about 220-230KHz. At the fracture the spectrum showed a narrow peak of frequency of about 131-139KHz.

6.2. Acoustic Emission from Long Flat Tensile Test Specimens

Specimens represented by Figs. (24) to (26) of the same steel B varied in their gauge, but have the same width and the same thickness.

This variation in length had several effects on the acoustic emission, such as the stress values and their distribution, where the values were lower and the distributions were less uniform in the case of the specimen with long gauge lengths compared with those of smaller gauge lengths.

Also using the same cross-head speed for the tests, the strain rate varied according to the variations of the gauge lengths; the longer the gauge length, the lower was the strain rate.

These two effects were clearly reflected on the acoustic emission counts which decreased with the increase in the gauge length.

The above figures showed that the acoustic emission counts rate for the different length specimens has a maximum peak prior to the yield point, but the value of that count rate peak is bound to be proportional to the specimen length.

The F.F.T. spectrum of the signals analysed from elastic pre-yielding and prior to fracture or at fracture regions showed that those three regions differ in their frequency range. But these frequency ranges are the same in the three different length specimen tests.

So the specimen length has very little effect on the frequency range of the acoustic emission signals.

6.3. Acoustic Emission from Non-Ferrous Flat Tensile Test Specimens

Fig. (27)-(29) represent the results of the tensile tests of Aluminium, Copper and Brass flat tensile test specimens. Two identical tensile specimens were prepared for each of the above non-ferrous metals and alloys. Tests carried out on these specimens showed that commercial pure Copper generated the highest number of acoustic emission counts; next was the commercial Aluminium alloy, and the quietest alloy was the Brass. Copper, having the most ductile of the three alloys, exhibited a large amount of plastic deformation. Aluminium alloy contains a large number of precipitates and many more interfaces between these precipitates and the matrix. These interfaces act as a vibration absorber. Brass was found to be the quietest alloy in this group. This is because Brass of this composition contains many lead particles. Lead absorbs vibration and provides a damping capacity to the Brass.

The F.F.T. spectrum of the signals generated from Copper specimens showed that there is a sharp peak at pre-yielding region of frequency about 202KHz and 228KHz for the other Copper specimen. This is due to the purity of the metal.

For Aluminium, the F.F.T. spectrum of the signals showed that the frequency range at pre-yielding region is between 98KHz-218KHz. This wide range frequency is due to the presence of a large number of precipitates in the metal.

For Brass, the predominant frequency range at the pre-yielding region is between 208-230KHz.

6.4. Acoustic Emission from Round Notched Specimens

For the round notched specimens the number of acoustic emissions increased with the increase in load. The number of acoustic emission counts were affected by two main factors:

(a) The sharpness of the notches which was measured as notch root radii.
(b) The chemical composition of the steels and the quantities of sulphides and oxides.

The figures from 30-56 show the relationships between the load, acoustic emission and counts rate plotted against time for the nine types of steel (C).

There are three curves for each type of root radii r=1.00mm, r=0.26mm, and r=0.16mm. Comparing each set of three figures for one type of steel together, it was clear that the number of acoustic emission counts increased significantly with the sharpness of the notch root radius where the numbers of acoustic emission counts were very high for notches of root radius r=0.16mm compared with the notch of root radii r=0.26mm and r=1.00mm. This was due to the fact that the sharper the notch (i.e. the smaller the notch root radius) the higher the stress concentration in the vicinity of the notch. This was again clear from the notch geometry calculation shown in tables (2-11) (i.e. the stress concentration factor K).

Examination of the fractured surfaces of the specimens showed that the notches with r=0.16mm were sharp enough to initiate fracture and propagate cracks from the notch root to the interior of the specimens; while in the case of the shallow notches fracture started in the interior of the specimen and the crack propagated from the centre outwards.

The charts of the load against time also showed that fracture, hence crack propagation, was faster in the case of the sharper notches.

This all confirmed that the number of acoustic emission counts increased with increase in the stress concentration and crack propagation.

Some results showed that the acoustic emission counts were higher in the case of the notch root radii r=1.00mm or r=0.26mm than in the case of r=0.16mm. That is because the transducer was attached to the grip surface and not to the specimen. Also, because the grip was a round one, not all the transducer surface has complete contact with grip surface. Also the attenuation of signals through the grip and the deformation of the specimen end in the grip can produce a large number of acoustic emissions. All these possibilities affect the recorded results.

6.5. The Effect of the Chemical Composition and Structure on the Acoustic Emission

The percentages of manganese and sulphur were varied in these steels during melting as shown in table (1).

These variations produced different microstructures and also varying quantities of manganese sulphide (MnS) and oxides for each type of the nine steels.

The volume fraction of the sulphide particles and the oxide particles were calculated, the results are shown in table (11).

The manganese sulphide particles were observed to be mainly type 1 (i.e. regular in shape).

The experimental results showed that the number of acoustic emission counts increased with the increase in the quantity of sulphides and oxides. On this trend it was expected that all steels of higher percentages of manganese and sulphur would give a higher number of acoustic emission counts compared with those steels with lower. But some of the steels with lower percentages of manganese and sulphur gave a higher number of acoustic emission counts. This was due to the presence of oxides in these steels (table 12).

Because the steels were hot rolled the manganese sulphide particles experienced some deformation and were elongated in the direction of rolling, while the oxide particles remained undeformed.

These oxide particles were more favourite sites of crack formation, hence they affected the generation of acoustic emission signals more than the sulphides and therefore produced higher numbers of acoustic emission counts compared to the sulphides.

On the other hand the size range of sulphides was small (0 um - 10 um) while the size range of oxides was much wider (0 - 70 um). These large oxide particles caused the production of more numbers of acoustic emission counts.

In general the effect of the sulphides and oxides on the acoustic emission counts was clear, but the acoustic emission counts were greatly affected by the presence of a sharp notch. This was in the same manner in which fracture is affected more by notches than the chemical composition. Therefore, acoustic emission technique can be successfully applied to monitor fracture.

6.6. Acoustic Emission from Three-Point Bending Test

Seven specimens of steel (A2) were tested. One specimen was plain (without any notch) and each pair of the remaining six specimens had a notch of a certain root radii (i.e. r= 0.127mm, r=12.7mm and r=25.4mm).

From the results in Fig. 57 to 60 it was shown that specimens of 0.127mm and 12.7mm root radii had been tested under the gain of 68dB. The first specimen of 25.4mm root radii was tested also under the same gain as before but there were no counts recorded. Therefore, the gain for the other specimen of 25.4mm changed to 76dB. Even using this high gain, the number of counts was still low.

From the above results it was concluded that the number of counts recorded from the sharper notches 0.127mm was higher than those recorded from the larger notch radii (12.7mm and 25.4mm). This can be justified by the fact that the sharper the notch the higher the stress concentration around the notch. Also the specimens of 12.7mm root radii generate more counts than that from the 25.4mm root radius. The higher gain used the higher the count recorded that appeared in testing the larger notches. The reason for this increase is due to the increase of the threshold level of the counter which then counted some of the background noise.

The plain specimen was tested under the same conditions as above, but using higher gain which was 78dB. This is because the plain specimen was free of notches to create a high stress concentration region, so that the number of counts generated was very low and the counts increased until the pre-yielding of the specimen due to the creation of high concentration regions in the specimen.

Acoustic emission signals recorded at a gain of 60dB while the acoustic emission counts recorded at a gain of 68dB to 78dB.

The F.F.T. spectrum analysis showed that the frequency range of the signal generated from the three-point bending test is between 130-251KHz.

The predominant frequency at the elastic region is between 130-230KHz, while in the pre-yielding region the frequency range is between 200-250KHz with central peak at about 235KHz. At fracture the frequency range is between 200-251KHz with central peak at about 247KHz.

The frequencies' ranges in the three-point bending were found to be different from that obtained from the tensile test. This is because in the tensile test the stress and strain are uniformly distributed so that any frequency generated can be related to a specific event taking place; while in the three-point bending the stress and strain are not uniform at all points in the specimen.

CHAPTER 7

CONCLUSION AND FURTHER WORK

7.1. Conclusion

Investigations were carried out on tensile tests of flat and round specimens of different types of steel and non-ferrous metals (Aluminium,Copper and Brass). Long gauge length specimens were tested to study the effect of length on the acoustic emission.

Acoustic emission phenomena were investigated from the three-point bending test specimens of different notch root radii. The results of these investigations showed the following conclusions:-

(1) The effect of carbon content in metal produces a higher number of acoustic emission counts than that produced from the lower carbon content. This effect was shown clearly in the tensile tests of 0.086%C, 0.15%C, and 0.67%C steel specimens. It has been found that steel of 0.67%C produces about nine times the acoustic emission counts produced by the 0.086%C steel and about four times the acoustic emission counts produced by the 0.15%C steel.

(2) The effect of specimen length on the acoustic emission counts showed that the specimen of short gauge length produced higher acoustic emission counts than from the long gauge length specimen.

(3) Different type of metals emit a different number of acoustic emission counts. This is shown from the tensile

test of Copper, Aluminium, and Brass specimens. Copper specimens produced a higher number of acoustic emission counts due to the purity of the metal. Aluminium alloy emitted less counts than the Copper. This is because the Aluminium alloy contains a large number of precipitates. Interfaces between these precipitates and the matrix act as vibration absorbers. The quietest metal was the Brass. The Brass used contains many Lead particles and these particles provide a damping capacity to the Brass.

(4) Acoustic emission was affected by the size of the notch radius. The sharper the notch, the higher the number of acoustic emissions generated, and the larger the notch, the less acoustic emission counts are generated. This is shown in the tensile test of notched round specimens.

(5) The presence of non-metallic particles such as oxides, produce higher acoustic emission counts. Also the presence of oxide particles reduces the effect of the notch size on the acoustic emission counts generation.

(6) In the three-point bending test, the effect of the notch size on the acoustic emission counts was shown very clearly, more so than in the tensile test. The sharper notch radius emits higher acoustic emission counts with low gain, while the larger notch radius

emits less acoustic emission counts even with using higher gain.

The three-point bending test of plain specimen (free of notch) showed that the increase in acoustic emission counts took place only prior to the fracture. For this test a high gain was needed to monitor the acoustic emission.

(7) Acoustic emission rate behaves constantly in most of the tests carried out. The rate has a maximum peak prior to the yielding and decreases sharply before starting a low rising prior to the fracture.

(8) A high gain was needed to monitor the acoustic emission from the tensile test, while low gain was needed to monitor the acoustic emission from the three-point bending test.

(9) The Fast Fourier transformation spectrum analysis of the signals recorded from the tensile tests showed that there are three distinguishable regions i.e. elastic, pre-yielding, and fracture. In the elastic region, the predominant frequency range is between 100-140KHz, while in the pre-yielding region the frequency range is between 200-230KHz. At fracture the frequency range is between 100-130KHz and the spectrum is represented in a clear peak at about 110KHz in most cases.

(10) The F.F.T. spectrum analysis of the signals recorded from the three-point bending tests showed that the predominant

frequency range in the elastic region is between 130-230KHz, while the frequency range in the pre-yielding region is between 200-250KHz with central peak at about 235KHz. At fracture the frequency range is between 200-251KHz with central frequency at about 247KHz.

(11) From the experimental results it was found that the number of acoustic emissions generated was affected by many factors such as type of metal, microstructures, the notch size, and specimen size.

However, the frequency content of the recorded acoustic emission signals was less affected by the above factors. But the frequency ranges of the signals were found to be affected by the type of test carried out i.e. tensile test or three-point bending test. The frequency range of the monitoring system used for the detection of acoustic emission is between 100-300KHz. A wider bandwidth monitoring system can give more information about the different activities taking place in the metal.

Finally, acoustic emission can be employed as a very useful technique for studying the deformation process in the metals and also as a very important non-destructive technique.

7.2. Suggestions for Further Work

(a) An acoustic emission monitoring and recording system with wider frequency bandwidth can be used to monitor and record the signals generated from the metals. A video tape recorder can be used to give wider frequency bandwidth to about 2MHz. Analyses of these signals on a wide frequency range will give more information about the changes taking place in the metal during the test than in the narrow frequency range.

(b) The transducer is considered the main part in the monitoring system of the acoustic emission. More work is needed to establish a relation between the output signals from the transducer (voltage signals) and the event which produced these signals.

(c) Acoustic emission pulses generated from the gripping region of the specimen due to the deformation taking place at the ends of the specimens. These pulses, monitored by the transducer attached to the middle of the specimen, made the technique less sensitive. So more work has to be done to reduce the emission of these pulses from the grips.

(d) Studying the effect of high and low temperatures on the acoustic emission characteristics from the three-point bending test by using a wider frequency bandwidth monitoring and recording system to be able to relate these signals generated with the events taking place in the specimens at different temperatures.

(e) Using the computer to calculate the number of acoustic emission counts of the signals which have been counted by the acoustic emission counter and comparing the two results.

APPENDIX

PROGRAMME LISTING AND DESCRIPTION

A.1 PROGRAMME LISTING AND DESCRIPTION

The complete programme consists of eleven separate programmes stored on flexible disc under separate file names. These programmes are :

FFTM	Master programmes which set parameters and access
FFTMa	Other programmes
FFTD	Instructs the DVM to sample the signal
FFTS	Standard FFT . 2048 point capacity
FFTB	Big FFT . 4096 point capacity
FFTBa	
FFT p & p	Print and plot frequency spectrum
FFTaut	Autocorrelation via FFT
IFFT	
SIGAV	Signal Averaging
FKILL	Erases all data files from disc

The complete programme is subdivided because there is insufficient memory for all the programmes and data.

Programme Variable Reference

G.V. = General Variable

Variable	Comments
A (*)	Decoding array
F (*)	Real part of main data/transform array
G (*)	Imaginary part of main data/transform array
Q (*)	Control parameters
T (*)	General. Used in FFT butterflies
U (*)	Multiplier in FFT. General
W (*)	Basic FFT multiplier
X (*)	Maximum of array. Split precision butterflies
Y (*)	Split precision butterflies
A $	Split precision butterflies
B $	Split precision butterflies
C $	ASCII Code for DVM
F $	Split precision F (*). File name string
G $	Split precision G (*).
I $	Redundant - not used
N $	File name string
S $	Main raw data string (coded)
A	G.V.
B	G.V.
C	G.V. Segment averaging repeat control
D	G.V. r18/2
E	G.V. Sample Interval
F	G.V. "Harmonic" Input frequency
G	G.V.
H	G.V. 2^L in FFT
I	G.V.
J	G.V.
K	G.V. Mean preFFT. Sum pre IFFT
L	G.V. FFT index. Counter in Zero Crossing

M	G.V. Power of 2 in FFT
N	Initially - data per segment
	Later - total data
P	G.V. Index in FFT
Q	G.V. Index in FFT
R	Error
S	Sampling frequency in "Harmonic"
T	G.V.
U	Bandwidth
V	Number of segments
W	Size of A(*)
X	G.V.
Y	G.V.
Z	G.V. Statistical d.o.f.
r1	Horizontal axis control
	Mean in FFTBa. Sum in IFFT
r2	Vertical axis control
r3	Horizontal axis control. Nyquist frequency component
r4	Previous analysis value of r18
r5	Total data points from DVM
r6	Smoothing parameter
r7	Indicates that previous analysis was in split precision
r8	Calculates r9
r9	Data window correction factor
r18	Number of data points per segment
r20	FFT parameter
r21	FFT parameter
r22	FFT parameter
r23	General FFT variable
Q (1)	Millisec to plot raw data
2	G.V.
3	Magnitude or PSD
4	Phase
5	Data window
6	dB range or Vertical axis volts value

7	Indicates some sort of repeat analysis
8	Specifies type of repeat
9	Controls repeat if too much data requested
10	Split precision i.e. FFTB
11	FFT print
12	FFT plot
13	Not used
14	Raw data plot
15	Start frequency output FFT. Lag time to plot
16	Stop frequency output FFT. Normalised autocorrelation
17	Triangular smoothing
18	Transform, autocorrelation or signal averaging analysis
19	Related to history of Q (18) for redimensioning
20	Related to history of Q (18) for redimensioning
21	dB scale vertical axis
22	Zero Crossing

```
0: "FFTM":wrt 6,""; gto +4
1: gto "Rep"
2: gto "Rep2"
3: gto "A"
4: dim Q[22],T[6],U[4],W[2],N$[6]
5: ent "Sample Interval or Frequency?",E;if E>1;1/E→E;0→Q[1]
6: fxd 5;wrt 6,1/E,"Hz",1000*E,"millisec"
7: "A":0→Q[10]→Q[18]
8: ent "Transform=0,Autoc.=1,Sig Av.=2",Q[18];if Q[18]=0;ent "Split=1",Q[10]
9: Q[19]→Q[20];Q[18]=2→Q[19]
10: "B":0→Q[9]→Q[1];ent "Manual=1,Harmonic=2",Q[1]
11: if Q[1]=1;gto "Manual"
12: if Q[1]=2;gto "Harmonic"
13: gto -3
14: "Manual":wrt 6,"Manual"
15: ent "Data Points per Segment?",N;cll 'Band'
16: if Q[9]=1;gto "A"
17: 0→Q[2];ent "Repeat Manual=1",Q[2];if Q[2]=1;gto -2
18: cll 'Outset';0→Q[2];ent "Repeat Man/Harm =1",Q[2];if Q[2]=1;gto "B"
19: gto "Data Window"
20: "Harmonic":wrt 6,"Harmonic"
21: ent "Frequency of Signal?",F;0→N;wrt 6,F,"Hz input"
22: ent "Data Points per Segement?",N;if N=0;gto +2
23: wrt 6,"No of cycles per segment=",int(NEF)→I;gto +3;if I=0;gto -1
24: 0→I;ent "No of cycles per segment?",I;if I=0;gto -3
25: wrt 6,"Data points per segment=",int(I/EF)→N;gto -3
26: fxd 5;wrt 6,"Actual Sampling Frequency=",NF/I→S
27: wrt 6,"Data points per cycle=",N/I;0→Q[2]
28: ent "Repeat Harmonic=1",Q[2];if Q[2]=1;gto -7
29: cll 'Band';if Q[9]=1;gto "A"
30: 0→Q[2];ent "Repeat in Harmonic=1",Q[2];if Q[2]=1;gto -8
31: cll 'Outset';0→Q[2];ent "Repeat Man/Harm =1",Q[2];if Q[2]=1;gto "B"
32: 1/S→E;gto "Data Window"
33: "Band":1→r6
34: 1→V;ent "No of Segments?",V;if Q[18]#1;ent "Smoothing(2n+1)?",r6
35: if Q[18]=0 and r6#1;0→Q[17];ent "Triangular Smoothing=1",Q[17]
36: fxd 0;wrt 6,"Segment Data=",N,"  No. Segments=",V
37: wrt 6,"Smoothing=",r6;if Q[17]=1;wrt 6,"Triangular"
38: VN→N;(r6-1)/2→r6;wrt 6,"Total Data=",N;cll 'Width';ret
39: "Width":if Q[7]#1;ent "Total Data Points?",r5
40: if Q[7]#1 and r5=0;N→r5
41: if N>r5;wrt 6,r5,"Available",N,"Requested";1→Q[9]
42: fxd 4;wrt 6,(2r6+1)V/NE→U,"Hz Bandwidth",√(1/UNE)→R,"Error=SD/mean"
43: wrt 6,2/R↑2→Z,"Stat d.o.f";N/V→r18
44: r18+(Q[18]=1)r18→r18
45: if Q[18]=0 and r18>2048;1→Q[10]
46: if r18-(Q[10]=1)r18/2>2048-(Q[18]=2)548;1→Q[9]
47: if r5>9999;1→Q[9]
48: if Q[10]=1;wrt 6,"Split"
49: ret
50: "Outset":if Q[8]=1;gto +5
51: -1→Q[22];ent "Zero Crossing Freq=1",Q[22]
52: if Q[22]=1;0→Q[22];ent "Total Zero Band, Volts?",Q[22];Q[22]/2→Q[22]
53: 0→Q[14];ent "Raw Data Plot=1,Plot only=2",Q[14]
54: if Q[14]#0;0→Q[1];ent "Millisec to plot?",Q[1];if Q[14]=2;gto +18
55: if Q[18]=1;gto +15
56: if Q[18]=2;gto +16
57: 0→Q[11]→Q[12];ent "FFT print=1",Q[11],"FFT plot=1",Q[12]
58: 0→Q[15];1/2E→Q[16];ent "Start Frequency?",Q[15]
59: ent "Stop Frequency?",Q[16]
60: if Q[8]=1;gto +3
```

```
61: 0→Q[3];ent "Magnitude=1,PSD=2",Q[3]
62: 0→Q[4];ent "Phase=1",Q[4]
63: if Q[12]#1;gto +4
64: if Q[12]=1;0→Q[21];ent "Decibel Scale=1",Q[21]
65: if Q[21]=0;0→Q[6];ent "Magnitude Volts Scale Value",Q[6]
66: if Q[21]=1;0→Q[6];ent "dB Range",Q[6];abs(Q[6])→Q[6]
67: if Q[3]=1;wrt 6,"Non statistical"
68: if Q[12]=1 or Q[14]#0 or Q[18]#0;dsp "Enter P1&P2if relcad....CONT";stp
69: ret
70: 1000Er18/2→Q[15];ent "Lag Time to plot,millisec?",Q[15]
71: 0→Q[16];ent "Normalised Autocorrelation=1",Q[16]
72: dsp "Enter P1&P2 if reload....CONT";stp
73: ret
74: "Data Window":chain "FFTMa",0,0
75: "Rep":0→Q[8];ent "Repeat:O/P=1,Window=2,Data=3",Q[8];if Q[8]=0;end
76: if Q[10]=1;1→r7
77: 1→Q[7];if Q[8]=3;r18→r4;gto "A"
78: 1→r6;ent "Smoothing(2n+1)?",r6
79: if r6#1;0→Q[17];ent "Triangular  Smoothing=1",Q[17]
80: wrt 6,"Smoothing=",r6;(r6-1)/2→r6;if Q[17]=1;wrt 6,"Triangular"
81: if Q[8]#2;gto +3
82: cll 'Width';cll 'Outset';0→I;ent "Repeat=1",I;if I=1;gto -4
83: gto "Data Window"
84: if Q[8]#1;gto +3
85: cll 'Width';cll 'Outset';0→I;ent "Repeat=1",I;if I=1;gto -7
86: chain "FFTp&p",0,0
87: gto -12
88: "Rep2":0→Q[8];ent "Repeat:O/P=1,Data=3",Q[8];if Q[8]=0;end
89: 1→Q[7];if Q[8]=3;r18→r4;gto "A"
90: if Q[18]#2;gto +2
91: 1→r6;ent "Smoothing(2n+1)?",r6;wrt 6,"Smoothing=",r6;(r6-1)/2→r6
92: if Q[8]=1 and Q[18]=2;cll 'Outset';chain "SIGAV",0,1
93: if Q[8]#1;gto +3
94: cll 'Outset';0→I;ent "Repeat=1",I;if I=1;jmp 0
95: chain "IFFT",0,1
96: gto -8
```

```
0: "FFTMa":gto +2
1: gto "Return1"
2: if Q[8]=3 and r18#r4 or Q[8]#1 and r7=1;-1→Q[8]
3: if (Q[18]=2)+(Q[20]=1)=1 and Q[7]=1;-1→Q[8]
4: if Q[18]#0;gto +9
5: fxd 4;wrt 6,"Frequency Range,Hz=",1/r18E,1/2E-1/r18E,1/r18E
6: 0→Q[5];if Q[14]=2;gto +7
7: ent "Data Window=1",Q[5]
8: if Q[5]#1;wrt 6,"Rectangular Window";gto +5
9: ent "Bingham=1,Bartlett=2,Hanning=3",Q[5]
10: if Q[5]=1;wrt 6,"Bingham Window"
11: if Q[5]=2;wrt 6,"Bartlet Window"
12: if Q[5]=3;wrt 6,"Hanning Window"
13: if Q[8]=-1;gto "Vfile"
14: if Q[7]=1;gto "Array"
15: "DVM Run":rem 724;clr 724
16: dim C$[26];fxd 0;for I=1 to 26;" "→C$[I];next I
17: "T1F2"→C$[23,26];0→I;ent "EXT trig=1",I;if I=1;"2"→C$[24,24]
18: ent "Range?",C$[22,22];"SE4SR"→C$[17,21];str(r5)→C$[12,16];"SN"→C$[11,12]
19: fxd 7;str(E)→C$[1,10];" D"→C$[1,2];wrt 6,"ASCII Code",C$;wrt 724,C$
20: "Vr>↑s9"→N$;asgn N$,9,0,X;if X#1;kill N$
21: open N$,1;asgn N$,9
22: "Vfile":rread 9,1;sprt 9,r5,N,V,E,U,R,Z,r6,r18,Q[*],"enc"
23: if Q[8]=-1;get "FFTMa",0,1
24: get "FFTD",0,0
25: "Return1":dim Q[22],T[6],U[4],W[2],N$[6]
26: asgn "Vr>↑s9",9;sread 9,r5,N,V,E,U,R,Z,r6,r18,Q[*]
27: "Fr@$q2"→N$;asgn N$,2,0,X;if X#1;kill N$
28: open N$,int(r18/30)+1;asgn N$,2
29: if Q[10]=1;r18/2→r18
30: r18/2+(Q[18]=2)r18/2→I;dim F[I],G[I],X[3]
31: "Array":
32: if Q[14]=0;gto "Zero Cross"
33: "FFTrdp":rread 1,1;sread 1,F[*];1→J;0→Q[2]
34: if Q[18]=0;sread 1,G[*]
35: gto +4
36: "Repeat":dsp "Reload,SetP1,P2...CONT";stp
37: if Q[2]=1;sread 1,F[*];J+1→J;wrt 6,"Segment",J
38: if Q[2]=1 and Q[18]=0;sread 1,G[*]
39: ina X;(Q[1]=0)1000Er18+Q[1]→r1;if Q[18]=1;r1/2→r1
40: r1/1000E→Q[1];pclr;if J=1;max(F[*])→X[1];max(G[*])→X[2];max(X[*])→r2
41: scl -r1/3.3,1.05r1,-1.5r2,1.2r2;pen# 2;fxd 3
42: xax -r2,r1/5,0,r1,1;deg;csiz 2,2,1.5,0;plt r1/3,-1.4r2,1
43: lbl "Time millisec"
44: yax 0,r2/2,-r2,r2,2;csiz 2,2,1.5,90;plt -r1/5,-r2/3,1
45: lbl "Amplitude Volts"
46: for I=1 to r18/2+(Q[18]=2)r18/2;if I>Q[1];gto +6
47: plt 1000(I-1)E,F[I]
48: next I;if Q[18]=2;gto +4
49: for I=r18/2+1 to r18;if I>Q[1];gto +3
50: plt 1000(I-1)E,G[I-r18/2]
51: next I
52: pen;0→Q[2];ent "Continue=0,Repeat Plot=1,Stop=2",Q[2]
53: if Q[2]#1;gto +3
54: 0→Q[1]→Q[2];ent "Millisec to plot?",Q[1];if J<V;ent "Next Segment=1",Q[2]
55: gto "Repeat"
56: if Q[2]=2 or Q[14]=2;1→Q[7];chain "FFTM",0,3
57: if Q[12]=1 or Q[18]#0;dsp "Reload,Set P1,P2...CONT";stp
58: "Zero Cross":
59: if Q[22]<0;gto "Cont"
60: rread 1,1;0→L→M→S
```

```
61: for I=1 to V+(Q[18]#2)V+(Q[10]=1)2V;sread 1,F[*]
62: if I=1;F[1]→X
63: for K=(I=1)+1 to r18/2+(Q[18]=2)r18/2
64: if X<-Q[22];1→S;if M=0;K→U[1]
65: if (F[K]>Q[22] and S=1)=0;gto +3
66: K+(I-1)r18/2→U[2]
67: L+1→L;0→S;1→M
68: F[K]→X;next K;next I;if U[2]=U[1];wrt 6,"No Crossing";gto +2
69: fxd 5;wrt 6,"Statistical Frequency,Hz",(L-1)/(U[2]-U[1])E;rread 1,1
70: 0→I;ent "Cont=0,Rep Zero Cross=1,Stop=2",I
71: if I=1;0→I;ent "Total Zero Band,Volts?",I;I/2→Q[22];gto -11
72: if I=2;1→Q[7];chain "FFTM",0,3
73: "Cont":if Q[18]=1;chain "FFTaut",0,0
74: if Q[18]=2;chain "SIGAV",0,0
75: if Q[10]#1;chain "FFTS",0,0
76: chain "FFTB",0,0
```

```
0: "FFTD":rread 9,1;sread 9,N;int((10400-N)/4)→W
1: dim S$[2N+16],F$[6],A[W];"Dt#?g1"→F$;asgn F$,1,0,I;if I#1;kill F$
2: open F$,int((N+W)/32)+1;asgn F$,1
3: buf "store",S$,3
4: dsp "READY TO SAMPLE";stp
5: tfr 724,"store",0,10
6: if rds("store")=-1;jmp 0
7: if N<=W;0→J;gto +3
8: for J=0 to 2W(int(N/W)-1) by 2W;for K=1 to W;cll 'D';next K
9: sprt 1,A[*];next J;ina A
10: for K=1 to N-Wint(N/W);cll 'D';next K
11: sprt 1,A[*];get "FFTMa",0,1
12: end
13: "D":num(S$[J+2K-1])→E;num(S$[J+2K])→F;bit(4,E)→G
14: shf(E,-12)→H;shf(H,12)→H;shf(F,4)→L;shf(F,-12)→M;shf(M,12)→M
15: shf(E,6)→P;1→Q;if P=1;.1→Q
16: if P=2;10→Q
17: (G+.1H+.01L+.001M)Q→A[K];if bit(5,E);-A[K]→A[K]
18: ret
```

```
0: "FFTS":rread 1,1;for C=0 to V-1
1: ina F,G;sread 1,F[*],G[*]
2: "Window":0+r9;if Q[5]=0;1+r9;gto "Zero Mean"
3: rad;for J=1 to N/V
4: if Q[5]=2;gto "Bartlett"
5: if Q[5]=3;gto "Hanning"
6: "Binghham":
7: "Bingham":1+r8;if J<N/10V+1;(1-cos(10π(J-1)V/N))/2+r8
8: if 1+9N/10V<J;(1+cos(10πV(J-1-9N/10V)/N))/2+r8
9: gto +5
10: "Bartlett":if J<=N/2V+1;2V(J-1)/N+r8
11: if 1+N/2V<J;2-2V(J-1)/N+r8
12: gto +2
13: "Hanning":.5(1-cos(2π(J-1)V/N))+r8
14: if J<=r18/2;F[J]r8+F[J];gto +2
15: G[J-r18/2]r8+G[J-r18/2]
16: r8(r8(Q[3]=2)+(Q[3]=1))+r9+r9;next J;Vr9/N+r9
17: "Zero Mean":
18: 0+K;for J=1 to N/V
19: if J<=r18/2;K+F[J]+K;gto +2
20: K+G[J-r18/2]+K
21: next J;KV/N+K;fxd 7;wrt 6,"Mean=",K
22: for J=1 to N/V;if J<=r18/2;F[J]-K+F[J];gto +2
23: G[J-r18/2]-K+G[J-r18/2]
24: next J
25: "Run FFT":r18/2+r20;r18/2+2+r21;r18/4+1+r22
26: 1/r18+A;smpy A*F+F;smpy A*G+G
27: "FFT":rad
28: 1+M;r20+I
29: I/2+I;if I#1;M+1+M;jmp 0
30: "Points&Power=r18,M":
31: 1+J;0+I
32: r20+K;I+1+I;if J<=I;gto +7
33: if I<=r18/2;F[I]+B;gto +2
34: G[I-r18/2]+B
35: if J<=r18/2;F[J]+A;B+F[J];gto +2
36: G[J-r18/2]+A;B+G[J-r18/2]
37: if I<=r18/2;A+F[I];gto +2
38: A+G[I-r18/2]
39: if J>K;J-K+J;K/2+K;jmp 0
40: J+K+J;gto -8;if J=r18;gto +1
41: for L=1 to M;2↑L+H;H/2+D;1+U[1];0+U[2]
42: cos(π/D)+W[1];-sin(π/D)+W[2]
43: for I=1 to D;for P=I to r20 by H;P+D+Q
44: F[Q]U[1]-G[Q]U[2]+T[1];F[Q]U[2]+G[Q]U[1]+T[2]
45: F[P]-T[1]+F[Q];G[P]-T[2]+G[Q]
46: F[P]+T[1]+F[P];G[P]+T[2]+G[P];next P
47: U[1]+K;KW[1]-U[2]W[2]+U[1];KW[2]+U[2]W[1]+U[2];next I;next L
48: F[1]-G[1]+r3
49: smpy .5F+F;smpy .5G+G;for J=2 to r22;r21-J+r23
50: F[J]+F[r23]+T;F[J]-F[r23]+F[r23];T+F[J-1]
51: G[J]+G[r23]+T;G[J]-G[r23]+G[r23];T+G[J-1]
52: next J
53: for J=r18/4+1 to 3r18/8;3r18/4+1-J+r23
54: F[J]+B;F[r23]+F[J];B+F[r23]
55: G[J]+B;G[r23]+G[J];B+G[r23];next J
56: for J=1 to r18/4;r18/4+J+r23
57: G[J]+T[1];-F[r23]+T[2];G[r23]+G[J]
58: T[1]+F[r23];T[2]+G[r23];next J
59: r18/2+D
60: cos(π/D)+W[1];-sin(π/D)+W[2];W[1]+U[1];W[2]+U[2]
```

```
61: cos(π(r18/2-1)/D)→U[3];-sin(π(r18/2-1)/D)→U[4]
62: for P=1 to r18/4;P+r18/4→Q
63: F[Q]U[1]-G[Q]U[2]→T[1];F[Q]U[2]+G[Q]U[1]→T[2]
64: F[Q]U[3]+G[Q]U[4]→T[3];F[Q]U[4]-G[Q]U[3]→T[4]
65: F[P]+T[1]→T[5];G[P]+T[2]→T[6]
66: F[P]+T[3]→F[Q];T[4]-G[P]→G[Q]
67: T[5]→F[P];T[6]→G[P]
68: U[1]→K;KW[1]-U[2]W[2]→U[1];KW[2]+U[2]W[1]→U[2]
69: U[3]→K;KW[1]+U[4]W[2]→U[3];U[4]W[1]-KW[2]→U[4];next P
70: for J=r18/4+1 to 3r18/8-1;3r18/4-J→r23
71: F[J]→B;F[r23]→F[J];B→F[r23]
72: G[J]→B;G[r23]→G[J];B→G[r23];next J
73: r3→F[r18/2];0→G[r18/2]
74: for I=1 to r18/2
75: "Mag":if Q[3]=1;2r(F[I]↑2+G[I]↑2)→X;gto +2
76: "PSD":if Q[3]=2;2E(N/V)(F[I]↑2+G[I]↑2)→X
77: if Q[4]=0 or C#0;0→Y;gto +3
78: "Phase":if F[I]=0;sgn(G[I])*90→Y;gto +2
79: deg;atn(G[I]/F[I])→Y;if F[I]<0;Y-sgn(Y)*180→Y
80: X→F[I];Y→G[I];next I
81: F[r18/2]/2→F[r18/2]
82: if C=0;rread 2,1;sprt 2,F[*],G[*],"end";gto +3
83: rread 2,1;ina G
84: sread 2,G[*];ara F+G→F;rread 2,1;sprt 2,F[*],"ens"
85: ina F,G;next C
86: "Segment Averaging":
87: rread 2,1;sread 2,F[*],G[*];1/Vr9→C
88: smpy C*F→F
89: rread 2,1;sprt 2,F[*],"ens"
90: rread 2,1
91: chain "FFTp&p",0,0
```

```
0: "FFTB":gto +2
1: gto "Ret"
2: "Sr@$q4"→N$;asgn N$,4,0,X;if X#1;kill N$
3: open N$,int(r18/30)+3;asgn N$,4
4: "Ssπ<v5"→N$;asgn N$,5,0,X;if X#1;kill N$
5: open N$,int(r18/30)+3;asgn N$,5
6: "OE#?g6"→N$;asgn N$,6,0,X;if X#1;kill N$
7: open N$,int(r18/30)+3;asgn N$,6
8: "OE#?g7"→N$;asgn N$,7,0,X;if X#1;kill N$
9: open N$,int(r18/30)+3;asgn N$,7
10: -1→C;rread 1,1;gto +4
11: dim Q[22],U[32],W[32],T[6],X[3]
12: rread 9,1;sread 9,C,Q[*],N,V,E,r5,r6,r9,r18;r18/2→r18
13: dim F[r18/2],G[r18/2]
14: 1+C→C;0→r9
15: chain "FFTBa",0,0
16: "Ret":
17: dim Q[22],U[32],W[32],T[6],X[3],Y[2],A$[4],B$[4],N$[6],I$[4]
18: rread 9,1;sread 9,C,Q[*],N,V,E,r5,r6,r9,r18
19: dim F$[2r18],G$[2r18]
20: rread 4,1;rread 5,1
21: for I=0 to r18/2-1 by 32;sread 4,U[*];sread 5,W[*]
22: for J=1 to 32
23: fts (U[J])→F$[4(I+J)-3,4(I+J)]
24: fts (W[J])→G$[4(I+J)-3,4(I+J)]
25: next J;next I;ina U,W
26: r18/2→D
27: cos(π/D)→W[1];-sin(π/D)→W[2];W[1]→U[1];W[2]→U[2]
28: cos(π(r18/2-1)/D)→U[3];-sin(π(r18/2-1)/D)→U[4]
29: for P=1 to r18/4;P+r18/4→Q
30: stf(F$[4P-3,4P])→X[1];stf(F$[4Q-3,4Q])→X[2]
31: stf(G$[4P-3,4P])→Y[1];stf(G$[4Q-3,4Q])→Y[2]
32: X[2]U[1]-Y[2]U[2]→T[1];X[2]U[2]+Y[2]U[1]→T[2]
33: X[2]U[3]+Y[2]U[4]→T[3];X[2]U[4]-Y[2]U[3]→T[4]
34: X[1]+T[1]→T[5];Y[1]+T[2]→T[6]
35: X[1]+T[3]→X[2];T[4]-Y[1]→Y[2]
36: fts (X[2])→F$[4Q-3,4Q];fts (Y[2])→G$[4Q-3,4Q]
37: fts (T[5])→F$[4P-3,4P];fts (T[6])→G$[4P-3,4P]
38: U[1]→K;KW[1]-U[2]W[2]→U[1];KW[2]+U[2]W[1]→U[2]
39: U[3]→K;KW[1]+U[4]W[2]→U[3];U[4]W[1]-KW[2]→U[4];next P
40: for J=r18/4+1 to 3r18/8-1;3r18/4-J→r23
41: F$[4J-3,4J]→B$;F$[4r23-3,4r23]→F$[4J-3,4J];B$→F$[4r23-3,4r23]
42: G$[4J-3,4J]→B$;G$[4r23-3,4r23]→G$[4J-3,4J];B$→G$[4r23-3,4r23];next J
43: fts (0)→F$[4r18/2-3,4r18/2]→G$[4r18/2-3,4r18/2]
44: for I=1 to r18/2;stf(F$[4I-3,4I])→X[1];stf(G$[4I-3,4I])→X[2];gto +1
45: "Mag":if Q[3]=1;2r(X[1]↑2+X[2]↑2)→X;gto +2
46: "PSD":if Q[3]=2;2E(N/V)(X[1]↑2+X[2]↑2)→X
47: if Q[4]=0 or C#0;0→Y;gto +3
48: "Phase":if X[1]=0;sgn(X[2])*90→Y;gto +2
49: deg;atn(X[2]/X[1])→Y;if X[1]<0;Y-sgn(Y)*180→Y
50: fts (X)→F$[4I-3,4I];fts (Y)→G$[4I-3,4I];next I
51: if C=0;rread 2,1;sprt 2,F$,G$,"end";gto +5
52: rread 2,1
53: sread 2,G$
54: for I=1 to r18/2;fts (stf(F$[4I-3,4I])+stf(G$[4I-3,4I]))→F$[4I-3,4I]
55: next I;rread 2,1;sprt 2,F$,"ens"
56: if C<V-1;get "FFTB",0,11
57: "Seg Av":
58: rread 2,1;sread 2,F$,G$;1/Vr9→C
59: for I=1 to r18/2;fts (Cstf(F$[4I-3,4I]))→F$[4I-3,4I];next I
60: rread 2,1;sprt 2,F$,"ens"
61: rread 2,1
62: chain "FFTp&p",0,0
```

```
0: "FFTBa":0→r1;rread 6,1;rread 7,1
1: for Z=0 to 1
2: sread 1,F[*],G[*]
3: if Q[5]=0;1→r9;gto "ZM"
4: rad;for I=1 to .5N/V;I+Z.5N/V→J
5: if Q[5]=2;gto "Bartlett"
6: if Q[5]=3;gto "Hanning"
7: "Binghham":
8: "Bingham":1→r8;if J<N/10V+1;(1-cos(10π(J-1)V/N))/2→r8
9: if 1+9N/10V<J;(1+cos(10πV(J-1-9N/10V)/N))/2→r8
10: gto +5
11: "Bartlett":if J<=N/2V+1;2V(J-1)/N→r8
12: if 1+N/2V<J;2-2V(J-1)/N→r8
13: gto +2
14: "Hanning":.5(1-cos(2π(J-1)V/N))→r8
15: if I<=r18/2;F[I]r8→F[I];gto +2
16: G[I-r18/2]r8→G[I-r18/2]
17: r8(r8(Q[3]=2)+(Q[3]=1))+r9→r9;next I
18: "ZM":
19: 0→K;for I=1 to .5N/V
20: if I<=r18/2;K+F[I]→K;gto +2
21: K+G[I-r18/2]→K
22: next I;KV/N→K;K+r1→r1;if Z=1;fxd 7;wrt 6,"Mean=",r1
23: "OE":
24: rread 4,1;rread 5,1;sprt 4,F[*];sprt 5,G[*]
25: for I=1 to r18/4;F[2I-1]→G[I];next I
26: rread 5,1;sread 5,F[*]
27: for I=1 to r18/4;F[2I-1]→G[I+r18/4];next I
28: if Z=0;sprt 6,G[*];gto +2
29: sprt 7,G[*]
30: rread 4,1;sread 4,F[*]
31: for I=1 to r18/4;F[2I]→G[I];next I
32: rread 5,1;sread 5,F[*]
33: for I=1 to r18/4;F[2I]→G[I+r18/4];next I
34: if Z=0;sprt 6,G[*];gto +2
35: sprt 7,G[*]
36: next Z;if Q[5]#0;Vr9/N→r9
37: rread 4,1;rread 5,1;rread 6,1;rread 7,1
38: for Z=1 to 2
39: ina F,G;sread 6,F[*];sread 7,G[*]
40: "Run FFT":r18/2→r20;r18/2+2→r21;r18/4+1→r22
41: "ZMn":for I=1 to r18/2
42: F[I]-r1→F[I];G[I]-r1→G[I];next I
43: 1/2r18→A;smpy A*F→F;smpy A*G→G
44: "FFT":rad
45: 1→M;r20→I
46: I/2→I;if I#1;M+1→M;jmp 0
47: 1→J;0→I
48: r20→K;I+1→I;if J<=I;gto +7
49: if I<=r18/2;F[I]→B;gto +2
50: G[I-r18/2]→B
51: if J<=r18/2;F[J]→A;B→F[J];gto +2
52: G[J-r18/2]→A;B→G[J-r18/2]
53: if I<=r18/2;A→F[I];gto +2
54: A→G[I-r18/2]
55: if J>K;J-K→J;K/2→K;jmp 0
56: J+K→J;gto -8;if J≐r18;gto +1
57: for L=1 to M;2↑L→H;H/2→D;1→U[1];0→U[2]
58: cos(π/D)→W[1];-sin(π/D)→W[2]
59: for I=1 to D;for P=I to r20 by H;P+D→Q
60: F[Q]U[1]-G[Q]U[2]→T[1];F[Q]U[2]+G[Q]U[1]→T[2]
```

```
61: F[P]-T[1]→F[Q];G[P]-T[2]→G[Q]
62: F[P]+T[1]→F[P];G[P]+T[2]→G[P];next P
63: U[1]→K;KW[1]-U[2]W[2]→U[1];KW[2]+U[2]W[1]→U[2];next I;next L
64: F[1]-G[1]→r3
65: smpy .5F→F;smpy .5G→G;for J=2 to r22;r21-J→r23
66: F[J]+F[r23]→T;F[J]-F[r23]→F[r23];T→F[J-1]
67: G[J]+G[r23]→T;G[J]-G[r23]→G[r23];T→G[J-1]
68: next J
69: for J=r18/4+1 to 3r18/8;3r18/4+1-J→r23
70: F[J]→B;F[r23]→F[J];B→F[r23]
71: G[J]→B;G[r23]→G[J];B→G[r23];next J
72: for J=1 to r18/4;r18/4+J→r23
73: G[J]→T[1];-F[r23]→T[2];G[r23]→G[J]
74: T[1]→F[r23];T[2]→G[r23];next J
75: r18/2→D
76: cos(π/D)→W[1];-sin(π/D)→W[2];W[1]→U[1];W[2]→U[2]
77: cos(π(r18/2-1)/D)→U[3];-sin(π(r18/2-1)/D)→U[4]
78: for P=1 to r18/4;P+r18/4→Q
79: F[Q]U[1]-G[Q]U[2]→T[1];F[Q]U[2]+G[Q]U[1]→T[2]
80: F[Q]U[3]+G[Q]U[4]→T[3];F[Q]U[4]-G[Q]U[3]→T[4]
81: F[P]+T[1]→T[5];G[P]+T[2]→T[6]
82: F[P]+T[3]→F[Q];T[4]-G[P]→G[Q]
83: T[5]→F[P];T[6]→G[P]
84: U[1]→K;KW[1]-U[2]W[2]→U[1];KW[2]+U[2]W[1]→U[2]
85: U[3]→K;KW[1]+U[4]W[2]→U[3];U[4]W[1]-KW[2]→U[4];next P
86: for J=r18/4+1 to 3r18/8-1;3r18/4-J→r23
87: F[J]→B;F[r23]→F[J];B→F[r23]
88: G[J]→B;G[r23]→G[J];B→G[r23];next J
89: r3→F[r18/2];0→G[r18/2]
90: sprt 4,F[*];sprt 5,G[*]
91: next Z
92: 2r18→r18
93: rread 9,1
94: if C>0;gto +2
95: sprt 9,C,Q[*],N,V,E,r5,r6,r9,r18;gto +2
96: sprt 9,C,"ens"
97: get "FFTB",0,1
```

```
0: "FFTp&p":
1: if Q[10]=1;gto "Split Smoothing"
2: if Q[7]=1;ina F,G;rread 2,1;sread 2,F[*],G[*]
3: if r6=0;gto "Display"
4: "Smooth":for I=1 to r18/2;0→X
5: if I-1<r6;0→G[I];gto +4
6: if r18/2-I<r6;0→G[I];gto +3
7: if Q[17]#1;for J=-r6 to r6;X+F[I+J]→X;next J;X/(2r6+1)→G[I];gto +2
8: for J=-r6 to r6;X+(1-abs(J)/(r6+1))F[I+J]→X;next J;X/(r6+1)→G[I]
9: next I;ara G→F;rread 2,1;sread 2,G[*],G[*];gto "Display"
10: "Split Smoothing":if Q[7]=1;rread 2,1;sread 2,F$,G$
11: if r6=0;gto "Display"
12: "Split Smooth":for I=1 to r18/2;0→X
13: if I-1<r6;fts (0)→G$[4I-3,4I];gto +8
14: if r18/2-I<r6;fts (0)→G$[4I-3,4I];gto +7
15: if Q[17]=1;gto +4
16: for J=-r6 to r6;X+stf(F$[4(I+J)-3,4(I+J)])→X
17: next J
18: fts (X/(2r6+1))→G$[4I-3,4I];gto +3
19: for J=-r6 to r6;X+(1-abs(J)/(r6+1))stf(F$[4(I+J)-3,4(I+J)])→X;next J
20: fts (X/(r6+1))→G$[4I-3,4I]
21: next I;G$→F$;rread 2,1;sread 2,G$,G$
22: "Display":
23: if Q[11]#1;gto "Plot"
24: if Q[3]=1;fxd 8;wrt 6,"          Frequency              Magnitude"
25: if Q[3]=2;wrt 6,"Frequency                   PSD"
26: if Q[4]#1;gto +2
27: wrt 6,"                                                  Phase+/cos"
28: for I=int(Q[15]r18E)+1 to int(Q[16]r18E)+(Q[16]#1/2E);jmp 2(I>r18/2)+1
29: if Q[10]#1;wrt 6,I/r18E,F[I],G[I];gto +2
30: wrt 6,I/r18E,stf(F$[4I-3,4I]),stf(G$[4I-3,4I])
31: next I
32: "Plot":pclr;if Q[12]#1;gto "Rep"
33: if Q[3]=0 and Q[4]=1;360→r2
34: Q[15]→r1;Q[16]→r3;if Q[6]#0 and Q[21]=0;Q[6]→r2;gto +4
35: if Q[10]#1;max(F[*])→r2;gto +3
36: ina X;for I=1 to r18/2;stf(F$[4I-3,4I])→X[1];max(X[*])→X[2];next I
37: X[2]→r2
38: if Q[21]=0;gto +10
39: for I=1 to r18/2
40: if Q[10]=0;gto +5
41: if stf(F$[4I-3,4I])=0;fts (-Q[6])→F$[4I-3,4I];gto +6
42: fts (20log(stf(F$[4I-3,4I])/r2))→F$[4I-3,4I]
43: if stf(F$[4I-3,4I])<-Q[6];fts (-Q[6])→F$[4I-3,4I];gto +4
44: gto +3
45: if F[I]=0;-Q[6]→F[I];gto +2
46: 20log(F[I]/r2)→F[I];if F[I]<-Q[6];-Q[6]→F[I]
47: next I
48: scl r1+(r1-r3)/4,r3+.1(r3-r1),-r2/5,1.1r2;pen# 4;fxd 1
49: xax 0,(r3-r1)/5,r1,r3,1;deg;csiz 2,2,1.5,0;plt r1+(r3-r1)/3,-r2/6,1
50: lbl "Frequency Hz"
51: if Q[3]=0;gto "Phasep"
52: if Q[21]#1;gto +6
53: Q[6]→r2
54: scl r1+(r1-r3)/4,r3+.1(r3-r1),-1.2r2,.1r2;pen# 1;fxd 0
55: yax r1,10,-r2,0,1;csiz 2,2,1.5,90;plt r1-(r3-r1)/5.5,-.8r2,1
56: if Q[3]=1;lbl "Magnitude dB";gto +6
57: lbl "PSD dB";gto +5
58: csiz 1.95;fxd 3;if Q[3]=2;fxd 7;csiz 1.7,2
59: yax r1,r2/5,0,r2,1;csiz 2,2,1.5,90;plt r1-(r3-r1)/5.5,r2/4,1
60: if Q[3]=1;lbl "Magnitude Volts";gto +2
```

```
61: lbl "PSD  Volts↑2 / Hz"
62: for I=int(Q[15]r18E)+1 to int(Q[16]r18E)+(Q[16]#1/2E);jmp 2(I>r18/2)+1
63: if Q[10]#1;plt I/r18E,F[I];gto +2
64: plt I/r18E,stf(F$[4I-3,4I])
65: next I;pen
66: "Phasep":if Q[4]#1;gto "Rep"
67: 0→I;ent "Plot Phase=1",I;if I#1;gto "Rep"
68: scl r1+(r1-r3)/4,r3+.1(r3-r1),-252,216;fxd 0;pen# 2;csiz 1.5,2
69: yax r3,90,-180,180,2;csiz 2,2,1.5,90;plt r3+.05(r3-r1),-160,1
70: lbl "Phase Lead Over Cosine"
71: for I=int(Q[15]r18E)+1 to int(Q[16]r18E)+(Q[16]#1/2E);jmp 2(I>r18/2)+1
72: if Q[10]#1;plt I/r18E,G[I];gto +2
73: plt I/r18E,stf(G$[4I-3,4I])
74: next I;pen
75: "Rep":chain "FFTM",0,1
```

```
0: "IFFT":gto +3
1: gto "Output"
2: "Zero Sum":
3: 0→K;for J=1 to r18
4: if J<=r18/2;K+F[J]→K;gto +2
5: K+G[J-r18/2]→K
6: next J;wrt 6,"Sum =",K;K→r1
7: "Run FFT":r18/2→r20;r18/2+2→r21;r18/4+1→r22
8: "FFT":rad
9: 1→M;r20→I
10: I/2→I;if I#1;M+1→M;jmp 0
11: "Points&Power=r18,M":
12: 1→J;0→I
13: r20→K;I+1→I;if J<=I;gto +7
14: if I<=r18/2;F[I]→B;gto +2
15: G[I-r18/2]→B
16: if J<=r18/2;F[J]→A;B→F[J];gto +2
17: G[J-r18/2]→A;B→G[J-r18/2]
18: if I<=r18/2;A→F[I];gto +2
19: A→G[I-r18/2]
20: if J>K;J-K→J;K/2→K;jmp 0
21: J+K→J;gto -8;if J=r18;gto +1
22: for L=1 to M;2↑L→H;H/2→D;1→U[1];0→U[2]
23: cos(π/D)→W[1];sin(π/D)→W[2]
24: for I=1 to D;for P=I to r20 by H;P+D→Q
25: F[Q]U[1]-G[Q]U[2]→T[1];F[Q]U[2]+G[Q]U[1]→T[2]
26: F[P]-T[1]→F[Q];G[P]-T[2]→G[Q]
27: F[P]+T[1]→F[P];G[P]+T[2]→G[P];next P
28: U[1]→K;KW[1]-U[2]W[2]→U[1];KW[2]+U[2]W[1]→U[2];next I;next L
29: smpy .5F→F;smpy .5G→G;for J=2 to r22;r21-J→r23
30: F[J]+F[r23]→T;F[J]-F[r23]→F[r23];T→F[J-1]
31: G[J]+G[r23]→T;G[J]-G[r23]→G[r23];T→G[J-1]
32: next J
33: for J=r18/4+1 to 3r18/8;3r18/4+1-J→r23
34: F[J]→B;F[r23]→F[J];B→F[r23]
35: G[J]→B;G[r23]→G[J];B→G[r23];next J
36: for J=1 to r18/4;r18/4+J→r23
37: G[J]→T[1];-F[r23]→T[2];G[r23]→G[J]
38: T[1]→F[r23];T[2]→G[r23];next J
39: r18/2→D
40: cos(π/D)→W[1];sin(π/D)→W[2];W[1]→U[1];W[2]→U[2]
41: cos(π(r18/2-1)/D)→U[3];sin(π(r18/2-1)/D)→U[4]
42: for P=1 to r18/4;P+r18/4→Q
43: F[Q]U[1]-G[Q]U[2]→T[1]
44: F[Q]U[3]+G[Q]U[4]→T[3]
45: F[P]+T[1]→T[5]
46: F[P]+T[3]→F[Q]
47: T[5]→F[P]
48: U[1]→K;KW[1]-U[2]W[2]→U[1];KW[2]+U[2]W[1]→U[2]
49: U[3]→K;KW[1]+U[4]W[2]→U[3];U[4]W[1]-KW[2]→U[4];next P
50: for J=r18/4+1 to 3r18/8-1;3r18/4-J→r23
51: F[J]→B;F[r23]→F[J];B→F[r23]
52: next J
53: for I=1 to r18/2-1;r18/2-I→r22;r22+1→r23;F[r22]→F[r23]
54: next I;r1→F[1];0→F[r18/2]→F[r18/2-1]
55: for I=1 to r20;(r20/(r20-I+1))F[I]→F[I];next I
56: smpy 2F→F;rread 2,1;sprt 2,F[*],"end"
57: rread 2,1
58: "Output":
59: if Q[7]=1;ina F;rread 2,1;sread 2,F[*]
60: "Display":if Q[16]=1;1/F[1]→C;smpy CF→F
```

```
61: pclr;Q[15]→r3;if Q[15]>1000Er18/2;1000Er18/2→Q[15]
62: ina X;for I=1 to Q[15]/1000E;F[I]→X[1];max(X[*])→X[2];next I;X[2]→r2
63: if Q[16]=1;drnd(r2,1)→r2
64: scl -r3/4,1.1r3,-1.5r2,1.2r2;pen# 2;fxd 3
65: xax -r2,r3/5,0,r3,1;deg;csiz 2,2,1.5,0;plt r3/3,-1.4r2,1
66: lbl "Time millisec"
67: fxd 3;csiz 1.7
68: yax 0,r2/2,-r2,r2,1;csiz 2,2,1.5,90;plt -r3/5.5,-.9r2,1
69: if Q[16]=1;lbl "Norm Autocorrelation";gto +2
70: lbl "Autocorrelation Volts↑2"
71: for I=1 to r3/1000E;jmp (I>r18/2)+1
72: plt (I-1)1000E,F[I]
73: next I;pen
74: "Rep":chain "FFTM",0,2
```

```
0: "FFTaut":
1: asgn "Fy&k>3",3,0,X;if X#1;kill "Fy&k>3"
2: open "Fy&k>3",int(r18/30)+1;asgn "Fy&k>3",3
3: rread 1,1;for C=0 to V-1
4: ina F,G;sread 1,F[*]
5: "Zero Mean":
6: 0→K;for J=1 to N/V
7: K+F[J]→K
8: next J;KV/N→K;wrt 6,"Mean=",K
9: for J=1 to N/V;F[J]-K→F[J]
10: next J
11: "Run FFT":r18/2→r20;r18/2+2→r21;r18/4+1→r22
12: 1/r18→A;smpy A*F→F
13: "FFT":rad
14: 1→M;r20→I
15: I/2→I;if I#1;M+1→M;jmp 0
16: "Points&Power=r18,M":
17: 1→J;0→I
18: r20→K;I+1→I;if J<=I;gto +7
19: if I<=r18/2;F[I]→B;gto +2
20: G[I-r18/2]→B
21: if J<=r18/2;F[J]→A;B→F[J];gto +2
22: G[J-r18/2]→A;B→G[J-r18/2]
23: if I<=r18/2;A→F[I];gto +2
24: A→G[I-r18/2]
25: if J>K;J-K→J;K/2→K;jmp 0
26: J+K→J;gto -8;if J=r18;gto +1
27: for L=1 to M;2↑L→H;H/2→D;1→U[1];0→U[2]
28: cos(π/D)→W[1];-sin(π/D)→W[2]
29: for I=1 to D;for P=I to r20 by H;P+D→Q
30: F[Q]U[1]-G[Q]U[2]→T[1];F[Q]U[2]+G[Q]U[1]→T[2]
31: F[P]-T[1]→F[Q];G[P]-T[2]→G[Q]
32: F[P]+T[1]→F[P];G[P]+T[2]→G[P];next P
33: U[1]→K;KW[1]-U[2]W[2]→U[1];KW[2]+U[2]W[1]→U[2];next I;next L
34: F[1]-G[1]→r3
35: smpy .5F→F;smpy .5G→G;for J=2 to r22;r21-J→r23
36: F[J]+F[r23]→T;F[J]-F[r23]→F[r23];T→F[J-1]
37: G[J]+G[r23]→T;G[J]-G[r23]→G[r23];T→G[J-1]
38: next J
39: for J=r18/4+1 to 3r18/8;3r18/4+1-J→r23
40: F[J]→B;F[r23]→F[J];B→F[r23]
41: G[J]→B;G[r23]→G[J];B→G[r23];next J
42: for J=1 to r18/4;r18/4+J→r23
43: G[J]→T[1];-F[r23]→T[2];G[r23]→G[J]
44: T[1]→F[r23];T[2]→G[r23];next J
45: r18/2→D
46: cos(π/D)→W[1];-sin(π/D)→W[2];W[1]→U[1];W[2]→U[2]
47: cos(π(r18/2-1)/D)→U[3];-sin(π(r18/2-1)/D)→U[4]
48: for P=1 to r18/4;P+r18/4→Q
49: F[Q]U[1]-G[Q]U[2]→T[1];F[Q]U[2]+G[Q]U[1]→T[2]
50: F[Q]U[3]+G[Q]U[4]→T[3];F[Q]U[4]-G[Q]U[3]→T[4]
51: F[P]+T[1]→T[5];G[P]+T[2]→T[6]
52: F[P]+T[3]→F[Q];T[4]-G[P]→G[Q]
53: T[5]→F[P];T[6]→G[P]
54: U[1]→K;KW[1]-U[2]W[2]→U[1];KW[2]+U[2]W[1]→U[2]
55: U[3]→K;KW[1]+U[4]W[2]→U[3];U[4]W[1]-KW[2]→U[4];next P
56: for J=r18/4+1 to 3r18/8-1;3r18/4-J→r23
57: F[J]→B;F[r23]→F[J];B→F[r23]
58: G[J]→B;G[r23]→G[J];B→G[r23];next J
59: r3→F[r18/2];0→G[r18/2]
60: for I=1 to r18/2;F[I]↑2+G[I]↑2→F[I];next I;F[r18/2]→G[1]
```

```
61: for I=1 to r18/2-1;r18/2-I→r22;r22+1→r23
62: F[r22]→F[r23]→G[I+1]
63: next I
64: if C=0;rread 2,1;sprt 2,F[*],G[*],"end";gto +5
65: rread 2,1;rread 3,1;sprt 3,G[*],"end";ina G
66: sread 2,G[*];ara F+G→F;rread 2,1;sprt 2,F[*],"ens";ina G,F
67: rread 3,1;sread 3,G[*];sread 2,F[*];ara F+G→G
68: rread 2,1;sread 2,F[*];sprt 2,G[*],"end"
69: ina F,G;next C
70: "Segment Averaging":
71: rread 2,1;sread 2,F[*],G[*];1/V→C
72: smpy C*F→F;smpy C*G→G
73: chain "IFFT",0,0
```

```
0: "SIGAV":gto +2
1: rread 8,1;sread 8,G[*];gto "Smoothing"
2: "SA#!?8"→N$;asgn N$,8,0,X;if X#1;kill N$
3: open N$,int(r18/30)+1;asgn N$,8
4: rread 1,1;ina F,G
5: for J=1 to V;sread 1,F[*]
6: ara F+G→G;next J;1/V→C;smpy CG→G;sprt 8,G[*]
7: "Smoothing":if r6=0;ara G→F;gto "Display"
8: for I=1 to r18;0→X
9: for J=-r6 to r6
10: if I+J<1;X+G[I+J+r18]→X;gto +3
11: if I+J>r18;X+G[I+J-r18]→X;gto +2
12: X+G[I+J]→X
13: next J
14: X/(2r6+1)→F[I];next I
15: "Display":
16: pclr;1000Er18→r3
17: max(F[*])→r2
18: scl -r3/3.3,1.05r3,-1.5r2,1.2r2;pen# 1;fxd 2
19: xax -r2,r3/5,0,r3,1;deg;csiz 2,2,1.5,0;plt r3/3,-1.4r2,1
20: lbl "Time millisec"
21: fxd 3
22: yax 0,r2/2,-r2,r2,1;csiz 2,2,1.5,90;plt -r3/4,-.9r2,1
23: lbl "Average Magnitude Volts"
24: for I=1 to r18;plt (I-1)1000E,F[I];next I;pen
25: "Rep":chain "FFTM",0,2
```

```
0: "FKILL":dim A$[6]
1: "Dt#?g1"→A$;cll 'A'
2: "Fr@$q2"→A$;cll 'A'
3: "Fy&k>3"→A$;cll 'A'
4: "Sr@$q4"→A$;cll 'A'
5: "Ssπ<v5"→A$;cll 'A'
6: "OE#?g6"→A$;cll 'A'
7: "OE#?g7"→A$;cll 'A'
8: "SA#!?8"→A$;cll 'A'
9: "Vr>↑s9"→A$;cll 'A'
10: end
11: "A":
12: asgn A$,1,0,X;if X#1;kill A$
13: ret
```

REFERENCES

1. Schofield, B.H. "Acoustic emission under applied stress". ASD-TDR-63-509, Lessels and Associates, Waltham, MA, 1963.

2. Hutton, P.H. Materials Evaluation. MAEVA, Vol. 26, 1968, pp. 125-129.

3. Beattie, A.G. "Characteristics of acoustic emission signals generated by a phase transformation". 1972 Ultrasonic Symposium Proceedings, Institute of Electrical and Electronic Engineers, pp. 13-17.

4. Graham, L.J. and Alers, G.A. "Spectrum analysis of acoustic emission in A533-B steel". Rockwell International, Thousand Oaks, California, presented at the ASNT 1973 Spring Convention, Los Angeles, California (March, 1973).

5. Bassim, M.N., Hay, D.R. and Lanteigne, J. "Wave form analysis of acoustic signals from a mild steel". Materials Evaluation, May 1976, pp. 109-113.

6. Kline, R.A. "Spectral analysis of acoustic emission signals". Master's Thesis, The John Hopkins University, Baltimore, MD 1975.

7. Hartman, W.F. and Kline, R.A. "Variations in frequency content of acoustic emission extension of HF-1 steel". Material Evaluation, July 1977, pp. 47-51.

8. Arthur E. Lord, J.R. "Acoustic emission". Physical Acoustics, Vol. 11, pp. 289-353, 1975.

9. Liptai, R.G. (1963). "Acoustic emission - A surface phenomenon", pp. 287-341. South West Research Institute: San Antonio, Texas.

10. Schofield, B.H. "Acoustic emission under applied stress". Lessels and Associates, Boston, Mass., Contract No. AF33(616)-540, progress report 11 (1961).

11. Schofield, B.H. "Investigation of applicability of acoustic emission". AFML-TR-65-106, Lessels and Associates, Waltham, Mass. (May 1965).

12. Liptai, R.G. "An investigation of the acoustic emission phenomena". PhD. Thesis, University of Michigan, Ann Arbor, Mich. (1963).

13. Tatro, C.A. and Liptai, R.G. "Acoustic emission from crystalline substances". Proceedings of the Symposium on Physics and Non-destructive Testing, Southwest Research Institute, San Antonio, Tex., pp. 145-158 (Oct. 1962).

14. Fisher, R.J. and Lally, J.S. "Microplasticity detected by an acoustic technique". Canadian Journal of Physics, Vol. 45, pp. 1147-1159 (1967).

15. Liptai, R.G., Dunegan, H.L. and Tatro, C.A. "Acoustic emission generated during phase transformations in metals and alloys". Lawrence Radiation Laboratory, UCRL-50525, University of California, Livermore, California,

(September, 1968).

16. Agarwel, A.B.L. "An investigation of the behaviour of the acoustic emission from metals and a proposed mechanism for its generation". Ph.D. Thesis, University of Michigan, Ann Arbor, Mich. (1968).

17. Frederick, J.R. "Use of acoustic emission in non-destructive testing". Seminar Annual Report, 1971-3-P, Sept. 1969-Feb. 1970, University of Michigan, Ann Arbor, Mich. (June, 1970).

18. Frederick, J.R. and Felbeck, D.K. "Dislocation motion as a source of acoustic emission". ASTM STP 505, pp. 129-139, 1971.

19. Schuyler, I.I. and Feiertag, T.H. "Acoustic emission testing program". Progress report on tensile testing through Oct. 1970". LA-4724-MS, Los Alamos Scientific Laboratory, Los Alamos, N. Mex. (March, 1972).

20. Romine, H.E. (1961). "Determination of the driving force for crack initiation from acoustic records of G_C tests in high strength materials for rocket motor cases". NWL Rep. No. 1779, U.S. Naval Weapons Laboratory.

21. Dunegan, H.L., Harris, D.O. and Tatro, C.A. "Fracture analysis by use of acoustic emission". California University, Livermore, Lawrence Radiation Laboratory, Feb. 6, 1969, Contract W-7405-eng-48.

22. Gergerich, W.W., and Hartbower, C.E. (1967). Int. J. Fracture Mech., 3, 185.

23. Hartbower, C.E., Gerberich, W.W., and Liebowitz, H. "Investigation of crack growth stress wave relationships". Engineering Fracture Mech. 1, pp. 291-308 (1968).

24. Jones, M.H., and Brown, W.F., Jr. "Acoustic detection of crack initiation in sharply notched specimens". Material Research and Standard Vol. 4, pp. 120-129 (March, 1964).

25. Baker, G.S. "Acoustic emission in metals as a non-destructive testing tool". Materials Evaluation, pp. 125-127 (July, 1968).

26. Pollock, A.A. and Randon, J.C. "Acoustic emissions in the fracture toughness test of a mild steel". Imperial College, Mechanical Engineering Dept., Fracture Group, Report No. FG-26, April 1970.

27. Randon, J.C. and Pollock, A.A. "Acoustic emission and energy transfer during crack propagation". Imperial College, Mechanical Engineering Dept., Fracture Group, Report No. 31, July 1970.

28. Dunegan, H.L. "Using acoustic emission technology to preduct structural failure". Feb. 1975, Metals Engineering Quarterly.

29. King, S.P. and Grigory, S.C. "Acoustic emission from flawed heavy section steel plates". Materials Evaluation, pp. 30-36 (Feb. 1975).

30. Mirabibe, M. "Application of acoustic emission to the study of the fracture of steel". Mem. Soci. Rev. Met., 1974, 71, (9), 27-39. BISI 13314, Sept. 1975.

31. Bassim, M.N., Hay, D.R., Lanteigne, J. "Waveform analysis of acoustic signals from a mild steel". Materials Evaluation, pp. 109-113 (May, 1976).

32. Harris, D.O. and Dunegan, H.L. "Applications of acoustic emission to industrial problems" Acoustic Emission-5, NDT, 1974, June, 137.

33. Hart, S.D. "On the possibilities for the use of acoustic emission for non-destructive testing of welds and welded structures". Welding in the World, 12, 1974, 61.

34. Hutton, Philip H. "A.E. - a new tool for evaluating structural soundness". BNWL-SA-2449, Battelle Memorial Institute, Richland, Washington, 1969.

35. DeKante, J.C.F. "Emitting materials: state of affairs of a very promising technique: the acoustic emission analysis". N73-16656, August 1972.

36. Ono, K., Huang, G. and Hatano, H. "A.E. characteristics of structural steels". 8th World Conference on NDT, Cannes, France, 1976.

37. Dunegan, H.L. and Green, A.T. "Factors affecting acoustic emission response from materials". ASTM STP 505, pp. 100-133, 1971.

38. Green, A.T. and Hartbower, C.E. "Development of a non-destructive testing technique to determine flaw criticality". Advanced Research Project Agency Order 1244, Program Code 8D10, Contract K33615-68-C-1705, May, 1970.

39. Parry, D.L. "Non-destructive flaw detection in nuclear power installations". USAEC Report, Conference Proceedings, Incipient Failure Diagnosis for Assuring Safety and Availability of Nuclear Power Plants, Gatinburg, Tenn.,Nov. 1967.

40. Ireland, D.R., Wullert, R.A., and Scott, V.G. "Connecticut yankee reactor vessel radiation surveillance program". Battelle-Columbus Laboratory.

41. Tangri, K., Toronchuk, J.P. and Lloyd, D.J. "A.E. from polycrystalline copper and iron silicon".

42. Nabarro, F.R.N. "Theory of crystal dislocations". p. 510, 1967.

43. Gillis, P.P. "Some fundamental aspects of the theory of acoustic emission". Materials Science and Engineering 14 (1974), 103-108.

44. Pollock, A.A., Acoustic emission, "Acoustic emission amplitudes". Non-destructive testing, Vol. 6, No. 5, Oct. 1973.

45. Graham, L.J. and Alers, G.A. "Acoustic emission in frequency domain". Monitoring Structural Integrity by Acoustic Emission, ASTM 1974, ASTM special Technical Publication (STP-521), pp. 11-39.